WILEY

ELECTRICALLY SMALL, SUPERDIRECTIVE, AND SUPERCONDUCTING ANTENNAS

R. C. HANSEN

Electrically Small, Superdirective, and Superconducting Antennas

R.C. Hansen

A John Wiley & Sons, Inc., Publication

Electrically Small, Superdirective, and Superconducting Antennas

Electrically Small, Superdirective, and Superconducting Antennas

R.C. Hansen

A John Wiley & Sons, Inc., Publication

Published by John Wiley & Sons, Inc., Hoboken, New Jersey
Published simultaneously in Canada

Library of Congress Cataloging-in-Publication Data:
Hansen, Robert C.
Electrically small, superdirective, and superconducting antennas / by R.C. Hansen.
p. cm.
Includes bibliographical references and index.
ISBN-13: 978-0-471-78255-1
ISBN-10: 0-471-78255-6
1. Antennas (Electronics) I. Title.

TK7871.6.H35156 2006
621.382′4—dc22

2005056820

Printed in the United States of America

10 9 8 7 6 5 4 3 2 1

This Book is Dedicated to These Intrepid
Warriors Against Nut-House Antennas
Dick Adler
Jack Belrose
Ben Dawson
Jim Hatfield
Larry Hurzon
Rick Ridgley

Books by R. C. Hansen:
Microwave Scanning Antennas (3 volumes)
Significant Phased Array Papers
Geometric Theory of Diffraction
Moment Methods in Antennas and Scattering
Phased Array Antennas
www.rchansen.com

Contents

Preface

Harold Wheeler, in his classic 1947 papers, created the field of electrically small antennas. This field has long been important for frequencies below roughly 1 GHz, where a half-wavelength is about 6 inches. These electrically small antennas have characteristics in common that limit performance: low radiation resistance, high reactance, low efficiency, narrow bandwidth, and increased loss in the matching network. Most of these limitations are shared by two other classes of antennas: superdirective antennas and superconducting antennas. This book is divided into three interrelated chapters: Chapter 1 on electrically small antennas, Chapter 2 on superdirective antennas, and Chapter 3 on superconducting antennas. Each chapter includes extensive references and an author list. An overall subject index is provided at the end of the book. We antenna engineers have done what is possible by rearranging the wires; future significant advances will come through use of new low-loss magnetic materials and through use of circuits to compensate for impedance deficiencies. Both areas are addressed.

Many engineers interested in these topics have not had the benefit of early papers on these three subject areas. This book aims to be a primer on what has been investigated and what works. Over the years many ideas on improving electrically small antennas have appeared. These are discussed under three categories: designs that work, clever physics but bad numbers, and pathological antennas. In retrospect, the simplest antennas are the best: dipoles with or without fatness or loading; patches with appropriate substrates. There are no wideband electrically small antennas, unless efficiency is sacrificed for bandwidth. The relatively new field of Non-Foster circuits may change this situation.

Harold A. Wheeler. Fundamental Limitations of Small Antennas. *Proc IRE* Vol. 35, Dec. 1947, pp. 1479–1484.

Harold A. Wheeler. A Helical Antenna for Circular Polarization. *Proc IRE* Vol. 35, Dec. 1947, pp. 1484–1488.

Chapter 1

Electrically Small Antennas

1.1 INTRODUCTION

An electrically small antenna (ESA) is a dipole-type antenna with length less than $\lambda/2$ (λ is wavelength), a monopole-type antenna with length less than $\lambda/4$, or a loop-type antenna with conductor length less than $\lambda/3$. All of these are constrained by fundamental limitations on bandwidth versus size. There are also constraints on impedance matching versus number of matching sections, for lossless matching circuits. Lossy matching circuits working into a large VSWR have a significantly increased loss; see Section 2.6. Non-Foster matching circuits are discussed in Section 2.7. Under canonical types of ESA are included loaded dipoles, patches with uncommon substrates, loops both air and magnetic core, and dielectric resonator antennas. Sections 1.2 and 1.3 are of historical interest, and are for those readers who tend to reinvent old ideas. Some clever ideas have been found to be impractical; see Section 1.4. A long list of antenna ideas resembling science fiction is given in Section 1.5.

1.2 FUNDAMENTAL LIMITATIONS

1.2.1 Wheeler–Chu–McLean

The concept of a limitation on the bandwidth of an ESA was probably due to Wheeler (1947). He considered a cylindrical volume with capacitor plates normal to the axis. With simple theory the susceptance was obtained (assuming no fringing), along with the shunt radiation conductance. The "Radiation Power Factor" (RPF) was then $k^3a^2b/6$, where the cylinder radius and length are a and b (throughout $k = 2\pi/\lambda$). Wheeler's RPF is approximately equal to bandwidth. The same result was obtained by Wheeler using a multiturn inductor whose diameter is $2a$ and length is b. These simple formulas for loops and capacitors are unfortunately only grossly approximate. See also Wheeler (1975). A year later, Chu (1948) published a more exact analysis, using low-order TE and TM modes. Chu, and all contributors since, enclosed the ESA in a hypothetical sphere of radius a. In this sphere are TE and

Electrically Small, Superdirective, and Superconducting Antennas, by R. C. Hansen.

TM spherical modes. Chu assumed that the modes are orthogonal in power, an assumption that is discussed below. The difficulty is in separating the nonradiating power from the total power (energy). As the latter is infinite, Chu devised a stratagem based on the recurrence relations for spherical Bessel functions. A continued fraction expansion allowed a ladder network to be expressed for each spherical mode. The calculations are simple for the lowest TE and the lowest TM mode. Antenna reactance was expressed in low-order spherical Bessel functions, and Q, defined as usual by $Q = 2\omega W/P$, is obtained by differentiating the reactance to get average stored energy W. P is the power dissipated (expended). The result, for a single lowest TE mode, or a single lowest TM mode, is:

$$Q = \frac{1}{ka} + \frac{1}{k^3 a^3} \tag{1.1}$$

For $Q \gg 1$, the half-power bandwidth equals $1/Q$. Note that the result in Hansen (1981) is incorrect.

The concept of low-order spherical modes was extended to antenna gain by Harrington (1960), who showed that the maximum directivity for the lowest-order mode was 3, a value twice that for a Hertzian dipole. As this is related to the lowest mode Q, it may offer insight on why the Chu Q has not been approached in practice.

Collin and Rothschild (1964) and Collin (1998) bypass the Chu ladder formulation and calculate energy directly. The total time average energy in the field is given by an integral of the spherical mode functions, from the sphere radius to infinity. This integral is infinite; to obtain the energy stored in the evanescent field, the radiated energy is subtracted. The latter is the real part of the radial component of the complex Poynting vector divided by the energy flow velocity. This yields Q in terms of spherical mode functions. For the lowest mode the result is just Equation 1.1. This has been reprised by McLean (1996) with the result of Equation 1.2; he also shows that when both the lowest TE and lowest TM modes are excited (circular polarization), the Q is:

$$Q = \frac{1 + 3k^2 a^2}{2\left(1 + k^2 a^2\right) k^3 a^3} \tag{1.2}$$

This result differs from twice Equation 1.1 because the TE mode also stores a small amount of electric energy and conversely for the TM mode. See also Fante (1969).

A different approach was taken by Thiele et al. (2003), based on the far-field pattern of a small source. A "pattern" Q is based on the integral of pattern over visible space and that integral over all space, including invisible. Their Q values are higher than those of Chu. An electrically small dipole with sinusoidal current distribution was used to provide the fields for the integrations. These pattern Q values are 8 times larger than Equation 1.1 predicts. Dipole bandwidth calculations were also made by Hujanen (2005).

Kalafus (1969) calculates Q for higher modes as well, using series expansions for the integrands of energy. Then coefficients of polynomials representing Q are given. Another calculation of Q due to higher modes is by Harrington (1960).

An egregious example of claiming antennas that violate the fundamental limitations on small antennas is by Underhill and Harper (2002, 2003). For a short folded dipole of length L they have reactance proportional to kL. However, it is well known that the folded dipole reactance is four times that of the constituent dipole, which is proportional to $1/kL$. For a small loop of diameter D they have radiation resistance proportional to kD^2, when it is widely accepted that it is proportional to k^4D^4. These errors appear to be due to applying static formulations to electromagnetic problems.

Another paper claims that orthogonal TE and TM modes produce a gain of 3 and a Q half that of either mode (Kwon, 2005). Both are in error; the input power and the peak power density are both doubled, leaving the gain at 1.5 and the Q that of one mode.

An erroneous calculation of bandwidth limitations occurred because of confusion between total energy, stored energy, and radiated energy. This resulted in a bandwidth of 16π times the fundamental limit for VSWR ≤ 2 (Chaloupka, 1992).

Geyi (2003a, 2003b) reexamines the task of maximizing the ratio D/Q, directivity divided by Q. He corrects some inconsistencies in Fante (1969), with the result that maximum D/Q for a directive antenna (with both TE and TM modes) is $3/Q$, whereas that for an omnidirectional antenna is, as expected, $3/2Q$.

Turning now to typical values of Q versus ka, Figure 1.1 shows Q versus ka, where sphere radius is a. Curves are shown for efficiencies of 100% (perfect matching), 50%, 10%, and 5%. The lower efficiencies represent additional loss, so the Q values are reduced. Q for a moderately fat dipole, of *length/radius* = 20, is shown in Figure 1.1 as a small circle; dipole length is 0.2λ. This Q of roughly 27 is considerably higher than the Chu 100% efficiency curve; the dipole does not make effective use of the spherical volume. To obtain performance closer to the minimum Q curve the spherical volume must be used more effectively; a dipole is essentially one dimensional. A more effective design using three dimensions is a Cloverleaf dipole with coupling loops over a ground plane (or double cloverleaf dipole without ground plane) developed by Goubau (1976). This antenna, as sketched in Figure 1.2, in symmetric form requires $ka = 1.04$ and gives an octave bandwidth, or $Q = \sqrt{2}$ (see small circle in Fig. 1.1). However, the performance is attributed both to electric and magnetic modes; the single mode Q is $2\sqrt{2}$. An improved version has been developed by Friedman (1985). Another version, but with less bandwidth, is by Jung and Park (2003).

1.2.2 Foster's Reactance Theorem Versus Smith Chart

In 1924 R. M. Foster published a paper showing that a lossless reactance always has a positive slope of reactance with frequency. This has become known as Foster's reactance theorem (1924). Such networks have their poles and zeroes on the real axis, and they alternate. See also Bode (1945) and Guillemin (1935). Because all antennas have a virtual loss due to the radiation resistance, Foster's theorem should

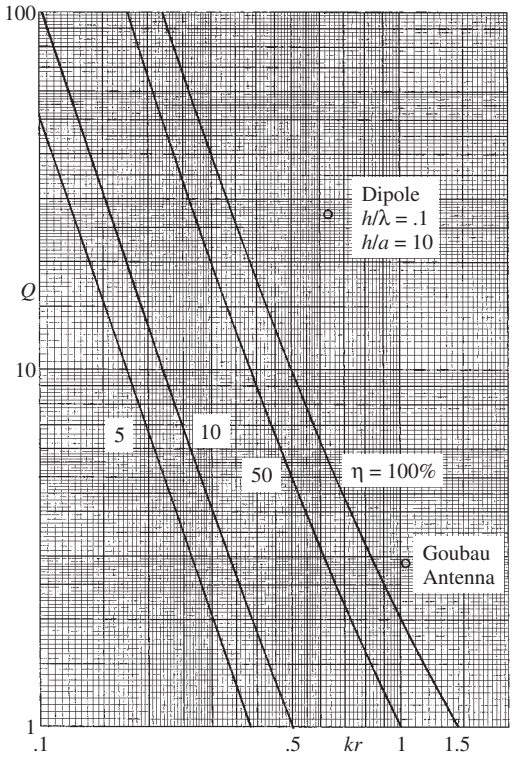

Figure 1.1 Fundamental limitation on Q

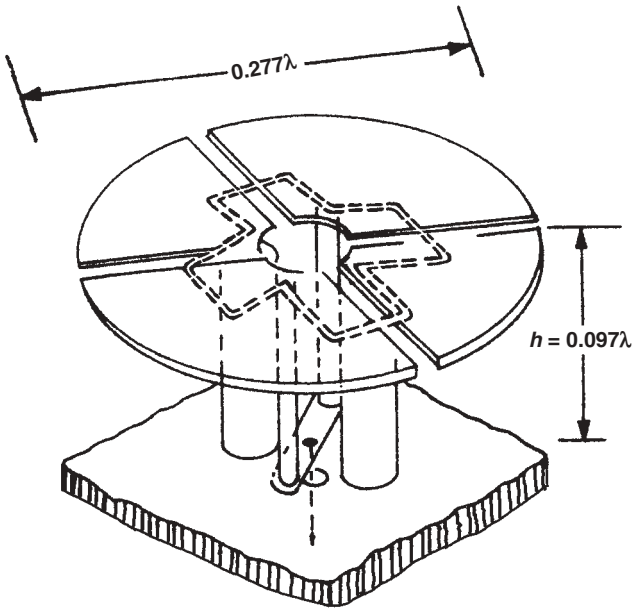

Figure 1.2 Goubau antenna

not apply. There has been some controversy regarding whether Foster's reactance theorem applies to antennas, and in particular, to electrically small antennas. Best (2004a) claims that it does not apply near antiresonance, where the reactance is rapidly changing sign. Others such as Geyi et al. (2000) claim that Foster's theorem does apply. Yaghjian and Best (2004, 2005) invoke a far-field "dispersion energy," which is the integral involving the complex far-field pattern and the antenna conductivity. If σ is dispersive, this energy integral adds to the reactance calculation, and voids the Foster theorem for antennas, as expected.

All of these discussions concerning antenna Q are mostly irrelevant: Q is only important (and useful) when it is large enough that half-power bandwidth is $1/Q$. Bandwidth and impedance are the crucial parameters in all antenna considerations. As usual bandwidth is between upper frequency f_2 and lower frequency f_1, at a center frequency of f_0:

$$\mathrm{BW} = \frac{f_2 - f_1}{f_0} \tag{1.3}$$

From a practical standpoint the applicability of the Foster theorem to antennas is irrelevant. The proper question to ask is: Does the impedance locus of an antenna always travel clockwise with increasing frequency around the Smith chart? To demonstrate that this is true, a computer program was written to calculate dipole impedance versus frequency, using the Carter impedance formulation involving Sine and Cosine Integrals. Figures 1.3 and 1.4 show the resistance and reactance versus dipole length in wavelengths over a range 0.2 to 1.5, for *length*/*radius* = 500. Similar data for *length*/*radius* = 20 are given in Figures 1.5 and 1.6. As asserted by Best, it is

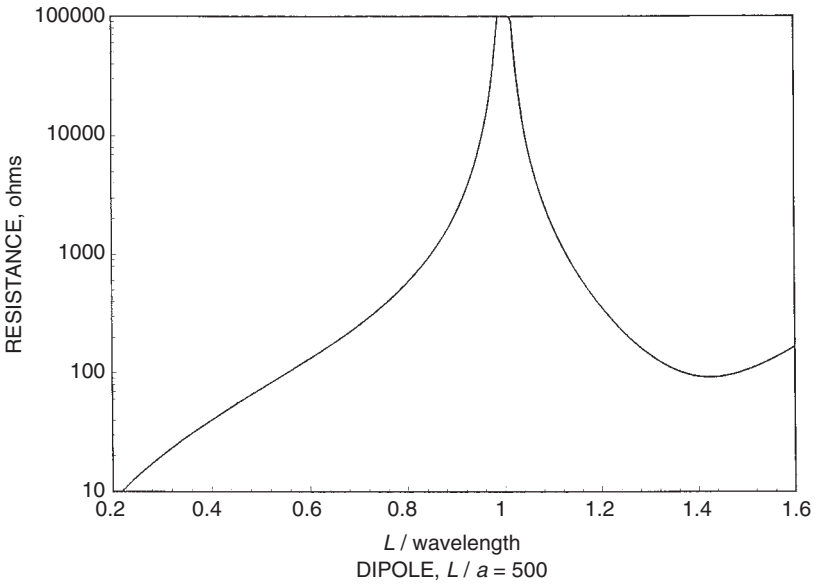

Figure 1.3

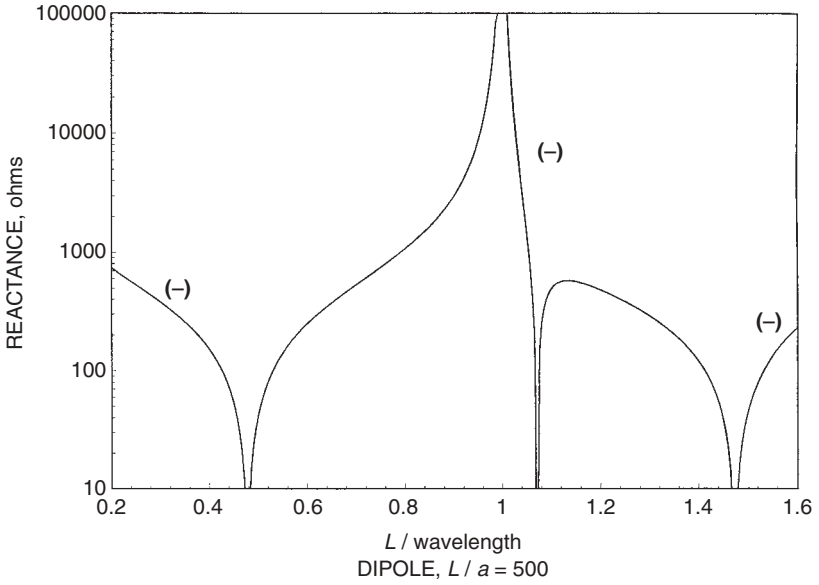

Figure 1.4

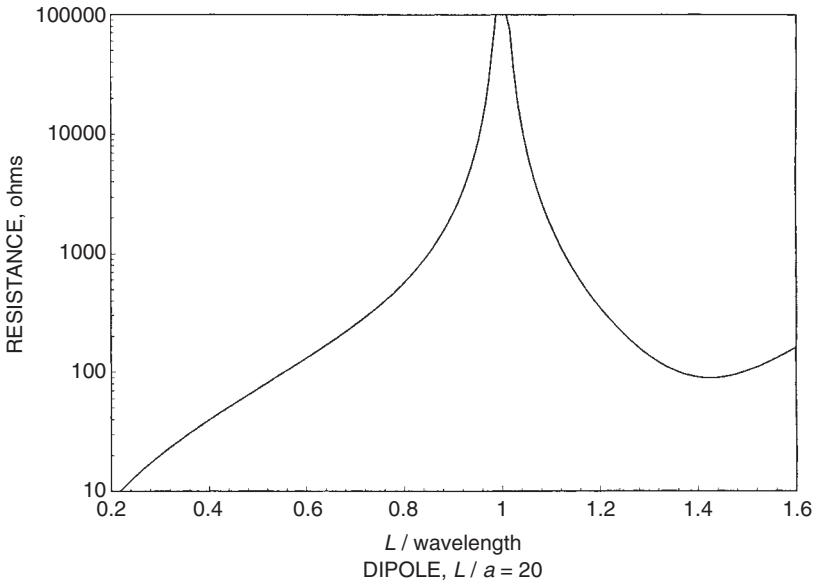

Figure 1.5

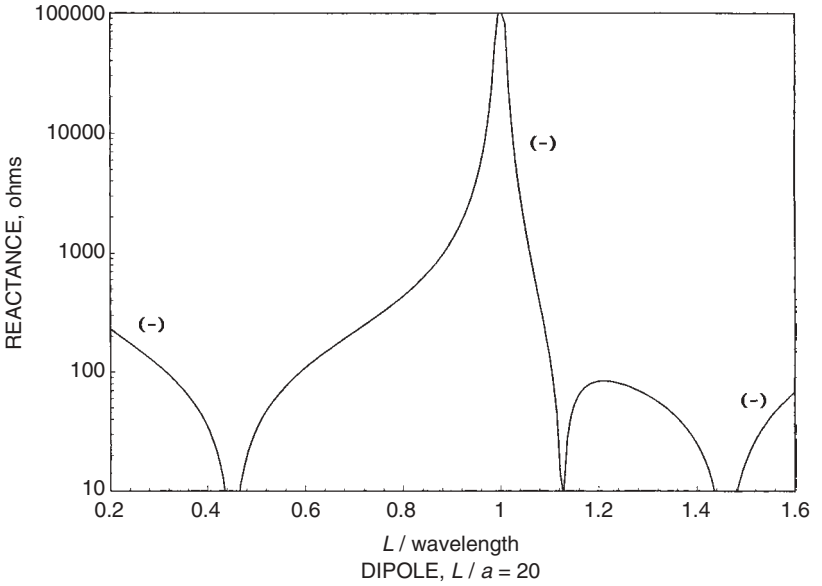

Figure 1.6

immediately obvious that there are impedance regions where the reactance slope does not obey Foster's theorem. However, Figure 1.7 is a Smith chart showing the dipole impedance over the same range, and it is clear that the rotation is always clockwise. Figure 1.8 is for *length*/*radius* = 20, and again the rotation is clockwise. When the impedance locus has resonances with small loops on the Smith chart, the rotation is still clockwise. We believe that this result holds true for all types of antennas.

1.2.3 Fano's Matching Limitations

The fundamental limits on matching were derived more than 50 years ago by R. M. Fano (1950a, 1950b). Matthaei, Young, and Jones (1964) in their treatise gave solutions to the simultaneous equations developed by Fano:

$$\frac{\tanh na}{\cosh a} = \frac{\tanh nb}{\cosh b}$$
$$\cosh nb = \Gamma \cosh na \tag{1.4}$$
$$\sinh b = \sinh a - 2\delta \sin\frac{\pi}{2n}$$

Here there are n matching sections (including the antenna as one), δ is decrement,[1] and a and b are parameters to be determined. Γ is the reflection coefficient. These

[1] δ is $1/Q$ of the load at band edges.

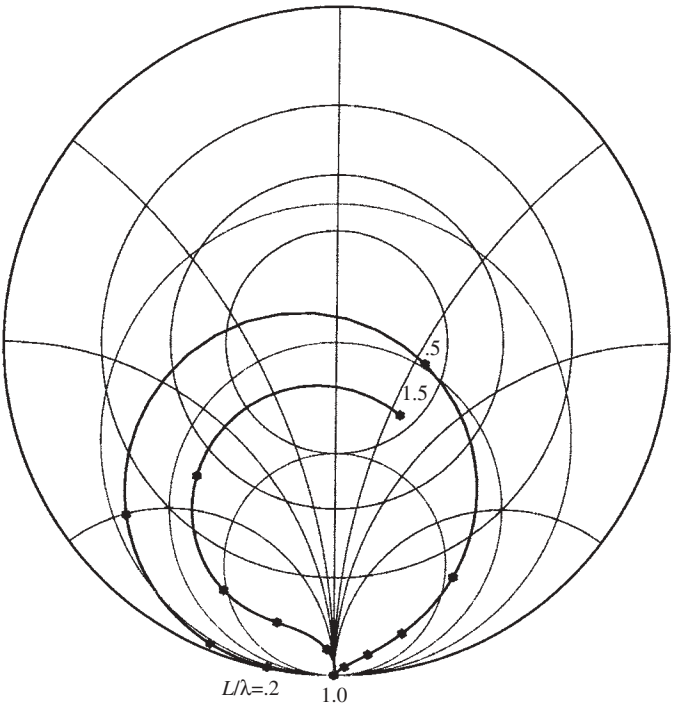

DIPOLE; *L/a*=500

Figure 1.7

simultaneous equations were solved by Matthaei et al. (1964), with results presented in graphical form. Subsequently Newton–Raphson (Stark, 1970) was used by this author to obtain precise values of a and b for both equal ripple VSWR ≤ 2 and VSWR ≤ 5.8328 (half-power) cases. For VSWR ≤ 2, Table 1.1 gives values of a, b, and δ. Note that $n = 1$ is for the antenna alone. Corresponding values for half-power (VSWR ≤ 5.828) are given in Table 1.2. The bandwidth improvement factor is just δ for $n = 1$ divided by δ for $n > 1$. Table 1.3 from Hansen (1998) gives these bandwidth improvement factors.

Typically an electrically small antenna represents one resonant circuit; an additional matching circuit doubles the half-power bandwidth, or increases the VSWR = 2 bandwidth by 2.31. A second matching circuit makes a significant improvement for all VSWR; however, more circuits offer diminishing returns. The limit, using many matching circuits, is only a factor 3.2 for half-power, or 3.8 for VSWR = 2. These results are all for lossless matching circuits; lossy circuits will of course increase the bandwidth and decrease the efficiency.

Impedance matching is a well-understood practice; a good exposition is in Chapter 5 of Collin (2001). For the special case of a transmit antenna, a novel

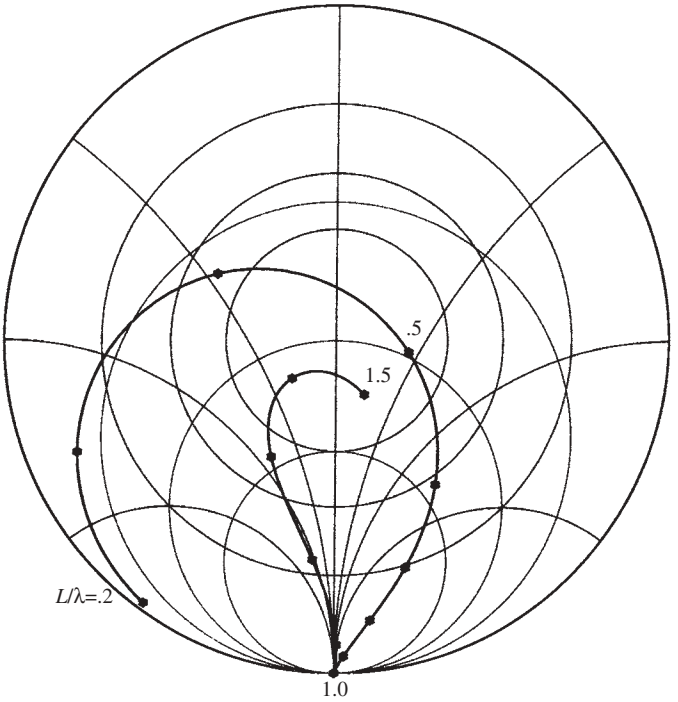

DIPOLE; *L/a*=20

Figure 1.8

Table 1.1 VSWR ≤ 2

n	*a*	*b*	δ
1	1.81845	0.32745	1.33333
2	1.03172	0.39768	0.57735
3	0.76474	0.36693	0.46627
4	0.62112	0.33112	0.42416
5	0.52868	0.30027	0.40264
∞	0	0	0.34970

Table 1.2 VSWR ≤ 5.828

n	*a*	*b*	δ
1	1.14622	0.65848	0.35355
2	0.76429	0.56419	0.17416
3	0.59982	0.47449	0.14394
4	0.50164	0.41026	0.13207
5	0.43483	0.36284	0.12589
∞	0	0	0.11032

Table 1.3 Maximum bandwidth improvement factors

Number of Additional Matching Circuits	VSWR = 2	Half-Power
1	2.3094	2.0301
2	2.8596	2.4563
3	3.1435	2.6772
4	3.3115	2.8083
∞	3.8128	3.2049

technique uses a circulator, a directional coupler, and a phaser to adjust the phase of the reflected power and return it to the antenna (Brennan, 1992).

A network matching into a large VSWR will experience an increased loss; see Section 2.6. Non-Foster matching circuits are covered in Section 2.7.

1.3 ELECTRICALLY SMALL ANTENNAS: CANONICAL TYPES

The term electrically small antennas applies to antennas whose dimensions are small compared to the wavelength. As will be shown, these are mostly dipoles or loops, or minor modifications of these. Various techniques for improving performance are discussed below.

Both short dipoles and small loops are superdirective; the directivity remains at 1.5 as the dimensions decrease, but the radiation resistance decreases and the reactance increases. Thus the bandwidth is narrow, the efficiency may be low, and the necessary tolerances will be small. See Chapter 2 for more discussion of superdirectivity.

1.3.1 Dipole Basic Characteristics

First take the case of a dipole (or monopole) that is transmitting. A typical equivalent circuit is shown in Figure 1.9. The dipole radiation resistance, loss resistance, and reactance are R_r, R_a, and X_a. The source and matching circuit has loss resistance and reactance R_ℓ and X_ℓ and load resistance R. The important parameters are the radiated power efficiency and the bandwidth. Assume that at the center frequency the antenna is matched, $X_\ell = -X_a$. Then the efficiency η at center frequency is:

$$\eta = \frac{R_r}{R_r + R_\ell + R_a} \tag{1.5}$$

Equation 1.5 of course states the well-known fact that efficiency is the ratio of radiation resistance to total circuit resistance; clearly, the R_r should be as large as feasible and equal to R_ℓ. For a short dipole of half-length h and a simple monopole also of length h, the radiation resistance is:

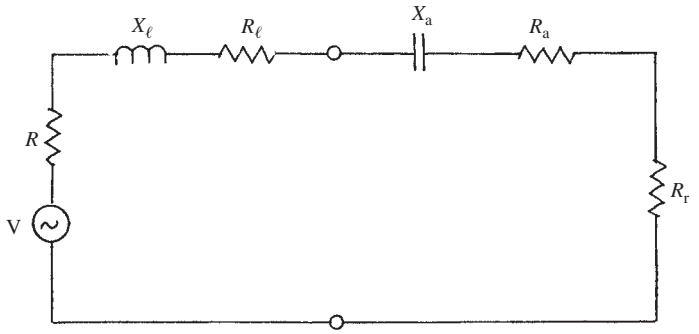

Figure 1.9 Transmitting dipole equivalent circuit

$$\begin{aligned} R_r &= 20k^2h^2 \quad \text{dipole} \\ R_r &= 10k^2h^2 \quad \text{monopole} \end{aligned} \tag{1.6}$$

The loss resistance is a simple function of the dipole dimensions; the reactance also involves the dimensions but is subject to modification through structural changes. The reactance and loss resistance formulas for simple dipoles/monopoles are:

$$\begin{aligned} X_a &= 120\left(1-\ell n\frac{n}{a}\right)\cot kh \quad \text{dipole} \\ X_a &= 60\left(1-\ell n\frac{h}{a}\right)\cot kh \quad \text{monopole} \\ R_a &= \frac{a}{2\delta}R_{dc}\frac{1}{3} = \frac{hR_a}{3\pi a} \quad \text{dipole} \end{aligned} \tag{1.7}$$

Here δ is skin depth, and R_s is resistivity in *ohms*/□. This formula for loss resistance is valid for short antennas (triangular current distributions) where the loss is 1/3 that for uniform current and for dipole radius large in skin depths. For a fixed h/a, the resistance is independent of length. Surface resistivity of copper at room temperature is $1.5E-7\sqrt{f}$, with f in Hz. A typical value of R_s for copper at 200 MHz is 2.6 mohm. Figure 1.10 shows the dipole parameters, using a fixed h/a = 100. Reactance for other thicknesses can be found by multiplying the reactance from Figure 1.10 by a normalized thickness factor:

$$\frac{\ell n\dfrac{h}{a}-1}{\ell n100-1} \tag{1.8}$$

Figure 1.11 gives this factor. Note that a flat strip dipole of width w is equivalent to a cylindrical dipole of radius $w/4$. The radiation resistance, over the range of h/λ from 0.005 to 0.01, varies from 0.02 ohms to 8 ohms; the reactance varies from –14,000 to –600 ohms. Not surprisingly, the efficiency is close to 100%, dipping only to 88% at h/λ = 0.005.

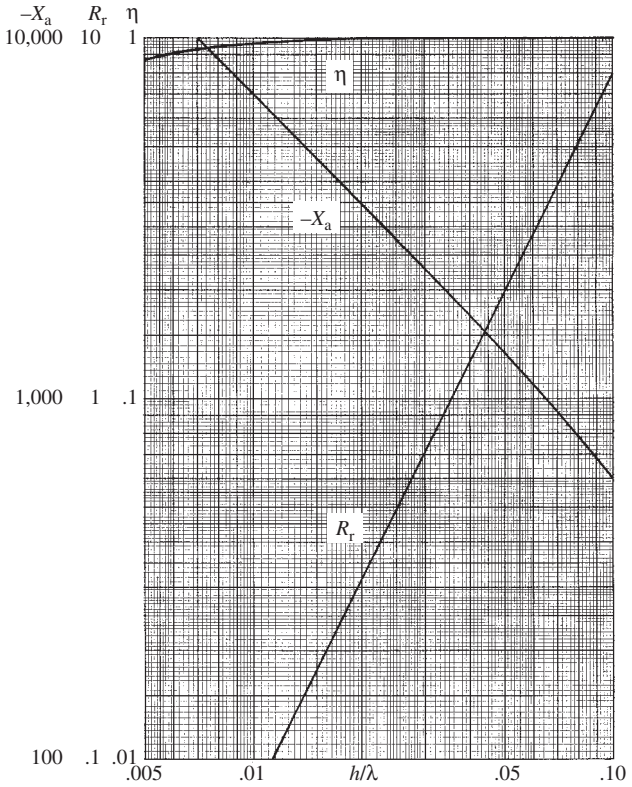

Figure 1.10 Dipole parameters

A simple bandwidth calculation assumes that the radiation resistance is constant with frequency, the loss resistance is negligible, and $Q = 1/\omega_o RC$, where $\omega = 2\pi f$ and the antenna reactance is $X = 1/\omega C$. Using a series equivalent circuit the impedance divided by R is:

$$\frac{Z}{R} = \frac{\omega RC + j(\omega^2 LC - 1)}{\omega RC} \tag{1.9}$$

$$\frac{Z}{R} = 1 + jQ\left(\frac{\omega}{\omega_0} - \frac{\omega_0}{\omega}\right) \tag{1.10}$$

The VSWR, abbreviated as V, becomes:

$$V = \frac{\sqrt{1+Q^2V^2} + QV}{\sqrt{1+Q^3V^2} - QV} \tag{1.11}$$

$$v = \frac{\omega}{\omega_0} - \frac{\omega_0}{\omega} = \text{BW} \tag{1.12}$$

$$Q^2v^2 = \frac{(V-1)^2}{4V} \tag{1.13}$$

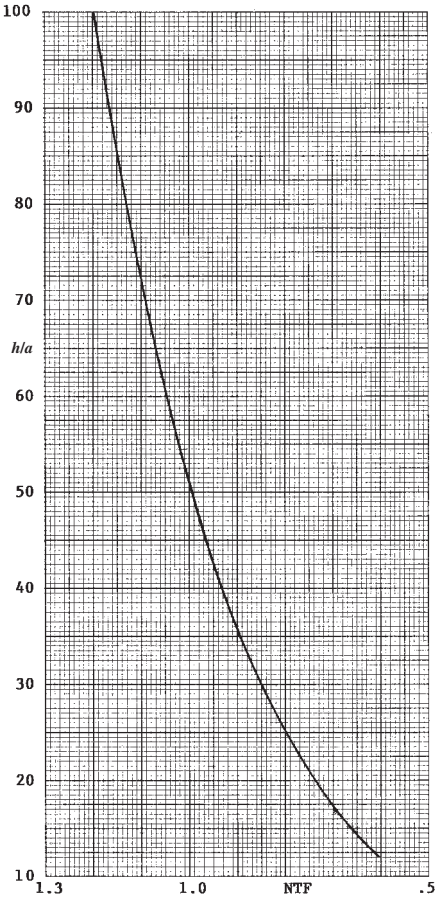

Figure 1.11 Normalized thickness factor

If bandwidth is defined as $(\omega_2 - \omega_1)/\omega_0$ for a given V, the Q bandwidth product becomes:

$$Q \cdot \mathrm{BW} = \frac{V-1}{2\sqrt{V}} \quad \text{(antenna only)} \tag{1.14}$$

A calculation useful for any thin dipole starts with the reactance derivative formula of Harrington (1968):

$$Q = \frac{\omega_0 d\,X/d\omega}{R_0} \quad \text{(antenna only)} \tag{1.15}$$

For the reactance and resistance, the Carter formula codified by Hansen (1976) is simplified for self impedance; $x_o = 0$ in the formula. Note that the series coefficients should be A(–2) = A(2) = 1, A(–1) = A(1) = $-4\cos$kd, A(3) = $2(1 + 2\cos^2$kd). The half power bandwidth is given approximately by:

$$\mathrm{BW} = 1/Q \tag{1.16}$$

To determine the utility of this result for low Q dipoles, exact bandwidth was calculated as the difference between two frequencies that satisfy:

$$V = \frac{[Z + R_0][Z - R_0]}{[Z + R_0][Z - R_0]} \tag{1.17}$$

A conjugate impedance match at the center frequency ω_o is used. The load resistance R_o equals the antenna radiation resistance at ω_o, and the matching reactance equals the negative of the antenna reactance X_o at ω_o. No losses are included; matching coil Q could easily be included. Results when a matching *network* is included are given by Hujanen et al. (2005).

Fig. 1.12 shows BW = 2/Q and exact bandwidth for half power: VSWR = $3 + \sqrt{8}$; the 2/Q results are surprisingly accurate for Q as small as 2. Similar calculations for VSWR = 2 are given in Fig. 1.13. Again 1/Q is accurate for Q ≥ 3.

Next a look at bandwidth vs dipole length. Given the dipole half-length h/λ, h/a, and VSWR, the $\omega_2 > \omega_o$ and $\omega_1 < \omega_o$ that satisfy Equation 1.17 can be found using

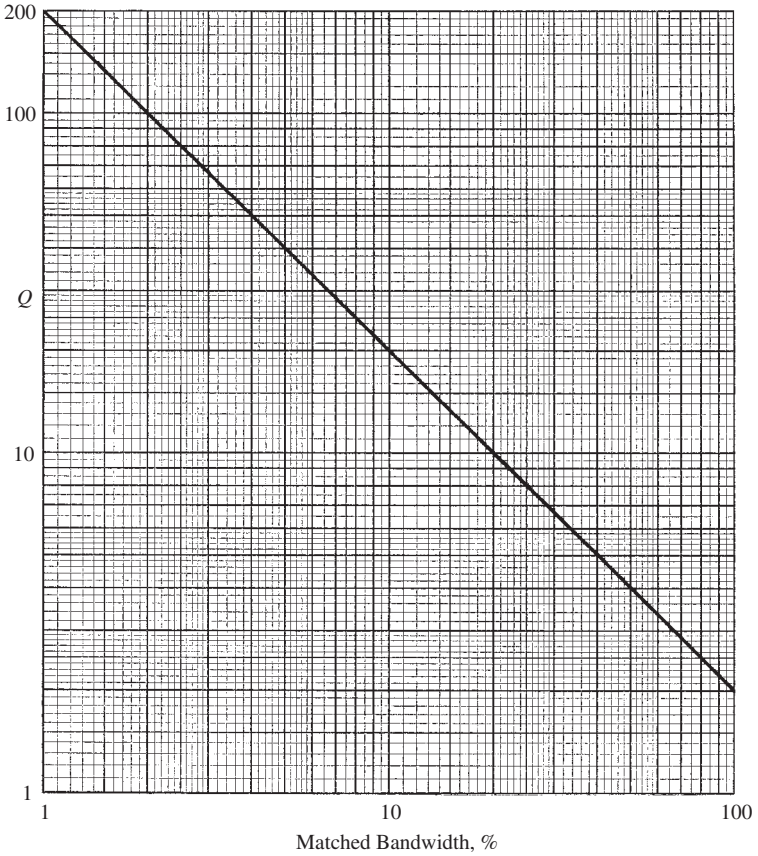

Figure 1.12 *Q* versus bandwidth, half power

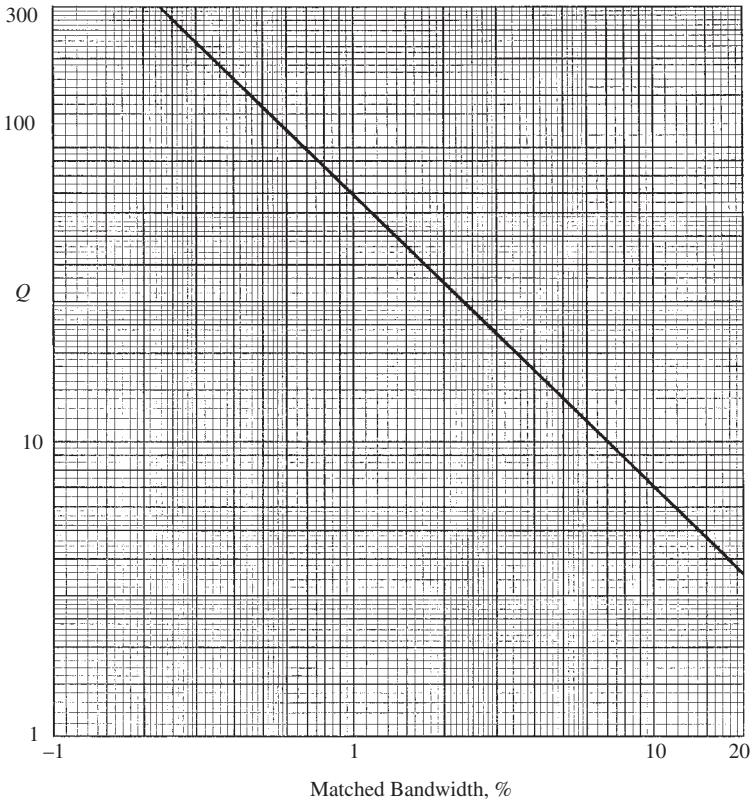

Figure 1.13 Q versus bandwidth, VSWR = 2

a root finder, in this case WEGSTEIN (1960) rooter. This subroutine is advantageous in that is does not require explicit derivatives.

Figure 1.14 gives % bandwidth for VSWR ≤ 2 for dipole lengths from 0.1λ to 0.4λ. Two curves are shown, for $L/a = 20$ and $L/a = 10$. The latter case is a fairly fat dipole; the equivalent flat strip dipole has length/width of only 2.5. The fatter dipole has bandwidth from 0.4% to 26%. These values are compared with those from Equation 1.15, which for VSWR ≤ 2 is:

$$BW = \frac{Q}{2\sqrt{2}} \tag{1.18}$$

The $L/a = 10$ case results from Equation 1.18 are shown as the small circles of Figure 1.14. The numbers for the $L/a = 10$, $L/\lambda = 0.2$ case will be informative. At center frequency f_o the impedance of the dipole is $8.308 - j\ 139.0$ ohms. At the upper VSWR = 2 frequency $f_2 = 1.01760/f_o$ the dipole impedance is $8.618 - j\ 135.5$ ohms. The matching inductive reactance is $1.0176 \times 139.0\,n = 141.4$ ohms. The net reactance at f_2 is 5.974 ohms. These values inserted into Equation 1.17 give VSWR = 2 and a bandwidth of 3.43%.

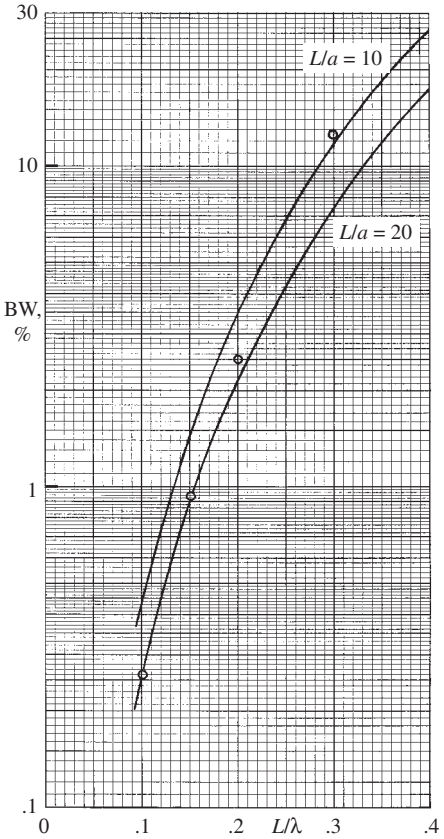

Figure 1.14 VSWR = 2 dipole bandwidth

These calculations assume that the matching inductance is lossless. In practice it will have losses, and this loss will widen the bandwidth and lower the efficiency. Also, a transformer is often used to transform the low radiation resistance to a convenient value such as 50 ohms. All transformers have loss and again the bandwidth is improved at the cost of efficiency. To reduce the losses, both the matching inductor and transformer can be made of HTS material; *see* Chapter 3. To convert bandwidth for any VSWR, given bandwidth for VSWR = 2:

$$\mathrm{BW} = \mathrm{BW}_2 \frac{\sqrt{2}(\mathrm{VSWR} - 1)}{\sqrt{\mathrm{VSWR}}} \tag{1.19}$$

The quantity most useful for evaluating short receiving antennas is effective length ℓ_e, which gives the open circuit voltage produced by a unit electric field strength: $V_{oc} = \ell_e E$. For a short dipole, $\ell_e = h$, independent of frequency. The equivalent circuit is the same as Figure 1.9 for transmitting. The low R_r and large X lead of course to a narrow bandwidth. For a receiving antenna the goal is to deliver as much of the incident power to the load. The receiving case is thus the same as the transmitting case: Minimize losses and utilize a good matching network.

Bandwidth is easily measured by connecting the antenna to a network analyzer, such as the HP 8510. This gives return loss (RL), which is:

$$\mathrm{RL} = \frac{(\mathrm{VSWR}+1)^2}{(\mathrm{VSWR}-1)^2} \tag{1.20}$$

or

$$\mathrm{VSWR} = \frac{\sqrt{\mathrm{RL}}+1}{\sqrt{\mathrm{RL}}-1} \tag{1.21}$$

Q can be measured with a time-domain procedure (Liu et al., 1999).

1.3.1.1 Resistive and Reactive Loading

Distributed resistive loading can be used to make a broadband dipole (Wu and King, 1965; Shen and Wu, 1967; Shen, 1967; Taylor, 1968; Lally and Rouch, 1970). Unfortunately, this technique is not effective for short dipoles; results are good for dipole lengths of the order of a wavelength. Distributed loading also helps short pulse response (Kanda, 1978, 1994; Esselle and Stuchly, 1990), but again only for longer dipoles. To avoid the drop in efficiency produced by resistive loading, distributed capacitive loading has been used (Rao et al., 1969). Again short dipoles do not benefit. Other loadings include impedance loads at two locations (Lin et al., 1970), multiple loads (Fanson and Chen, 1973), and loading with a resonant circuit at one location (Smith, 1975). Again these are not useful for a short dipole. S/N performance has been analyzed by Maclean and Saini (1981).

It has been accepted practice for many years to improve the performance of a short monopole (whip) by inserting an inductor into the whip. A pioneering work was by Bulgerin and Walters (1954). They performed a series of experiments on short, fat monopoles of various lengths at 100 MHz. For each length a number of loading points was used. Because of the relatively large gaps where the loading coil was located, these data have not been widely circulated. Also, modern ferrite toroid coils offer much higher Q values. Harrison (1963) analyzed the loaded monopole (dipole) with superposition of asymmetrically excited dipoles. However, because the coupled integral equations for the current distribution on an asymmetric dipole have not been solved except in principle, the current distribution used for each asymmetrically excited dipole was obtained from a zero-order solution. With this approach, Harrison calculated input impedance, current, and loading inductor currents for several lengths and a for number of loading coil Q values. The results showed a gradual increase in efficiency as the load point moved closer to the dipole ends; the data essentially stopped at a 2/3 load point, that is, 2/3 from the feed to the end. Czerwinski (1965, 1966) measured monopoles with distributed inductance where the monopole is a helix of small diameter with tapered pitch. For narrow band operation, a discrete coil offers better performance than does a helix (see Fig. 1.15). Moment Method calculations, described below, have indicated that the maximum efficiency point occurs closer to the feed than the 2/3 value predicted by the approximate theories.

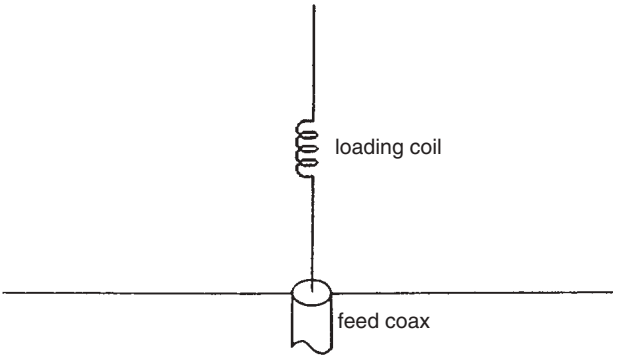

Figure 1.15 Inductively loaded monopole

The Moment Method calculations (Hansen, 1975a, 1975b) use piecewise sinusoidal expansion and test functions, a Galerkin stationary form. Carter mutual impedances are used, in a convenient subroutine (Hansen, 1972). A simultaneous equation solver provides the currents, from which input impedance is found. Discrete loading is included by adding the loading $R + jX$ to the matrix of mutual impedances at the proper segment junction. The load is added to the self-impedance on the diagonal for that segment. A restriction on the use of the Moment Method occurs for fat monopoles: Each segment must have a length-to-diameter ratio sufficiently large that the filamentary current approximation can be employed. At the same time, there must be sufficient segments to accurately represent the current distribution. When the wire is too fat for the number of segments used, the susceptance exhibits a shift. Also the number of segments must be chosen such that a segment junction occurs at each desired loading point. If N is the number of symmetrical segments on the dipole wire, I is the segment number at the loading point to dipole half-length (or monopole length),

$$\frac{N}{2I} = \frac{1}{1-\gamma} \tag{1.22}$$

The ratio of distance from feed to load to dipole half-length is γ. All data presented here were obtained by using $N = 12$, which allowed loading points of 1/6, 1/3, 1/2, 2/3, and 5/6 to be considered. Results were spot checked with $N = 6$ and 48 to validate the runs.

In principle the loading inductor functions by keeping the current distribution nearly constant from the feed to the load point, thereby increasing the current moment. Because the radiation resistance varies as current moment squared and the effective length varies with current moment, it is clear that inductive loading will improve short monopole performance (Fournier and Pomerleau, 1978). There is a value of loading reactance that allows the current to approximate a constant value out to γh with a linear dropoff beyond. This value of inductance is, however, insufficient to produce input impedance resonance. The resonant value of load produces a modest current peak just beyond γh so that the current moment is increased by an additional amount over that expected from the constant current model. Figure 1.16

shows two typical current distributions calculated for a thin dipole using $N = 40$. Figures 1.17 through 1.19 show the resonant input resistance as a function of the load point γ for lengths of monopole $h/\lambda = 0.05$, 0.1, and 0.15, for loading coil $Q = \infty$, 300, and 100, and for two monopole length-to-radius ratios $h/a = 50$ and 500.

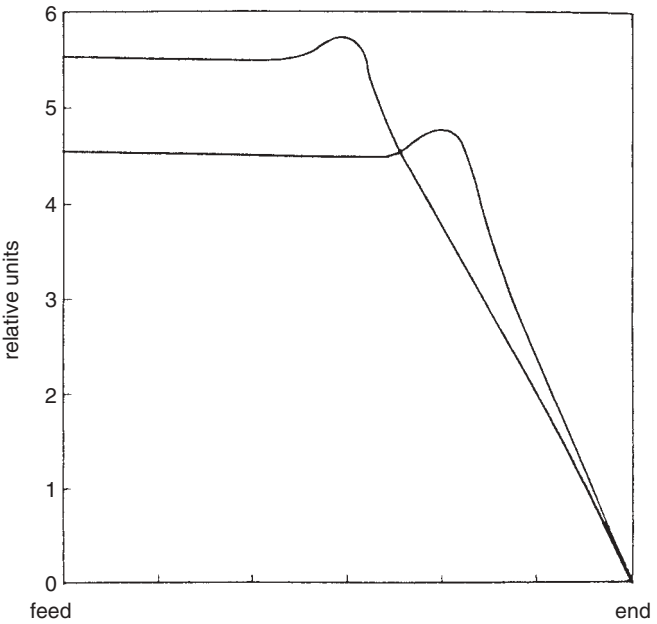

Figure 1.16 Current distributions for loading at 1/2 and 2/3 points. Courtesy of Hansen, R.C. Formulation of Echelon Dipole Mutual Impedance for Computer. *Trans IEEE* Vol. AP-20, Nov. 1972, pp. 780–781.

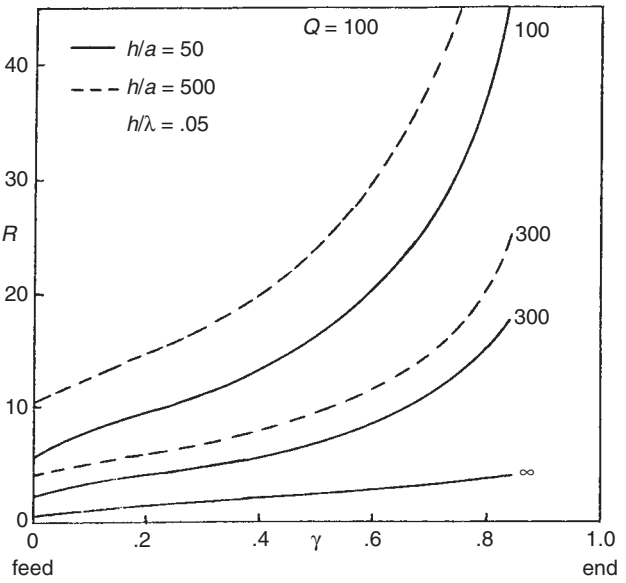

Figure 1.17 Input resistance versus loading point. Courtesy of Hansen, R.C. Formulation of Echelon Dipole Mutual Impedance for Computer. *Trans IEEE* Vol. AP-20, Nov. 1972, pp. 780–781.

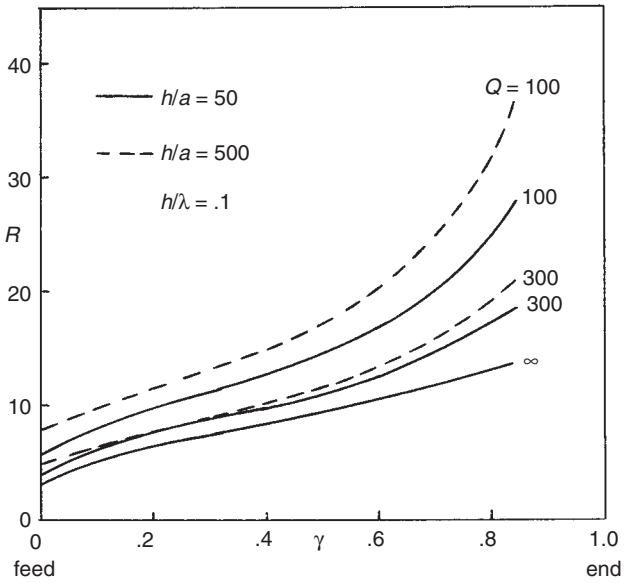

Figure 1.18 Input resistance versus loading point. Courtesy of Hansen, R.C. Formulation of Echelon Dipole Mutual Impedance for Computer. *Trans IEEE* Vol. AP-20, Nov. 1972, pp. 780–781.

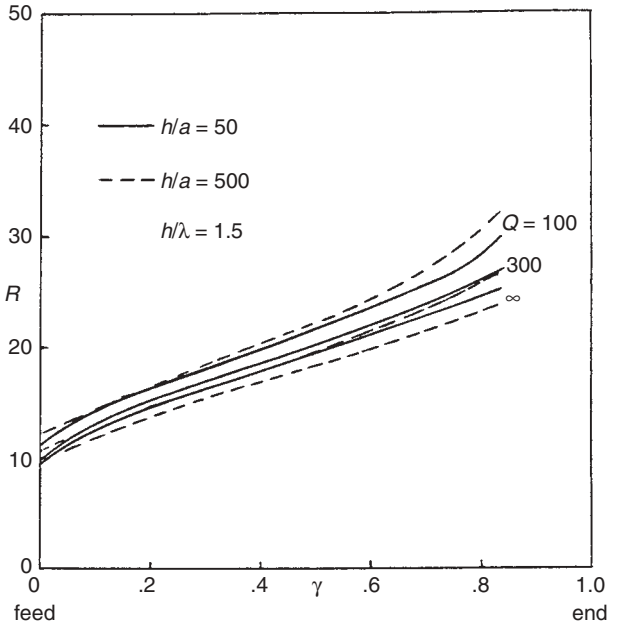

Figure 1.19 Input resistance versus loading point. Courtesy of Hansen, R.C. Formulation of Echelon Dipole Mutual Impedance for Computer. *Trans IEEE* Vol. AP-20, Nov. 1972, pp. 780–781.

Radiation resistance improvement factor β is given in Figures 1.20 and 1.21 for the same cases. It should be noted in Figures 1.17 through 1.19 that a significant part of the input resistance is due to coil losses, and this is reflected in the efficiency values. An empirical fit has been made to the radiation resistance enhancement factors based on the model of a current rising to a peak and then linearly dropping to zero at the wire end. The improvement factor β is the ratio of loaded to unloaded radiation resistance, and is:

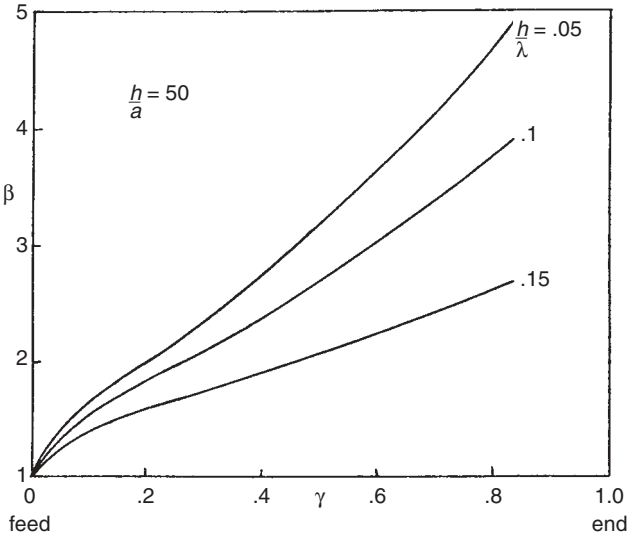

Figure 1.20 Radiation resistance improvement factor. Courtesy of Hansen, R.C. Efficiency and Matching Tradeoffs for Inductively Loaded Short Antennas. *Trans IEEE* Vol. COM-23, April 1975a, pp. 430–435.

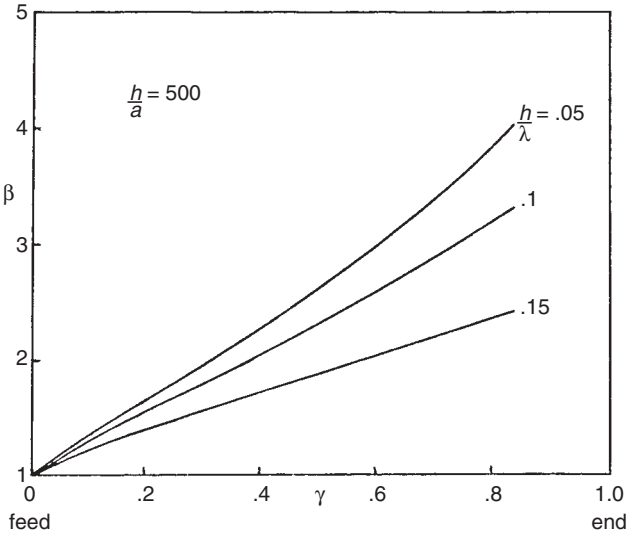

Figure 1.21 Radiation resistance improvement factor. Courtesy of Hansen, R.C. Efficiency and Matching Tradeoffs for Inductively Loaded Short Antennas. *Trans IEEE* Vol. COM-23, April 1975a, pp. 430–435.

$$\beta = \left[1 + \gamma + \frac{\gamma^{1/2}}{2}\left(1 - \frac{h/\lambda}{0.25}\right)\right]^2 \tag{1.23}$$

This will be used later in finding efficiency transition values. It is interesting to note that the radiation resistance improvement can for short antennas be larger than 4, the value that obtains with uniform antenna current. As mentioned, these results are due to the current peaking at or just beyond the load point.

As the load point moves toward the end, the loading reactance must increase to maintain resonance, finally becoming infinite at the end. For monopole lengths below roughly 0.1λ, the antenna reactance increases linearly (inversely) with length; the loading reactance does also, as seen in Figure 1.22. Here values for three loading points are shown. Figure 1.23 gives the factor $\alpha = X_{LOAD}/X_{ANT}$ for the same three load points. An empirical fit to be used later is just $\alpha = 1/(1 - \gamma)$.

Efficiency versus load point γ is of interest. Figures 1.24 and 1.25 give efficiency for $h/a = 50$ and 500, $h/\lambda = 0.05$, 0.1, and 0.15, and loading coil $Q = \infty$, 300, and 100. With ferrite toroid coils, Q values approaching 300 are practical over the HF-UHF range; the higher permeability cores are typified by the $Q = 100$ values. Lengths below 0.05λ are usually not practical as the efficiency is well below 50%. At the other extreme, monopoles longer than 0.15λ are seldom loaded as their radiation resistance and bandwidth are more tractable. Of course, the fatter monopoles have

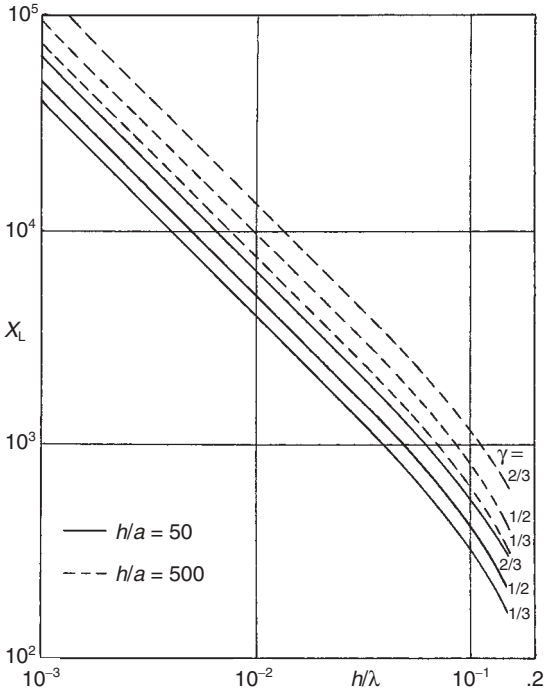

Figure 1.22 Resonant loading reactance. Courtesy of Hansen, R.C. Efficiency and Matching Tradeoffs for Inductively Loaded Short Antennas. *Trans IEEE* Vol. COM-23, April 1975a, pp. 430–435.

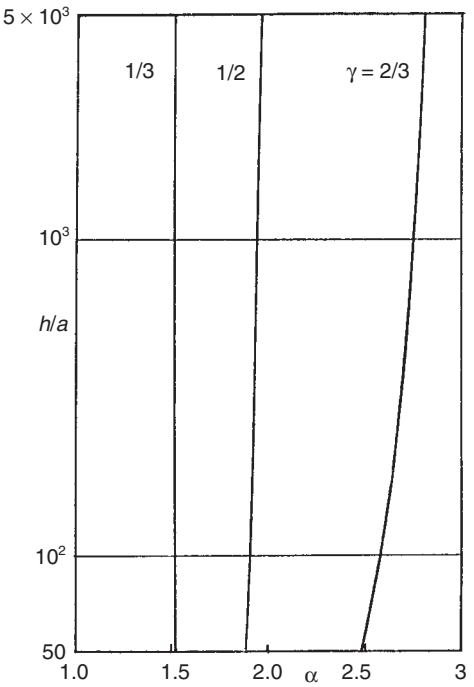

Figure 1.23 Ratio of loading reactance to antenna reactance. Courtesy of Hansen, R.C. Efficiency and Matching Tradeoffs for Inductively Loaded Short Antennas. *Trans IEEE* Vol. COM-23, April 1975a, pp. 430–435.

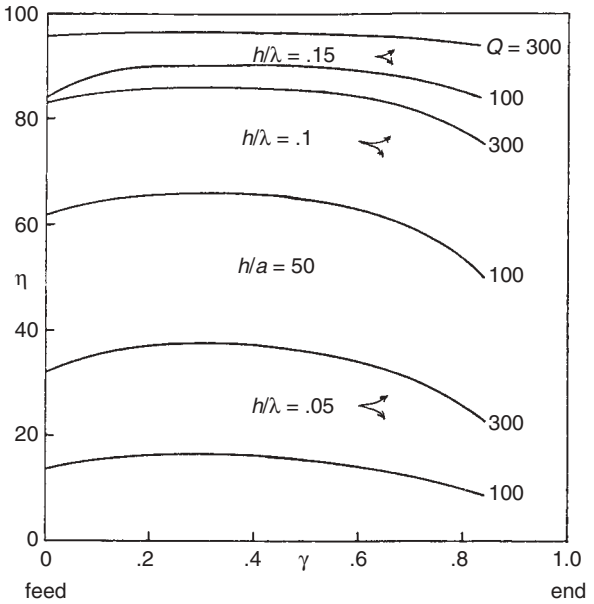

Figure 1.24 Efficiency versus loading point. Courtesy of Hansen, R.C. Efficiency and Matching Tradeoffs for Inductively Loaded Short Antennas. *Trans IEEE* Vol. COM-23, April 1975a, pp. 430–435.

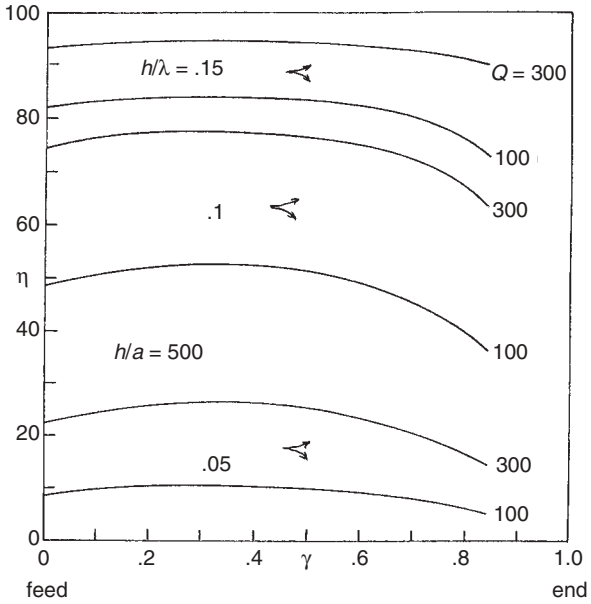

Figure 1.25 Efficiency versus loading point

higher efficiency as there is less antenna reactance to offset. Maximum efficiency occurs for a loading point between 0.3 and 0.4 from the feed, although the efficiency varies slowly with load point. There is no apparent variation of the maximum point with Q or with monopole length. It should be noted that when the loading coil is located at the feed, the efficiency is always lower. Thus for maximum efficiency the inductive load should be located at roughly $0.4h$. However, in most cases a small sacrifice in efficiency should be made to obtain a higher input resistance. Figures 1.17 through 1.19 show the input (radiation) resistance versus γ, and the tradeoff may be made between these figures and Figures 1.24 and 1.25. Antenna copper loss is not included as it is always much smaller than the loading coil loss.

An efficiency transition formula has been derived. Efficiency η is:

$$\eta = \frac{Q\beta R_r}{Q\beta R_r + \alpha X} \tag{1.24}$$

where for short monopoles $R_r = 10k^2h^2$ and $X = 60(\ell n\ h/a - 1)/kh$. Putting $\eta = 0.5$ and using the empirical formulas for α and β gives the h/λ for 50 percent efficiency:

$$\frac{h}{\lambda} = \frac{1}{2\pi}\left(\frac{6(\ell n\ h/a - 1)}{Q(1-\gamma)\left[1+\gamma+\gamma^{1/2}(1-4h/\lambda)/2\right]^2}\right)^{1/3} \tag{1.25}$$

As the $(1 - 4h/\lambda)$ factor has a weak influence on the result, the equation is readily solved by iteration. Note that the transition length varies as the cube root of Q and

even more slowly with h/a. For lengths below the transition length the efficiency drops rapidly, in the limit as f^3, or as length/wavelengths cubed. Use of HTS materials can improve η, but it is the loading coil that needs to be HTS. Even with the coil at the base this conclusion is still true. Thus the important overall conclusion: With ordinary inductances, loading of monopoles shorter than 0.06λ is not practical because of the low efficiency. There are, of course, special cases where the application is sufficiently important to warrant acceptance of low efficiencies, for example, VLF transmitting antennas.

A remark on bandwidth is in order. With an ideal loading coil ($Q = \infty$), the bandwidth is essentially unchanged by loading. Although the radiation resistance is substantially increased by loading, the slope of reactance is correspondingly increased, so the overall Q, which is the inverse of fractional bandwidth, is essentially unchanged. Real loading coils will have losses, with Q in the 100–300 range for ferrite toroids and in the 50–100 range for air core coils. These coil losses will of course decrease antenna Q and increase bandwidth.

1.3.1.2 Other Loading Configurations

Instead of a half-bowtie monopole, a wire frame monopole can be used (Wong and King, 1986), as sketched in Figure 1.26. This is a zigzag meander construction; an adjacent parasitic monopole is of similar shape. Performance is roughly equal to a $\lambda/4$ monopole, with half the length.

A novel inductive loading scheme winds a coil around a sphere, to give the maximum inductance for a given spherical volume (Best, 2004b, 2005b) (see Fig. 1.27).

A folded dipole may also be loaded to reduce its size. The folded dipole is often used because it offers a 4 : 1 impedance step up over a dipole, and this ratio can be changed over wide limits by making the two arms of different diameter (Guertler, 1950; Hansen, 1982). When the folded dipole is short, the transmission line currents see a low impedance, thus reducing the effectiveness of the element. One way of

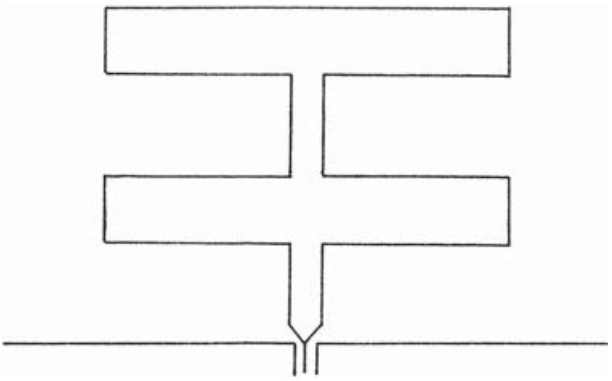

Figure 1.26 Wire frame monopole. Courtesy of Wong, J.L. and King, H.E. Height-Reduced Meander Zigzag Monopoles with Broad-Band Characteristics. *Trans IEEE* Vol. AP-34, May 1986, pp. 716–717.

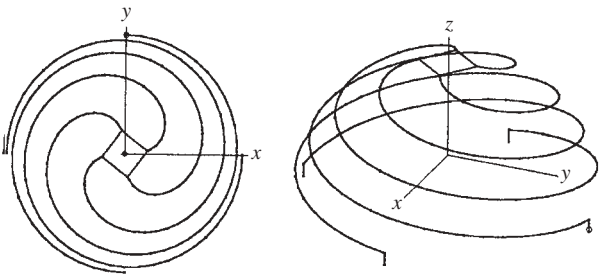

Figure 1.27 One-turn, four-arm spiral. Courtesy of Best, S.R. The Radiation Properties of Electrically Small Folded Spherical Helix Antennas. *Trans IEEE* Vol. AP-52, April 2004b, pp. 953–960.

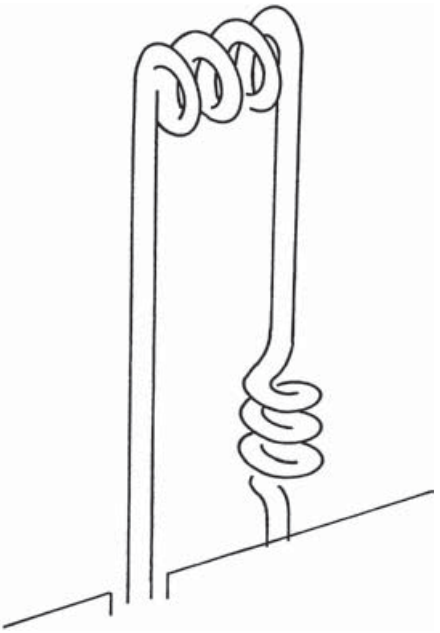

Figure 1.28 Loaded folded monopole. Courtesy of Harrison, C.W. and King, R.W.P. Folded Dipoles and Loops. *Trans IRE* Vol. AP-9, March 1961, pp. 171–187.

overcoming this shorting out effect, and making the folded dipole usable at lower frequencies, is to use a series impedance at the ends where the two arms join, in the center of the folded arm, or both. Figure 1.28 shows the general configuration. A short folded dipole has radiating currents in a triangular distribution, like a dipole, with maximum radiating current at the feed (and shorted) end and zero current at the other end where the arms join. Insertion of an inductor reduces the transmission line currents but probably has no effect on the radiating currents if the dipole is short. Analyses have been made of the end-loaded folded dipole (Harrison and King, 1961) and of the base-loaded folded monopole (Leonhard et al., 1955), but calculations of the radiation resistance as a function of loading are not available. Basically the short loaded folded dipole will have a more useful input reactance—not very large as that of the same length dipole nor very small as that of the unloaded folded

dipole. Radiation properties are probably not much affected. The ability to produce broadband behavior through judicious choice of loading is as yet a very poorly understood situation.

To sum up, inductively loading a short dipole gives the best trade of performance versus space. Top hat loading is effective, if space allows (Francavilla et al., 1999). Loops are inefficient, but ferrite-cored loops are good for receive. Fat dipoles such as bowtie dipoles offer good bandwidth. If space allows, the Goubau antenna offers the best performance for a given small volume; see Section 1.2.1. There are no ultrawideband electrically small antennas.

1.3.2 Patch and Partial Sleeve

1.3.2.1 Titanate or Metaferrite Substrate

The conventional patch antenna is not electrically small, but it may be so when constructed with a high-ε substrate. Ceramic substrates embodying barium, strontium, calcium, etc. titanates may have a large range of ε, perhaps to $\varepsilon > 100$ (Middleton, 2002). When used as a substrate for a patch, the resonant width is decreased by $\sqrt{\varepsilon}$. Such a patch can be electrically very small, and along with the reduced size goes a narrower bandwidth and tighter tolerances. Bandwidth, for VSWR $\preceq 2$, is approximately $4t/\sqrt{2\varepsilon_r}\,\lambda_0$, where t is the substrate thickness. A thorough treatment of patch antennas is given by Balanis (2005). A closely related antenna, the dielectric resonator antenna, is discussed in Section 1.3.4.

What if a low-loss material with both μ and ε was used as a patch substrate; how would the characteristics change? A first answer was given by Hansen and Burke (2000), where a square patch with μ, ε substrate was analyzed via a transmission line model. This zero-order analysis assumed that the patch length was resonant, $a/\lambda = 1/\sqrt{2\mu\varepsilon}$, and the edge susceptance was omitted. The edge (radiation) conductance is given by (Wheeler, 1965):

$$G = \frac{1}{120\pi^2}\int_0^{\pi} \frac{\sin^2\left[\dfrac{\pi}{2\sqrt{\mu\varepsilon}}\cos\theta\right]\sin^3\theta\, d\theta}{\cos^2\theta} \tag{1.26}$$

In many works, it is stated that an approximation valid for small a/λ (large με) is:

$$G \simeq \frac{a^2}{90\lambda^2} = \frac{1}{360\mu\varepsilon} \tag{1.27}$$

A similar approximation stated to be valid for large a/λ (small με) is:

$$G \simeq \frac{a}{120\lambda^2} = \frac{1}{240\sqrt{\mu\varepsilon}} \tag{1.28}$$

It will be shown that Equation 1.28 for large με is good, whereas Equation 1.27 for small με is poor. Figure 1.29 shows the exact integral, along with the two approximations, for με = 1 to 10; a 128-point Gaussian integrator was used. In this figure, half of the conductance is used as the patch has two radiating slots. Note that the

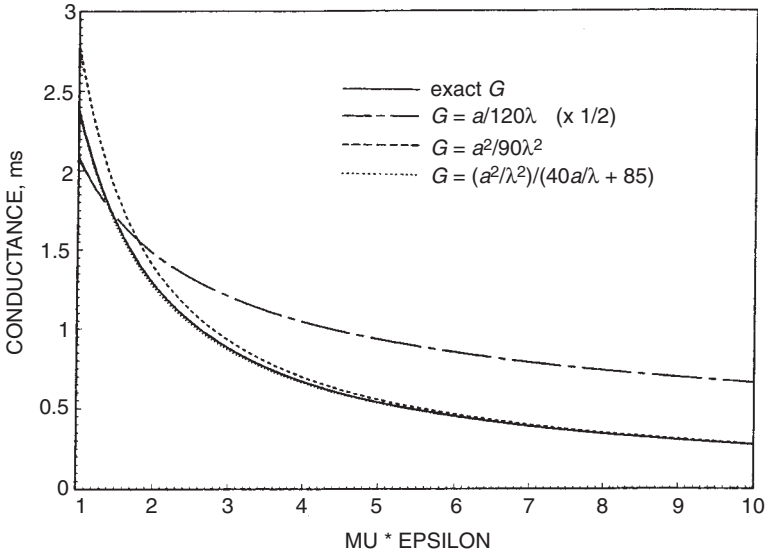

Figure 1.29 Exact and approximate square patch radiation conductance. Courtesy of Hansen, R.C. and Burke, M. Antennas with Magneto-Dielectrics. *Microwave Optical Tech Lett* Vol. 26, 20 July 2000, pp. 75–78.

large με approximation is useful for με > 3. The small approximation is good for με < 1. Even with an added factor of ½ as shown in Figure 1.29, the approximation is poor for με = 1. A good fit is given for the entire range of με = 1 to 10 by:

$$G \simeq \frac{1}{40\sqrt{\mu\varepsilon}+170\mu\varepsilon} \tag{1.29}$$

This conductance will be used with the transmission-line analysis. From Wheeler (1965), the characteristic admittance of a wide microstrip line is:

$$Y_0 = \frac{a\sqrt{\varepsilon}}{\eta t\sqrt{\mu}} = \frac{\lambda}{2\eta\mu t} \tag{1.30}$$

where $\eta = 120\pi$ and t is the dielectric thickness. It should be noted that, for the resonant patch, the characteristic impedance involves only μ. The radiation quality factor is $Q = \pi Y_o/4G$ (Wheeler, 1947), and the VSWR = 2 bandwidth BW is $1/\sqrt{2}Q$ (with matched load). The result is that the zero-order bandwidth is:

$$\mathrm{BW} = \frac{96\sqrt{\mu/\varepsilon}\, t/\lambda_0}{\sqrt{2}[4+17\sqrt{\mu\varepsilon}]} \tag{1.31}$$

Unfortunately, this result is not simply a function of μ/ε. The bandwidth result (Balanis, 2005; Hansen, 1998):

$$\mathrm{BW} \simeq \frac{4\sqrt{\mu}\, t/\lambda_0}{\sqrt{2\varepsilon}} \tag{1.32}$$

is seen to be fair for $\varepsilon = 1$ to 2 and poor for $\varepsilon > 2$. The other approximate result:

$$\mathrm{BW} \simeq \frac{16t/\lambda_0}{3\sqrt{2\varepsilon}} \tag{1.33}$$

is fair for $\varepsilon > 4$ and poor for $\varepsilon < 4$. However, Equation 1.31 is accurate for the entire range of $\mu\varepsilon$.

The resonant patch length is reduced by $\sqrt{\mu\varepsilon}$. Two cases are of interest.

Case 1: $\mu = \varepsilon$. If μ is put equal to ε and the small $\mu\varepsilon$ result were applicable, then this shortened patch would enjoy the same bandwidth as the same-sized air patch. A more accurate evaluation is obtained by setting $\mu = \varepsilon$ in Equation 1.31; the result is:

$$\mathrm{BW} \simeq \frac{96t/\lambda_0}{\sqrt{2}\,[4+17\varepsilon]} \tag{1.34}$$

A comparison of values from Equation 1.31 with Equation 1.34 where $\varepsilon = 10$ and $\mu = 1$ shows that only a small improvement in bandwidth results. Specifically, for $\mu = \varepsilon = 10$, the improvement in bandwidth is only 5%. However, the patch length is shortened by $1/\mu$.

Case 2: $\varepsilon = 1$, $\mu > 1$. A substrate with $\varepsilon = 1$ and $\mu > 1$ would offer a modest increase in bandwidth over the $\varepsilon = 1 = \mu$ patch. For $\mu \gg 1$, the increase in bandwidth would be 21/17 = 1.235. Compared to a typical patch with $\varepsilon = 3$ and $\mu = 1$, the improvement in bandwidth is 330%.

Metaferrites is the term given to a lamination of layers, where each thin layer has a pattern of short segments of a mixture of high-μ materials. The objective is to realize a large μ and a modest ε, with low loss (Walser, 2001).

1.3.2.2 Partial Sleeve

The partial sleeve antenna, which is a two-dimensional transmission line antenna, was developed by Nash and others at the University of Illinois Antenna Lab in the early 1950s, but data were published only in reports to USAF ASD. The antenna consists of a square or rectangular plate located adjacent to a ground plane and shorted to the ground plane. A feed is connected at a point that gives a convenient impedance level, as shown in Figure 1.30. A capacitor may be used to tune the end of the sleeve. The ground plane and the sleeve may be curved in either dimension. The term sleeve arose as such an antenna may be used on a curved aircraft surface. Typical sizes are separation 1/10 the length, and length from 0.01λ to 0.1λ. The radiating portion of the antenna consists of a U-shaped slot, which for small lengths will have a nearly triangular distribution of current. Radiation from the two side slots will mostly cancel out, leaving the end slot as the primary source. However, the side slots act as a form of loading to increase the current moment of the primary radiator. Assuming a square plate or sleeve, the current moment of the end slot is $5L/6$, which is 1.67 times better than that of a short dipole of length L. This is the same improvement factor (2.78 in radiation resistance) produced by the dipole with optimum inductive loading in the dipole. Both the transmission line antenna and

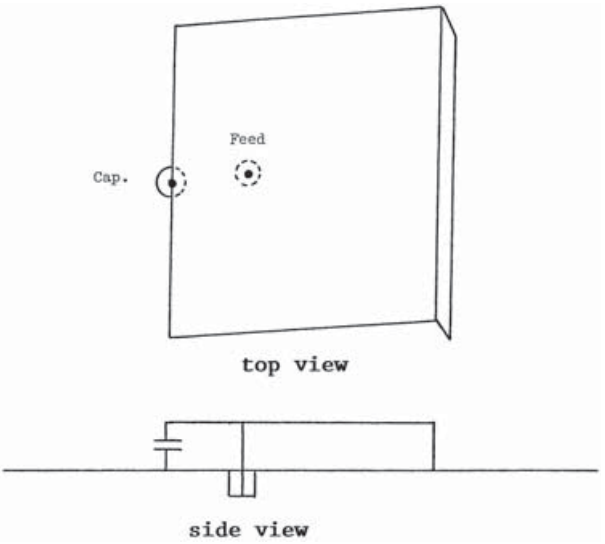

Figure 1.30 Partial sleeve antenna

the partial sleeve are useful when λ/4 of length is available but are not attractive when short because of the low impedance.

The important fact about the partial sleeve is that it led to the invention of the ubiquitous patch antenna by Deschamps and Sichak (1953). It is also the PIFA (Planar Inverted F Antenna): a flat plate shorted at one end and fed by a coax near the open end. The PIFA is widely used for portable communications devices. The plate may be square or narrow, and the shorting plate may be the full width or part of the width. The PIFA is not quite an ESA, so its extensive coverage is not included here. Taga (1992) gives data on resonant frequency. Pinhas and Shtrikman (1988) give data for resonant PIFA bandwidth versus plate-screen spacing for several widths. Both theory and measurement data are given. Taga and Tsunekawa (1987) also provide data on bandwidth versus plate-screen spacing.

1.3.3 Loop Basic Characteristics

It is usually desirable for small loops to have a pattern that is omnidirectional in the plane of the loop. This requires the loop diameter D to be less than roughly 0.1λ (Balanis, 2005). When the loop has multiple turns, the winding length must be $\leq 0.1\lambda$. The equivalent circuit is simply the inductive reactance X in series with the radiation resistance R_r and the loss resistance R_l. For a loop with N turns, the radiation resistance is proportional to N^2 and to the square of effective permeability.

$$R_r = \frac{5\pi^2 N^2 k^4 D^4 \mu_e^2}{4} \tag{1.35}$$

Magnetic core effects are discussed below.

1.3.3.1 Air Core Loop

The single turn loop will be treated first. Now a single conductor, single turn, will act as a very thin tube of conductor because of skin effect. Rosa and Grover (1916) give the inductance of an infinitely thin tube bent into a circle, from which the reactance in ohms is:

$$X = 60\pi kD\left[\left(1+\frac{a^2}{D^2}\right)\ell n\frac{4D}{a}-2\right] \tag{1.36}$$

Here D is the mean diameter of the loop and a is the tube radius. Most practical single turn loops will have $D \gg a$, so the reactance is well approximated by:

$$X = 60\pi kD\left(\ell n\frac{4D}{a}-2\right) \tag{1.37}$$

If the loop diameter is much larger than the wire diameter, the proximity effect, which tends to concentrate the current on the inside of the loop, can be neglected (Smith, 1972). Then:

$$R_\ell = \frac{D}{2a\sigma\delta} = \frac{R_s D}{2a} \tag{1.38}$$

Here R_s is the surface resistivity, in *ohms*/□. Figure 1.31 gives R_sD/a versus D/a and frequency. The efficiency formula is the same as for dipoles:

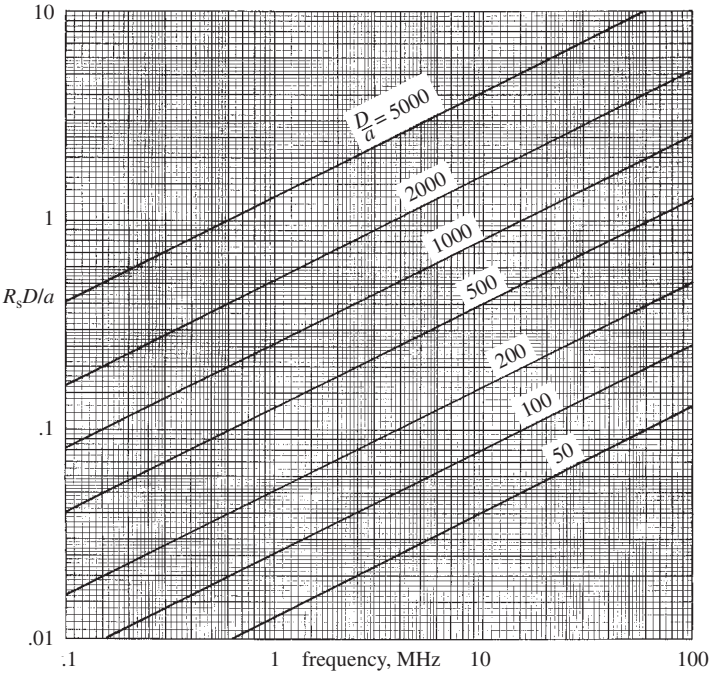

Figure 1.31 Loss factor for copper

$$\eta = \frac{R_r}{R_r + R_\ell} \tag{1.39}$$

Immediately, the efficiency is found to be:

$$\eta = \frac{5\pi^2 k^4 D^4}{5\pi^2 k^4 D^4 + 2R_s D/a} \tag{1.40}$$

Efficiency is shown in Figure 1.32 for $D/a = 50$. The Q is given by:

$$Q = \frac{240\pi kD(\ell n 4D/a - 2)}{5\pi^2 k^4 D^4 + 2R_s D/a} \tag{1.41}$$

Because small loops have high Q, half-power bandwidth becomes:

$$\text{BW} \simeq 1/Q \tag{1.42}$$

Half-power bandwidth is given in Figure 1.33. It is a minimum for:

$$\frac{D}{\lambda} = \frac{1}{2\pi}\left[\frac{2RsD/a}{15\pi^2}\right]^{\frac{1}{4}} \tag{1.43}$$

The bandwidth × efficiency merit factor is:

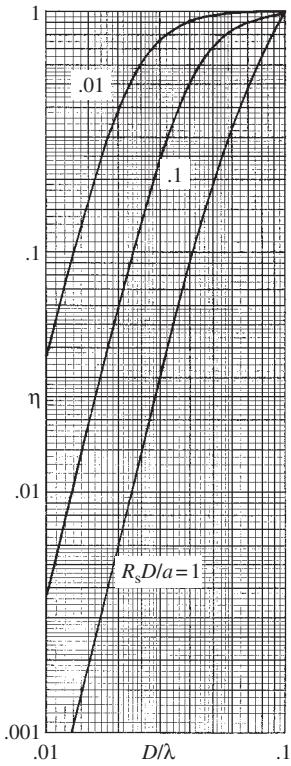

Figure 1.32 Loop efficiency, $D/a = 50$

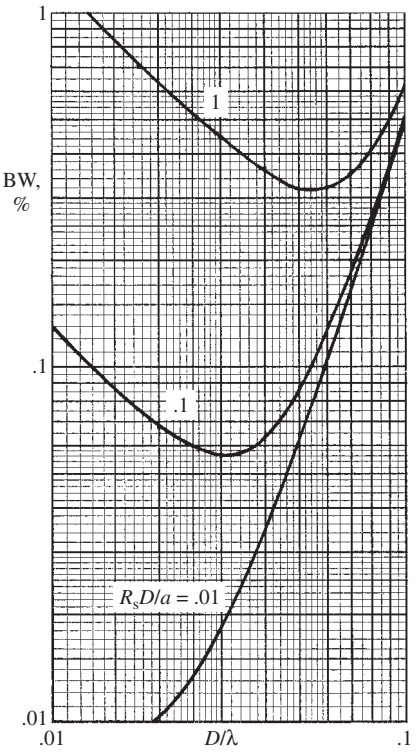

Figure 1.33 Loop bandwidth, $D/a = 50$

$$\mathrm{BW}\cdot\eta = \frac{R_r}{X} = \frac{\pi k^3 D^3}{48(\ell n 4D/a - 2)} \tag{1.44}$$

For the largest feasible small loop, $D/\lambda = 0.1$, and for $D/a = 50$, the bandwidth × efficiency product is:

$$\mathrm{BW}\cdot\eta = 0.004922 \tag{1.45}$$

Figure 1.34 shows R_r, X, and $\mathrm{BW}\cdot\eta$ for $D/a = 50$. The range of D/λ is 0.01 to 0.1. As expected, the radiation resistance and bandwidth × efficiency product are small. Because the loop resistivity enters into both, data are shown for $R_sD/a = 1$, 0.1, and 0.01. All of these graphs are for $D/a = 50$; the R_s values are 0.02, 0.002, and 0.0002. For copper, these values cover the range of 0.6 MHz to 6 GHz.

The air core loop may be squished into a narrow rectangle to allow convenient mounting on a platform. It must be remembered that loop performance is proportional to area.

1.3.3.2 Multiturn Air Loop

A typical multiturn air core loop is either circular or square in shape, with a winding of rectangular cross section, that is, many layers with each layer having

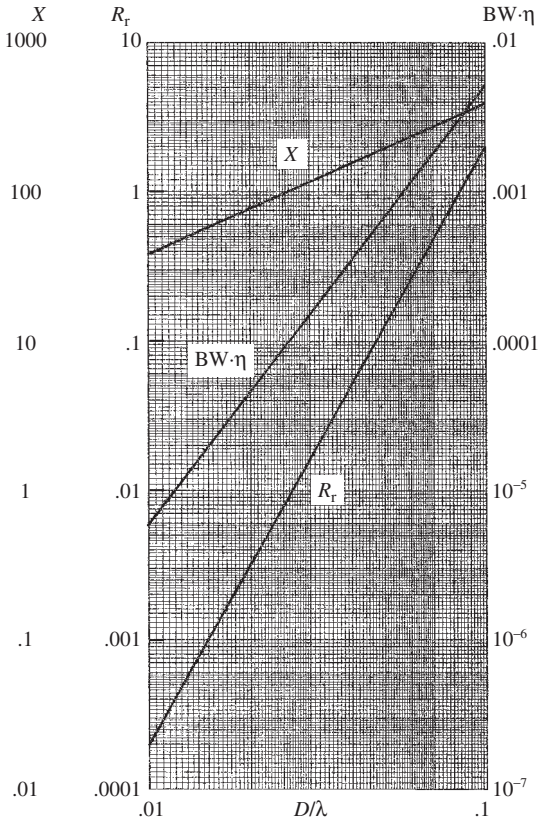

Figure 1.34 Loop parameters, $D/a = 50$

many turns. Such a loop is a short multilayer solenoid, with reactance given approximately by:

$$X = 60\pi N^2 kD\left(\ell n\frac{9D}{b} - 1\right) \tag{1.46}$$

Solenoid diameter and axial length are D and b. This result, derived by Maxwell (Rosa and Grover, 1916), is adequate for comparative purposes. Such coils are usually designed for optimum Q; the only parameters that significantly affect radiation resistance are diameter and number of turns. Various formulas are available for optimum design of multilayer solenoids. That of Butterworth (Terman, 1943) requires b, D, and winding radial thickness t to obey:

$$3t + 2b = D \tag{1.47}$$

Examination of the loss formulas for short multilayer solenoids shows that the loss of the optimum designs varies slowly as the ratio t/b changes around unity. Because a coil with square winding cross section is physically attractive, the loss results will be quoted for $t = b$. Then for the optimum, $t/D = 0.2$ and the Butterworth parameter

$Kb/D = 2.8$. Assuming the wires are spaced with one wire diameter air gap, the ratio of AC and DC resistance, using Butterworth's H and G functions, is:

$$\frac{R_{ac}}{R_{dc}} = H + 0.49GN \simeq H + \frac{GN}{2} \tag{1.48}$$

If now the wire diameter is large in skin depths, which may not be a valid assumption but yields an upper bound, H and G may be approximated by $H \simeq a/2\delta \simeq 2G$, giving:

$$\frac{R_{ac}}{R_{dc}} = \frac{a}{2\delta}\left(1 + \frac{N}{4}\right) \tag{1.49}$$

The lower limit is, of course, $R_{ac} = R_{dc}$. $R_{dc} = ND/a^2\sigma$, which gives the coil resistance:

$$R_\ell = \frac{NR_s D}{2a}\left(1 + \frac{N}{4}\right) \tag{1.50}$$

Although this value was derived under a number of assumptions, it is weak only in the assumption of wire diameter large in skin depths. The corresponding reactance is given by:

$$X = 168\pi N^2 kD \tag{1.51}$$

With these reactance and resistance results, the efficiency and BW × efficiency merit factors may be obtained. For the efficiency:

$$\eta = \frac{5\pi^2 Nk^4 D^4}{5\pi^2 Nk^4 D^4 + 2R_s \dfrac{D}{a}\left(1 + \dfrac{N}{4}\right)} \tag{1.52}$$

The Q is found to be:

$$Q = \frac{672\pi NkD}{5\pi^2 Nk^4 D^4 + 2R_s \dfrac{D}{a}\left(1 + \dfrac{N}{4}\right)} \tag{1.53}$$

The bandwidth-efficiency merit factor is independent of N, and is:

$$\mathrm{BW}\cdot\eta = \frac{5\pi k^3 D^3}{672} \tag{1.54}$$

This result is similar to that for a single turn loop with $D/a = 50$.

1.3.3.3 Magnetic Core Loop

The most common loop with a magnetic core is the "loop stick," a single layer winding on a cylindrical ferrite rod. Equation 1.35 gives radiation resistance in terms of effective permeability μ_e and turns N. The effective permeability of a ferrite or other magnetic core depends on the length-to-diameter ratio of the core, with large ratios required to realize μ_e close to the intrinsic permeability of the material. Therefore, ferrite core loops will usually be long but not large in diameter.

Figure 1.35 gives effective permeability, normalized to permeability, as a function of core length-to-diameter ratio (Wait, 1953a). Effective permeability, normalized by the shape factor $L/2a$, is given in Figure 1.36. Whether the coil is distributed over most of the length of the core or lumped at the center is not critical and affects mainly distributed capacity and the flux enhancement of the end turns. The core need not be solid, as thin ferrite walls will give a significant increase of flux density.

For a long single-layer solenoid of many turns and with ferrite core, the reactance is given by:

$$X_a = \frac{30\pi^2 N^2 k L \kappa \mu_e}{\left(\frac{L}{2a}\right)^2} \tag{1.55}$$

where L is now the length of the core and a the radius of the winding rather than the radius of the wire; κ is Nagaoka's constant (Langford-Smith, 1953), which for large L/a is approximately $1 - \frac{0.8}{(L/a)}$, and thus for $L/a \gg 1$ is nearly unity. There exist formulas for calculating loss of long air core solenoids, but formulas for computing loss of ferrite core solenoids are very poor. Because the derivation of formulas of sufficient generality to be of use here is too arduous a task, a simpler but adequate scheme will be used. If low-loss ferrites are utilized, and if the coil dimensions are in the neighborhood of optimum, the coil Q will vary slowly with dimensions, number of turns, etc. That is, the Q maximum is very broad. Table 1.4 gives para-

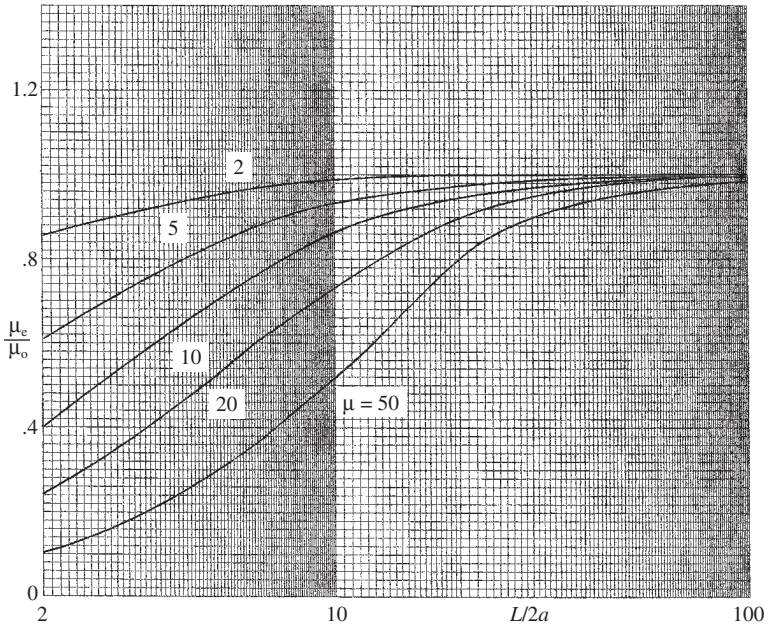

Figure 1.35 Effective permeability of solid core

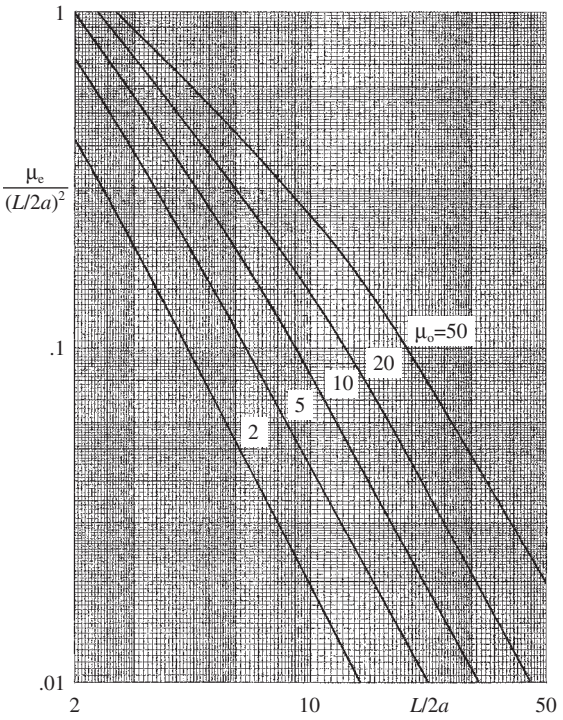

Figure 1.36 Shape factor for cylindrical core

Table 1.4 TDK ferrite cores

	K5	K6a	K8
upper frequency, MHz	8	50	200
μ	290	25	16
$\tan\delta$	0.008	0.004	0.004
curie temp, °C	>280	>450	>500

meters for TDK materials, and it may be observed that the maximum Q is roughly independent of frequency from 50 MHz to 200 MHz. Of course at higher frequencies the ferrite permeability is lower so that copper and dielectric losses tend to play a larger role.

Using the previously defined symbols, the principal parameters, starting with the radiation resistance, are:

$$R_r = \frac{5\pi^2 N^2 k^4 L^4 \mu_e^2}{4\left(\frac{L}{2a}\right)^4} \tag{1.56}$$

$$X = \frac{30\pi^2 N^2 kL\mu_e}{\left(\frac{L}{2a}\right)^2} \tag{1.57}$$

The core length is L; the core radius is a and the coil radius is also a, as the coil wire is usually of small diameter. The factor $L/2a$ is separated as it controls μ_e/μ. Loss resistance is:

$$R_\ell = \frac{30\pi^2 N^2 kL\mu_{\text{eff}} \tan\delta}{\left(\frac{L}{2a}\right)^2} \tag{1.58}$$

Efficiency and bandwidth × efficiency merit factors are, again, neglecting the effect of distributed capacity on bandwidth:

$$\eta = \frac{k^3 L^3 \dfrac{\mu_{\text{eff}}}{(L/2a)^2}}{k^3 L^3 \dfrac{\mu_{\text{eff}}}{(L/2a)^2} + 24\tan\delta} \tag{1.59}$$

$$\text{BW}\cdot\eta = \frac{k^3 L^3 \mu_{\text{eff}}}{24(L/2a)^2} \tag{1.60}$$

In all these formulas, the shape of the coil and the core effect are contained in the factor $\mu_e/(L/2a)^2$. In the curves of Figure 1.36, this shape factor is plotted as a function of length-to-diameter ratio of the core. It can be seen that most cores will have shape factors between 0.1 and 1, with a few perhaps as low as 0.01. Accordingly, calculations of loop antenna parameters were made with three values of shape factor: 1, 0.1, and 0.01. In Figure 1.37 are plotted R/N^2, X/N^2, and R_r/N^2 for a shape factor of 1. Note that the number of turns is included by multiplying all these values by N^2. The value of $\tan\delta$ for R_l is 0.004. Also the vertical scales for R_l and R_r are different, so the crossing of these two in Figure 1.37 does not represent $\eta = 50\%$. Efficiency and bandwidth × efficiency merit factors are given in Figure 1.38. In the figures, values of $\mu_e/(L/2a)^2$ are 1 (solid line), 0.1 (dashed line), and 0.01 (dot-dash line).

The effective permeability data in Figure 1.35 were obtained by Wait (1953a). He assumed that the core was a prolate spheroid, with coil around the center of the spheroid. For thin rod cores this is a good approximation. Using the spheroidal functions the boundary conditions are matched, resulting in:

$$\frac{\mu_e}{\mu} = \frac{1}{1 + (\mu - 1)(\eta_0^2 - 1)Q_1(\eta_0)} \tag{1.61}$$

Note that the spheroidal coordinates are (η, δ). Q_1 is a spheroidal wave function:

$$Q_1 = \frac{\eta}{2}\ell n\frac{\eta+1}{\eta-1} - 1 \tag{1.62}$$

The coordinate η_0 is:

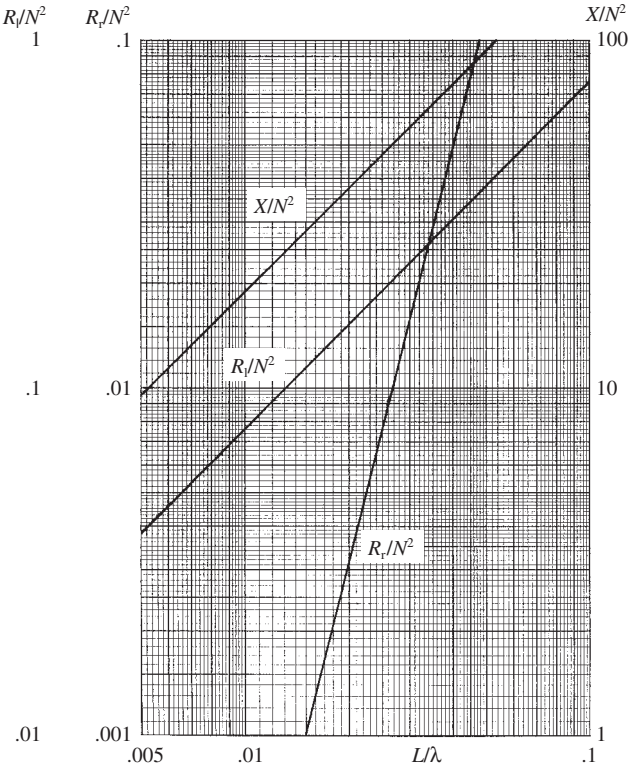

Figure 1.37 Magnetic core loop parameters; $L/2a = 1$

$$\eta_0 = 1\Big/\sqrt{1-4a^2/L^2} \tag{1.63}$$

where L is core length and a is core radius. These equations result in Figure 1.35, where μ_e/μ is plotted versus $L/2a$. Higher-permeability cores need to be longer to reach the intrinsic permeability. It was discovered that most of the flux density is near the surface of the core, so that hollow cores could be used. This problem was also solved by Wait (1953b), using prolate spheroidal geometry. In Figure 1.39, core external and internal radii are a and a'. The results are:

$$\frac{\mu_e}{\mu} = 1 + BQ_1' \tag{1.64}$$

where:

$$B = \frac{B_1[Q_1(\eta_0) - \mu\eta_0 Q'(\eta_0)] - \eta_0(\mu - 1)}{B_1(\mu - 1)\,Q_1(\eta_0)\,Q_1'(\eta_0) + \mu Q_1(\eta_0) - \eta_0 Q_1'(\eta_0)} \tag{1.65}$$

$$B_1 = \frac{(\mu - 1)\eta_1}{Q_1(\eta_1) - \mu\eta_1 Q_1'(\eta_1)} \tag{1.66}$$

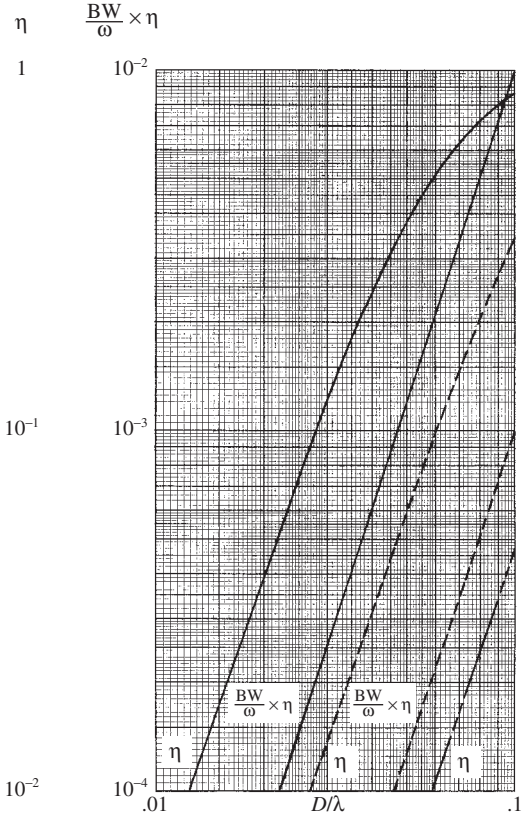

Figure 1.38 Ferrite loop parameters

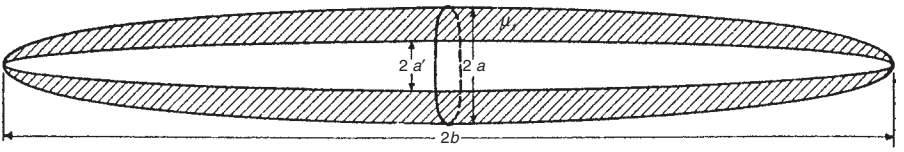

Figure 1.39 Loop with hollow prolate spheroidal core

$$Q_1' = \frac{1}{2}\ell n\frac{\eta+1}{\eta-1} - \frac{\eta}{\eta^2-1} \tag{1.67}$$

Figure 1.40 gives μ_e versus $L/2a$ for $\mu = 50$, and Figure 1.41 is for $\mu = 200$. These design data have proved satisfactory for loopstick antenna design. In summary, a ferrite loop antenna should first use as high a permeability ferrite as possible, and second, the length (of core) should be as large as feasible. When length L is fixed, then the core should be made stubby, that is, with low $L/2a$ as the improvement in coil area increases faster than effective permeability decreases.

It should also be noted that both efficiency and radiation Q are independent of number of turns. Thus the low efficiencies of Figure 1.38 are inescapable and are a

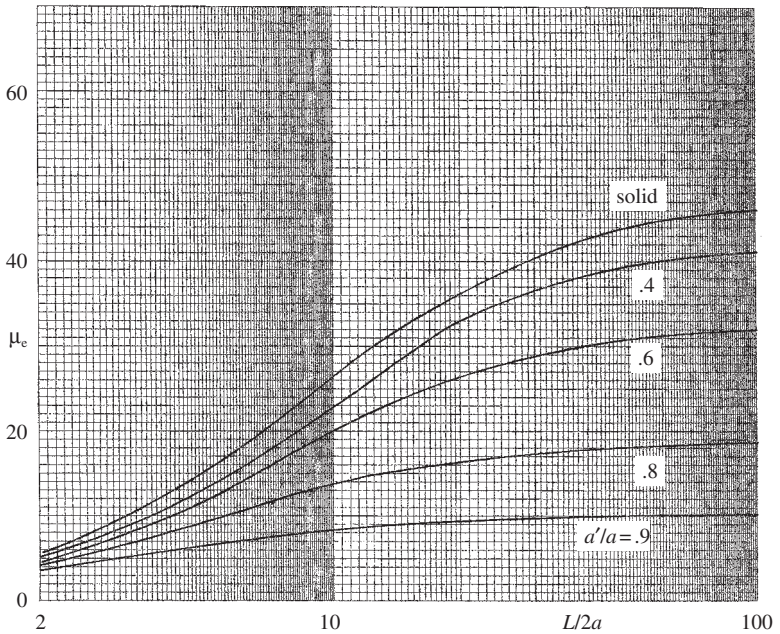

Figure 1.40 Effective permeability of hollow core, $\mu_0 = 50$

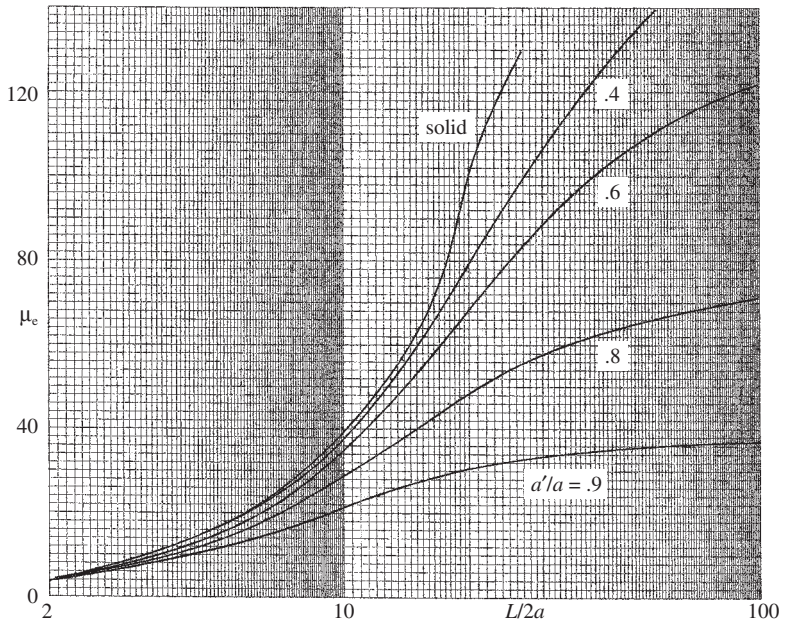

Figure 1.41 Effective permeability of hollow core, $\mu_0 = 200$

result of the intrinsically poor performance of a loop small in wavelengths. A short folded dipole has similar low efficiency. Parameters for $L > 0.1\lambda$ are not shown, as the loop is resonant just above $L = 0.1\lambda$.

1.3.3.4 Receiving Loops

The effective length for a single-turn air core receiving loop is:

$$\ell_{\text{eff}} = \frac{\pi k D^2}{4} \tag{1.68}$$

and when this is normalized to open-circuit voltage per unit field strength in volts per wavelength,

$$\frac{\ell_{\text{eff}}}{\lambda} = \frac{V_{\text{oc}}}{\lambda E} = \frac{k^2 D^2}{8} \tag{1.69}$$

Now for low distributed capacitance, as before, the voltage at the preamp is simply the open-circuit voltage multiplied by the circuit Q:

$$\frac{V}{\lambda E} = \frac{k\ell_{\text{eff}} X}{2\pi(R_\ell + R_{\text{r}})} \tag{1.70}$$

where the tuning capacitor loss and input circuit loss are assumed to be small with respect to R_{l} and R_{r}. With current technology, this assumption is quite valid. Using values of X, R_{l}, and R_{r} previously derived, the output voltage for a single-turn loop is:

$$\frac{V}{\lambda E} = \frac{30\pi k^3 D^3 \left(\ell n \dfrac{4D}{a} - 2\right)}{5\pi^2 k^4 D^4 + 2R_{\text{s}} \dfrac{D}{a}} \tag{1.71}$$

This merit factor, normalized output voltage, is plotted in Figure 1.42 for three values of the loss factor $R_{\text{s}}D/a$ as before. Effective length depends only on D/λ as shown. The output voltage peaks for:

$$\frac{D}{\lambda} = \frac{1}{2\pi}\left[\frac{6R_{\text{s}}D/a}{5\pi^2}\right]^{\frac{1}{4}} \tag{1.72}$$

Just as the lower loss factor gave higher efficiency, the lower loss factor here gives a higher output voltage, with a higher peak.

For a magnetic core loop the effective length is now:

$$\ell_{\text{eff}} = \frac{\pi}{4} N k D^2 \mu_{\text{e}} \tag{1.73}$$

and this normalized as before, using the shape factor $\mu_{\text{e}}/(L/2a)^2$, is:

$$\frac{\ell_{\text{eff}}}{\lambda} = \frac{V_{\text{oc}}}{\lambda E} = \frac{N k^2 L^2 \mu_{\text{e}}}{8(L/2a)^2} \tag{1.74}$$

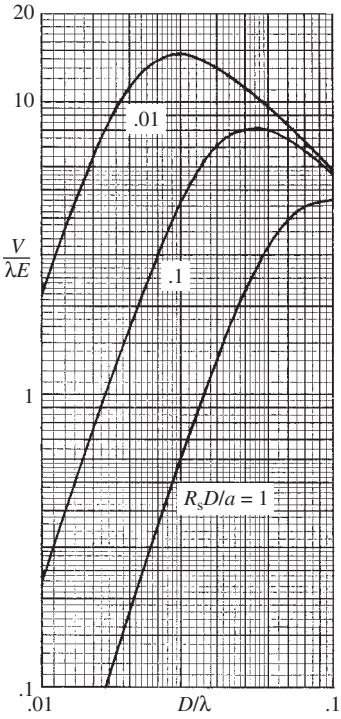

Figure 1.42 Receiving loop merit factor; $D/a = 50$

The normalized output voltage is simply:

$$\frac{V}{\lambda E} = \frac{\ell_e Q}{\lambda} = \frac{Nk^2 L^2 \mu_e X}{8(L/2a)^2 (R_r + R_\ell)} \tag{1.75}$$

Using previously developed results for R_l, X, R_r, the output voltage merit factor becomes:

$$\frac{V}{\lambda E} = \frac{3Nk^2 L^2 \mu_e}{\left(\frac{L}{2a}\right)^2 \left[\frac{k^3 L^3 \mu_e}{\left(\frac{L}{2a}\right)^2} + 24 \tan\delta\right]} \tag{1.76}$$

This merit factor is shown in Figure 1.43 for three values of the shape factor $\mu_e/(L/2a)^2$, as before. The value of $\tan\delta$ used is 0.01. The output voltage merit factor is larger for larger D/λ.

Noise reception must be discussed, as it is sometimes said that loop antennas pick up less noise. At sufficiently low frequencies (VLF) and close to electrical storms, the antenna may be in the near-field of the source such that the wave impedance is higher than 120π. In these cases, the dipole/monopole will pick up more noise than the loop. But at any usable communications frequency this does not

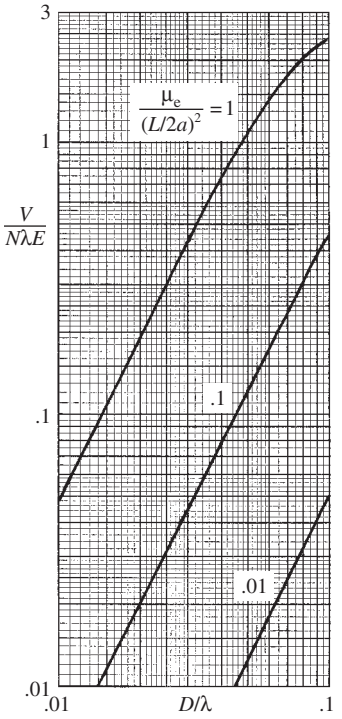

Figure 1.43 Receiving loop merit factor, tan δ = 0.01

happen; loops treat signal and noise equally. Precipitation static also may affect a dipole more than a loop. In many cases, the noise of a loop is low because its signal is also low.

1.3.3.5 Vector Sensor

A vector sensor is six antennas, three of which are electric dipoles (dipole antennas) and the other three magnetic dipoles (loop antennas). Typically the loops and dipoles are all orthogonal and are cocentered. Figure 1.44 is a sketch of such a vector sensor. This configuration has been called the CART antenna, after Compact Array Radiolocation Technology (Hatke, 1993). Here, the capabilities and limitations of vector sensors, using electrically small antennas, are investigated. Emphasis is on the practical problems of impedance matching, bandwidth, and gain degradation.

For angle-of-arrival (AOA) applications, the vector sensor should be isotropic, that is, be effective for all angles of incidence. Single-turn loops should be no larger than 0.1λ in diameter, as larger loops have patterns that are not omnidirectional and have impedance swings.

Many papers on AOA estimation using vector sensors state that loops respond to magnetic field whereas dipoles respond to electric field, thereby implying that this is why performance is better than that obtained by tripoles, for example. This is a misconception: Loops are magnetic field sensors and dipoles are electric field

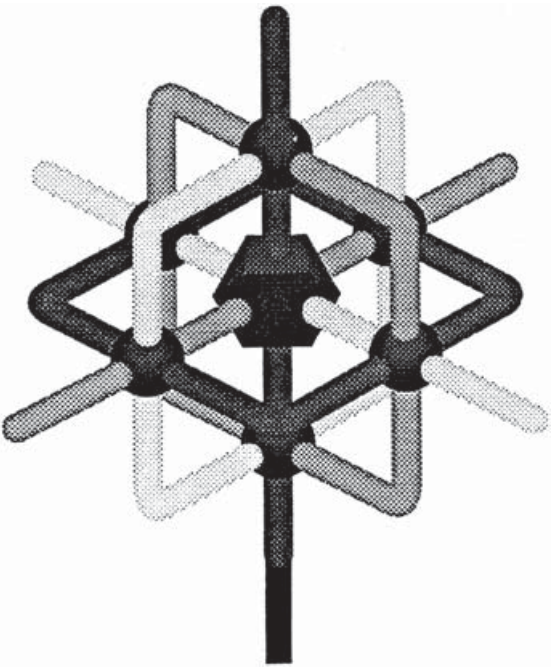

Figure 1.44 Notional vector sensor. Courtesy of Hatke, G.F. Conditions for Unambiguous Source Location Using Polarization Diverse Arrays. *IEEE 27th Asilomar Conf* 1993, pp. 1365–1369.

sensors only in the near-field region, where distance between source and antenna is less than a wavelength. For all practical applications vector sensor sources are in the far-field; both loops and dipoles couple to the incident field, which has both E and H, with $E/H = 120\pi$.

The salient advantage of a vector sensor is that it allows Poynting vector (AOA) to be determined. This is possible because the response of a dipole depends simply on the angle between the dipole axis and AOA, and the response of a small loop depends simply on the angle between the loop axis and AOA. By taking ratios of the three dipole outputs the scale factors are removed, leaving angular functions of AOA. Similarly, ratios of the three loop outputs yield additional angular functions; these together allow AOA to be estimated. Collectively the six antennas are isotropic, so that polarization nulls are effectively removed. Now some ambiguity suppression and signal discrimination is feasible. As each antenna has its own preamplifier, the gains can be adjusted to provide equal sensitivities, taking into account the dipole and loop efficiencies. The behavior of a coplanar loop-dipole pair has been analyzed by Overfelt (1998). For the loop and dipole to act independently, the relative phasing must be 90°.

It is crucial that the loop arms for a coplanar loop and dipole not contact the dipole arms. This means that the loop arms must connect across the dipole arms either by an insulated feed-through or an insulated bypass outside the dipole conductor. Figure 1.45 sketches a possible configuration in which the dipole arms are tubes,

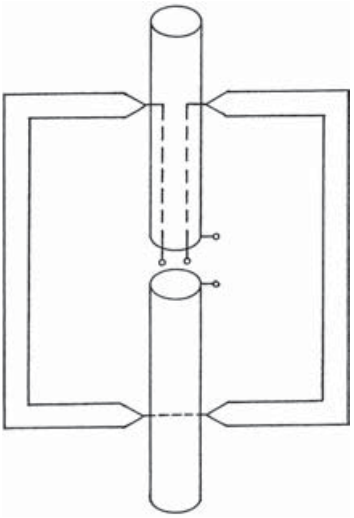

Figure 1.45 Coplanar loop and dipole

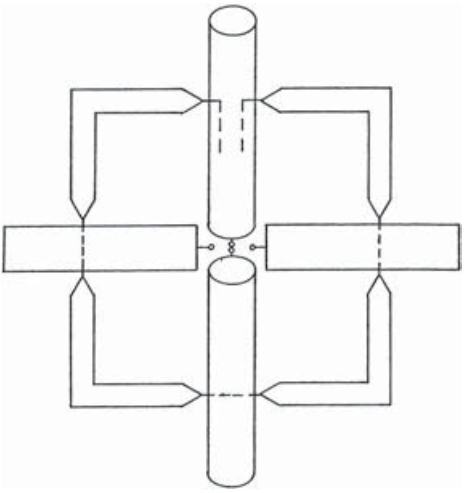

Figure 1.46 Coplanar loop and two dipoles

with a twin line feed for the loop contained in one of the tubes. The dipole plane and the loop plane could be offset to avoid intersections, but although this is easy for one loop plus one dipole, it does not alleviate the problem for three loops and three dipoles. An easy fabrication for one loop plus one dipole would be to print a loop and feed line on one side of a board and print a dipole on the other side. But three boards cannot be "egg-crated" together without cutting some conductors, thereby necessitating pigtail or wire bond connections.

Figure 1.46 shows a loop and two dipoles, all coplanar. Each dipole arm would need to allow two loop sides to connect through the arm; maintenance of symmetry will be a challenge. Each loop will connect through four dipole arms, as sketched

in Figure 1.46. Also, each loop feed point will need a shunt tuning capacitor, so that the twin line can be effectively utilized as a matching transformer (details given below). Each dipole arm connect through will need to accommodate two independent loops but for three arms a tuning capacitor as well. This imposes fabrication and assembly difficulties.

Segmented loops, which allow larger diameters, require multiple feed lines; a two-segment configuration is sketched in Figure 1.47. Both dipole arms contain twin line feeds that are paralleled at the final feed point. One pair is reversed, so that the current around the loop is in the same direction.

A vector sensor consists of three loops and three dipoles. Because any single antenna has at least one null direction for a given polarization, use of orthogonal antennas removes nulls. Because all signals will be in the far-field of the antenna, there will be some redundant outputs from a vector sensor. The plane wave response will involve both E and H fields. The principal difference among redundant signals is due to the patterns. For example, the dominant electric field pattern of a dipole, normalized to unity, is:

$$E = \frac{\cos(kh\cos\theta) - \cos kh}{\sin\theta} \tag{1.77}$$

where $k = 2\pi/\lambda$, h is dipole half-length, and θ is measured from the dipole axis. For a loop coplanar with the dipole, the loop normalized electric field is:

$$E = J_1(ka\sin\theta) \tag{1.78}$$

where J_1 is the Bessel function, a is the loop radius, and θ is measured from the loop axis. Loops and dipoles small in wavelengths will behave approximately the same.

Orthogonal cocentered dipoles have zero coupling, as the radial component of the near electric field from a dipole is zero in the normal plane through the dipole

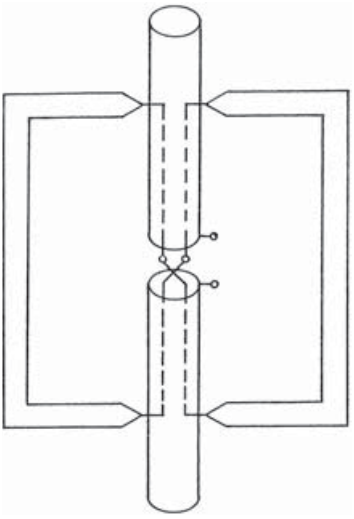

Figure 1.47 Coplanar segmented loop and dipole

center. Similarly, orthogonal cocentered loops have zero coupling. A constant current loop has only an H_ϕ, and this flux does not enter the loop. Thus a vector sensor made of thin orthogonal dipoles and loops should provide six terminals that are decoupled from each other.

Because the determination of Poynting vector direction, either direct or implicitly, involves all six antenna outputs, fabrication and assembly asymmetries must be minimized and the feed-matching circuits must produce sufficiently small phase and amplitude errors. For a specific vector sensor implementation an error analysis should be made, relating mechanical and electrical errors to error in Poynting vector. This error function can then be incorporated into the AOA estimation algorithm.

There are many papers on the algorithms for processing vector sensor outputs, such as maximum likelihood, MUSIC, and ESPRIT; see Ko, Zhang, and Nehorai (2002) for references.

1.3.4 Dielectric Resonator Antenna

The dielectric resonator antenna (DRA) is simply a block of low-loss dielectric placed on a ground plane. A precursor was probably a short monopole surrounded by a centered cylindrical dielectric (pillbox); the monopole is the same height as the pillbox (James and Burrows, 1973). As expected, a short monopole may be resonated by high ε, but the bandwidth is reduced. Long et al. (1983) introduced the DRA, where the dielectric body is resonant. They considered both rectangular slab dielectrics and cylindrical (pillbox) dielectrics. A rectangular block DRA can

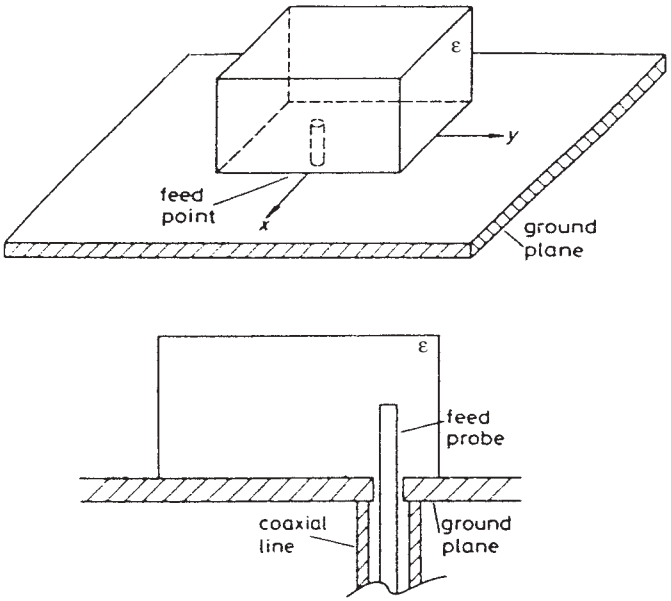

Figure 1.48 DRA with probe feed. Courtesy of McAllister, M.W., Long, S.A., and Conway, G.L. Rectangular Dielectric Resonator Antenna. *Electronics Lett* Vol. 19, 17 March 1983, pp. 218–219.

be fed by a probe (McAllister et al., 1983) as sketched in Figure 1.48, fed by a microstrip (Mridula et al., 2004), or by a microstrip line with a tee (Bijumon et al., 2005). Circular disk (pillbox) DRA (McAllister et al., 1984) have been fed by a microstrip excited slot (Leung and To, 1997); an inverted microstrip (Leung et al., 1997a); a waveguide with a slot in the guide top wall-ground plane (Eshrah et al., 2005a); a waveguide with a probe extending into both the guide and the DRA (Eshrah et al., 2005b); and a vertical metal strip on the disk exterior, with the strip connected to a feed line (Leung et al., 2000). Unusual DRA shapes include a hemisphere fed by a slot in the ground plane with microstrip excitation (Leung et al., 1995); a half-cylinder with axis parallel to the ground plane and fed by a probe (Mongia, 1989; Kishk et al., 1999); a cylindrical ring with axis normal to the ground plane and fed by a microstrip (Leung et al., 1997c); and conical dielectric shapes (Kishk et al., 2002). A further reduction in size results from a metal top plate connected to a center grounded rod (Mongia, 1997). A different configuration utilizes a tall, narrow, and thin high-ε dielectric slab normal to the ground plane and fed by a metal strip along the flat side, with a thicker, low-ε block attached (Moon and Park, 2000; see Fig. 1.49). Size reduction also occurs when metallic plates connected to the ground plane are placed at the *E* walls (of a rectangular DRA). This, however, also reduces the bandwidth (Cormos et al., 2003). Some bandwidth can be recovered by adding a grounded metal strip on an *H* wall, thus exciting also a higher mode (Li and Leung, 2005). Another bandwidth enhancement technique top loads a circular disk with a thin, high-ε disk of larger diameter (Leung et al., 1997b).

Because of the needs of mobile communications devices there has been work on dual band DRA. Two rectangular blocks placed on either side of a coupling slot produce two narrow band responses (Fan and Antar, 1997). A circular disk fed by a stripline can produce dual band response if the feed line is properly placed (Kumar

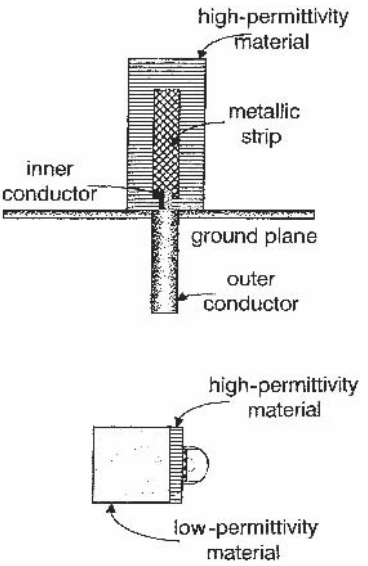

Figure 1.49 Rectangular DRA with high ε vertical strip. Courtesy of Moon, J.-I. and Park, S.-O. Dielectric Resonator Antenna for Dual-Band PCS/IMT-2000. *Electronics Lett* Vol. 36, 8 June 2000, pp. 1002–1003.

et al., 2005). An oval cylindrical disk, by proper choice of diameters, produces dual band operation (Paul et al., 2004). An alternate geometry uses a circular disk with a concentric circular cavity, fed by microstrip lines at right angles (Sung et al., 2004). Finally, a circular disk of modest ε with a higher-ε, smaller-diameter, and smaller-height disk inside, with a probe feed provides dual band operation (Nannini et al., 2003). All of these dual band configurations have a few percent (VSWR = 2) bandwidth in each band.

Field distributions inside a cylindrical dielectric were studied via Moment Method by Glisson et al. (1983) and by Kajfez et al. (1984). Analyses of resonant frequency and Q of rectangular DRA were made by Mongia (1992) and by Mongia and Ittipiboon (1997). Details on calculations are given below. For cylindrical DRA, Tsuji et al. (1982) and Mongia and Bhartia (1994) derived the relevant equations. Measurements of DRA Q appear to have been made primarily on cylindrical DRA (Mongia et al., 1994a, 1994b). Although a high ε considerably reduces the size of a DRA, metallic loading such as a top plate (Mongia, 1997) or a side plate (Li and Leung, 2005) can further reduce the size. Luk and Leung (2003) have extensively covered the art of DRA.

Most of the analyses and experiments have been made on the cylindrical or spherical configuration, because the wave functions are well-known cylindrical or spherical harmonics, which allow easy satisfaction of the boundary conditions. In contrast, rectangular DRA usually require a numerical method such as the Moment Method. But for practical antennas the rectangular DRA is the best choice: It is low profile and easy to fabricate; the three dimensions provide versatility in resonant frequency, polarization, and bandwidth. Thus only the rectangular DRA is considered in detail here.

It is analogous to the conventional patch antenna, where the patch-dielectric-ground plane form a cavity supporting the dominant TM mode. Polarization and pattern for the DRA are similar to those of the patch antenna. However in a rectangular DRA the length-to-width ratio may need to be adjusted to give an omnidirectional pattern. Circular polarization requires proper location of the feed. Increasing ε_r reduces the size by $\sqrt{\varepsilon_r}$, but the bandwidth is also reduced. Dielectric loss is an important factor as it reduces efficiency and gain.

The analysis given here is from Mongia and Ittipiboon (1997). Let the ground plane be the X-Z plane, with Z the resonant direction, and let the dielectric block have length ℓ (along Z), width w, and height h. Their wave numbers are:

$$k_x = \frac{\pi}{w}, \quad k_y = \frac{\pi}{2h}, \quad k_z^2 = \varepsilon k^2 - k_x^2 - k_y^2 \tag{1.79}$$

The indicial equation for resonance is:

$$k_z \tan\frac{k_z \ell}{2} = \sqrt{(\varepsilon - 1)k^2 - k_z^2} \tag{1.80}$$

These combine to give an equation for $k_z\ell$, from which the resonant frequency can be found:

$$k_z^2\left[1+\varepsilon\tan^2\frac{k_z\ell}{2}\right]=(\varepsilon-1)\left(k_x^2+k_y^2\right) \tag{1.81}$$

In terms of convenient design parameters ℓ/h and w/h, Equation 1.81 becomes:

$$k_z^2\ell^2\left[1+\varepsilon\tan^2\frac{k_z\ell}{2}\right]=\frac{\pi^2}{4}(\varepsilon-1)\left(\frac{\ell}{h}\right)^2\left[1+\left(\frac{2h}{W}\right)^2\right] \tag{1.82}$$

Given ε, ℓ/h, and w/h this equation is solved by this author by a Newton-Raphson rooter (Stark, 1970), a good choice as the required derivative function is easily found. Figure 1.50 shows $k_z\ell$ versus ℓ/h for values of w/h = 1, 2, 5, and 10. The curves are accurate within 1% for ε from 10 to 40, and probably higher ε. It should be noted that $k_z\ell$ is a function of only e and of the ratios of dimensions. Because $\ell/\lambda_g = k_z\ell/2\pi$, the resonant guide length approaches $\lambda_g/2$ as ℓ/h becomes large, and as w/h becomes small. The resonant value $kd\ell$ is now found from:

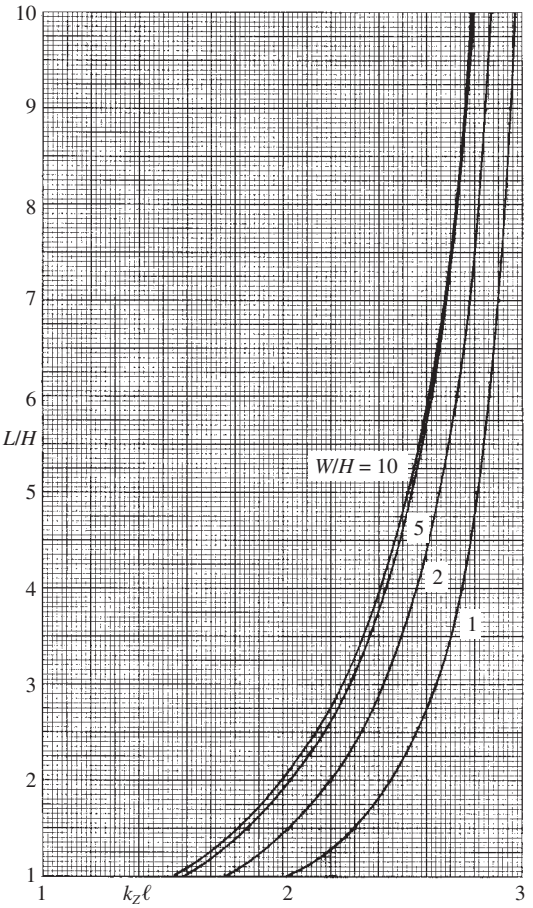

Figure 1.50

$$k^2\ell^2 = \frac{1}{\varepsilon}\left[k_z^2\ell^2 + \frac{\pi^2}{4}\left(\frac{\ell}{h}\right)^2\left[1+\left(\frac{2h}{w}\right)^2\right]\right] \tag{1.83}$$

The resonant frequency f_r is given by:

$$f_r = 0.3k\ell/2\pi \tag{1.84}$$

where f_r is in gigaherz and ℓ is in millimeters.

In free space wavelengths, the square root of Equation 1.83 is divided by 2π to get ℓ/λ. For example, $\varepsilon = 20$, $\ell/h = 5$, $w/h = 5$, $k_z\ell = 2.5421$, $\ell/\lambda_g = 0.4046$, and the resonant length is $\ell/\lambda = 0.314$.

Bandwidth for a matched load and for VSWR ≤ 2 is given by:

$$\text{BW} = \frac{P}{\sqrt{2}W} \tag{1.85}$$

The radiated power P is given by (Mongia and Ittipiboon, 1997):

$$P = \frac{640k^4\omega^2\varepsilon_0^2(\varepsilon-1)^2\sin^2\left(\frac{k_z\ell}{2}\right)}{k_z^2k_y^2k_z^2} \tag{1.86}$$

Energy times 2ω is:

$$2\omega W = \frac{\omega\varepsilon_0\varepsilon w\ell h(k_x^2+k_y^2)(1+\text{sinc}\,k_z\ell)}{16} \tag{1.87}$$

Since $\omega\varepsilon_0 = k/120\pi$, the bandwidth becomes:

$$\text{BW} = \frac{128k^5(\varepsilon-1)^2\sin^2\frac{k_z\ell}{2}}{3\sqrt{2}\pi\varepsilon w\ell hk_z^2k_y^2k_z^2(k_x^2+k_y^2)(1+\text{sinc}\,k_z\ell)} \tag{1.88}$$

Inserting dimensional ratios:

$$BW = \frac{512(\varepsilon-1)^2\left(\frac{w}{h}\right)^3(k\ell)^5\sin^2\frac{k_2\ell}{2}}{3\sqrt{2}\pi^7\varepsilon\left(\frac{\ell}{h}\right)^4\left[1+\left(\frac{w}{2h}\right)^2\right]k_z^2\ell^2(1+\text{sinc}\,k_z\ell)} \tag{1.89}$$

It is interesting to note that the bandwidth is a function only of ε and the ratios ℓ/h and w/h. Figure 1.51 shows bandwidth for VSWR = 2, for $\varepsilon = 20$, and for w/h = 2, 5, and 10. The range of ℓ/h is 1 to 10. As expected, longer and wider DRA have more bandwidth. Figure 1.52 shows bandwidth for $\varepsilon = 40$ for the same parameters. The bandwidth is reduced close to the $\varepsilon^{1.5}$ factor that has been suggested for large ε. Finally, Figure 1.53 gives bandwidth for a square DRA, with $\varepsilon = 20$ and 40. These bandwidths are the intrinsic values for the dielectric resonator; the effect of the feed on efficiency and bandwidth can be expected to be important.

A brief comparison with a conventional patch is now made. For the DRA take $\varepsilon = 20$, a square ($\ell = w$) dielectric, with $\ell/h = 40$. The value of $k\ell$ is 1.6637 so that

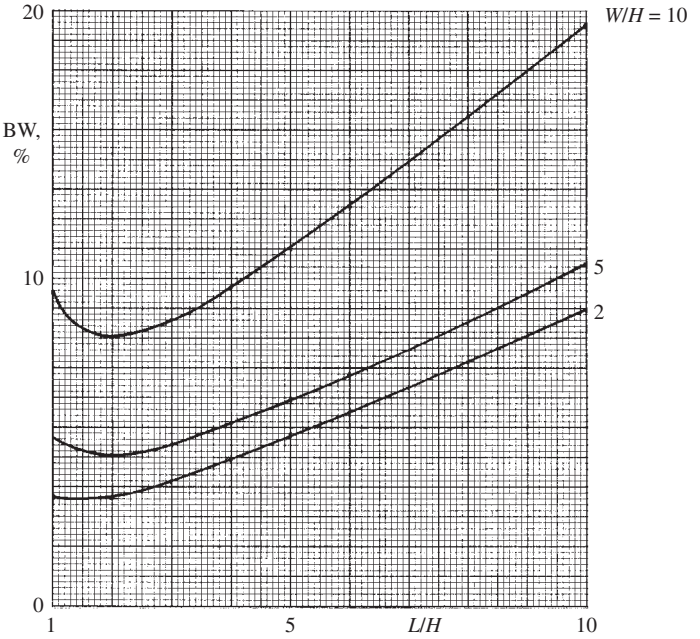

Figure 1.51 DRA VSWR = 2 matched bandwidth, ε = 20

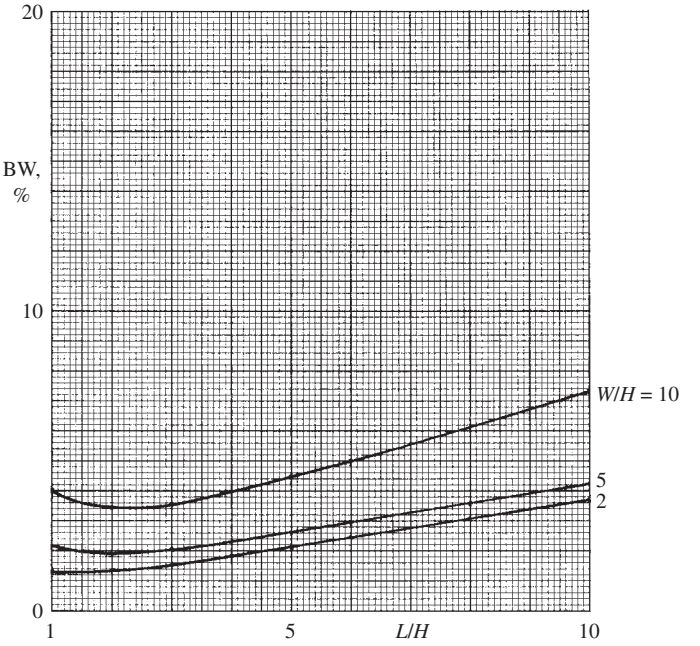

Figure 1.52 DRA VSWR = 2 matched bandwidth, ε = 40

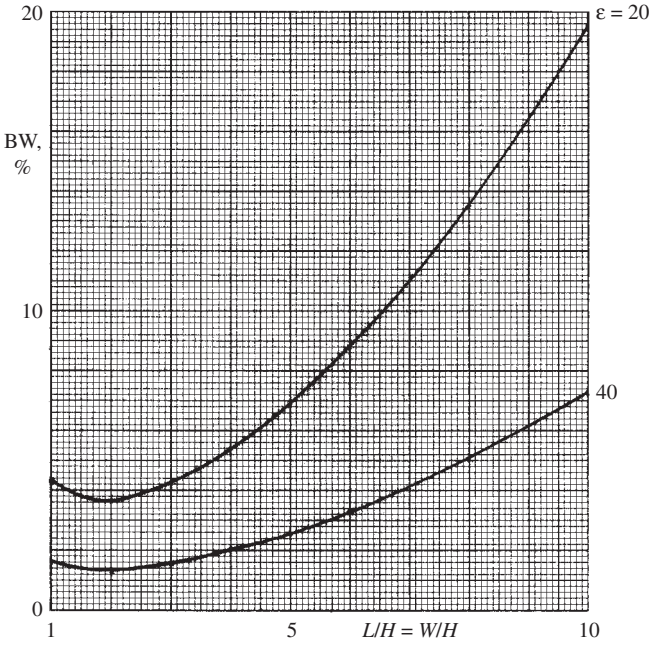

Figure 1.53 Square DRA VSWR = 2 matched bandwidth

$\ell/\lambda_0 = 0.2648$, and $h/\lambda_0 = 0.0662$. VSWR = 2 bandwidth is 5.38%. For the square patch, use $\varepsilon = 3$. Patch bandwidth is approximately:

$$\mathrm{BW} = \frac{4t}{\sqrt{2\varepsilon}\lambda_0} \tag{1.90}$$

Using the same bandwidth, the patch thickness is $t/\lambda_0 = 0.03295$. The patch length is: $\ell/\lambda_0 = 1/2\sqrt{\varepsilon} = 0.2887$. The DRA and patch lengths are nearly the same, with nearly the same resonant frequency, but the DRA thickness is about double that of the patch.

1.4 CLEVER PHYSICS, BUT BAD NUMBERS

1.4.1 Contrawound Toroidal Helix Antenna

The first example of an ESA concept that was clever and sound, but has unfortunate characteristics (tight tolerances, low radiation resistance, etc.), is the contrawound toroidal helix antenna (CWTHA). This was invented and patented by Corum (1986, 1988), who started with a coil of many turns bent into a ring or toroid. Inexplicably, some years later the patent office granted patents for the CWTHA to former lab assistants of Corum! Applying a voltage at the terminals produces a ring of current, like a single-turn loop. Then a second toroidal coil is added in the same volume,

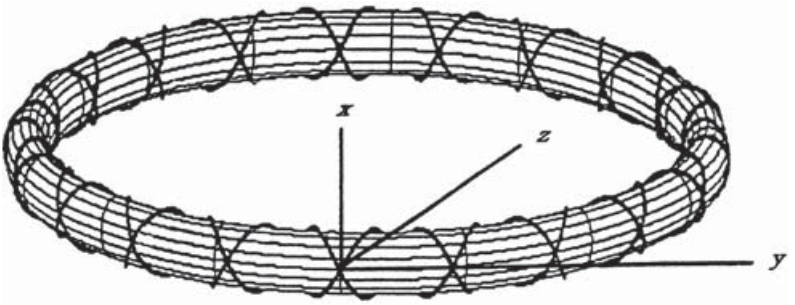

Figure 1.54 Contrawound toroidal helix (on foam core). Courtesy of Hansen, R.C. and Ridgley, R.D. Fields of the Contrawound Toroidal Helix Antenna. *Trans IEEE* Vol. AP-49, Aug. 2001, pp. 1138–1141.

but wound in the opposite direction. If the second winding is excited 180° out of phase with the first, the loop currents cancel. Figure 1.54 is a sketch of a CWTHA; the loop lines represent lines of magnetic flux. The feeds are at the origin. However, the currents around the turns add, and a vertical (dipole) electric field is created. The CWTHA was heavily promoted by others without any careful measurements or calculations. MacLean and Rahman (1978) showed that the CWTHA coordinates could be exactly written in terms of a single spherical coordinate variable. A ring-bar analysis, adapted from TWT work, was performed by Hansen and Ridgley (1999); this was followed by an exact analysis (Hansen and Ridgley, 2001) using exact geometry. The exact vector potential integrals were integrated numerically. It was shown that any combination of dimensions that gave an omnidirectional pattern (in the plane of the toroid) produced a very small ratio of dipole/loop fields. Thus the mechanical and excitation tolerances are very tight. The corresponding radiation resistance is low, where the reactance is modest. When the dimensions produce resonance, the radiation resistance is again low and the bandwidth narrow (Hansen, 2001). Figures 1.55 and 1.56 show resistance and reactance for a 20-turn model, with the ratio of toroid diameter to turn diameter of 10. Figure 1.57 shows the azimuth pattern. Even a two-turn CWTHA, which can be implemented with printed flat strips, is narrowband. (Hansen, 2002). Other approximate analyses are by Miron (2001) and Pertl et al. (2005); the second paper is about patterns and has no information about the critical areas of tolerances, radiation resistances, impedance, etc. See also Hansen (2005). So the CWTHA was a good idea, but the very tight tolerances and low radiation resistances doomed it.

1.4.2 Transmission Line Antennas

The transmission line antenna, sketched in Figure 1.58, is simply a wire or strip over a ground plane. The wire length is usually $\lambda/4$ or less, and the height above the ground plane is much less. A shunt stub or capacitor may be employed at the end. This antenna is essentially a vertical monopole loaded by a wire parallel to the ground plane (King et al., 1960; Prasad and King, 1961; Guertler, 1977). The loading may allow the monopole to have a nearly uniform current, with nearly quadrupling

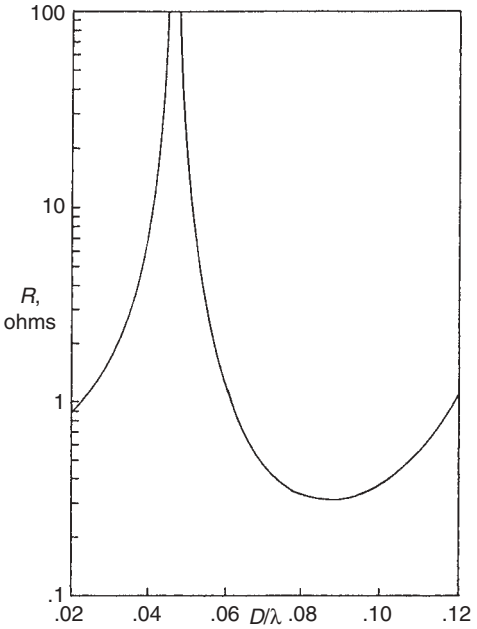

Figure 1.55 Resistance of 20 turn CWTHA. Courtesy of Hansen, R.C. Resonant Contrawound Toroidal Helix Antenna. *Microwave Optical Tech Lett* Vol. 29, 20 June 2001, pp. 408–410.

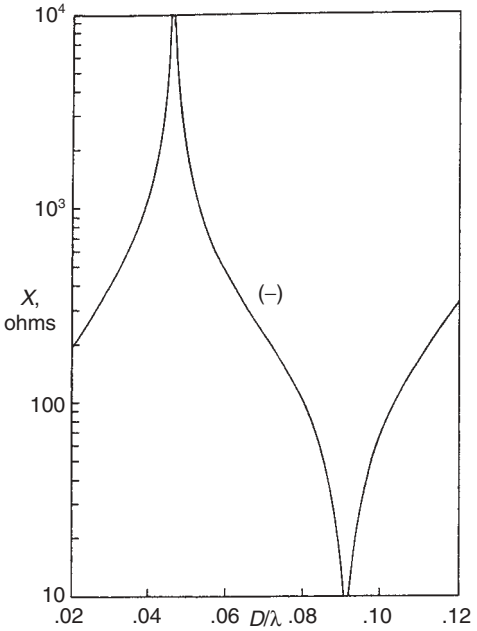

Figure 1.56 Reactance of 20 turn CWTHA. Courtesy of Hansen, R.C. Resonant Contrawound Toroidal Helix Antenna. *Microwave Optical Tech Lett* Vol. 29, 20 June 2001, pp. 408–410.

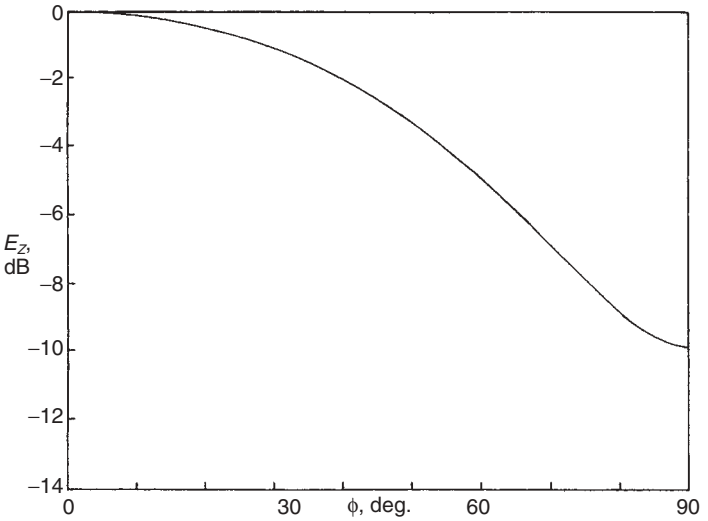

Figure 1.57 Azimuth pattern of 20 turn CWTHA. Courtesy of Hansen, R.C. Resonant Contra-wound Toroidal Helix Antenna. *Microwave Optical Tech Lett* Vol. 29, 20 June 2001, pp. 408–410.

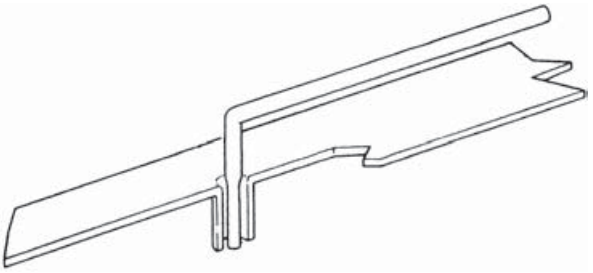

Figure 1.58 Transmission line antenna. Courtesy of King, R.W.P. et al. Transmission-Line Missile Antennas. *Trans IRE* Vol. AP-8, Jan. 1960, pp. 88–90.

of the monopole-alone radiation resistance. In that case, the radiation resistance would be $40k^2h^2$, where h is the monopole height. Thus the limitation on the transmission line antenna is the low radiation resistance.

1.4.3 Halo, Hula Hoop, and DDRR Antennas

A small loop antenna can be folded, as sketched in Figure 1.59. This has been called the Halo Loop (Harrison and King, 1961). It could also be the result of bending a folded dipole into the halo shape. A narrow bandwidth results. The closely spaced half-loop conductors carry opposing currents, resulting in a radiation resistance reduction of 5 : 1, and a reactance increase of 2 : 1, over the folded dipole, for half-wave size. For smaller antennas the performance is even poorer. Radiation resistance is roughly $30k^2a^2$, with a the loop radius.

The Hula Hoop antenna is simply a short monopole with capacitive loading bent into a hoop to save space (Boyer, 1963; Nakano et al., 1993; see Fig. 1.60). The wire

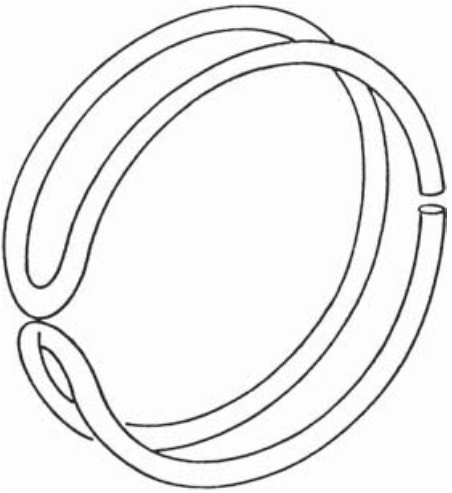

Figure 1.59 Halo loop

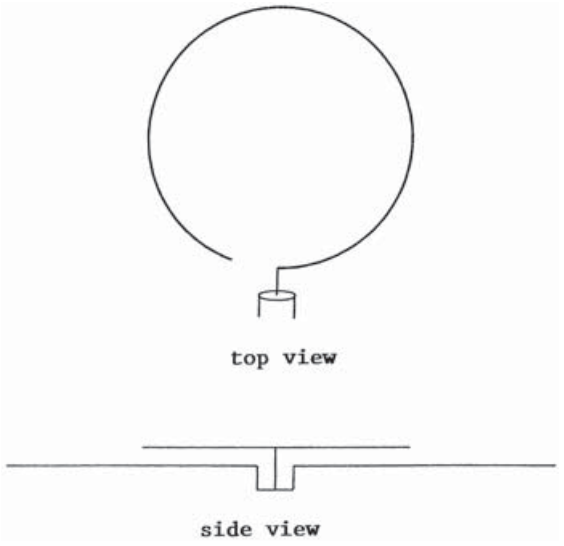

Figure 1.60 Hula hoop antenna

is λ/4 in length. It was observed by Burton and King (1963) that such an antenna behaves essentially the same if the wire is straight or in a hoop, and thus the radiation resistance is again $30k^2h^2$. Although the silhouette is low, the resistance is very low. If the wire length is electrically short, the reactance becomes very high and the resistance even lower. Thus this antenna experienced only a brief flurry of interest before being consigned to history.

The simplest top loading of a short monopole is with a top hat, a metal plate at the monopole end, which acts as a capacitive load. A large hat might produce a

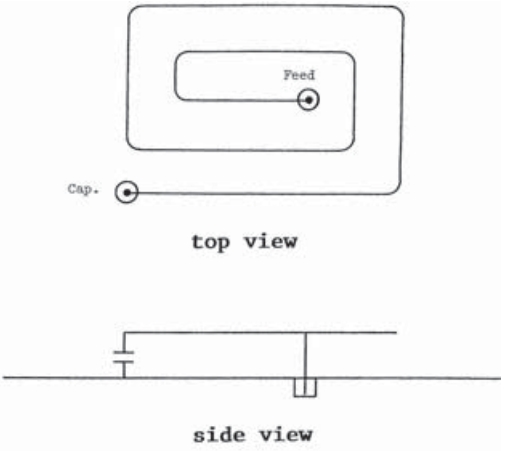

Figure 1.61 DDRR antenna

nearly constant current in the monopole, with nearly quadruple the radiation resistance, but the hat diameter would be larger than the monopole length. A Moment Method analysis of a monopole with large top disk was given by Simpson (2004), who found that the load could produce resonance, but the resulting bandwidth was narrow.

More elaborate transmission line antennas were developed by Fenwick (1965). Here the single capacitive wire above ground plane is replaced by a meandering wire, by a planar strip spiral, or by a partially counterwound planar strip spiral. The end opposite from the feed may be grounded or connected to a resistor. These configurations tend to be less effective than a top plate. See also Hallbjorner (2004). The transmission line may be zigzagged, to reduce the length (Lee and Mei, 1970).

When a simple planar wire spiral, with the outside end connected to the ground plane by a capacitor, is used as the top load (Wanselow and Milligan, 1966), the radiation resistance is improved somewhat, but the resonant circuit Q reduces the bandwidth. This configuration was called the direct driven resonant radiator (DDRR); the name was more impressive than the performance (see Fig. 1.61).

Top loading schemes for MF and HF monopoles are described and evaluated by Trainotti (2001).

1.4.4 Dielectric Loaded Antennas

The first attempt in this roughly chronological chronicle was to encapsulate a short dipole in dielectric, in the hope that the result would be similar to that produced by loading a loop with a high-permeability core. Unfortunately, the loop and dipole are not analogs; there are no magnetic currents.

In gross terms dielectric loading of antennas is undesirable; the current is decreased by $1/\varepsilon_r$ (Wheeler, 1947; Schelkunoff and Friis, 1952). Dipoles or monopoles with dielectric sleeves have been investigated for over 40 years. Polk (1959) analyzed a biconical dipole embedded in a dielectric sphere, using the Schelkunoff transmission line approach. For a short biconical the reactance was reduced by the dielectric, but the bandwidth was also reduced. Grimes (1958) showed that a dielectric sleeve around a dipole would affect the impedance due to ε, but not from μ. Galejs (1962, 1963) used a spherical mode approach for a short dipole in a dielectric sphere. Using the lowest mode, he showed that the efficiency × bandwidth varies as $9\varepsilon/(\varepsilon + 2)^2$. For $\varepsilon = 1$ this factor is one, of course, and for large ε it approaches $9/\varepsilon$. The maximum occurs for $\varepsilon = 2$, and is 1.125. This contradicts the results of Wheeler (1958), who assumed a dielectric surface tangential to *E*. The results of Galejs were recapitulated by Chatterjee (1985). Measurements were made of short probes with dielectric sleeves by Birchfield and Free (1974): The sleeves improved the impedance match, but data are sparse. A Moment Method analysis of dielectric coated dipoles was made by Richmond and Newman (1976). Resonant conductance increased roughly linearly with $(\varepsilon - 1)/\varepsilon\ \ell n\ b/a$, where *a* is the dipole radius and *b* is the sleeve radius. Bandwidth is reduced, but no data are given. See also Popovic and Djorkjevic (1981). Smith (1977) in a brief note indicates that the efficiency × bandwidth product is reduced by the addition of the dielectric, based on the work of Galejs. A cylindrical dielectric or ferrite sleeve on a dipole was treated as a resonator by James et al. (1974) and James and Henderson (1978). See also Fujimoto et al. (1987). The external field has a continuous eigenvalue spectrum, and the cavity has discrete modes. Their perturbation approach ensures that the cavity fields are only slightly changed by loss and by radiation. A variational method is then used to find the fields. Results show decrease in efficiency (due to material losses) and decrease in bandwidth. The degradation appears less when $\mu = \varepsilon$ for the dielectric. Reduced dipole length, for resonance, may not compensate adequately for the lower efficiency and smaller bandwidth. Returning now to subresonant cladding, King and Smith (1981) formulated an integral equation for the currents; only a few results are given. Sinha and Saoudy (1990) did a Weiner–Hopf analysis of a dielectric coated dipole; the asymptotic approximation of current shows unexplained small changes in impedance with ε. An FDTD approach was used by Bretones et al. (1994), for the case where sleeve thickness equals wire radius, with $\varepsilon = 3.2$. A small shift in impedance peaks was observed. Francavilla et al. (1999) added a circular dish top hat to a monopole, with dielectric between hat and ground plane. Cylindrical wave functions and mode matching were used. As ε was increased the resonant frequency decreased, and the bandwidth decreased, both as expected. See also Janapsatya and Bialkowski (2004). A different use of dielectric loading uses a permeable bead placed on a long monopole, to make the monopole act as a $\lambda/4$ monopole (Kennedy et al., 2003).

Dielectric coatings on monopoles or dipoles can produce resonance at lengths well below $\lambda/4$, but the lower efficiency and lower bandwidth are generally a poor trade. Better results are obtained by inserting a series inductor as mentioned in Section 1.3.1.1.

1.4.5 Meanderline Antennas

The resonant size of a dipole can be reduced by meandering the conductor, as in Figure 1.62 (Rashed and Tai, 1991). For resonance the wire length is roughly half-wave. These antennas can be used over a ground plane at quarter-wave spacing, or as a patch. A meanderline monopole for a notebook computer has been described by Lin et al. (2005). Meander patches have been used by the HTS community; see Section 3.3.2. Probe feeding was used by Chang and Kuo (2005). A less effective arrangement inserts a folded dipole crosswise in the center of a monopole (Altshuler, 1993).

Although the meander monopole antenna can be resonant in a width (or length) below λ/4, there are several significant disadvantages (Best, 2003a). The closely spaced wires store reactive energy, which reduces bandwidth. Radiation resistance tends to be that of a monopole with the physical length, not the wire length; thus it is often low. And the wire length introduces nonnegligible loss resistance.

1.4.6 Cage Monopole

A novel monopole loading scheme uses a cage of four monopoles with a loading wire at the top of each; the monopoles are independently fed (Breakall et al., 2002, 2003). Each monopole is connected to a transmission line transformer to raise the low radiation resistance; then the four transformer coax are connected in parallel (see Fig. 1.63). Moment Method simulations have been concerned with modeling the ground wires and the earth. A simple understanding of how this antenna works is provided by a model of four closely spaced dipoles, all much shorter than λ/4. Unlike the monopoles, where the top loads make the vertical current nearly constant, the short dipoles have a triangular current, but for understanding impedance and performance the cage of dipoles is adequate. If one dipole alone has impedance Z_{11}, the mutual impedances Z_{12}, Z_{13}, and Z_{14} will be very close to Z_{11}, but with somewhat less reactance, as the dipoles are closely spaced. Then the impedance of each dipole

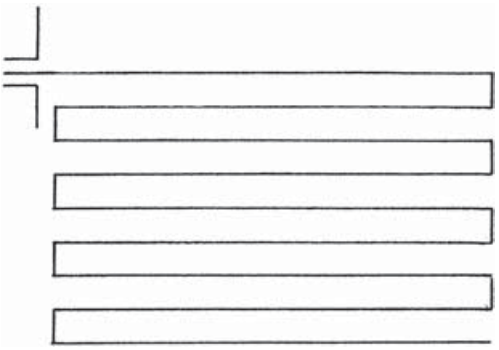

Figure 1.62 Meanderline antenna. Courtesy of Rashed, J. and Tai, C.-T. A New Class of Resonant Antennas. *Trans IEEE* Vol. AP-39, Sept. 1991, pp. 1428–1430.

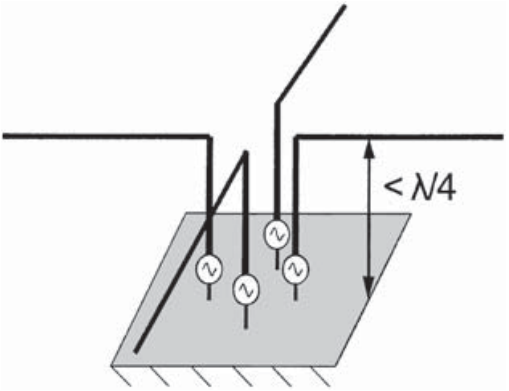

Figure 1.63 Cage monopole

in the cage is closely $4Z_{IN}$. The impedance transformation process does not change this basic result. Thus the Q of the cage is essentially that of one monopole as fat as the cage. Better performance (easier matching) would result from using a single fat monopole (four or more wires connected together at the feed point) with an equivalent top load. Thus the separate feeding is of no value as the monopoles are eventually connected together.

1.5 PATHOLOGICAL ANTENNAS

Claims on these antennas typically have performance characteristics that violate the physical laws we work under.

1.5.1 Crossed-Field Antenna

The crossed-field antenna (CFA) was conceived by Hately and Kabbary in the late 1980s. It was based on several "new" principles: that E and H fields could be created independently, that Maxwell's displacement current produces magnetic fields, and that near-fields could be avoided. The basic geometry is shown in Figure 1.64: Two horizontal circular metallic disks form a capacitor that is excited by the transmitter, but it is alleged that the displacement current between the plates produces an azimuthal magnetic field. Two hollow metallic circular cylinders are stacked vertically, and above the horizontal plates. The transmitter also excites the cylinders, but 90° out of phase with the plate excitation. An electric field is produced by the cylinders, as sketched. Because of Poynting vector, the H and E fields radiate a wave into space. Several of these CFAs have been built, at MF. Later versions have incorporated a large flare structure into the upper cylinder, presumably to increase the electric field in Figure 1.64. To quote the authors, "E and H fields are produced from separate electrodes," "the two fields are compelled to cross at right angles in the

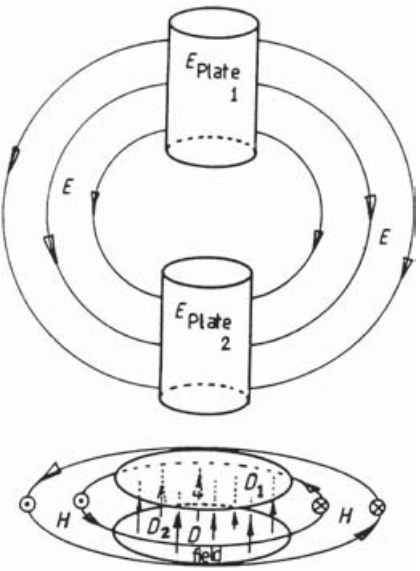

Figure 1.64 CFA geometry

interaction zone," "any CFA is capable of radiation over a decade of frequency," and "Moment Method cannot be used to model CFA, as it only models currents" (see Kabbary, Hately, and Stewart, 1989; Kabbary, Khattab, and Hately, 1997; Kabbary et al., 1999; Hately, Kabbary, and Khattab, 1991; see also U.K. patent 2215524 and U.S. patent 5155495). It is significant that peer-reviewed antenna journals have not accepted papers on CFA.

A critical analysis was made by Smith (1992). He performed a simple circuit analysis on one of the CFA antennas, with the result that the efficiency is below 50% and the Q is roughly 20. This value is due to the "fatness" of the CFA monopole. Belrose (2000a, 2000b) did both a Moment Method analysis and experiments on a CFA (Fig. 1.65). This experimental model closely follows a CFA built at Tanta, Egypt. Both the E cylinders and the H plates were high Q (low radiation resistance), and the 90° phasing resulted in power oscillating between the cylinders and plates, further increasing loss. The NEC simulation and measurements both showed that, unlike the claims of Kabbary, (1) the relative voltage drives of the disk and cylinder are not critical; (2) in the vicinity of the CFA "electrodes," the wave impedance is much greater than 120π ohms; and (3) the CFA gain is not sensitive to the relative phase of the two voltage drives. The Moment Method calculations agreed well with measured data.

Hatfield (2000) calculated that for a typical CFA to maintain the ratio of E to H of 120π, the plates would require a voltage of more than one megavolt. Kabbary and Hately apparently do not understand that both the H plates and the E cylinders produce near-fields, that the impedance of these near-fields is not 120π, and that it varies with distance. Furthermore, the near-fields are not orthogonal.

Figure 1.65 CFA built and tested by Belrose

All measurements made by Kabbary et al. are doubtful for the following reasons. Almost all CFAs were mounted on top of buildings, where the building had at least a partial metal skin. Almost all CFA measurements were made at radio transmitting sites, where extensive ground wire systems existed. In at least one case, the measurement inspectors were denied access to the phasing and matching cabinet. In at least one case a hidden ground cable was discovered. In general the tuning and adjustment of the CFA has proved difficult, and all performances have been narrow band. A variant of the CFA is the EH antenna, but the "principles" are the same. Foolishness leads to fraud? (Robert Park)

1.5.2 Snyder Dipole

A dipole with built-in coaxial matching stubs was invented by Snyder (1984a, 1984b); wideband performance was claimed. The Snyder dipole is sketched in Figure 1.66; the radiating currents are indicated in the figure. This configuration can be decomposed into the parallel combination of three structures: a thin wire

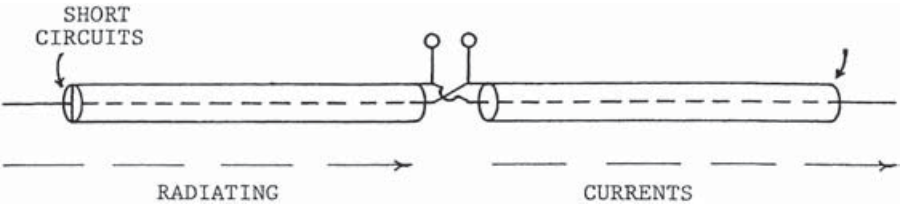

Figure 1.66 Snyder dipole

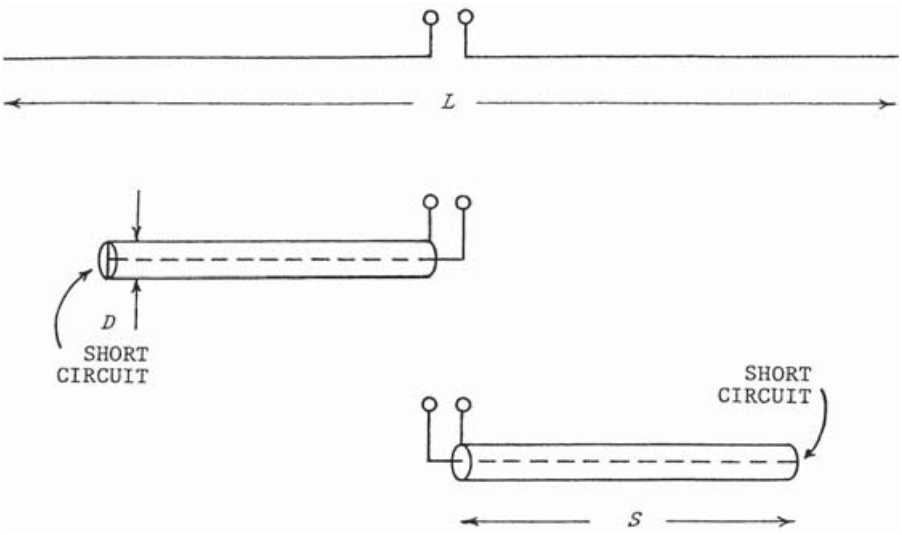

Figure 1.67 Snyder dipole components

dipole and two short-circuited transmission line stubs (see Fig. 1.67). Thus an equivalent circuit for this antenna is simply composed of dipole and transmission line components. Note that the coaxial structure shields the stub currents, preventing them from radiating, as long as the stubs are near resonant length. Call the dipole length L, the length of each stub S, and the diameter D; the wall thickness is assumed to be negligible. It is convenient to normalize the electrical stub length by the resonant electrical stub length and the stub diameter by the dipole length:

$$\alpha = \frac{\sqrt{\varepsilon} kS}{\pi/2} \quad \text{and} \quad \beta = D/L \tag{1.91}$$

ε is the stub transmission line dielectric constant, and the characteristic impedance is given by:

$$Z_{0\ell} = \frac{60}{\sqrt{\varepsilon}} \ell n D/2a \tag{1.92}$$

where a is the wire radius. The input impedance of one stub, where $k = 2\pi/\lambda$, is:

$$Z_s = jZ_{0\ell} \tan \alpha \pi/2 \tag{1.93}$$

If the dipole impedance is called Z_d, the input impedance of the Snyder dipole will be:

$$Z_{in} = \frac{Z_S Z_d}{Z_S + 2Z_d} \tag{1.94}$$

Note that this is different from that of a folded dipole, whose impedance is given by (Stutzman and Thiele, 1981):

$$Z_{in} = \frac{4Z_S Z_d}{Z_S + 2Z_d} \tag{1.95}$$

This folded dipole result is four times the Snyder formula; both contain the parallel combination of dipole and two stubs.

The Snyder dipole is used with a matching transformer; an approximate value for its impedance Z_0 can be indicated by a simple analysis. An admittance $G + jB$ connected to a circuit of characteristic admittance $Y_0 = 1/Z_0$ has a VSWR given implicitly by:

$$Y_0 G\left(V^2 + 1\right) = V\left(Y_0^2 + G^2 + B^2\right) \tag{1.96}$$

For VSWR = 2 this reduces to:

$$Y_0 = \frac{5G}{4} \pm 1/4\sqrt{9G^2 - 16B^2} \tag{1.97}$$

When a simple resonant matching circuit is used optimally, the VSWR has a peak of two near center frequency and rises at band edges. Thus near resonance, the dipole susceptance B_d and the stub susceptance B_s are both small, giving the approximate result that Y_0 should be 2 G_d or 0.5 G_d. It will appear that the second is a good choice.

Snyder (1984b) uses as comparison a thin wire dipole with no matching transformer. This is obviously unfair. The comparison dipole used here uses a resonant tuning circuit as well as a transformer. This makes a fair comparison between the Snyder dipole, where the tuning is provided by coaxial stubs, and a dipole where the tuning is provided by a lumped resonant circuit at the feed terminals. A parallel resonant circuit is used in parallel with the feed terminals (see Fig. 1.68). The admittance of this circuit is given by:

$$Y_{ckt} = (1 + jQH)/R \tag{1.98}$$

where $H = f/f_0 - f_0/f$, $Q = 2\pi f_0 RC$, and $f_0^2 = 1/4\pi^2 LC$. It is convenient to use Q and R/Q as input parameters. Q should be selected very large so that the matching circuit loss does not increase the bandwidth. The parameter R/Q can be determined for maximum bandwidth. The matching transformer ratio, or, equivalently, the characteristic impedance of the dipole plus circuit, is selected to make VSWR = 2 at the resonant peak.

The Snyder dipole and the comparison dipole model have been implemented by this author in computer programs for ease of determining optimum results. A wire diameter of 0.005 times dipole length is used.

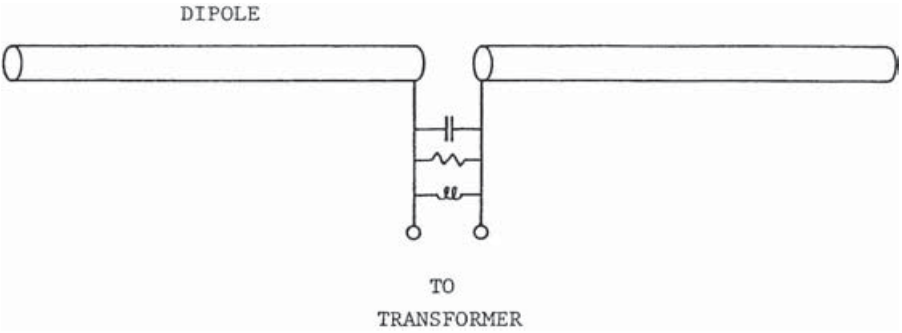

Figure 1.68 Dipole with matching circuit

For the comparison dipole with matching resonant circuit, the circuit Q is set at 1000, a value sufficiently large as to have little effect on bandwidth. The matching circuit is tuned to dipole resonance. It may be possible to improve the bandwidth somewhat by staggering the dipole and circuit resonance frequencies, but this is not done here. As occurred for the Snyder dipole, the optimum match impedance is a little less than twice the resonant resistance; $Z_0 = 126$ ohms. To find the optimum pair of values of R/Q and Z_0, a number of values of R/Q are used. For each R/Q, the value of Z_0 is adjusted to make the VSWR peak around resonance equal to two. Finally, the bandwidth of each pair is evaluated, and the largest is chosen. Note that R/Q must be carefully chosen; it controls the circuit reactance that offsets the dipole reactance. The value used was 30. Use of lower-Q matching circuit components will increase bandwidth; a value of $Q = 100$ significantly improves bandwidth but lowers efficiency. The bandwidth was 21.0%.

For the Snyder dipole, taking $\alpha = 1$, which is for a stub that is resonant at the dipole resonant frequency, the maximum VSWR = 2 bandwidth occurs for $Z_{0\ell} = 45$ ohms and $Z_0 = 127$ ohms; the normalized bandwidth is 20.7% Calculations were made by picking values of α and $Z_{0\ell}$, then adjusting Z_0 to make the VSWR peak around center frequency equal to two. This allows the low and high VSWR = 2 frequencies to be determined, hence the bandwidth. When the stub is tuned off the dipole resonance, the bandwidth decreases; this is typical of matching of high-Q circuit (the dipole) with a high-Q resonant circuit. Maximum bandwidth for $\alpha = 0.95$ occurs for $Z_{0\ell} = 42$ ohms and $Z_0 = 110$ ohms; the normalized bandwidth is 18.3%

At center frequency where the coaxial stubs are resonant, the radiating currents on the Snyder dipole are just those of an equivalent fat plain dipole. Thus the basic gain is expected to be that of a dipole: 1.64 or 2.15 dB. In the center of the band and at band edges, where the VSWR = 2, there is a mismatch loss of 0.51 dB. In addition, the gain is reduced by the loss in the coaxial stubs, both due to dissipation in the coaxial dielectric and in the metallic conductors. A further gain reduction occurs away from center frequency, where the stubs are no longer resonant. This results in currents flowing from the inside of the stub around the open end to the outside. These exterior currents will radiate, and in some parts of the frequency

band their radiation will oppose the primary radiation; thus there will be a gain reduction. So the bandwidth calculations presented here are optimistic, in that the dipole gain diminished by the mismatch loss will not be realized over the entire bandwidth.

One might consider replacing the Snyder dipole with twin conductor stubs, but this configuration is not equivalent to the coaxial stub antenna. In the Snyder dipole the return stub current is shielded, whereas in the twin conductor stubs the currents nearly cancel.

In summary, the Snyder dipole performance is no better than a fat dipole of the same diameter as the stub diameter. At band edges it is worse because of stub transmission line currents that flow on the outside of the stubs away from resonance; this was not included in the simple analysis used here.

1.5.3 Loop-Coupled Loop

In this configuration a large tuned parasitic loop is excited by a coplanar, but eccentric, small loop (Dunlavy, 1971; see Fig. 1.69). The large loop couples loss to the small loop, thereby increasing bandwidth and decreasing efficiency, but the gain is low for the large size. This antenna is also dispersive (Barrick, 1986). For some years this loop was sold commercially by a U.S. company.

Because both loops are small in wavelengths, the performance can be analyzed by simple circuit theory. Figure 1.70 shows the equivalent circuit of the two loops. For the large single-turn loop, R_r is the radiation resistance, R_ℓ is the loss resistance, L is the inductance, and C is the tuning capacitor. For the small loop the loss resistance is $R_{\ell 1}$, the inductance is L_1, and the load resistance is R_0. The mutual inductance is X_m. The circuit equations are:

$$V = I_1 \underbrace{[R_r + R_\ell + j(X_c + X_\ell + X_m)]}_{A} - I_2 \underbrace{[R_0 + R_{\ell 1} + j(x_{\ell 1} + X_m)]}_{B} \qquad (1.99)$$

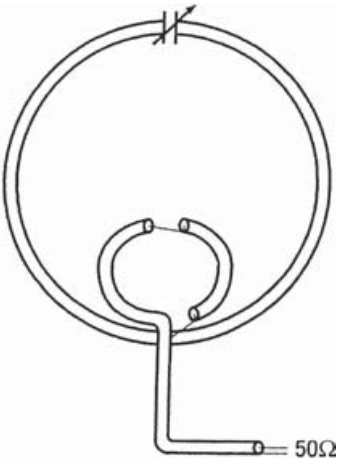

Figure 1.69 Loop coupled loop

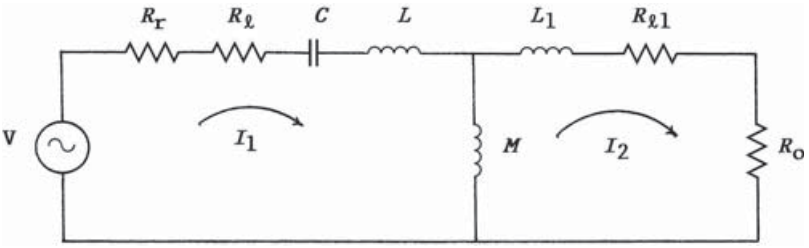

Figure 1.70 Loop coupled loop equivalent circuit

$$O = \underset{C}{I_1 jX_m} - \underset{B}{I_2 [R_0 + R_{\ell 1} + j(X_{\ell 1} + X_m)]} \tag{1.100}$$

The complex brackets are called A and B for brevity. The solution for the two currents is:

$$I_1 = \frac{V}{A-C} \quad I_2 = \frac{VC}{B(A-C)} \tag{1.101}$$

The power delivered to the load resistor as a result of the induced voltage is:

$$P_l = I_2 I_2^* R_0 = V^2 R_0 \left[\frac{C}{B(A-C)}\right]\left[\frac{C}{B(A-C)}\right]^* \tag{1.102}$$

To maximize this power the quantity $B(A - C)$ times its conjugate should be minimized. If the loop dimensions are fixed, the minimization occurs when $X_c = -X_\ell$, that is, the big loop is tuned for the desired frequency. This gives received power as a function of the resistances, the mutual inductance, and the small loop inductance:

$$P_l = \frac{V^2 R_0 X_m^2}{[R_0 + R_{\ell 1} + j(X_{\ell 1} + X_m)][R_0 + R_\ell + j(X_{\ell 1} + X_m)]^* \\ [R_r + R_\ell + jX_m][R_r + R_\ell + jX_m]^*} \tag{1.103}$$

Because the maximum diameter of the large loop is roughly 0.1λ to avoid pattern breakup and impedance swings, the large loop reactance is significant while the radiation resistance and loss resistance are typically much smaller than one ohm. Thus the power can be approximated with the result:

$$P_l = \frac{V^2 R_0}{(X_{\ell 1} + X_m)^2} \tag{1.104}$$

In comparison, the large loop by itself, when matched, has a power delivered to the load of:

$$P = \frac{V^2 R_0}{(R_r + R_\ell + R_0)^2} \tag{1.105}$$

The efficiency of the loop-coupled loop system is now found from the ratio of its power to the single loop power just derived. This ratio is given by:

$$\eta_t = \frac{P_1}{P} = \frac{(R_r + R_\ell + R_0)^2}{(X_{\ell 1} + X_m)^2} \tag{1.106}$$

Overall performance of the loop-coupled loop system now requires this efficiency to be multiplied by that of the single large loop, which is:

$$\eta = \frac{R_r}{R_r + R_\ell} \tag{1.107}$$

It is immediately clear that the resistances in the numerator are all very small, whereas the reactances in the denominator, although less than those for the large loop, are still much larger than the resistances. Thus the transfer efficiency is very small. The formulas for the approximate mutual inductance between single-turn coplanar but noncoaxial loops are complicated (Grover, 1946). Very roughly, the ratio of mutual inductance to self-inductance varies as a $\sqrt{d/D}$, where d is the diameter of the small loop and D is the diameter of the large loop. It appears that the mutual inductance term in Equation 1.106 may be comparable to the self-inductance of the small loop. In any case, the transfer efficiency is very small. It might be thought that the load resistance in Equation 1.106 could be increased in order to increase the transfer impedance. However, this would violate the assumptions made in reducing Equation 1.103 to Equation 1.104. It is expected that if the load resistance value were raised, and the exact formulas used, the transfer impedance would still be very small. The single loop efficiency, which multiplies the transfer efficiency, may or may not be small. For the 0.1λ-diameter loop the radiation resistance is 1.923 ohms, and it should be easy to build a loop of a large conductor with high efficiency. However, most loops are much smaller than 0.1λ, and for these the efficiency may be poor, as the radiation resistance varies as the diameter in wavelengths to the fourth power. Thus in all cases the efficiency of the loop coupled loop system is small. Belrose (2003, 2005a, 2005b) has modeled the loop-coupled loop with the NEC-4 Moment Method code and has performed measurements on a model that he constructed. Because he was interested in modeling the effect of the earth on the antenna, a Moment Method analysis was appropriate. His results show in detail that the efficiency of the antenna is very poor, and that the bandwidth is very narrow, because of the high Q of the large loop. The conclusion is that if a loop antenna is needed for a given application, it should be a single loop tuned with a capacitor. Whether the loop is comprised of single turn or multiple turns will depend on a variety of other factors.

1.5.4 Multiarm Dipole

A multiarm dipole represents an idea that has reappeared, phoenix like, many times from the ashes of critical engineering evaluation (Turner and Richard, 1968). The concept is simple. In Figures 1.71 and 1.72 each pair of arms is cut to a different

Figure 1.71 Multi arm dipole

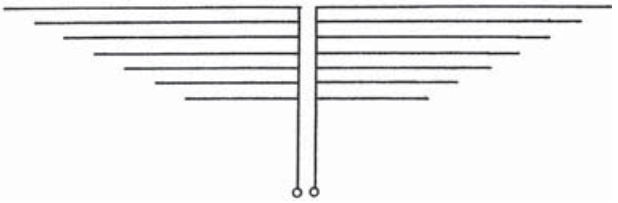

Figure 1.72 Multi arm dipole. Courtesy of Turner, E.M. and Richard, D.J. Development of an Electrically Small Broadband Antenna. *Proc 18th Symp USAF Ant Res Dev Prog* Oct. 1968, Allerton, IL.

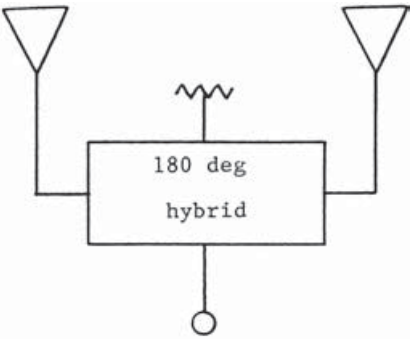

Figure 1.73 Complementary pair antenna

frequency, and so the ensemble should be broadband. However, whether the arms are resonant or short, the ensemble acts like a single fat antenna because of mutual coupling among the closely spaced arms. The result is again a narrowband antenna resulting from a lack of basic understanding of antennas and mutual coupling.

1.5.5 Complementary Pair Antenna

In the complementary pair antenna (Schroeder, 1964, 1969; Schroeder and Soo Hoo, 1976) two antennas are connected to the side arms of a 180° hybrid junction (see Fig. 1.73). The concept is that the reactances are cancelled because of the π phase, whereas the radiation resistances are added. Hybrids with highly mismatched (and usually not quite equal) loads give only a partial reactance cancellation. The cancellation may also vary with frequency. Furthermore, the environment of the two antennas may make the reactances somewhat different. Thus the reactance cancel-

lation may be only partial. Mutual coupling between the two antennas will also affect the hybrid performance. When the volume occupied by the two antennas is utilized by a single, fatter, antenna, the complementary pair advantage disappears. The single antenna is simpler.

1.5.6 Integrated Antenna

This is the name given by Turner and Meinke to an electrically small antenna that has a semiconductor element, usually a transistor, connected in the interior of an antenna. The first discussion of integrating semiconductor electronics into antennas was given by Frost, who conceived a parametric amplifier using portions of the antenna as resonant circuits (Frost, 1960, 1964). This work was followed at OSU, where an amplifier was integrated with the antenna, although in a more conventional sense (Copeland et al., 1964). For the integrated antennas, although many configurations have been devised, the most common is a folded monopole with capacitive "top hat." The transistor is inserted at the top hat junction (see Fig. 1.74). Other connections of the transistor have been tried; this is the broadband configuration (Flachenecker and Meinke, 1967). The transistor can be located just below the top hat or can be near the feed point, with the location affecting the frequency of minimum VSWR. Operation of this scheme can be understood by considering only the example of Figure 1.74, with the transistor just below the top plate. Effectively all the induced voltage appears from base to emitter, as the folded monopole operating as a loop will yield a much smaller voltage. Thus the transistor acts as a variable resistance inserted at the loop of the folded dipole, with the resistance value depending on the bias level. Such a loaded folded antenna was discussed above. The resistance makes the folded monopole broadband, with no increase in output voltage. The transistor may also be used as a variable reactance circuit to add capacitance to tune the monopole inductance. However, this application and the broadband application are only partly compatible, with the relative effectiveness of each depend-

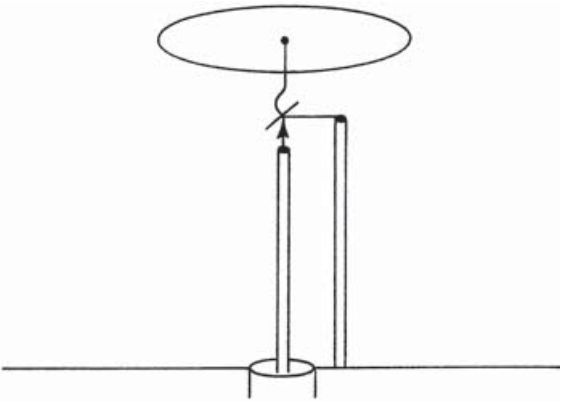

Figure 1.74 Integrated antenna. Courtesy of Flachenecker, G. and Meinke, H.R. Active Antennas with Transistors. *Can Int Electronics Conf Rec* Sept. 1967, pp. 142–143.

ing on the transistor drive phase angle. The integrated antenna has an effective length like that of the top hat monopole alone, but the transistor loss broadens the bandwidth, reduces efficiency, and introduces appreciable noise (Maclean and Ramsdale, 1975). Instabilities incurred in active loading of dipoles was examined by Fanson and Chen (1974). After years of high-level hype, the consensus was reached that the optimum placement of active devices is not in the antenna, but at the antenna terminals. Subsequent amplification can be accomplished with appropriate band limiting for noise factor control.

1.5.7 Antenna in a NIM Shell

In another attempt to beat the fundamental limits on bandwidth of an electrically small antenna, such as a short dipole, Ziolkowski and colleagues (2003) have placed a thin shell around a short dipole, with the shell diameter also small in wavelengths (see Fig. 1.75). When the shell has the ideal properties of a negative index metamaterial (NIM), it can act as an impedance transformer over that part of the dispersion curve versus frequency where the NIM property exists. It is claimed that the shell can greatly increase radiation resistance and bandwidth of the dipole and decrease reactance. And Wheeler–Chu–McLean is violated not by a modest increase in bandwidth, but by orders of magnitude!!!

Alas, the electrically small, thin NIM shell is made of that well-known material, UNOBTAINIUM. NIM require at least one of several awkward features: an array of long (in wavelengths), closely spaced wires parallel to the E field; a conducting ground plane not small in wavelengths (for mushroom NIM); and conductive waveguide walls that allow circuit elements. None of these configurations fits into an electrically small, thin shell. Closely spaced and long wires (in wavelengths) greatly attenuate the field transmitted through, although several papers have shown the field without attenuation. The reviewers should be ashamed.

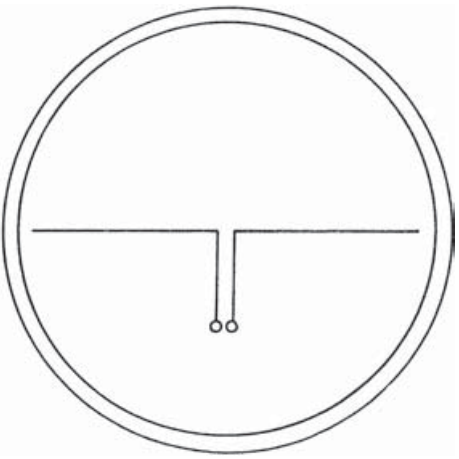

Figure 1.75 NIM shell and dipole

A further difficulty is that the metallic inclusions that are integral to any NIM are small in wavelengths and are close to the dipole wire in wavelengths. Just as a plethora of higher-order wire dipoles results in one lowest-order wire dipole, because of mutual coupling, the NIM inclusions have their induced currents and scattering properties altered with the resulting loss of NIM properties.

To quote Robert Park, "It never pays to underestimate the human capacity for self-deception."

1.5.8 Fractal Antennas

The science of fractals was developed by Mandelbrot and published in seminal books (1977, 1983). Fractal antennas have incurred a large interest and a large number of papers in recent years. Only the most significant are mentioned here. This activity arose because there is very little new in antennas, and fractal antennas are a new frontier. In addition, the mathematics is fairly simple, and the antenna forms are neat. For ESA the forms are either monopoles (dipoles) or loops, and there are five general categories, each with its initiator and generator. These are shown in the various stages:

von Koch (1870–1924) snowflake, 1904; (Puente et al., 1998; Baliarda et al., 2000a). Figure 1.76 shows stages. Figure 1.77 shows a segment that could be a monopole.

Sierpinski (1882–1969) gasket (Puente et al., 1996; Baliarda et al., 2000b). Figure 1.78 shows stages. Figure 1.79 shows a segment that could be a monopole.

Hilbert (1862–1943) curve (Vinoy et al., 2001; Anguera et al., 2003). Figure 1.80 shows monopoles.

Minkowski (1864–1909) island, circa 1890 (Cohen, 1995; Best, 2003b). Figure 1.81 shows monopoles. Figure 1.82 shows loops.

Peano (1858–1932) curves (Zhu et al., 2004). Figure 1.83 shows monopoles.

Most of the papers concern Sierpinski monopoles.

Fractals occur in many places in nature, and in biology in particular. Ferns, leaves, and coral are among the many examples. Fractals may be useful in scattering from rough surfaces or ocean waves (Jaggard, 1990). However, there is nothing in Maxwell's equations that indicates any particular spatial periodicity in performance parameters, so one must look to the world of practical antennas to see whether fractal mathematics would improve performance. Wideband antennas such as the spiral, the log-periodic dipole array (LPDA), and the TEM horn have in common the Frequency Independent Principle: The feed point excites a small geometry first. If this geometry is a resonant active region, it radiates. If not, the exciting currents are passed on without significant change to a subsequent larger active region. The active regions start small at the feed point and become large at the end of the antenna. In the spiral antenna, the active region is an annulus that starts immediately

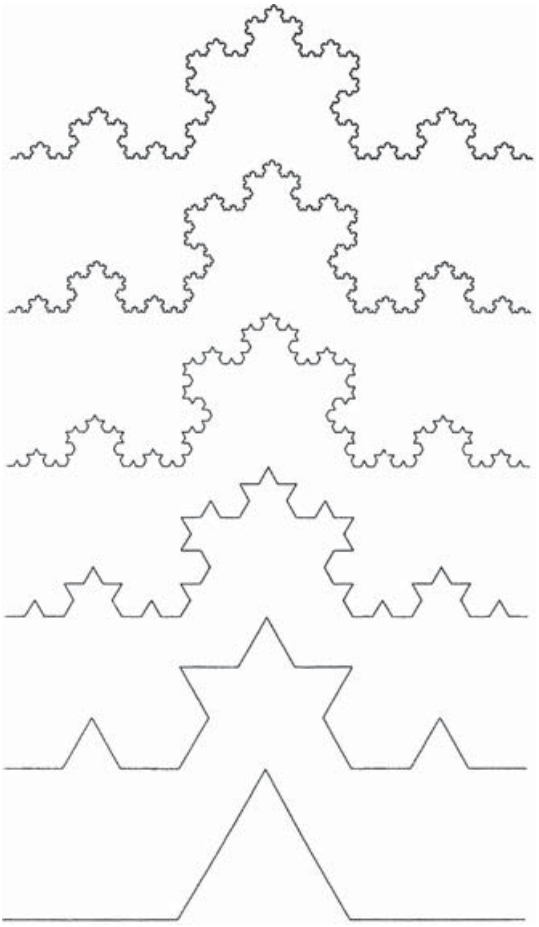

Figure 1.76 von Koch stages

around the feed point and as frequency increases moves to the periphery of the spiral at the lowest operating frequency. Similarly, the LPDA has a high-frequency resonant region consisting of short dipoles near the feed and longer, lower-frequency dipoles situated along the boom. The active region for the lowest frequency contains long dipoles at the big end of the LPDA (see Fig. 1.84). Similarly, the TEM horn radiation is primarily from the throat region at high frequencies and primarily from the mouth region at low frequencies.

Fractals, in contrast, tend to behave in just the opposite manner. The classic Mandelbrot diagram (see Fig. 1.85) starts with a large figure at the origin (feed point); smaller replicas are then clustered at strategic points around the large figure, and even smaller figures are clustered around each of these medium-sized figures, etc. Thus the feed point occurs at the large structure instead of at the small active

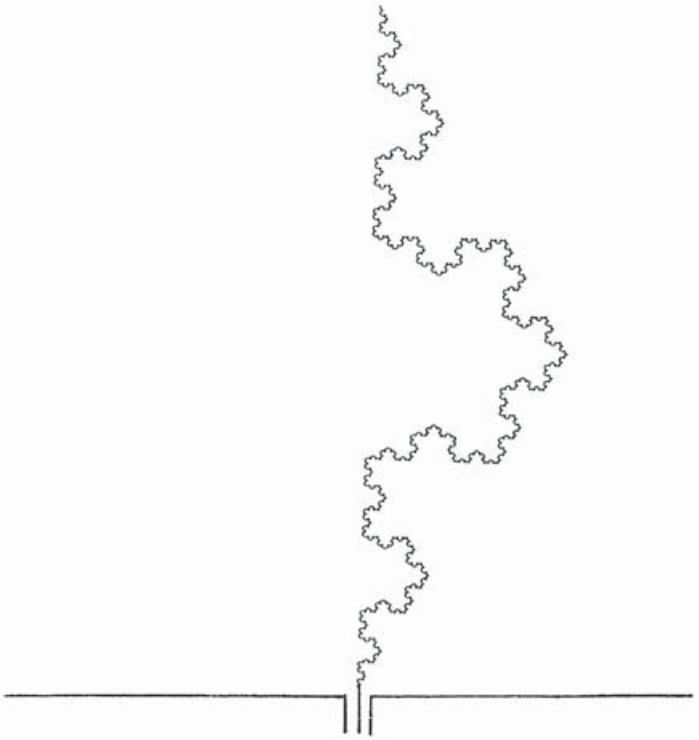

Figure 1.77 von Koch monopole

region; the currents to excite the small structures must travel through the large structure, clearly violating the principles of broadband radiation.

Best and Morrow (2002, 2003) have shown that, for the von Kock, Hilbert, Minkowski, and Peano fractal antennas, although their space-filling nature reduces resonant frequency, the strong coupling between parallel segments with opposite currents reduces the antenna effective length. Also, reactance is increased over that of simple antennas such as dipoles and bowties, thereby reducing bandwidth. Hilbert fractal antennas with narrow bandwidth at resonance are shown by Zhu et al. (2003) and by Guterman et al. (2004). Similarly, Koch fractal antennas have narrow bandwidth at resonance (Best, 2002b). The Sierpinski holes in the bowtie shape produce higher-frequency resonances, but these make a multiple narrow band antenna rather than a broadband antenna (see Puente-Baliarda, 1998; Liang and Chia, 1999; Soler et al., 2002). The resonant frequency of wire monopoles such as Hilbert, Minkowski, and meander is controlled primarily by wire length (Best and Morrow, 2002, 2003; Best 2002a). Self-resonant ESA, because their input resistance is not small (Best, 2005a), do not need the matching circuit loss enhancement described in Section 2.6. Thus we may conclude that in general fractal antennas should not be expected to contribute performance improvement in size or bandwidth.

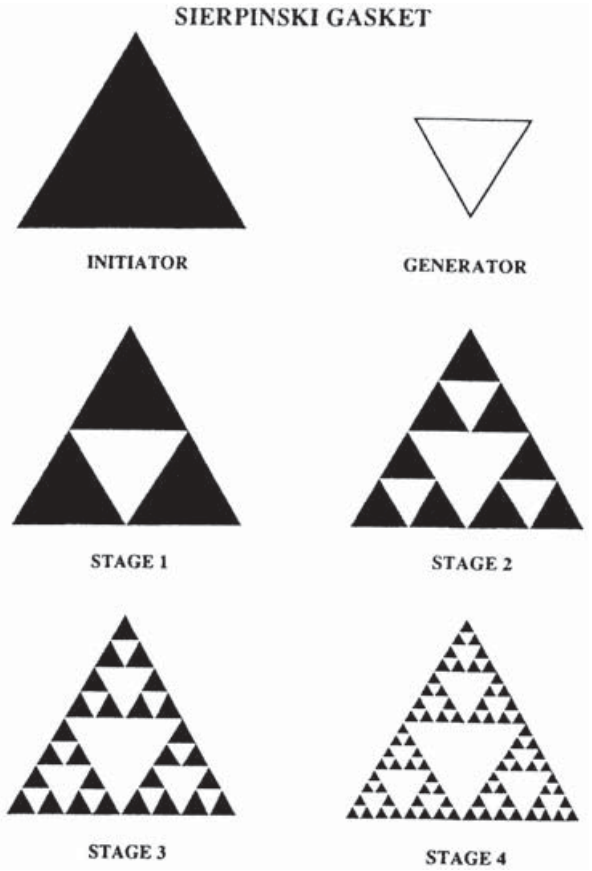

Figure 1.78 Sierpinski stages

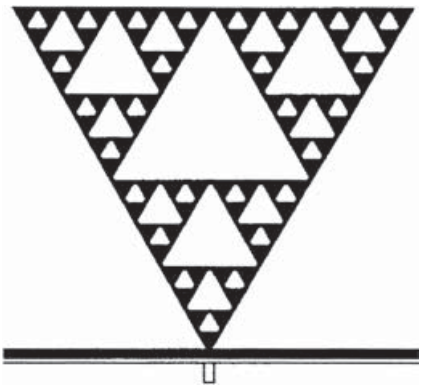

Figure 1.79 Sierpinski monopole

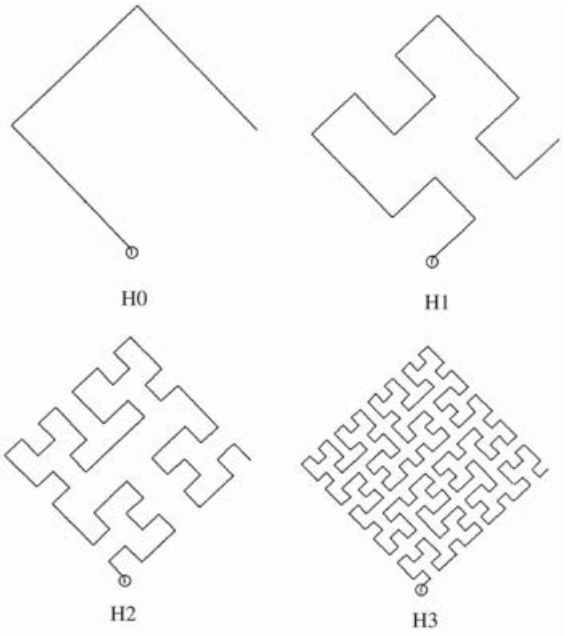

Figure 1.80 Hilbert monopoles

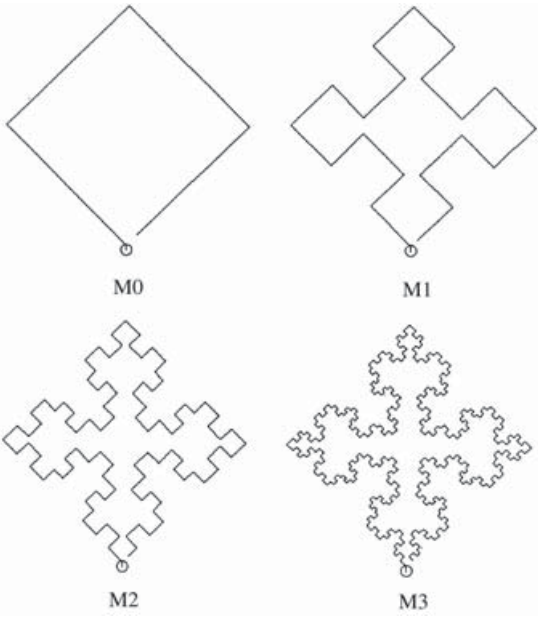

Figure 1.81 Minkowski monopoles

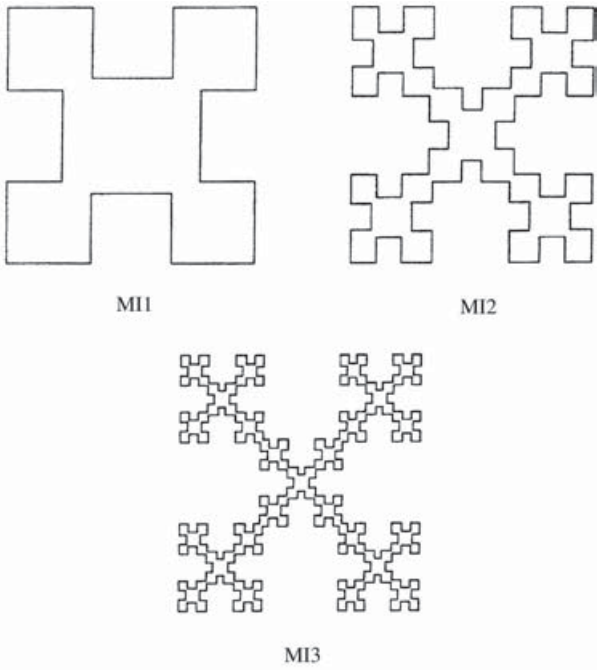

Figure 1.82 Minkowski loops

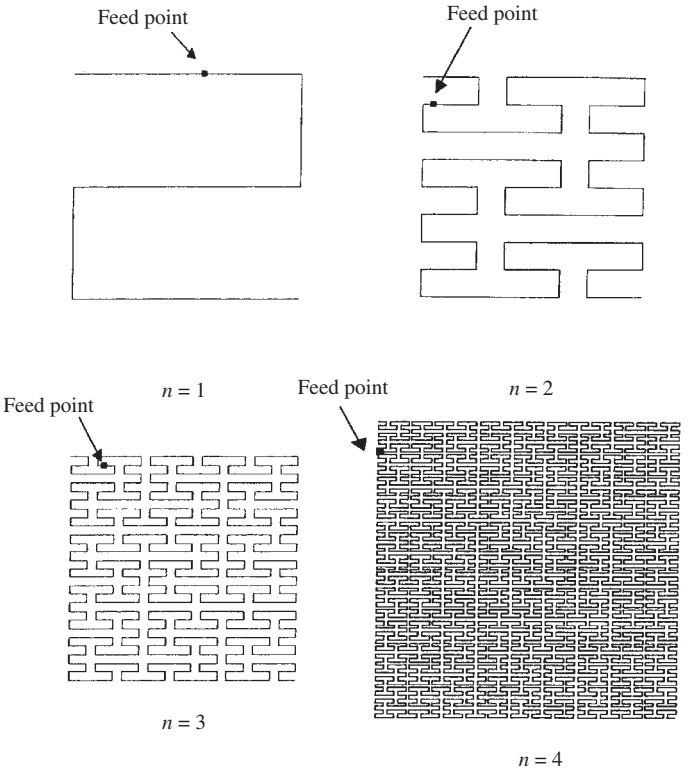

Figure 1.83 Peano curves

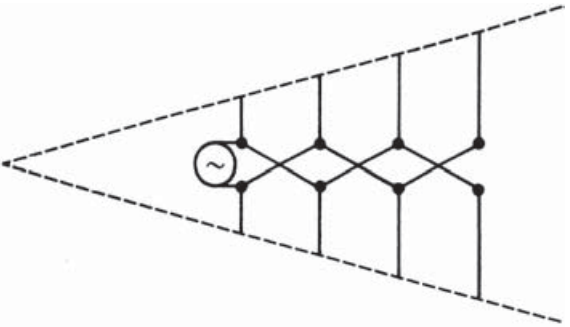

Figure 1.84 Log-periodic dipole array

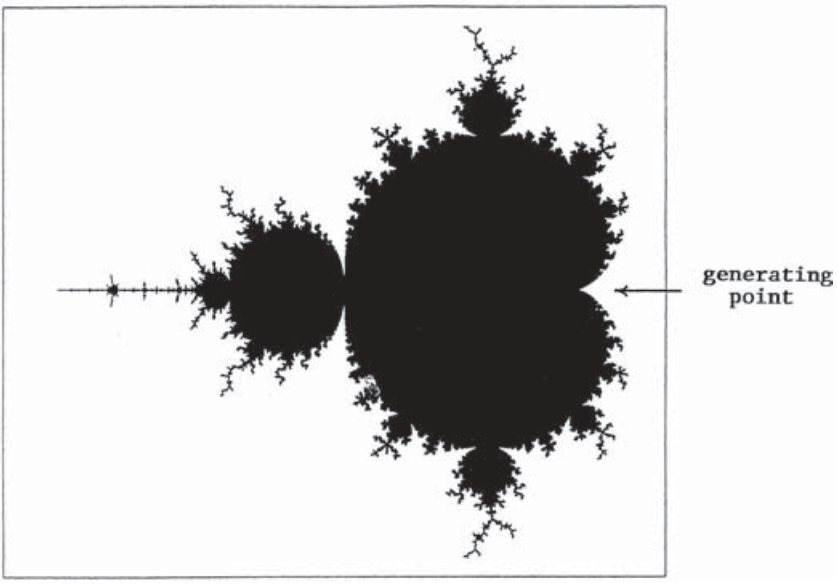

Figure 1.85 Original Mandelbrot fractal

Electrically small planar monopoles, broadly speaking, have only two design parameters besides height. These are the fatness and the wire length (for a wire monopole). It is well known that fat monopoles, such as bowtie monopoles, have much wider bandwidth than wire monopoles. A wire monopole can become resonant even if the overall height is small in wavelengths. Best (2002a, 2003a) compared ESA resonant wire antennas of meander, Koch fractal, meander helix, Hilbert fractal, and Minkowski fractal. The wire length-controlled resonance and the bandwidth were essentially the same. The increase in resistance usually did not affect bandwidth significantly because of a larger radiation resistance. For loops the wire length affects efficiency, because of a small radiation resistance. Gonzalez et al. (2003) showed that space-filling monopoles, such as meander, Hilbert fractal, and Peano fractal, store a lot of

energy in the near-field and have more loss. Thus the bandwidth and efficiency are both diminished. If wire length is used to produce resonance in an ESA, the wires should be disposed to minimize cross-polarization and to maximize radiation resistance. Generally, higher-order fractal designs have less bandwidth and lower efficiency. A closely spaced meanderline monopole is better than Kock and Hilbert fractal monopoles, but fat bowties or top-loaded fat dipoles are better.

The Sierpinski monopole is slightly poorer in efficiency and thus slightly better in bandwidth, because of slightly higher loss resistance, than a solid bowtie. The Sierpinski holes in the bowtie shape produce higher frequency resonances, but these make a multiple narrow band antenna rather than a broadband antenna.

Fractal array designs, such as Cantor set arrays, are outside the scope of this book, but they offer no advantages and have high sidelobes; there are much better nonuniformly spaced array designs available. An array design related to fractals uses difference sets (a brand of combinatorial mathematics) to formulate a thinned array with constant sidelobe envelope (Leeper, 1999).

A careful review of the many papers on fractal antennas shows that they offer no advantages over fat dipoles, loaded dipoles, and simple loops with or without magnetic core. Nonfractals are always better.

1.5.9 Antenna on a Chip

A few years ago a large telecommunications company announced an "antenna on a chip," an antenna so small that it resided on the printed circuit board. Measurements were made with the chip connected to a network analyzer by a small diameter coax. Results were excellent. Later, when the cable was removed and the antenna was activated by the circuit board, the antenna did not operate. This was another case of an unbalanced antenna connected to a coax cable; the cable often makes an excellent radiator! All announcements on the chip antenna ceased. Similar problems occurred in most of the CWTHA tests.

1.5.10 Random Segment Antennas

It has become fashionable to design wire antennas with some type of optimizer program, almost independent of good physics or high-quality performance. The results sometimes have wire segments in all directions; see Figure 1.86 for an example. A long total wire length may achieve resonance in a small volume, but there are several disadvantages. If Z is the normal monopole direction, the X currents tend to cancel, as do the Y currents. However, in certain directions the cross-polarized field may not be negligible. Longer total wire length increases loss resistance, reduces efficiency, and increases reactance. And generally the bandwidth is narrow. Examples are Altshuler and Linden (2004), Choo et al. (2005), Altshuler (2005), and Best (2002a, 2003a). Use of fractals and meanderlines to fill space (Gonzalez-Arbesu et al., 2003; Best and Morrow, 2002) suffers from the same problems.

"Do not confuse inexperience with creativity" (Linda Whittaker), is appropriate here.

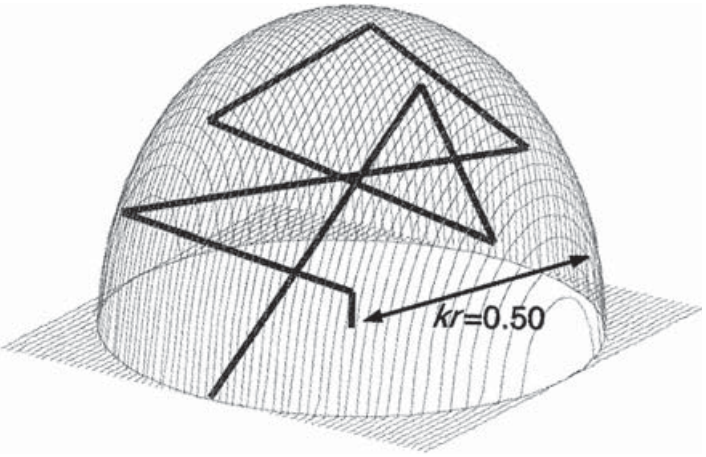

Figure 1.86 Random segment antenna. Courtesy of Choo, H., Rogers, R.L., and Ling, H. Design of Electrically Small Wire Antennas Using a Pareto Genetic Algorithm. *Trans IEEE*. Vol. AP-53, March 2005, pp. 1038–1046.

1.5.11 Multiple Multipoles

The fundamental limitations on antennas make it clear that the maximum bandwidth of an ESA occurs when both the electric dipole mode and the magnetic dipole mode are excited. For many years an effort has been made to show that higher-order modes, or multipoles, could also be excited within the imaginary enclosing small sphere, and thereby invalidate Chu's results. Grimes (1995, 1996) improperly applied Poynting's theorem to individual modes and "derived" a non-Maxwellian equation for the conservation of power. Grimes (1997, 1999) produced a "standing energy density" (reactive power) that cannot be derived from electrodynamics. It was stated that ESA Q could be as low as zero! It is well known from antenna theory that a dipole along the axis of a loop, with the dipole center in the loop plane, has zero mutual impedance to the loop. McLean (1995), using Moment Method, showed this but, more importantly, showed that a coplanar dipole and loop were coupled and that the dipole and loop energy densities were interrelated. Notwithstanding, Grimes (2000a, 2000b) claimed that two loop-dipole pairs used "energy that returns from the radiation field to the antenna," and that when the pairs are excited for CP, "large near-field energy is not supported." In a review paper (Grimes, 2001) it was stated again that $Q = 0$ was possible. Collin (1998) gives a detailed critique of how Grimes has bent the laws of electrodynamics.

The several Grimes papers only vaguely explain how to produce higher-order multipoles in a small volume. Of course, for the lowest-order TE and TM modes a dipole along the loop axis suffices. In a patent (Grimes, 1989) it is suggested that the lowest-order mode may be produced by a dipole, the next mode may be produced by two parallel dipoles fed 180° out of phase, etc., and similarly for the loops (see Fig. 1.87). Of course, what happens is that the mutual coupling of three closely spaced dipoles is very strong, with the result that all the dipoles revert to a single

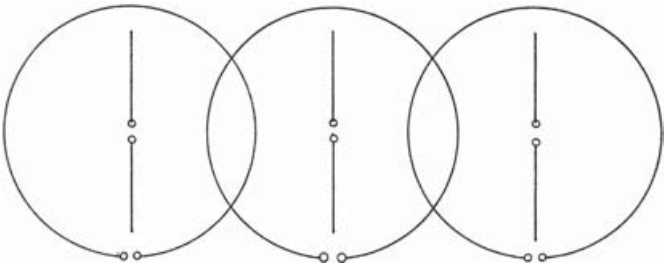

Figure 1.87 Multipoles, after Grimes (1989)

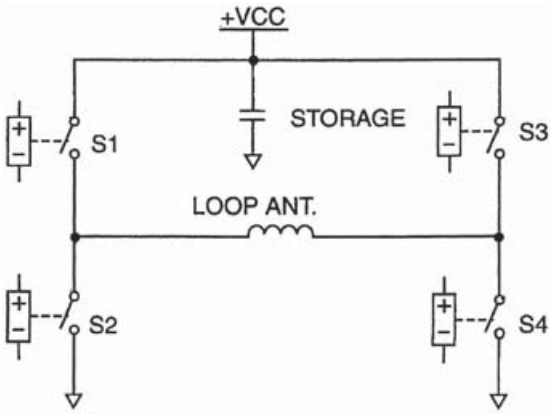

Figure 1.88 Merenda switching circuit

fatter dipole, but of course with reactance changed. This is much like the multiarm dipole of Section 1.5.4. Similar effects can be expected from the loops. Also damaging is that the dipoles and loops must be connected to the external world by wire segments inside the enveloping sphere. These wires cross-couple the multipoles and become part of the antenna. It is not surprising that there are no credible measurements of antennas that beat the Chu limit.

As Robert Park states in *Voodoo Science: The Road from Foolishness to Fraud*: "Where accepted laws of electrodynamics must be changed to give the researcher the results he wants, he is almost certainly wrong."

1.5.12 Switched Loop Antenna

The switching of energy between a capacitor and a loop to provide wideband operation was invented by Merenda (2001). As shown in Figure 1.88, an energy storage device (capacitor) and a loop are connected with a DC supply by four switches. Figure 1.89 depicts the cycle: Current flows through the loop for the first 60° of cycle, building up to a peak value. During the next 60° the loop is short circuited; the current decays somewhat. For the next 120° the loop excitation is reversed; the

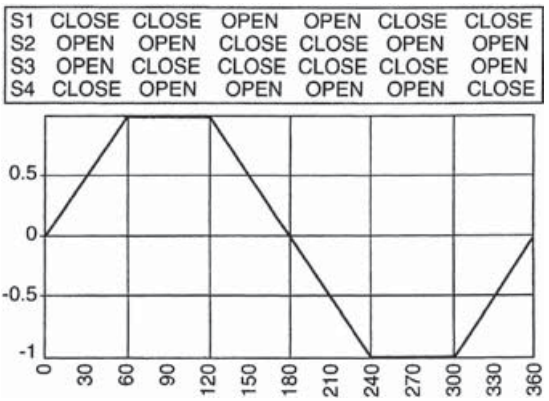

Figure 1.89 Merenda switching cycle

current decays to zero and builds up in the opposite direction. From 240° to 300° the loop is again shorted, thus allowing a slow current decay. Finally, from 300° to 360° the current decays to zero and starts the buildup in the next cycle. The capacitor and power supply are connected to the loop during the current increasing cycles. The waveform of Figure 1.89 approximates a sine wave, the RF carrier.

The question arises: How does this switching scheme differ from simply connecting a capacitor in parallel with the loop and connecting both to an RF source? The switching circuit effectively generates the RF carrier. Disadvantages of the Merenda circuit are that the waveform of Figure 1.90 contains, in addition to the RF carrier frequency, some higher harmonics, which cause interference, corrupt the signal modulation, and reduce efficiency somewhat, and that the switching circuit transistors will reduce the DC to RF carrier efficiency and introduce noise. In both cases the antenna is basically a loop with a shunt capacitor; the bandwidth will be limited by the Q of the tuned loop.

"The absolute ingenuity of this idea almost blinds one to its utter worthlessness" (Air Marshall Tedder), is appropriate here.

1.6 ESA SUMMARY

Although there have been many attempts to make electronically small antennas that out-perform the fundamental imitations, or even to come close to them, none has succeeded. The Wheeler–Chu–McLean fundamental limitations are absolute, regardless of government needs or expenditures. What has changed over the years is that the attempts have become more sophisticated, although in each case, basic principles were ignored.

Clever antenna design can make the most of available space; a reasonable objective is to get close to the limits. In general dipole-type ESA should use as much area (and volume) as feasible, for example, bowtie, to take advantage of "free" bandwidth. Judicious inductive loading is also productive. Bandwidth can be improved

further through use of clever matching networks. HTS materials will affect these conclusions only by allowing more efficient matching sections to be used. Non-Foster matching circuits will become very important.

The reader is urged to read the fascinating *Voodoo Science* by Robert Park (2000): "Foolishness, if pursued can lead to denial, and that sometimes leads to fraud."

REFERENCES

ALTSHULER, E.E. A Monopole Antenna Loaded with a Modified Folded Dipole. *Trans IEEE*, Vol. AP-41, July 1993, pp. 871–876.

ALTSHULER, E.E. AND LINDEN, D.S. An Ultrawide-Band Impedance-Loaded Genetic Antenna. *Trans IEEE*, Vol. AP-52, Nov. 2004, pp. 3147–3150.

ALTSHULER, E.E. A Method for Matching an Antenna Having a Small Radiation Resistance to a 50-Ohm Line. *Trans IEEE*, Vol. AP-53, Sept. 2005, pp. 3086–3089.

ANGUERA, J. et al. The Fractal Hilbert Monopole: A Two-Dimensional Wire, *Microwave Optical Tech Ltrs*, Vol. 36, 20 Jan. 2003, pp. 102–104.

BALANIS, C.A. *Antenna Theory*, John Wiley & Sons, 2005.

BALIARDA, C.P., ROMEU, J., AND CARDAMA, A. The Koch Monopole: A Small Fractal Antenna, *Trans IEEE*, Vol. AP-48, Nov. 2000a, pp. 1773–1781.

BALIARDA, C.P. et al. An Iterative Model for Fractal Antennas: Application to the Sierpinski Gasket Antenna, *Trans IEEE*, Vol. AP-48, May 2000b, pp. 713–719.

BARRICK, D. Miniloop Antenna Operation AND Equivalent Circuit, *Trans IEEE*, Vol. AP-34, Jan. 1986, pp. 111–114.

BELROSE, J.S. Characteristics of the CFA Obtained by Numerical and Experimental Modeling, *Proc IEEE BTS Symp*, 2000a.

BELROSE, J.S. The Crossed Field Antenna-Analyzed by Simulation and Experiment, *ICAP-JINA Conf on Antennas and Prop, Davos*, 2000b.

BELROSE, J.S. Electrically Small Transmitting Loops—Part 1. *Radcom* June 2003, pp. 65–67; Part 2, July 2004, pp. 88–90.

BELROSE, J.S. Electrically Small Transmitting Loops. *IEEE APS Symp Digest*, 2005a.

BELROSE, J.S. Performance Analysis by Experiment and Simulation of Small Tuned Transmitting Loop Antennas. *IEEE APS Symp Digest*, 2005b.

BEST, S.R. A Comparison of the Performance Properties of the Hilbert Curve Fractal and Meander Line Monopole Antennas. *Microwave Optical Tech Lett* Vol. 35, 20 Nov. 2002a, pp. 258–262.

BEST, S.R. On the Multiband Behavior of the Koch Fractal Monopole Antenna. *Microwave Optical Tech Lett* Vol. 35, 5 Dec. 2002b, pp. 371–374.

BEST, S.R. A Comparison of the Resonant Properties of Small Space-Filling Fractal Antennas. *IEEE Ant Wireless Propagation Lett* Vol. 2, 2003a, pp. 197–200.

Best, S.R. On the Significance of Current Vector Alignment in Establishing the Resonant Frequency of Small Space-Filling Wire Antennas. *IEEE Ant Wireless Propagation Lett* Vol. 2, 2003b, pp. 201–204.

Best, S.R. The Foster Reactance Theorem and Quality Factor for Antennas. *IEEE Ant Wireless Propagation Lett* Vol. 3, 2004a, pp. 306–309.

Best, S.R. The Radiation Properties of Electrically Small Folded Spherical Helix Antennas. *Trans IEEE* Vol. AP-52, April 2004b, pp. 953–960.

Best, S.R. A Discussion on the Quality Factor of Impedance Matched Electrically Small Wire Antennas. *Trans IEEE* Vol. AP-53, Jan. 2005a, pp. 502–508; correction Jun. 2005, p. 2133.

Best, S.R., Low Q Electrically Small Linear and Elliptical Polarized Spherical Dipole Antennas. *Trans IEEE* Vol. AP-53, March 2005b, pp. 1047–1053.

Best, S.R. and Morrow, J.D. The Effectiveness of Space-Filling Fractal Geometry in Lowering Resonant Frequency. *IEEE Ant Wireless Propagation Lett* Vol. 1, 2002, pp. 112–115.

Best, S.R. and Morrow, J.D. On the Significance of Current Vector Alignment in Establishing the Resonant Frequency of Small Space-Filling Wire Antennas. *IEEE Ant Wireless Propagation Lett* Vol. 2, 2003, pp. 201–204.

Bijumon, P.V. et al. T-Strip-Fed High-Dielectric Resonator Antenna for Broadband Applications. *Microwave Optical Tech Lett* Vol. 47, 5 Nov. 2005, pp. 226–228.

Birchfield, J.L., and Free, W.R. Dielectrically Loaded Short Antennas. *Trans IEEE* Vol. AP-22, May 1974, pp. 471–472.

Bode, H.W. *Network Analysis and Feedback Amplifier Design*. D. Van Nostrand Co., 1945.

Boyer, J.M., Hula-Hoop Antennas: A Coming Trend? *Electronics* 11 Jan. 1963, pp. 44–46.

Breakall, J.K. et al. A Novel Short AM Monopole Antenna with Low-Loss Matching System. *Proc IEEE Broadcast Tech Symp Washington DC*, 2002.

Breakall, J.K. et al. Testing and Results of a New, Efficient Low-Profile AM Medium Frequency Antenna System. *Proc NAB Broadcast Engineering Conf* 2003.

Brennan, P.V. Impedance Matching Method Using Passive Lossless Feedback. *Proc IEE*, Vol. 139H, Oct. 1992, pp. 397–400.

Bretones, A.R. et al. Time Domain Analysis of Dielectric-Coated Wire Antennas and Scatterers. *Trans IEEE* Vol. AP-42, June 1994, pp. 815–819.

Bulgerin, M.A. and Walters, A.B. *NOLC—Report 154*. 1954, pp. 67–83.

Burton, R.W. and King, R.W.P. Theoretical Considerations and Experimental Results for the Hula-Hoop Antenna. *Microwave J* Vol. 6, Nov. 1963, pp. 89–90.

Chaloupka, H. On the Frequency Bandwidth of Functionally Small Antennas. *Proc URSI Symp EM Theory* Aug. 1992, pp. 266–268.

Chang, T.-N. and Kuo, C.-C. Meander Antenna with Backside Tuning Stubs. *Trans IEEE* Vol. AP-53, April 2005, pp. 1274–1277.

Chatterjee, R., *Dielectric and Dielectric-Loaded Antennas*. John Wiley & Sons, 1985, Chap. 7.

Choo, H., Rogers, R.L., and Ling, H. Design of Electrically Small Wire Antennas Using a Pareto Genetic Algorithm. *Trans IEEE* Vol. AP-53, March 2005, pp. 1038–1046.

Chu, L.J. Physical Limitations of Omni-Directional Antennas. *J Appl Physics* Vol. 19, Dec. 1948, pp. 1163–1175.

Cohen, N. Fractal Antennas—Part 1. *Commun Q* Summer 1995, pp. 7–22.

Collin, R.E. Minimum Q of Small Antennas. *J EM Waves Appl* Vol. 12, 1998, pp. 1369–1393.

Collin, R.E. *Foundations for Microwave Engineering,* 2nd Ed. John Wiley & Sons, 2001.

Collin, R.E. and Rothschild, S. Evaluation of Antenna Q. *Trans IEEE* Vol. AP-12, Jan. 1964, pp. 23–27.

Copeland, JR. et al. Antennafier Arrays. *Trans IEEE* Vol. AP-12, March 1964, pp. 227–233.

Cormos, D. et al. Compact Dielectric Resonator Antenna for WLAN Applications. *Electronics Lett* Vol. 39, Apr.3, 2003, pp. 588–590.

Corum, J.F. *Toroidal Antenna*. U.S. Patent Number 4,622,558, 11 Nov. 1986.

Corum, J.F. *Electromagnetic Structure and Method*. U.S. Patent Number 4,751,515, 14 June 1988.

Czerwinski, W.P. On Optimizing Efficiency and Bandwidth of Inductively Loaded Antennas. *Trans IEEE* Vol. AP-13, Sept. 1965, pp. 811–812.

Czerwinski, W.P. On a Foreshortened Center-Fed Whip Antenna. *Trans IEEE* Vol. VC-15, Oct. 1966, pp. 33–40.

Deschamps, G.A. and Sichak, W. Microstrip Microwave Antenna. *Proc 1953 USAF Antenna R&D Symp, Allerton, IL*. Oct. 1953.

Dunlavy, J.H. Jr. *Wide Range Tunable Transmitting Loop Antenna*. U.S. Patent 3,588,905, June 1971.

Eshrah, I.A. et al. Theory and Implementation of Dielectric Resonator Antenna Excited by a Waveguide Slot. *Trans IEEE* Vol. 53, Jan. 2005a, pp. 483–494.

Eshrah, I.A. et al. Excitation of Dielectric Resonator Antennas by a Waveguide Probe: Modeling Technique and Wide-Band Design. *Trans IEEE* Vol. 53, March 2005b, pp. 1028–1037.

Esselle, K.P. and Stuchly, S.S. Pulse-Receiving Characteristics of Resistively Loaded Dipole Antennas. *Trans IEEE* Vol. AP-38, Oct. 1990, pp. 1677–1683.

Fan, Z. and Antar, Y.M.M. Slot-Coupled DR Antenna for Dual-Frequency Operation. *Trans IEEE* Vol. AP-45, Feb. 1997, pp. 306–308.

FANO, R.M. Theoretical Limitations of the Broadband Matching of Arbitrary Impedances. *J Franklin Institute* Vol. 249, Feb. 1950a, pp. 139–154.

FANO, R.M. A Note on the Solution of Certain Approximation Problems in Network Synthesis. *J Franklin Institute* Vol. 249, March 1950b, pp. 189–205.

FANSON, P.L. AND CHEN, K.-M. Modification of Antenna Radiating Characteristics with Multi-Impedance Loading. *Trans IEEE* Vol. AP-21, Sept. 1973, pp. 715–721.

FANSON, P.L. AND CHEN, K.-M. Instabilities and Resonances of Actively and Passively Loaded Antennas. *Trans IEEE* Vol. AP-22, March 1974, pp. 344–347.

FANTE, R.L. Quality Factor of General Ideal Antennas. *Trans IEEE* Vol. AP-17, March 1969, pp. 151–155.

FENWICK, R.C. A New Class of Electrically Small Antennas. *Trans IEEE* Vol. AP-13, May 1965, pp. 379–383.

FLACHENECKER, G. AND MEINKE, H.R. Active Antennas with Transistors. *Can Int Electronics Conf Rec* Sept. 1967, pp. 142–143.

FOSTER, R.M. A Reactance Theorem. *BSTJ* Vol. 3, April 1924, pp. 259–267.

FOURNIER, M. AND POMERLEAU, A. Experimental Study of an Inductively Loaded Short Monopole Antenna. *Trans IEEE* Vol. VT-27, Feb. 1978, pp. 1–6.

FRANCAVILLA, L.A. et al. Mode-Matching Analysis of Top-Hat Monopole Antennas Loaded with Radially Layered Dielectric. *Trans IEEE* Vol. AP-47, Jan. 1999, pp. 179–185.

FRIEDMAN, C.H. Wide-Band Matching of a Small Disk-Loaded Monopole. *Trans IEEE* Vol. AP-33, Oct. 1985, pp. 1142–1148.

FROST, A.D. Parametric Amplifier Antenna. *Proc IRE* Vol. 48, June 1960, pp. 1163–1164.

FROST, A.D. Parametric Amplifier Antenna. *Trans IEEE* Vol. AP-12, March 1964, pp. 234–235.

FUJIMOTO, K. et al. *Small Antennas.* Research Studies Press, Wiley, 1987, Chap. 3.

GALEJS, J. Dielectric Loading of Electric Dipole Antennas. *J Res NBS* Vol. 66D, Sept.–Oct. 1962, pp. 557–562.

GALEJS, J. Small Electric and Magnetic Antennas with Cores of a Lossy Dielectric. *J Res NBS* Vol. 67D, July–Aug. 1963, pp. 445–451.

GEYI, W. Physical Limitations of Antenna. *Trans IEEE* Vol. AP-51, Aug. 2003a, pp. 2116–2123.

GEYI, W. A Method for the Evaluation of Small Antenna Q. *Trans IEEE* Vol. AP-51, Aug. 2003b, pp. 2124–2129.

GEYI, W., JARMUSZEWSKI, P., AND QI, Y. The Foster Reactance Theorem for Antennas and Radiation Q. *Trans IEEE* Vol. AP-48, March 2000, pp. 401–408.

GLISSON, A.W., KAJFEZ, D., AND JAMES, J. Evaluation of Modes in Dielectric Resonators Using a Surface Integral Equation Formulation. *Trans IEEE* Vol. MTT-31, Dec. 1983, pp. 1023–1029.

Goubau, G. Multi-Element Monopole Antennas. *Proc Workshop on Elec Small Ant* USARO, 6–7 May 1976, Durham, N. Carolina, pp. 63–67, AD-A031-845.

González-Arbesú, J.M., Blanch, S., and Romeu, J. Are Space-Filling Curves Efficient Small Antennas?. *IEEE Ant Wireless Propagation Lett* Vol. 2, 2003, pp. 147–150.

Grimes, C.A. and Grimes, D.M. A Clarification and Extension of Bandwidth and Q of Antennas Radiating Both TE and TM Modes. *Trans IEEE* Vol. EMC-38, May 1996, pp. 201–202.

Grimes, C.A. et al. Time-Domain Measurement of Antenna Q. *Microwave Optical Tech Lett* Vol. 25, 20 April 2000a, pp. 95–100.

Grimes, C.A. et al. Characterization of a Wideband, Low-Q, Electrically Small Antenna. *Microwave Optical Tech Lett* Vol. 27, 5 Oct. 2000b, pp. 53–58.

Grimes, D.M. Miniaturized Resonant Antenna Using Ferrites. *J Appl Physics* Vol. 29, March 1958, pp. 401–402.

Grimes, D.M. and Grimes, C.A. *Resonant Antenna*. U.S. Patent, 4,809,009, 28 Feb. 1989.

Grimes, D.M. and Grimes, C.A. Bandwidth and Q of Antennas Radiating TE and TM Modes. *Trans IEEE* Vol. EMC-37, May 1995, pp. 217–226.

Grimes, D.M. and Grimes, C.A. Power in Modal Radiation Fields: Limitations of the Complex Poynting Theorem and the Potential for Electrically Small Antennas. *J EM Waves Appl* Vol. 11, 1997, pp. 1721–1747.

Grimes, D.M. and Grimes, C.A. Radiation Q of Dipole-Generated Fields. *Radio Sci* Vol. 34, March–April 1999, pp. 281–296.

Grimes, D.M. and Grimes, C.A. Minimum Q of Electrically Small Antennas: A Critical Review. *Microwave Optical Tech Lett* Vol. 28, 5 Feb. 2001, pp. 172–177.

Grover, F.W. *Inductance Calculations.* Dover, 1946.

Guertler, R.J.F. Impedance Transformation in Folded Dipoles. *Proc IRE* Vol. 38, Sept 1950, pp. 1042–1047.

Guertler, R.J.F. Isotropic Transmission-Line Antenna and Its Toroid-Pattern Modification. *Trans IEEE* Vol. AP-25, May 1977, pp. 386–392.

Guillemin, E.A. *Communications Network*, *Vol. 2*. John Wiley & Sons, 1935, Chapter V.

Guterman, J., Moreira, A.A., and Peixeiro, C. Microstrip Fractal Antennas for Multistandard Terminals. *IEEE Ant Wireless Propagation Lett* Vol. 3, 2004, pp. 351–354.

Halbjörner, P. Electrically Small Unbalanced Four-Arm Wire Antenna. *Trans IEEE* Vol. AP-52, June 2004, pp. 1424–1428.

Hansen, R.C. Formulation of Echelon Dipole Mutual Impedance for Computer. *Trans IEEE* Vol. AP-20, Nov. 1972, pp. 780–781.

HANSEN, R.C. Efficiency and Matching Tradeoffs for Inductively Loaded Short Antennas. *Trans IEEE* Vol. COM-23, April 1975a, pp. 430–435.

HANSEN, R.C. Optimum inductive Loading of Short Whip Antennas. *Trans IEEE* Vol. VT-24, May 1975b, pp. 21–29.

HANSEN, R.C. Fundamental Limitations in Antennas. *Proc IEEE* Vol. 69, Feb. 1981, pp. 170–182.

HANSEN, R.C. Folded and T-Match Dipole Transformation Ratio. *Trans IEEE* Vol. AP-30, Jan. 1982, pp. 161–162.

HANSEN, R.C. *Phased Array Antennas*, John Wiley & Sons, 1998, Section 5.4.3.

HANSEN, R.C. Resonant Contrawound Toroidal Helix Antenna. *Microwave Optical Tech Lett* Vol. 29, 20 June 2001, pp. 408–410.

HANSEN, R.C. Two-turn Contrawound Toroidal Helix Antenna. *Microwave Optical Tech Lett* Vol. 33, 20 May 2002, pp. 251–252.

HANSEN, R.C. Comments on "An Analysis of the CWTHA's Resonance Currents and the Resulting Radiation Shapes". *Trans IEEE* Vol. AP-53, June 2005, p. 2132.

HANSEN, R.C. AND BURKE, M. Antennas with Magneto-Dielectrics. *Microwave Optical Tech Lett* Vol. 26, 20 July 2000, pp. 75–78.

HANSEN, R.C. AND RIDGLEY, R. Modes of the Contrawound Toroidal Helix Antenna. *Microwave Optical Tech Lett* Vol. 23, 20 Dec. 1999, pp. 365–368.

HANSEN, R.C. AND RIDGLEY, R.D. Fields of the Contrawound Toroidal Helix Antenna. *Trans IEEE* Vol. AP-49, Aug. 2001, pp. 1138–1141.

HARRINGTON, R.F. Field Computation by Moment Methods. *Macmillan*, 1968, pp. 10–81.

HARRINGTON, R.F. Effect of Antenna Size on Gain, Bandwidth, and Efficiency. *J Res NBS* Vol. 64D, Jan.–Feb. 1960, pp. 1–12.

HARRISON, C.W. Monopole with Inductive Loading. *Trans IEEE* Vol. AP-11, July 1963, pp. 394–400.

HARRISON, C.W. AND KING, R.W.P. Folded Dipoles and Loops. *Trans IRE* Vol. AP-9, March 1961, pp. 171–187.

HATELY, M.C., KABBARY, F.M., AND KHATTAB, M. An Operational MF Broadcast Antenna Using Poynting Vector Synthesis. *ICAP*, York, IEE Conf. Publ. 333, 1991, pp. 645–648.

HATFIELD, J.B. Magnetic Fields from Displacement Current Densities Generated by the Crossed Field Antenna. *IEEE Broadcast Tech Soc 50th Broadcast Symp* 28 Sept. 2000, pp. 1–3.

HATKE, G.F. Conditions for Unambiguous Source Location Using Polarization Diverse Arrays. *IEEE 27th Asilomar Conf* 1993, pp. 1365–1369.

HUJANEN, A. AND STEN, J.C.E. Bandwidth Limitations of Impedance Matched Ideal Dipoles. *Trans IEEE* Vol. AP-53, Oct. 2005, pp. 3236–3239.

Jaggard, D.L. On Fractal Electrodynamics. Chap. 6 in *Recent Advances in Electromagnetic Theory*, Kritikos, H.N. and Jaggard, D.L., Eds., Springer, 1990.

James, J.R. and Burrows, R.M. Resonance Properties of Dielectric-Loaded Short Unipoles. *Electronics Lett* Vol. 9, 12 July 1973, pp. 300–302.

James, J.R. and Henderson, A. Electrically Short Monopole Antennas with Dielectric or Ferrite Coatings. *Proc IEE* Vol. 125, Sept. 1978, pp. 793–803.

James, J.R., Schuler, A.J., and Binham, R.F. Reduction of Antenna Dimensions by Dielectric Loading. *Electronics Lett* Vol. 10, 27, June 1974, pp. 263–265.

Janapsatya, J. and Bialkowski, M.E. Reducing the Height of a Circular Array of Monopoles Using Top Hats and Dielectric Coatings. *Radio Sci* Vol. 39, RS3004, 2004.

Jung, J.-H. and Park, I. Electromagnetically Coupled Small Broadband Monopole Antenna. *IEEE Ant Wireless Propagation Lett* Vol. 2, 2003, pp. 349–351.

Kabbary, F.M., Hately, M.C., and Stewart, B.G. Maxwell's Equations and the Crossed-Field Antenna. *Electronics Wireless World*, March 1989, pp. 216–218.

Kabbary, F.M., Khattab, M., and Hately, M.C. Extremely Small High Power MW Broadcasting Antennas. *Int Broadcasting Convention*, 12–16 Sept. 1997, IEE Conf Publ 447, pp. 441–431.

Kabbary, F.M. et al. Four Egyptian MW Broadcast Crossed-Field-Antennas. *Proc NAB Conf Las Vegas* April 1999, pp. 235–241.

Kajfez, D., Glisson, A.W., and James, J. Computed Modal Field Distributions for Isolated Dielectric Resonators. *Trans IEEE* Vol. MTT-32, Dec. 1984, pp. 1609–1616.

Kalafus, R.M. On the Evaluation of Antenna Quality Factors. *Trans IEEE* Vol. AP-17, Nov. 1969, pp. 729–732.

Kanda, M. A Relatively Short Cylindrical Broadband Antenna with Tapered Resistive Loading for Picosecond Pulse Measurements. *Trans IEEE* Vol. AP-26, May 1978, pp. 439–447.

Kanda, M. Standard Antennas for Electromagnetic Interference Measurements and Methods to Calibrate Them. *Trans IEEE* Vol. EMC-36, Nov. 1994, pp. 261–273.

Kennedy, T.F., Long, S.A., and Williams, J.T. Modification and Control of Currents on Monopole Antennas Using Magnetic Bead Loading. *IEEE Ant Wireless Propagation Lett* Vol. 2, 2003, pp. 208–211.

King, R.W.P. et al. Transmission-Line Missile Antennas. *Trans IRE* Vol. AP-8, Jan. 1960, pp. 88–90.

King, R.W.P. and Smith, G.S. *Antennas in Matter—Fundamentals, Theory, and Applications*. MIT Press, 1981, Chap. 8.

Kishk, A.A., Glisson, A.W., and Junker, G.P. Study of Broadband Dielectric Resonator Antennas. *Antenna Applications Symposium, Allerton, IL*. 1999, pp. 45–68.

Kishk, A.A. et al. Conical Dielectric Resonator Antennas for Wide-Band Applications. *Trans IEEE* Vol. AP-50, April 2002, pp. 469–474.

Ko, C.C., Zhang, J., and Nehorai, A. Separation and Tracking of Multiple Broadband Sources with One Electromagnetic Vector Sensor. *Trans IEEE* Vol. AES-38, July 2002, pp. 1109–1116.

Kumar, A.V.P. et al. Microstripline Fed Cylindrical Dielectric Resonator Antenna for Dual-Band Operation. *Microwave Optical Tech Lett* Vol. 47, Oct. 20, 2005, pp. 150–153.

Kwon, D.-H. On the Radiation Q and the Gain of Crossed Electric ang Magnetic Dipole Moments. *Trans IEEE* Vol. AP-53, May 2005, pp. 1681–1687.

Lally, J.F. and Rouch, D.T. Experimental Investigation of the Broad-Band Properties of a Continuously Loaded Resistive Monopole. *Trans IEEE* Vol. AP-18, Nov. 1970, pp. 764–768.

Langford-Smith, F. *Radiotron Designer's Handbook*, 4th Ed. RCA, 1953, Chap. 10.

Lee, S.H. and Mei, K.K. Analysis of Zigzag Antennas. *Trans IEEE* Vol. AP-18, Nov. 1970, pp. 760–764.

Leeper, D.G. Isophoric Arrays-Massively Thinned Phased Arrays with Well-Controlled Sidelobes. *Trans IEEE* Vol. AP-47, Dec. 1999, pp. 1825–1835.

Leonhard, J. et al. Folded Unipole Antennas. *Trans IRE* Vol. AP-3, July 1955, pp. 111–116.

Leung, K.W. et al. Theory and Experiment of an Aperture-Coupled Hemispherical Dielectric Resonator Antenna. *Trans IEEE* AP-43, Nov. 1995, pp. 1192–1198.

Leung, K.W. et al. Excitation of Dielectric Resonator Antenna Using a Soldered-Through Probe. *Electronics Lett* Vol. 33, Feb. 27, 1997a, pp. 349–350.

Leung, K.W. et al. Bandwidth Enhancement of Dielectric Resonator Antenna by Loading a Low-Profile Dielectric Disk of Very High Permittivity. *Electronics Lett* Vol. 33, 24 April 1997b, pp. 725–726.

Leung, K.W. et al. Low-Profile Circular Disk DR Antenna of Very High Permittivity Excited by a Microstripline. *Electronics Lett* Vol. 33, 5 June 1997c, pp. 1004–1005.

Leung, K.W. et al. Circular-Polarized Dielectric Resonator Antenna Excited by Dual Conformal Strips. *Electronics Lett* Vol. 36, 16 March 2000, pp. 484–486.

Leung, K.W. and To, M.W. Slot-Coupled Dielectric Resonator Antenna Using a Proximity Feed on a Perpendicular Substrate. *Electronics Lett* Vol. 33, 25 Sept. 1997, pp. 1665–1666.

Li, B. and Leung, K.W. Strip-Fed Rectangular Dielectric Resonator Antennas with/without a Parasitic Patch. *Trans IEEE* Vol. AP-53, July 2005, pp. 2200–2207.

Liang, X. and Chia, M.Y.W. Multiband Characteristics of Two Fractal Antennas. *Microwave Optical Tech Lett* Vol. 23, Nov. 20, 1999, pp. 242–245.

Lin, C.C., Kuo, S.W., and Chuang, H.R. A 2.4-GHz Printed Meander-Line Antenna for USB-WLAN with Notebook-PC Housing. *IEEE Microwave Wireless Component Lett* Vol. 15, Sept. 2005, pp. 546–548.

Lin, C.J., Nyquist, D.P., and Chen, K.M. Short Cylindrical Antennas with Enhanced Radiation or High Directivity. *Trans IEEE* Vol. AP-18, July 1970, pp. 576–580.

Liu, G., Grimes, C.A., and Grimes, D.M. A Time-Domain Technique for Determining Antenna Q. *Microwave Optical Tech Lett* Vol. 21, 20 June 1999, pp. 395–398.

Long, S.A. McAllister, M.W., and Shen, L.C. The Resonant Cylindrical Dielectric Cavity Antenna. *Trans IEEE* Vol. AP-31, May 1983, pp. 406–412.

Luk, K.M. and Leung, K.W. *Dielectric Resonator Antennas.* Research Studies Press Ltd., 2003.

Maclean, T.S.M. and Ramsdale, P.A. Signal/Noise Ratio for Short Integrated Antennas. *Electronics Lett* Vol. 11, 6 Feb. 1975, pp. 62–63.

Maclean, T.S.M. and Rahman, F. Small Toroidal Antennas. *Electronics Lett* Vol. 14, 25 May 1978, pp. 339–340.

Maclean, T.S.M. and Saini, S.P.S. Efficiency and Signal/Noise Ratio of Short Linear Dipoles. *Electronics Lett* Vol. 17, 9 July 1981, pp. 492–494.

Mandelbrot, B.B. *Fractals: Form, Chance and Dimension*. W.H. Freeman, 1977.

Mandelbrot, B.B. *The Fractal Geometry of Nature*. W.H. Freeman, 1982.

Matthaei, G.L., Young, L., and Jones, E.M.T. *Microwave Filters, Impedance-Matching Networks, and Coupling Structures.* McGraw-Hill, 1964, Sections 4.09, 4.10.

McAllister, M.W. and Long, S.A. Resonant Hemispherical Dielectric Antenna. *Electronics Lett* Vol. 20, 2 Aug. 1984, pp. 657–659.

McAllister, M.W., Long, S.A., and Conway, G.L. Rectangular Dielectric Resonator Antenna. *Electronics Lett* Vol. 19, 17 March 1983, pp. 218–219.

McLean, J.S. The Application of the Method of Moments to the Analysis of Electrically-Small "Compound" Antennas. *EMC Symp Record* Aug. 1995, pp. 119–124.

McLean, J.S. A Re-Examination of the Fundamental Limits on the Radiation Q of Electrically Small Antennas. *Trans IEEE* Vol. AP-44, May 1996, pp. 672–676.

Merenda, J.T. *Radiation Synthesizer Systems and Methods.* U.S. Patent 6229494, 8 May 2001.

Middleton, W.M. *Reference Data for Engineers*, Section 4.20. Newnes-Butterworth-Heinemann, 2002.

Miron, D.B. A Study of the CTHA Based on Analytical Models. *Trans IEEE* Vol. AP-49, Aug. 2001, pp. 1130–1137.

Mongia, R.K. Half-Split Dielectric Resonator Placed on Metallic Plane for Antenna Applications. *Electronics Lett* Vol. 25, 30 March 1989, pp. 462–464.

Mongia, R.K. Theoretical and Experimental Resonant Frequencies of Rectangular Dielectric Resonators. *Proc IEE—H* Vol. 139, Feb. 1992, pp. 98–104.

Mongia, R.K. Reduced Size Metallized Dielectric Resonator Antennas. *IEEE AP Symp Dig* Vol. 35, 1997, pp. 2202–2205.

Mongia, R.K. and Bhartia, P. Dielectric Resonator Antennas–A Review and General Design Relations for Resonant Frequency and Bandwidth. *Intl J Microwave Millimeter-Wave Computer-Aided Engineering*, Vol. 4, 1994, pp. 230–247.

Mongia, R.K. and Ittipiboon, A. Theoretical and Experimental Investigations on Rectangular Dielectric Resonator Antennas. *Trans IEEE* Vol. AP-45, Sept. 1997, pp. 1348–1356.

Mongia, R.K., Ittipiboon, A., and Cuhaci, M. Measurement of Radiation Efficiency of Dielectric Resonator Antennas. *IEEE Microwave Guided Wave Lett* Vol. 4, March 1994a, pp. 80–82.

Mongia, R.K. et al. Accurate Measurement of Q-Factors of Isolated Dielectric Resonators. *Trans IEEE* Vol. MTT-42, Aug. 1994b, pp. 1463–1467.

Moon, J.-I., and Park, S.-O. Dielectric Resonator Antenna for Dual-Band PCS/IMT-2000. *Electronics Lett* Vol. 36, 8 June 2000, pp. 1002–1003.

Mridula, S. et al. Characteristics of a Microstrip-Excited High-Permittivity Rectangular Dielectric Resonator Antenna. *Microwave Optical Tech Lett* Vol. 40, Feb. 20, 2004, pp. 316–318.

Nakano, H. et al. A Curl Antenna. *Trans IEEE* Vol. AP-41, Nov. 1993, pp. 1570–1575.

Nannini, C. et al. A Dual-Frequency Dielectric Resonator Antenna. *Microwave Optical Tech Lett* Vol. 38, 5 July 2003, pp. 9–10.

Overfelt, P.L. Electric Lines of Force of an Electrically Small Dipole-Loop Antenna Array. *Trans IEEE* Vol. AP-46, March 1998, pp. 451–456.

Park, R.L. *Voodoo Science*. Oxford Univ. Press, 2000.

Paul, B. et al. A Compact Very-High-Permittivity Dielectric-Eye Resonator Antenna for Multiband Wireless Applications. *Microwave Optical Tech Lett* Vol. 43, 20 Oct. 2004, pp. 118–121.

Pertl, F.A., Smith, J.E., and Nutter, R.S. An Analysis of the CTHAs Resonance Currents and the Resulting Radiation Shapes. *Trans IEEE* Vol. AP-53, Jan. 2005, pp. 377–385.

Pinhas, S. and Shtrikman S. Comparison between Computed and Measured Bandwidth of Quarter-Wave Microstrip Radiators. *Trans IEEE* Vol. AP-36, Nov. 1988, pp. 1615–1616.

Polk, C. Resonance and Supergain Effects in Small Ferromagnetically or Dielectrically Loaded Biconical Antennas. *Trans IRE* Vol. AP-7, Dec. 1959, pp. S414–S423.

Popović, B.D., Djordjević, A.R., and Kirćanski, N.M. Simple Method for Analysis of Dielectric-Coated Wire Antennas. *Radio Electronic Engineer* Vol. 51, March 1981, pp. 141–145.

Prasad, S. and King, R.W.P. Experimental Study of Inverted L-, T-, and Related Transmission Line Antennas. *J Res NBS* Vol. 65D, Sept.–Oct. 1961, pp. 449–454.

Puente, C. et al. Fractal Multiband Antenna Based on the Sierpinski Gasket. *Electronics Lett* Vol. 32, 4 Jan. 1996, pp. 1–2.

Puente, C. et al. Small but Long Koch Fractal Monopole. *Electronics Lett* Vol. 34, 8 Jan. 1998, pp. 9–10.

Puente, C. et al. On the Behavior of the Sierpinski Multiband Fractal Antenna. *Trans IEEE* Vol. AP-46, April 1998, pp. 517–524.

Rao, B.L.J., Ferris, J.E., and Zimmerman, W.E. Broadband Characteristics of Cylindrical Antennas with Exponentially Tapered Capacitive Loading. *Trans IEEE* Vol. AP-17, March 1969, pp. 145–151.

Rashed, J. and Tai, C.-T. A New Class of Resonant Antennas. *Trans IEEE* Vol. AP-39, Sept. 1991, pp. 1428–1430.

Richmond, J.H. and Newman, E.H. Dielectric Coated Wire Antennas. *Radio Sci* Vol. 11, Jan. 1976, pp. 13–20.

Rosa, E.B. and Grover, F.W. Formulas and Tables for the Calculation of Mutual and Self-Inductance. *NBS Circular* 169, 18 Dec. 1916, p. 135.

Schelkunoff, S.A. and Friis, H.T. *Antennas—Theory and Practice.* John Wiley & Sons, 1952, Section 10.14.

Schroeder, K.G. The Complementary Pair—A Broadband Element Group for Phased Arrays. *IEEE AP Conv Rec* 1964, pp. 128–133.

Schroeder, K.G. *Complementary Pair Antenna Element Groups.* U.S. Patent 3,449,751, 10 June 1969.

Schroeder, K.G. and Soo Hoo, K.M. Electrically Small Complementary Pair (ESCP) with Interelement Coupling. *Trans IEEE* Vol. AP-24, July 1976, pp. 411–418.

Shen, L.-C. An Experimental Study of the Antenna with Nonreflecting Resistive Loading. *Trans IEEE* Vol. AP-15, Sept. 1967, pp. 606–611.

Shen, L.-C. and Wu, T.T. Cylindrical Antenna with Tapered Resistive Loading. *Radio Sci* Vol. 2, Feb. 1967, pp. 191–201.

Simpson, T.L. The Disk Loaded Monopole Antenna. *Trans IEEE* Vol. AP-52, Feb. 2004, pp. 542–550.

Sinha, B.P. and Saoudy, S.A. Rigorous Analysis of Finite Length Insulated Antenna in Air. *Trans IEEE* Vol. AP-38, Aug. 1990, pp. 1253–1258.

Smith, G.S. Proximity Effect in Systems of Parallel Conductors. *J Appl Phys* Vol. 43, May 1972, pp. 2196–2203.

Smith, D.L. The Trap-Loaded Cylindrical Antenna. *Trans IEEE* Vol. AP-23, Jan. 1975, pp. 20–27.

Smith, M.S. Properties of Dielectrically Loaded Antennas. *Proc IEE* Vol. 124, Oct. 1977, pp. 837–839.

Smith, M.S. Conventional Explanation for "Crossed Field Antenna". *Electronics Lett* Vol. 28, 13 Feb. 1992, pp. 360–361.

Snyder, R.D. *Broadband Antennae Employing Coaxial Transmission Line Sections.* U.S. Patent 4479130, 23 Oct. 1984a.

Snyder, R.D. The Snyder Antenna. *RF Design* Sept./Oct. 1984b, pp. 49–51.

Soler, J., Puente, C., and Puerto, A. A Dual-Band Bidirectional Multilevel Monopole Antenna. *Microwave Optical Tech Lett* Vol. 34, Sept. 20, 2002, pp. 445–448.

Stark, P.A. *Introduction to Numerical Methods.* MacMillan, 1970, p. 130.

Stutzman, W.L. and Thiele, G.A. *Antenna Theory and Design*. John Wiley & Sons, 1981.

Sung, Y., Ahn, C.S., and Kim, Y.S. Microstripline Fed Dual-Frequency Dielectric Resonator Antenna. *Microwave Optical Tech Lett* Vol. 42, 5 Sept. 2004, pp. 388–390.

Taga, T. Analysis of Planar Inverted-F Antennas and Antenna Design for Portable Radio Equipment. Chap. 5 in *Analysis, Design, And Measurement of Small And Low-profile Antennas*. Hirasawa, K. and Haneishi, M. Eds. Artech House, 1992.

Taga, T. and K. Tsunekawa. Performance Analysis of a Built-In Planar Inverted-F Antenna for 800 MHz Band Portable Radio Units. *Trans IEEE* Vol. SAC-5, June 1987, pp. 921–929.

Taylor, C.D. Cylindrical Transmitting Antenna: Tapered Resistivity and Multiple Impedance Loadings. *Trans IEEE* Vol. AP-16, March 1968, pp. 176–179.

Terman, F.E. *Radio Engineers' Handbook*. McGraw-Hill, 1943, Section 2.

Thiele, G.A., Detweiler, P.L., and Penno, R.P. On the Lower Bound of the Radiation Q for Electrically Small Antennas. *Trans IEEE* Vol. AP-51, June 2003, pp. 1263–1269.

Trainotti, V. Short Medium Frequency AM Antennas. *Trans IEEE Broadcasting* Vol. 47, Sept. 2001, pp. 263–284.

Tsuji, M. et al. Analytical and Experimental Considerations on the Resonant Frequency and the Quality Factor of Dielectric Resonators. *Trans IEEE* Vol. MTT-11, Nov. 1982, pp. 1952–1958.

Turner, E.M. and Richard, D.J. Development of an Electrically Small Broadband Antenna. *Proc 18th Symp USAF Ant Res Dev Prog* Oct. 1968, Allerton, IL.

Underhill, M.J. and Harper, M. Simple Circuit Model of Small Tuned Loop Antenna Including Observable Environmental Effects. *Electronics Lett* Vol. 38, 29 Aug. 2002, pp. 1006–1008.

Underhill, M.J. and Harper, M. Small Antenna Input Impedances That Contradict Chu-Wheeler Q Criterion. *Electronics Lett* Vol. 39, 29 May 2003, pp. 828–830.

Vinoy, K.J. et al. Hilbert Curve Fractal Antenna: A Small Resonant Antenna for VHF/UHF Applications. *Microwave Optical Tech Lett* Vol. 29, 20 May 2001, pp. 215–219.

Wait, J.R. Receiving Propagationerties of a Wire Loop with a Spheroidal Core. *Can J Tech* Vol. 31, Jan. 1953a, pp. 9–14.

Wait, J.R. The Receiving Loop with a Hollow Prolate Spheroidal Core. *Can J Tech* Vol. 31, June 1953b, pp. 132–137.

Walser, R.M. Electromagnetic Metamaterials. In *Complex Mediums II: Beyond Linear Isotropic Dielectrics*, Lakhtakia, A. Werner, S.W. Hodgkinson, I.J., Eds. Proc SPIE Vol. 4467, 2001, pp. 1–15.

Wanselow, R.D. and Milligan, D.W. A Compact, Low Profile, Transmission Line Antenna–Tunable over Greater than Octave Bandwidth. *Trans IEEE* Vol. AP-14, Nov. 1966, pp. 701–707.

Wegstein, J. Algorithm 2. *CACM* Vol. 3, Issue 2, 1960, p. 74.

Wheeler, H.A. Fundamental Limitations of Small Antennas. *Proc IRE* Vol. 35, Dec. 1947, pp. 1479–1484.

Wheeler, H.A. The Spherical Coil as an Inductor, Shield, or Antenna. *Proc IRE*, Vol. 46, Sept. 1958, pp. 1595–1602.

Wheeler, H.A. Transmission-Line Propagationerties of Parallel Strips Separated by a Dielectric Sheet. *Trans IEEE* Vol. MTT-13, Mar. 1965, pp. 172–185.

Wheeler, H.A. Small Antennas. *Trans IEEE* Vol. AP-23, July 1975, pp. 462–469.

Wong, J.L. and King, H.E. Height-Reduced Meander Zigzag Monopoles with Broad-Band Characteristics. *Trans IEEE* Vol. AP-34, May 1986, pp. 716–717.

Wu, T.T. and King, R.W.P. The Cylindrical Antenna with Nonreflecting Resistive Loading. *Trans IEEE* Vol. AP-13, May 1965, pp. 369–373; correction Nov. 1965 p. 998.

Yaghjian, A.D. and Best, S.R. Impedance, Bandwidth, and Q of Antennas. *Trans IEEE* Vol. AP-53, April 2005, pp. 1298–1324.

Zhu, J. and Engheta, N. Peano Antennas. *IEEE Ant Wireless Propagation Lett* Vol. 3, 2004, pp. 71–74.

Zhu, J., Hoorfar, A., and Engheta, N. Bandwidth, Cross-Polarization, and Feed-Point Characteristics of Matched Hilbert Antennas. *IEEE Ant Wireless Propagation Lett* Vol. 2, 2003, pp. 2–5.

Ziolkowski, R.W. and Kipple, A.D. Application of Double Negative Materials to Increase the Power Radiated by Electrically Small Antennas. *Trans IEEE* Vol. AP-51, Oct. 2003, pp. 2626–2640.

AUTHOR INDEX

Chapter 2

Superdirective Antennas

2.1 HISTORY AND MOTIVATION

A useful operational definition of antenna array superdirectivity (formerly called supergain) is directivity higher than that obtained with the same array length and elements uniformly excited (constant amplitude and linear phase). Superdirectivity applies in principle to ESA, to apertures, to arrays of isotropic elements, and to actual antenna arrays composed of nonisotropic elements such as dipoles, slots, and patches. Small dipoles and loops are superdirective; their directivity remains at 1.5 as size decreases. But their efficiency also decreases. Excessive array superdirectivity inflicts major problems in low radiation resistance (hence low efficiency), sensitive excitation and position tolerances, and narrow bandwidth. It is important to distinguish between directivity and gain. Gain as used in this book follows the antenna industry definition: Gain includes the effects of both losses (conductor and dielectric) and impedance mismatch. The IEEE and textbook definition, where only loss is included, is unrealistic and of little use; directivity includes neither loss nor impedance match. Thus the gain of a superdirective antenna may be low.

Taylor (1948) was one of the first to use the term "superdirectivity"; supergain should include efficiency, which in many cases would negate the directivity increase. He proposed a physical explanation of superdirectivity in terms of spherical modes and their cutoff due to dimensions. Taylor (1955) defined a most useful parameter: superdirective ratio (SDR). This is the ratio of array (or aperture) directivity to the directivity that would be obtained if the amplitude(s) were uniform, and the phase constant or progressive. It is the ratio of radiated power plus reactive power to radiated power, which for a broadside line source is:

$$\mathrm{SDR} = \frac{\displaystyle\int_{-\infty}^{\infty} \lceil f(u) \rceil^2 \, du}{\displaystyle\int_{-\pi L/\lambda}^{\pi L/\lambda} \lceil f(u) \rceil^2 \, du} \tag{2.1}$$

where $u = (L/\lambda)\sin\theta$.

Electrically Small, Superdirective, and Superconducting Antennas, by R. C. Hansen.

For other than broadside, the limits in the denominator change. For a long uniform amplitude line source the broadside SDR = 1, whereas for endfire SDR = 2. Values of SDR for 10λ uniform amplitude line sources are given by Stutzman and Thiele (1998):

broadside	SDR = 1.01
endfire	2.01
Hansen–Woodyard	8.23

Because Q may be expressed as the ratio of reactive power to radiated power,

$$Q = \frac{\displaystyle\int_{-\infty}^{-\pi L/\lambda} \lceil f(u) \rceil^2 \, du + \int_{\pi L/\lambda}^{\infty} \lceil f(u) \rceil^2 \, du}{\displaystyle\int_{-\pi L/\lambda}^{\pi L/\lambda} \lceil f(u) \rceil^2 \, du} \tag{2.2}$$

These two equations give SDR = 1 + Q.

Superdirectivity is a mature technical area, but many newer researchers have not been exposed to its capabilities and limitations. Thus this aims at providing a broad reference framework, as well as some more recent results. Probably the first work on this subject was due to Oseen, in 1922. The next work that appeared was dated 1938. A flurry of papers appeared around the World War II era, up to roughly 1960. Another burst of activity occurred from 1964 to 1974. Since then only a few papers have appeared. Details of these advances are given below.

2.2 MAXIMUM DIRECTIVITY

2.2.1 Apertures

The question arises whether a continuous aperture with amplitude and phase chosen appropriately can have an infinite directivity. Oseen (1922) discussed forming an arbitrarily narrow beam, analogous to the quantum mechanical "needle" radiation of Einstein, and the possibilities of superdirectivity. See Bloch et al. (1953, 1960) for a list of early references. Another early contributor was Franz (1943). Schelkunoff, in a classic paper (1943) on linear arrays, discussed, among other topics, array spacings less than λ/2, showing how equal spacing of the array polynomial zeros over that portion of the unit circle represented by the array gives superdirectivity. The field received wide publicity when La Paz and Miller (1943) purported to show that a given aperture would allow a maximum directivity. However, Bouwkamp and De Bruijn (1946) showed that they had made mathematical errors and that there was no limit on theoretical directivity. Thus the important theorem: A fixed aperture size can achieve (in theory) any desired directivity value. This theorem is now widely recognized, but the practical implications are less well known. Bloch et al. (1960) say that the theorem has been rediscovered several times; the practical limitations of superdirectivity occur as a surprise to systems engineers and others year after year!

Reid (1946) generalized the Hansen–Woodyard endfire directivity as $d \to 0$. The Bouwkamp and de Bruijn work was extended to a two-dimensional aperture by Riblet (1948). Kyle (1959) discussed transforming a linear superdirective distribution to a cylindrical distribution. Superdirective aperture design thus requires a constraint; see Section 2.3.

2.2.2 Arrays

2.2.2.1 Broadside Arrays of Fixed Spacing

An array with fixed length and number of elements represents a determinate problem. Clearly a maximum directivity exists. Uzkov (1946), and later Gilbert and Morgan (1955), showed that in the limit of zero element spacing the maximum directivity is:

$$D = \sum_{n=1}^{N-1} (2n+1)[P_n(\sin\theta)]^2 \tag{2.3}$$

The array has N elements, and broadside is $\theta = 0$. P_n is the Legendre Polynomial of order n. The broadside case is discussed next and the endfire case in Section 2.2.2.2.

Tai (1964) developed broadside array results starting with the mutual resistance series and then optimizing by setting derivatives to zero and evaluating the resulting matrix. He plotted directivity for $0 \le d/\lambda \le 2$ for isotropes, parallel dipoles, and collinear dipoles. For broadside in the $d = 0$ limit the Uzkov result is obtained:

$$D = \sum_{n=1}^{N-1} (2n+1)[P_n(0)]^2 \tag{2.4}$$

The Legendre Polynomial of argument 0 can be written as a product of factors (Burington, 1973); the result for maximum directivity is simply:

$$D \to \left(\frac{1 \bullet 3 \bullet 5 \bullet \bullet \bullet M}{2 \bullet 4 \bullet 6 \bullet \bullet \bullet (M-1)} \right), \quad \text{where } M = 2\,\text{AINT}\left(\frac{N+1}{2}\right) - 1 \tag{2.5}$$

The implicit function AINT provides the integer part. Here M is the number of odd elements or the number of even elements minus 1. Thus the result: 3- and 4-element arrays have the same limiting value, 5- and 6-element arrays have the same value, etc. This maximum directivity is plotted in Figure 2.1. The circles show the corresponding limiting directivity for Chebyshev arrays with 10 dB sidelobe ratio (SLR), and the squares are for 20 dB SLR. SLR is the ratio of main beam peak to highest sidelobe. The Chebyshev directivity is less, as the maximum directivity pattern does not have equal level sidelobes, and even in the case where there is only one sidelobe (backlobe), the Chebyshev result would be equal to the maximum value only if the sidelobe ratio were properly chosen. See Section 2.2 for a discussion of Chebyshev arrays.

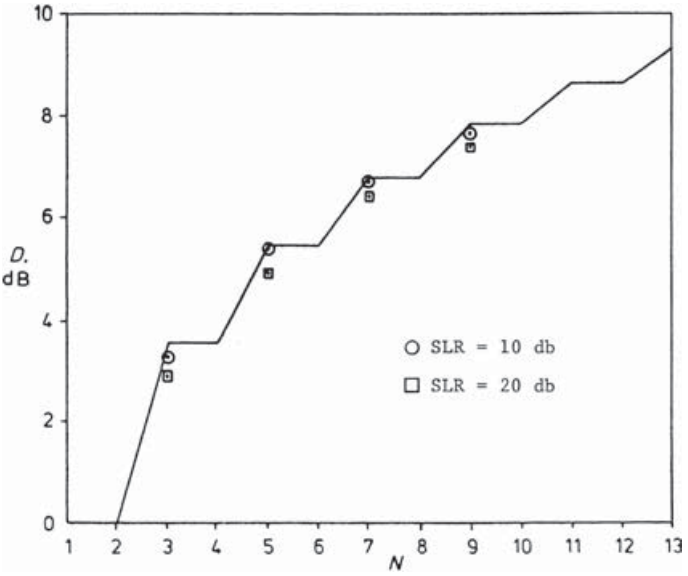

Figure 2.1 Maximum broadside directivity in zero spacing limit

Bloch, Medhurst, and Pool (1953) used a formulation involving mutual resistances (see Hansen, 1998; Section 2.4.3), but only very limited calculations were presented.

The maximum value of directivity can be found by using the Lagrange multiplier method (Sokolnikoff and Sokolnikoff, 1941). The directivity D of an array of isotropes at broadside can be written as:

$$D = \frac{\left(\sum_{n=1}^{N} A_n\right)^2}{\sum_{n=1}^{N}\sum_{m=1}^{N} A_n A_m \operatorname{sinc}[(n-m)2\pi d/\lambda]} \tag{2.6}$$

Here it is assumed that N array elements are isotropic and equally spaced by d. In the formulation in Equation 2.6, the array amplitudes are A_n and the sinc function $[(\sin x)/x]$ represents the mutual impedance between isotropic elements (Hansen, 1983) which is: 120 sinc kd. Although the directivity expression could be maximized directly, it is convenient to constrain the sum of the coefficients to unity, and then to minimize the denominator. The Lagrangian equations are:

$$2\sum_{n=1}^{N} A_n \operatorname{sinc}[(n-i)2\pi d/\lambda] - \beta = 0, \quad i = 1, 2, 3, \ldots, N;$$
$$\sum_{n=1}^{N} A_n = 1 \tag{2.7}$$

where β is the Lagrangian multiplier. Solving the first equation for $i = 1$ for β and substituting gives N equations in the unknown coefficients for an N-element array. These are easily solved by using simultaneous equation computer subroutines with multiple precision as needed. These were solved by hand for $N = 3, 5, 7$ by Pritchard (1953). Hansen (1983) compares the maximum directivity of small arrays with the uniform amplitude directivity versus element spacing (see Fig. 2.2). Above $d/\lambda = 0.5$, the two are very close. Also, some minor oscillations in the directivity curves have been smoothed out, as they are not important here. The coalescing of pairs of curves at zero spacing occurs because arrays of $2N$ and $2N - 1$ elements have the same number of degrees of freedom as previously mentioned.

To give an idea of the coefficients, input resistances, and pattern of a small array with modest superdirectivity, Table 2.1 shows the amplitude coefficients for an array of seven elements with quarter-wave spacing. Directivity is 5.21, and the pattern is the solid line in Figure 2.3. Also shown (dashed line) is the pattern of the same length array with half-wave spacing. Directivity of a corresponding uniform amplitude array is 3.64. Three of the input resistances in the table are negative; these

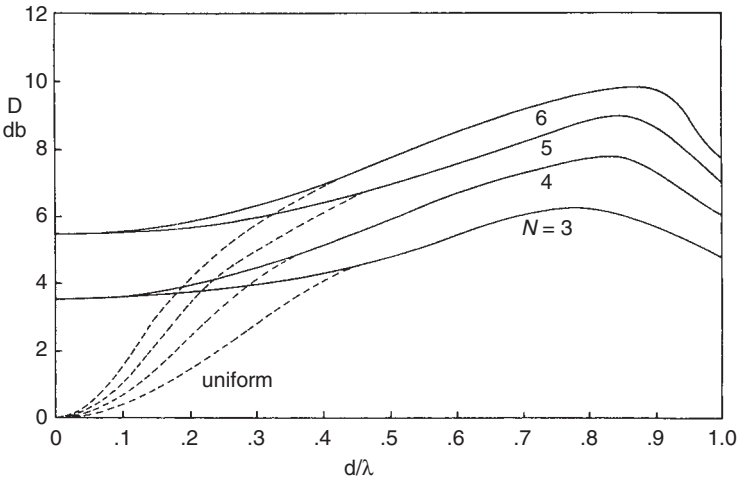

Figure 2.2 Maximum directivity for fixed spacing

Table 2.1 Seven-element superdirective array ($d = \lambda/4$)

Element Number	Amplitude	Resistance (ohms)
1	1.443	0.13299
2	–3.933	–0.04879
3	7.122	0.02694
4	–8.264	–0.02322
5	7.122	0.02694
6	–3.933	–0.04879
7	1.443	0.13299

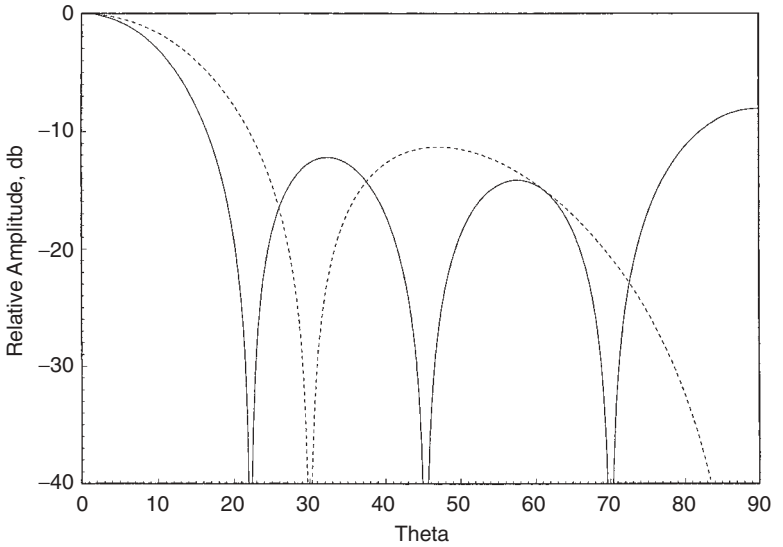

Figure 2.3 Maximum directivity array, $N = 7$, $d = \lambda/4$

elements have power flow in the reverse direction, a phenomenon not unusual in superdirective arrays.

An extreme example of a superdirective array was computed by Yaru (1951); this was a nine-element broadside array of isotropes with an overall length of $\lambda/4$. The design was a nominal Chebyshev pattern with 25 dB SLR. Because of the limitations of desk calculators circa 1950 the currents calculated by Yaru contain small errors, which were corrected (Jordan and Balmain, 1968). Correct values are:

$$I_1 = I_9 = 260{,}840.2268$$
$$I_2 = I_8 = -2{,}062{,}922.9994$$
$$I_3 = I_7 = 7{,}161{,}483.1266$$
$$I_4 = I_6 = -14{,}253{,}059.7032$$
$$I_5 = 17{,}787{,}318.7374$$

The net broadside current is 0.039! The superdirective ratio is 17.3!

Almost all papers have neglected the network used to feed the array elements, but Harrington (1965) sets up a matrix representing array element self- and mutual impedances. Directivity is a ratio of products of current and impedance matrices, which is then differentiated to find maximum D. An eigenvalue equation results with one nonzero eigenvalue. Unfortunately, no examples or calculations accompanied this work.

2.2.2.2 Endfire Arrays

The Uzkov–Gilbert–Morgan result for maximum endfire directivity as element spacing goes to zero is:

$$D = \sum_{n=0}^{N-1} (2n+1)[P_n(1)]^2 \tag{2.8}$$

Because $P_0\,(1) = 0$ and $P_n\,(1) = 1$ for $u > 0$, the directivity limit is:

$$D = \sum_{n=1}^{N-1} (2n+1) = N^2 \tag{2.9}$$

Although calculations are scarce, this result was validated by Tai (1964) and by Stearns (1961).

Endfire superdirectivity is produced by interference whereby the main beam is scanned into the invisible region where $|u| > \pi L/\lambda$ or $|\cos\theta_0| > 1$. This causes energy to be stored in the near-field, resulting in a large antenna Q.

W.W. Hansen and Woodyard (1938) developed an endfire line source with modest superdirectivity. This is of interest because the distribution can be sampled to get array excitations and because the amplitude is constant, a feature that is attractive for arrays. They observed that if the free-space phase progression along the aperture was increased, the space-factor power integral decreased faster than the peak value; thus the directivity increases up to a point. The endfire pattern, for a source of length L, is:

$$f(\theta) = \operatorname{sinc}\left(\frac{L}{2}(k\sin\theta - \beta)\right) \tag{2.10}$$

where β is the wavenumber over the aperture. Inverse directivity is proportional to:

$$\begin{aligned}\frac{1}{D} &\propto \frac{1}{\operatorname{sinc}^2\left(\frac{L}{2}(k-\beta)\right)} \int \operatorname{sinc}^2\left(\frac{L}{2}(k\sin\theta - \beta)\right)\cos\theta\, d\theta \\ &= \frac{1}{\operatorname{sinc}^2(\phi/2)}\left(\frac{\pi}{2} + \mathrm{Si}\phi + \frac{\cos\phi - 1}{\phi}\right)\end{aligned} \tag{2.11}$$

Here Si is the Sine Integral, and $\phi = L\,(k - \beta)$, the additional phase along the aperture (in addition to the progressive endfire phase). Maximum directivity of 7.2143 L/λ was determined to occur for $\phi = 2.922$ radians. In many books it is carelessly stated that π extra radians of phase are needed, but there is no physical reason for this; a better approximation to 2.922 is 3. Directivity increase over normal endfire is 2.56 dB, and the sidelobe ratio is 9.92 dB. The distribution is suitable for long arrays; for short arrays a computer optimization of phase is recommended; see Hansen (1992). A modest improvement was made by Goward (1947) by adjusting the endfire source amplitude.

The Hansen–Woodyard distribution is endfire. In general, the maximum directivity does not occur there. The most general solution for uniform amplitude would allow any element phases needed to maximize directivity. Such a solution could be formally realized for a given number of elements and spacing, but the equations would require a numerical solution. A slightly simpler problem was worked by Bach (1970); he started with a uniform-amplitude array of isotropic elements that was

phased to produce a main beam at θ_0. The interelement phase factor is $\delta = kd \sin \theta_0$, and the directivity is:

$$D = \frac{N}{1 + \frac{2}{N}\sum_{n=1}^{N-1}(N-n)\text{sinc}(nkd)\cos(n\delta)} \tag{2.12}$$

Calculations were made for 2-, 3-, 4-, and 10-element arrays for all beam angles, and for spacings up to λ. Figure 2.4 shows the results for 2- and 3-element arrays, and Figure 2.5 is for 4- and 10-element arrays. Figure 2.5 is striking in that high directivity occurs along a line roughly for $kd + \delta = 0$, or $\theta_0 = -\pi/2$, with peak directivity near endfire at λ spacing. Along the line roughly for $kd = \delta + 2\pi$ directivity is changing rapidly, perhaps owing to appearance of another lobe. Directivity values are shown at θ_0, but in some cases a "sidelobe" may have higher amplitude. Thus even for uniform amplitude an array is complex.

Lo and colleagues (1966) formulated maximum endfire directivity by setting derivatives of the array polynomial to zero. They compare D for a 10-element array of isotropes for four cases: D(U)—uniform amplitude, progressive endfire phase;

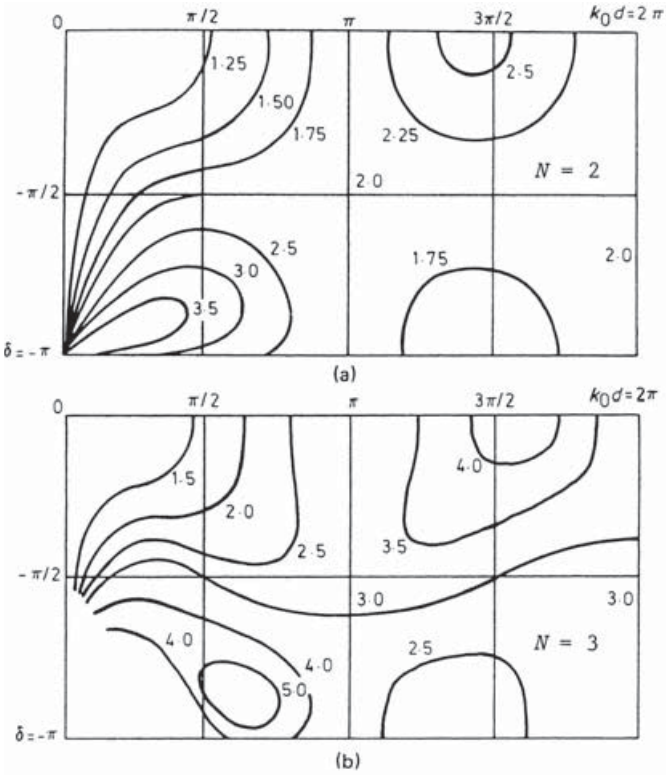

Figure 2.4 Uniform array directivity, $N = 2$ and 3. Courtesy of Bach, H. Directivity of Basic Linear Arrays. *Trans IEEE* Vol. AP-18, Jan. 1970, pp. 107–110.

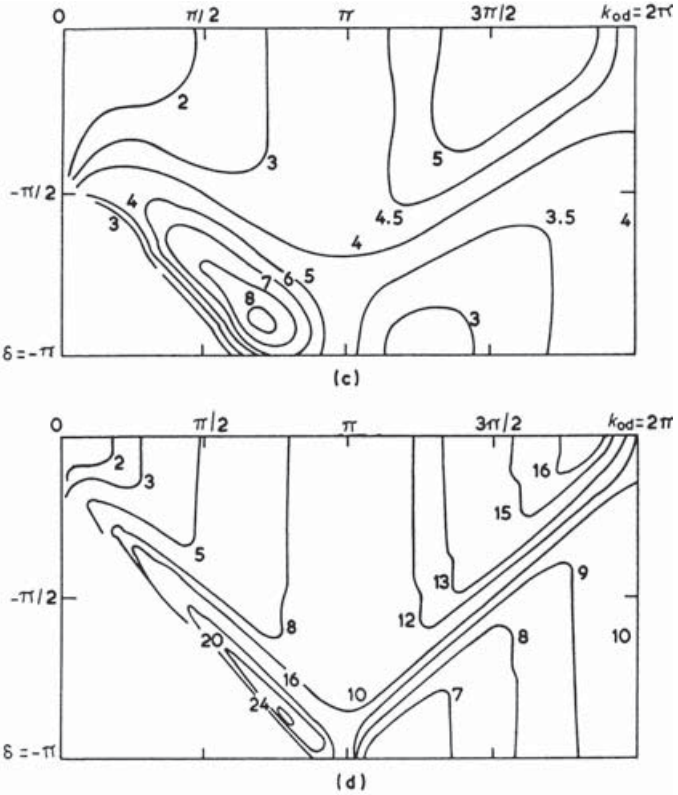

Figure 2.5 Uniform array directivity, $N = 4$ and 10. Courtesy of Bach, H. Directivity of Basic Linear Arrays. *Trans IEEE* Vol. AP-18, Jan. 1970, pp. 107–110.

D(OC)—amplitude optimized, progressive endfire phase; D(HW)—Hansen–Woodyard; $D(O)$—amplitude and phase optimized. Figure 2.6 shows results; for $d \leq \lambda/4$, which is the normal endfire range, the Hansen–Woodyard gives better directivity than the uniform amplitude or the optimized amplitude. Of course, the fully optimized case gives directivity equal to N^2 in the $d = 0$ limit. Note that Figure 2.6 (Lo, 1988) is a correction of Figure 4 of Lo et al. (1966). With the high directivity of D(O) goes severe bandwidth and tolerance problems; see Section 2.4.1.

Cheng and Tseng (1965) optimized directivity by using the Hermitian quadratic forms ratio; their calculations for an eight-element endfire array are not useful as the element spacing was $>\lambda/4$, thereby producing additional main lobes.

A special case of an endfire dipole array was investigated by Bacon and Medhurst (1969). Here four unequally spaced dipoles were used, with one dipole fed. Mutual resistances were used, with the spacings optimized. Array lengths of 0.5λ, 0.6λ, and 0.7λ were used. It was necessary to couple dipole 2 to dipole 4 (dipole 1 is fed). This configuration gave a maximum directivity of 19.7, with an overall length of $\lambda/2$. From the feed end spacings were 0.05λ, 0.25λ, and 0.20λ. A typical Yagi–Uda of 0.5λ length will have directivity of about 5 (Hansen, 2002). Hansen–

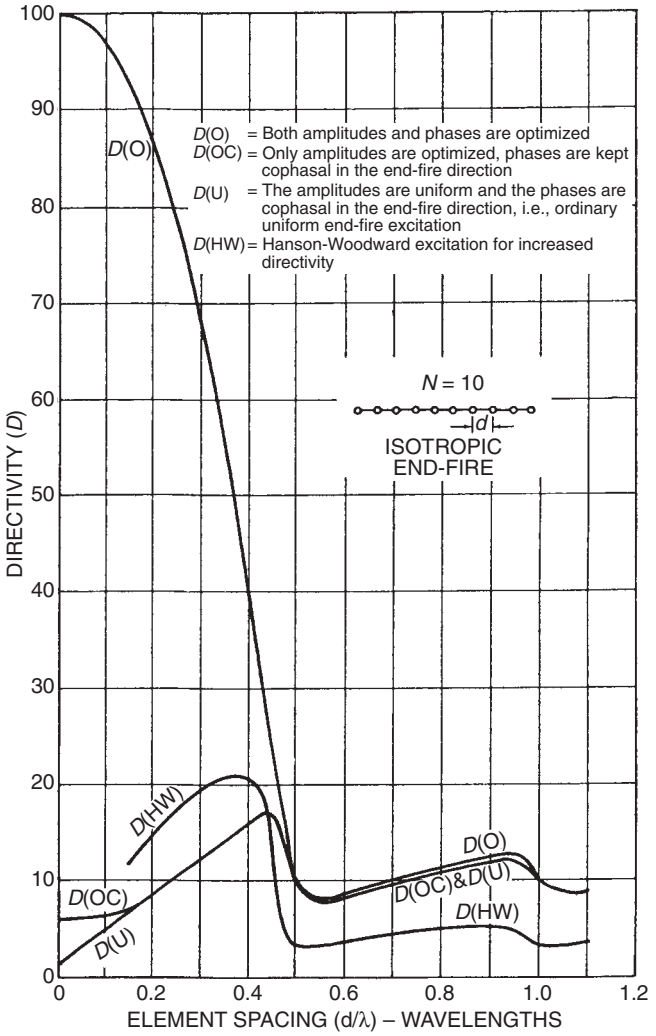

Figure 2.6 Linear endfire array directivity; various excitations. Courtesy of Lo, Y.T. Array Theory. Chapter 11 in *Antenna Handbook*, Lo, Y.T. and Lee, S.W., Eds. Van Nostrand, 1988.

Woodyard directivity would be 1.8 $L/\lambda = 3.6$. The superdirectivity ratio of 10.7 is accompanied by tight tolerances and a small input resistance.

Seeley (1963a, 1963b) investigated arrays of 2 and 3 loops; phasing was used to steer nulls. As expected, tolerances were tight.

2.3 CONSTRAINED SUPERDIRECTIVITY

To avoid impractical values of bandwidth, tolerances, and efficiency, it is useful to constrain the optimization process. Constraints can involve SDR, sidelobe level, Q,

tolerance, or efficiency. Probably the simplest, and most investigated, is a sidelobe constraint.

2.3.1 Dolph–Chebyshev Superdirectivity

The principles and design equations for arrays with equal-level sidelobes, Dolph–Chebyshev arrays, were covered in detail in Hansen (1998). However, Dolph's derivation (Dolph, 1946) and the formulas of Stegen are limited to $d \geq \lambda/2$. Riblet (1947) showed that this restriction could be removed, but only for N odd. For spacing below half-wave, the space factor is formed by starting at a point near the end of the Chebyshev ±1 region,[1] tracing the oscillatory region to the other end, then retracing back to the start end and up the monotonic portion to form the main beam half. Because the Mth-order Chebyshev has $M - 1$ oscillations, which are traced twice, and the trace from 0 to 1 and back forms the center sidelobe (in between the trace out and back), the space factor always has an odd number of sidelobes each side, or an even number of zeros. Hence only an odd number of elements can be formed into a Chebyshev array for $d < \lambda/2$. The pattern is given by:

$$T_M(a\cos\Psi + b), \qquad a = \frac{z_0 + 1}{1 - \cos kd} \tag{2.13}$$

$$b = \frac{z_0 \cos kd + 1}{\cos kd - 1} \tag{2.14}$$

where $\Psi = kd \sin\theta$. The value of z_0 is:

$$z_0 = \cosh\frac{\operatorname{arccosh} \mathrm{SLR}}{M} \tag{2.15}$$

The sidelobe ratio is:

$$\mathrm{SLR} = T_M(z_0) \tag{2.16}$$

Formulas have been developed by DuHamel (1953), Brown (1957, 1962), Salzer (1975), and Drane (1963, 1964). Those of Drane will be used here as they are suitable for computer calculation of superdirective arrays. The array amplitudes are:

$$A_n = \frac{\varepsilon_n}{4M}\sum_{m=0}^{M_1}\varepsilon_m\varepsilon_{M_2-m}T_m(x_n)[T_M(ax_n + b) + (-1)^n T_M(b - ax_n)] \tag{2.17}$$

where $\varepsilon_i = 1$ for $i = 0$ and is equal to 2 for $i > 0$; $x_n = \cos n\pi/M$. The integers M_1 and M_2 are, respectively, the integer parts of $M/2$ and $(M + 1)/2$. This result is valid for $d \leq \lambda/2$. Small spacings (highly superdirective arrays) may require multiple precision because of the subtraction of terms. Many arrays are half-wave spaced; for these the a and b reduce to:

[1] The exact starting point depends on N and kd.

$$a = \frac{1}{2}(z_0 + 1), \quad b = \frac{1}{2}(z_0 - 1) \tag{2.18}$$

For half-wave spacing this approach and that of Dolph give identical results! In fact, owing to the properties of the Chebyshev polynomial, the two space factors, in precursor form, are equal:

$$T_{N-1}\left(z_0^{N-1}\cos\frac{\Psi}{2}\right) \equiv T_M\left(\frac{z_0^M(\cos\Psi + 1) + \cos\Psi - 1}{2}\right), \quad N - 1 = 2M \tag{2.19}$$

where the superscripts on z_0 indicate that each must be chosen for the proper form. Because many computers have no inverse hyperbolic functions, it is convenient to rewrite the z_0 as:

$$z_0 = \frac{1}{2}\left[\mathrm{SLR} + \sqrt{\mathrm{SLR}^2 - 1}\right]^{1/M} + \frac{1}{2}\left[\mathrm{SLR} - \sqrt{\mathrm{SLR}^2 - 1}\right]^{1/M} \tag{2.20}$$

Directivity is given by:

$$D = \frac{\left[\sum_{n=1}^{N} A_n\right]^2}{\sum_{n=1}^{N}\sum_{m=1}^{N} A_n A_m \mathrm{sinc}[(n-m)kd]} \tag{2.21}$$

where the A_n coefficients are given by Equation 2.17. Directivity for arrays of three, five, seven, and nine elements has been calculated, for sidelobe ratios of 10 and 20 dB. The superdirectivity can be seen in Figures 2.7 and 2.8 for spacing below 0.5λ, as the ordinary directivity (using the Chebyshev coefficients that are independent of spacing) goes smoothly to 0 dB at zero spacing. The figures display these

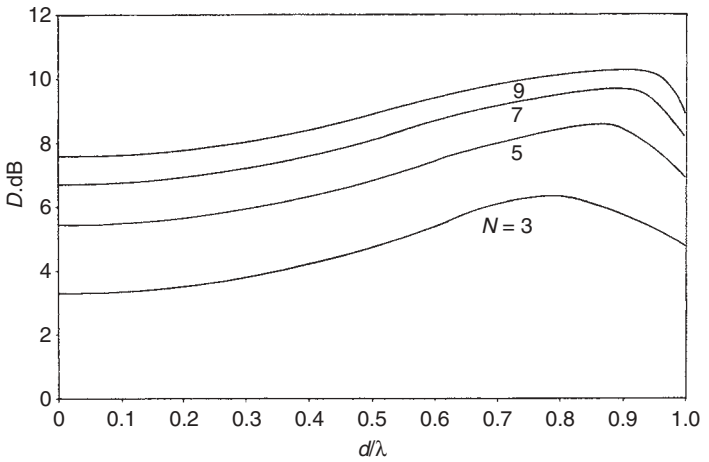

Figure 2.7 Chebyshev array directivity, SLR = 10 dB

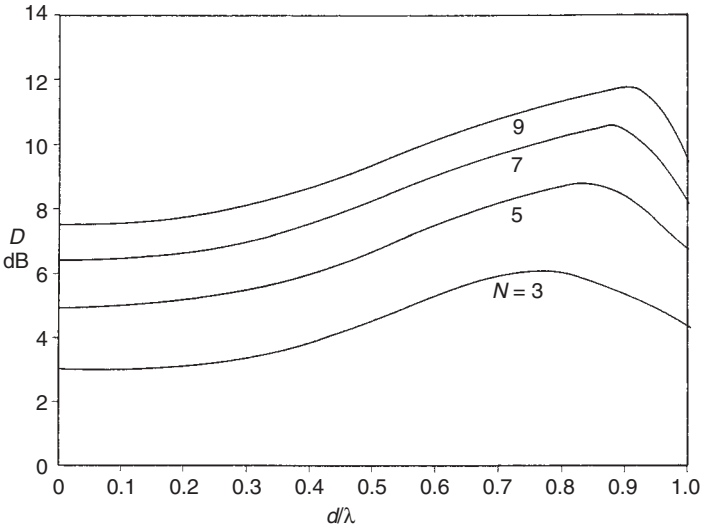

Figure 2.8 Chebyshev array directivity, SLR = 20 dB

calculated directivities versus element spacing. Thus a three-element array offers roughly 3 dB directivity for small spacings; five elements offers roughly 5 dB.

The Q is given by:

$$Q = \frac{120 \sum A_n A_m^*}{\sum_n \sum_m A_n A_m^* R_{nm}} \tag{2.22}$$

R_{nm} is the mutual resistance between the n and m elements. Normally the latter would, for thin wire dipoles, be computed by the efficient algorithm using Sine and Cosine Integrals developed by Hansen (1972). But superdirectivity typically involves subtracting large numbers, especially for Q. It is necessary to employ double precision in the calculation of the mutual resistances, and hence in the Sine and Cosine Integrals. Because such a subroutine could not be found, a Chebyshev economized series expansion, developed by Luke (1975), was used by this author to construct a double precision Sine and Cosine Integral subroutine. The results check all digits given in Abramowitz and Stegun (1970, Tables 5.1–5.3). Note the similarity between the D and Q formulas, Equation 2.21 and 2.22.

Riblet also showed (1947) that the Chebyshev polynomials T_n alone, of all real and complex polynomials, have the optimum properties that if the first null angle is specified the sidelobe level is minimized, and that if the sidelobe level is specified the first null angle is minimized. DuHamel (1953) modified the Dolph–Chebyshev design equations so that they would apply to a broadside or an endfire array of odd number of elements. He compared four endfire designs, for a seven-element array with $d/\lambda = 0.25$. These were uniform amplitude, normal phase (u); Hansen–Woodyard (HW); Schelkunoff, where the array polynomial zeroes are equally

Table 2.2 Comparison of four endfire array designs

	θ_3	SLR	I_4/I_1
U	99	13.3	1
HW	57	7.4	1
S	53	28	9.19
O	52	31	8.78

spaced on the unit circle (S); and an optimum design with the same SLR as the Schelkunoff design (O). Table 2.2 gives beamwidth, SLR, and ratio of largest to smallest current. Computing facilities circa 1953 did not allow calculation of either directivity or input resistances. Note that the element spacing is too large to allow significant superdirectivity, as borne out by the current ratios.

Another case of modest superdirectivity was given by Sanzgiri and Butler (1971). Stepwise sidelobe constraints were employed, and the optimum directivity was formulated as the ratio of two Hermetian quadratic forms, as previously described. Lagrangian methods were used to solve for max D. The array was broadside with nine elements at $d/\lambda = 0.6$. Several sidelobe envelopes were used; the case with constant $SLR = 20$ dB was typical. Directivity was 14.85, with SDR of 1.55. This very modest value was due to the large element spacing; significant SDR for a broadside array requires d/λ much less than 0.5.

Multiple power pattern constraints were used by Kurth (1974) with directivity optimization. Constraints on both main beam and sidelobe were used, leading to the common ratio of Hermitian quadratic forms solved by Lagrangian multipliers. A circular array of dishes was used as an example. Cox (1986) obtained a modest superdirectivity for an acoustic endfire array for various angular distributions of white noise. He also discussed "oversteering" past endfire to increase directivity. Apparently, the acoustics community was not familiar with Hansen–Woodyard!

Dawoud and Anderson (1978) used Chebyshev polynomials to optimize the ratio of beam peak value for a superdirective array to beam peak value for a uniformly excited cophasal array. As the beamwidth narrows, this ratio rapidly decreases. However there seems to be no simple relationship between this ratio and SDR. Another polynomial approach, by Dawoud and Hassan (1989), used Legendre polynomials instead of Chebyshev polynomials. The former yields slightly greater directivity for a broadside array with small spacing in wavelengths. The calculated directivities ($SDR = 6.2$) seem to be much too high for the 3 dB beamwidth shown.

2.3.2 Superdirective Ratio Constraint

By specifying an SDR, the designer can design the array and then evaluate bandwidth, tolerances, and efficiency. Using the definition of SDR provided by Taylor, the aperture or array problem was cast by Fong (1967) into a ratio of two Hermitian

quadratic forms, which are then solved by Lagrangian methods. Let the scalar product of coefficients be:

$$\langle A | A^* \rangle = \sum |A_n|^2 \tag{2.23}$$

where * indicates the complex conjugate. Call the row vector of complex array excitations **J** and the column vector of path-length phases **F**:

$$\mathbf{F} = \begin{vmatrix} \exp(-jkr_1 \sin\theta) \\ \vdots \\ \exp(-jkr_n \sin\theta) \end{vmatrix} \tag{2.24}$$

where r_n is the distance from the reference point to the nth element. For a uniformly spaced array, $r_n = (n - 1)\, d$. Now define matrices A and B, where A is:

$$|A| = |\mathbf{F}^*\rangle\langle\mathbf{F}| \tag{2.25}$$

and the elements of B are:

$$B_{nm} = \frac{1}{4\pi} \int f_1(\theta,\phi) \exp[-jkd(n-m)\sin\theta] d\Omega \tag{2.26}$$

The pattern of the ith element is f_i. Isotropic elements and a uniformly spaced array allow simplifications of A and B. The elements then become:

$$A_{nm} = \exp[-jkd(n-m)\sin\theta], \quad B_{nm} = \operatorname{sinc}[(n-m)kd] \tag{2.27}$$

Now the directivity can be written in abbreviated form:

$$D = \frac{\langle \mathbf{J}|A|\mathbf{J}^* \rangle}{\langle \mathbf{J}|B|\mathbf{J}^* \rangle} \tag{2.28}$$

The tolerance sensitivity S is defined as the ratio of variance of peak field strength produced by errors of variance σ_T^2 (Uzsoky and Solymar, 1956):

$$S = \frac{\sigma_E^2}{\sigma_j^2} = \frac{\dfrac{(\Delta E)^2}{E^2}}{\sigma_j^2} = \frac{\dfrac{\sigma_j^2 \langle \mathbf{J}|\mathbf{J}^* \rangle}{\langle \mathbf{J}|A|\mathbf{J}^* \rangle}}{\sigma_j^2} = \frac{\langle \mathbf{J}|\mathbf{J}^* \rangle}{\langle \mathbf{J}|A|\mathbf{J}^* \rangle} \tag{2.29}$$

Thus sensitivity is also written in abbreviated form. Q is conveniently found from $Q = SD$, or:

$$Q = \frac{\langle \mathbf{J}|\mathbf{J}^* \rangle}{\langle \mathbf{J}|B|\mathbf{J}^* \rangle} \tag{2.30}$$

The directivity is a ratio of two Hermitian quadratic forms, with B positive definite and A at least positive semidefinite. Thus all the eigenvalues of the associated equation are zero or positive real. Because A is a single-term dyad there is one nonzero eigenvalue. The eigenvector (excitation) is given by:

$$|\mathbf{J}\rangle = |B|^{-1}\mathbf{F}\rangle \tag{2.31}$$

The corresponding maximum directivity is given by:

$$D_{\max} = \left\langle \mathbf{F} | B |^{-1} \mathbf{F}^* \right\rangle \tag{2.32}$$

In many applications it is important to maximize D/T, directivity/system noise temperature. This is equivalent to maximizing signal-to-noise ratio S/N. To do this the element pattern in the integral for B_{nm} is multiplied by the antenna noise temperature $T(\theta, \phi)$. Then the excitation vector that maximizes S/N or D/T is that of Equation 2.31.

Another ratio that can be directly minimized is beam efficiency: the fraction of power contained within the main beam, null-to-null. This is:

$$\eta_b = \frac{\left\langle \mathbf{J} | A | \mathbf{J}^* \right\rangle}{\left\langle \mathbf{J} | B | \mathbf{J}^* \right\rangle} \tag{2.33}$$

To avoid the practical difficulties of finding the complex roots of a complex polynomial of high order, Winkler and Schwartz (1972) transformed that problem into one of finding the eigenvalues of a real matrix. This is numerically much faster, and readily available subroutines can be used. Maximum directivity (equivalent to SNR for a uniform noise field) was calculated for a four-element array of isotropes. Their calculations show that for broadside array spacing less than $\lambda/5$ the Q rises very fast while directivity is slowly increasing. Thus for this broadside array the tolerance factor[2] $T = D/Q$ increases very fast as $d \to 0$. For an endfire array, both Q and D are increasing as $d \to 0$, but again the tolerance factor increases very fast.

A related constrained D optimization used as a constraint the integral of current squared divided by radiated power (Margetis et al., 1998). This constraint is related to the SDR constraint.

A different approach was taken by Rhodes (1971), who optimized directivity of a line source subject to a fixed SDR. The pattern and aperture distribution are expanded in a series of prolate spheroidal functions. The SDR of Taylor was generalized to include edge effects (element pattern). When the SDR approaches a large value, the aperture distribution approaches a delta function spike at each end. For a given SLR, the series of spheroidal functions provides the maximum directivity that can be achieved.

2.3.3 Bandwidth or *Q* Constraint

Bandwidth is probably the most useful constraint. Constraining Q is equivalent, because for narrowband antennas (and all superdirective antennas are narrowband), the 3 dB bandwidth is simply $1/Q$. Again the problem is formulated as the ratio of two Hermitian quadratic forms, by Lo, Lee, and Lee (1966) and Cheng (1971). Using a scalar p proportional to the Lagrangian multiplier, the problem can be reduced to a complex polynomial of $2(N-1)$ degrees of freedom in p, for an N-element array.

[2] see Section 2.4.3.

Unfortunately, solving such an equation for large N is extremely tedious. See Winkler and Schwartz (1972) for an alternative solution. The paper lists quadratic ratios for directivity and Q, for the uniform case, optimum directivity, and optimum directivity for a prescribed Q. They also compared several endfire cases, as discussed in Section 2.2.2.2. See Section 2.4.1 for additional bandwidth data.

Kovacs and Solymar (1956) treated the inverse problem: Given directivity for an array configuration, find the excitation that minimizes Q. They showed that the minimum Q increases as D^2 for a fixed array size.

2.3.4 Phase or Position Adjustment

An iterative perturbation approach was used by Cheng (1971) to provide optimum directivity for an array. This was applied first to a ring array of uniformly spaced isotropic elements. Both amplitudes and phases were adjusted. The directivity increased rapidly with decreasing ring diameter below 2λ. Because amplitudes are difficult (expensive in hardware and losses) to adjust, phase-only optimization was applied to a 12-element ring array; for diameters less than 3λ, or element spacings less than 0.78λ, roughly 2 dB increase in D is obtained.

Phase-only optimization of an endfire array of isotropes was given by Voges and Butler (1972); they used steepest descent to solve for maximum directivity. Their 10-element array had spacing of $d = 0.4\lambda$, so there is some uncertainty about the pattern, due to $d > \lambda/4$. The SDR was 1.71. Q was just above 4, a value slightly less than a corresponding Hansen–Woodyard array.

Optimization of D by varying the interelement spacing in a linear array was performed by Butler and Unz (1967). Steepest descent methods were used on quadratic forms. A seven-element array was optimized with uniform amplitude. The maximum D agreed with the maximum calculated by Tai (1964) of 11.5. The SDR was 1.92; the spacings were symmetric, and changed slightly.

2.3.5 Tolerance Constraint

Because tolerances, in excitation amplitude and phase, in element position, and in element orientation, are critical for superdirective arrays, it is logical to optimize superdirectivity subject to a constraint on tolerances. Tseng and Cheng (1967) assumed standard deviations for element amplitude, for phase, and for element position. Directivity was maximized by reducing the Hermitian ratio to a determinantal equation; the matrix equation was solved via standard computer eigenvector routines. An example was calculated: an equally spaced eight-element endfire array of short dipoles; the normal directivity for $d = 0.3\lambda$ was 12.6, while the no-error optimum value was 45, an SDR of 3.57. Modest phase or amplitude errors transformed a directivity curve that was increasing as $d \to 0$ into a curve that turned down around $d \sim 0.35\lambda$ to 0.4λ, and rapidly decreased as $d/\lambda \to 0$. Endfire arrays appear to be more sensitive to errors, perhaps because the sidelobe region occupies more of the pattern volume.

Uzsoky and Solymar (1956) introduce a tolerance factor T that is the ratio of Q to D: $T = Q/D$. It has also been used by Lo et al. (1966), but called the sensitivity factor S. This factor is important as it tells whether Q is increasing faster than D as the SDR increases. They show that for endfire arrays, the uniform case has $T \sim 1$ over a wide range of spacings; the Hansen–Woodyard has $T \sim 0.3$ over a wide range of spacings; the amplitude-optimized case gives a rapidly rising T for spacings below about 0.2λ; the fully optimized case T rapidly rises for spacings below about 0.45λ. Thus the Q is rising fast (roughly exponentially) while the directivity is rising slowly.

A different approach was taken by Newman et al. (1978); they defined a sensitivity factor, which was the sum of element current magnitudes squared divided by the magnitude of the sum of currents. Also defined was a safety factor, and of course errors in terms of rms values of amplitude, phase, and position errors. For sidelobe fidelity in the –20, –30, and –40 dB region, the sensitivity factor should be 10^3, 10^4, and 10^5. Using a safety factor of one, the total allowable error (1σ) was roughly 3%, 1%, and 0.3%. Gilbert and Morgan (1955) maximized directivity subject to a fixed "background pattern" (see also Section 2.4.3).

2.4 BANDWIDTH, EFFICIENCY, AND TOLERANCES

2.4.1 Bandwidth

The first of three major difficulties with superdirective arrays is bandwidth, which rapidly becomes a problem as the element spacing decreases below $\lambda/2$ for broadside arrays or below $\lambda/4$ for endfire arrays. Thus the Q is of concern; for narrowband antennas, half-power *bandwidth* $\simeq 1/Q$ and the impedance *matched bandwidth* $\simeq 2/Q$. Note that the VSWR ≤ 2 bandwidth is given by $1/\sqrt{2}\,Q$. The ratio of stored to dissipated energy, Q, can similarly be written in terms of array coefficients and mutual coupling, which for isotropic elements is:

$$Q = \frac{\sum_{n=1}^{N} A_n^2}{\sum_{n=1}^{N}\sum_{m=1}^{N} A_n A_m \operatorname{sinc}[(n-m)2\pi d/\lambda]} \tag{2.34}$$

Directivity D is given by:

$$D = \frac{\left(\sum_{n=1}^{N} A_n\right)^2}{\sum_{n=1}^{N}\sum_{m=1}^{N} A_n A_m \operatorname{sinc}[(n-m)kd]} \tag{2.35}$$

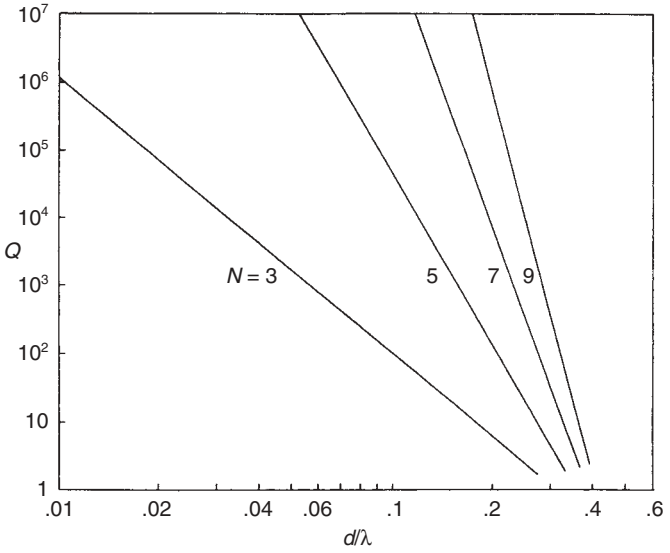

Figure 2.9 Q of broadside Chebyshev arrays versus element spacing

Calculations have shown (Hansen, 1981b) that, for broadside arrays of fixed length, both directivity and Q increase with the number of elements as expected. Figure 2.9 shows Q of Chebyshev arrays of odd numbers of elements versus element spacing. An array with an even number of elements has a slightly higher Q than the array with the next larger odd number of elements, possibly because the odd-element sampling is more efficient. Figures 2.10 and 2.11 show Q versus directivity for Chebyshev arrays two wavelengths long. For all the cases computed, Q varied approximately linearly with directivity. Figure 2.12 shows log Q versus directivity for odd arrays with lengths 1λ, 2λ, and 5λ. The circles represent points calculated in double precision; extended precision is required for arrays of more elements than those shown in the figure. The straight lines are drawn through the uniform excitation directivity point (equal to D_0) with slope of π, where $D_0 = 1 + 2L/\lambda$. There is at this time no physical significance to using this value of slope, but it is suggested by calculations of Rhodes (1974) on superdirective line sources. In making a best straight-line fit to the set of points for each of the three arrays, the slopes were in fact clustered around the value of 3.14. However, it is difficult to perform this fit with precision because, as pointed out by Rhodes, the curve of $\log Q$ versus directivity has an oscillatory behavior for low values of Q. If the assumptions above are true, superdirective broadside array behavior is predicted by the equation:

$$\log Q = \pi(D - D_0) \tag{2.36}$$

The 20 dB Chebyshev data of Figure 2.8 are close to this result. Thus the superdirective array clearly fits into the category of fundamental limitations in antennas

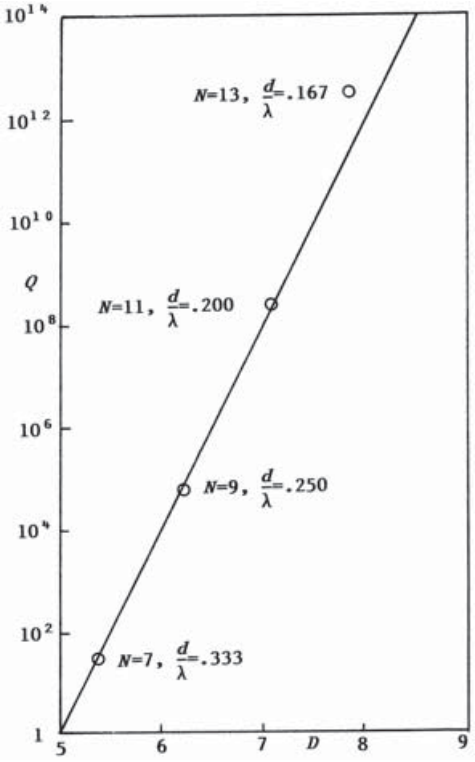

Figure 2.10 Q Versus Directivity, SLR = 10 dB, $L = 2\lambda$

(Hansen, 1981a). Whether the assumed slope of π can be physically justified remains an interesting problem at this time.

The Q to be expected from an array of isotropes is approximately a function of the number of elements divided by d/λ. Figure 2.13 shows this relationship for many arrays; each array is represented by a circle. Spacings larger than 0.3λ are not included, as the amount of superdirectivity achieved is small for these. $\text{Log}\, Q$ is approximately linear with $N\lambda/d$; the straight-line fit in the figure is:

$$\log Q \simeq 0.16043\left(\frac{N\lambda}{d}\right) - 1.53476 \tag{2.37}$$

These data allow the array designer to estimate the degree of superdirectivity (Q) for a given array geometry.

Calculations of performance have been made for superdirective linear arrays of parallel dipoles. Collinear dipoles are not considered, as they would overlap neighbors. Figure 2.14 shows $\log Q$ versus directivity for arrays two wavelengths long. Both 0.1λ and 0.5λ dipoles are used. Again, $\log Q$ versus G is a straight line. As expected, the half-wave dipole array has higher Q than the corresponding

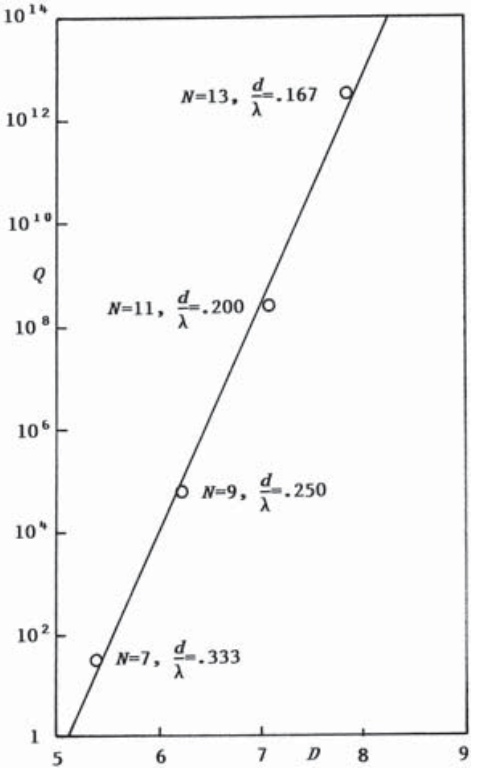

Figure 2.11 Q Versus directivity, SLR = 20 dB, $L = 2\lambda$

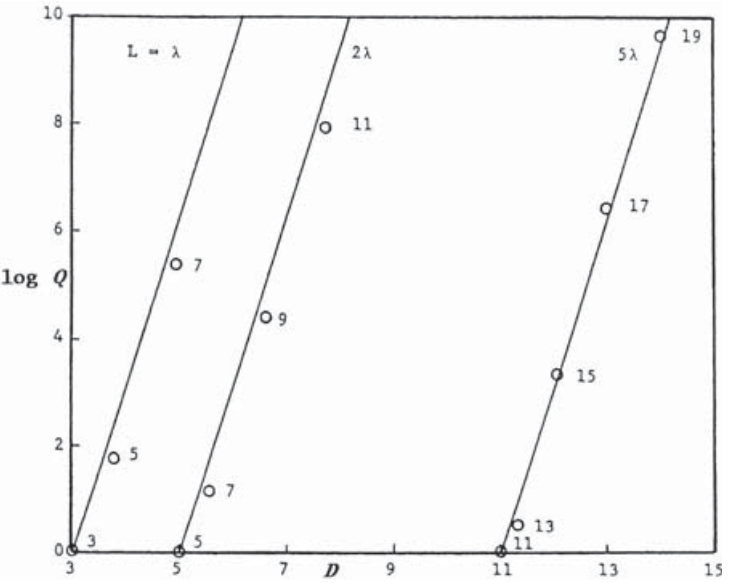

Figure 2.12 Q verse maximum directivity, odd arrays of isotropes

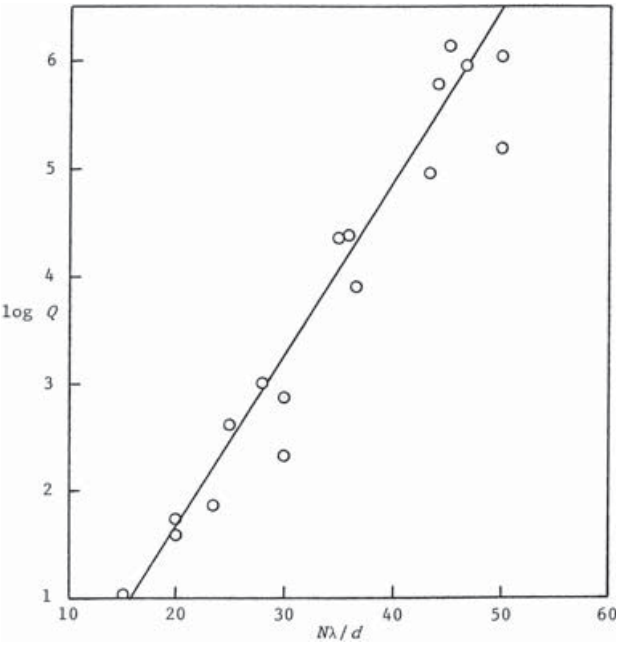

Figure 2.13 Q of broadside linear SD arrays of isotropes

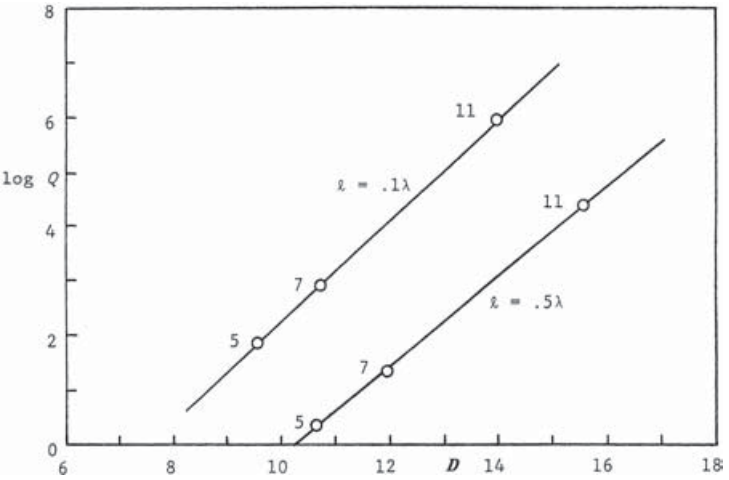

Figure 2.14 Q of 2λ broadside arrays of parallel dipoles

isotropic array, owing to energy storage in the dipole near-field. Withv short (0.1λ) dipoles this energy storage is much larger, resulting in much higher Q.

For endfire linear parallel dipole arrays, the variation of log Q with directivity is again linear, but the slope changes as the length of the array changes. Figure 2.15

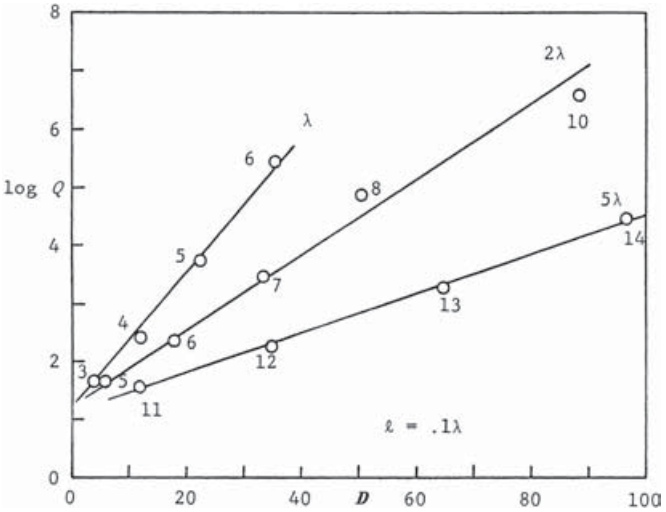

Figure 2.15 Q of endfire arrays of parallel dipoles

gives data for arrays of lengths 1λ, 2λ, and 5λ; the number of elements in each array is shown in the figure (Hansen, 1998).

2.4.2 Efficiency

A second undesirable feature of superdirective arrays is low efficiency, due both to matching network losses (see Section 2.6) and to losses in the antenna elements. Both losses are caused by the low radiation resistances of these arrays. In many cases, but not all, the elements at the array center show the lowest radiation resistance; calculations for many small broadside arrays of an odd number of isotropes show that $R_{\text{rad}} \propto 1/\sqrt{Q}$. Figure 2.16 shows these data, where each circle represents one array. The straight-line log-log fit is:

$$R_{\text{rad}} \simeq \frac{0.8058}{\sqrt{Q}} \tag{2.38}$$

Odd arrays were used as there are more variables per length, allowing better control of SD.

Loss resistance of cylindrical or strip dipoles is easily computed: a dipole of length ℓ, radius a, made of material with surface resistance R_s, has a loss resistance R_{loss} of:

$$R_{\text{loss}} = \frac{R_s \ell (1 - \operatorname{sinc} k\ell)}{4\pi a \sin^2 \frac{1}{2} k\ell} \tag{2.39}$$

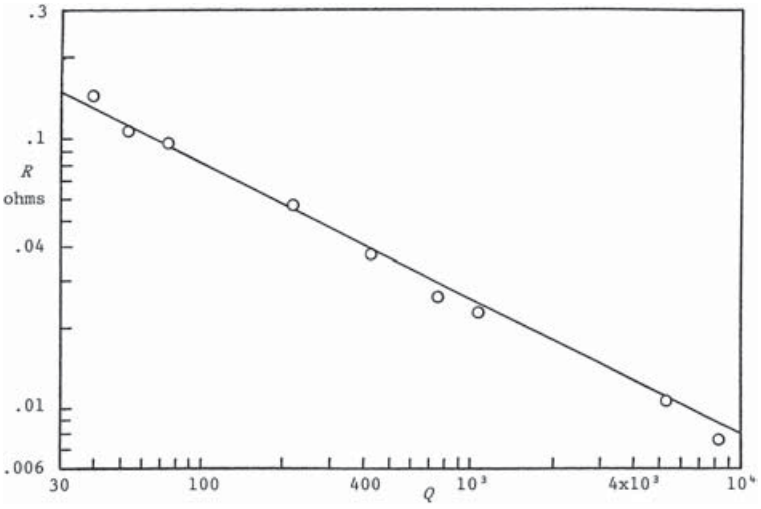

Figure 2.16 Q Verse R; broadside arrays

For half-wave or resonant dipoles, $R_{loss} = R_s \ell/4\pi a$. Strip dipoles are equivalent to cylindrical dipoles, with strip width equal to $4a$. Copper wires have an ideal surface resistivity of:

$$R_s \simeq 0.000261\sqrt{f\ \text{MHz}} \tag{2.40}$$

Over the range of 10 to 1000 MHz, R_s varies from 0.000825 to 0.00825 ohm/□. Using a value of $\ell/a = 25$, a moderately fat dipole, the loss resistance varies from 0.0066 ohm at 10 MHz to 0.066 ohm at 1 GHz. When these typical loss resistance numbers are compared with the radiation resistance values of Figure 2.16, it is clear that superdirective array efficiency may be a severely limiting consideration. Use of high-temperature superconductor (HTS) materials in the array and feed network can produce high efficiencies, but now the Q is that from Figures 2.14 and 2.15.

2.4.3 Tolerances

The third significant problem with superdirective arrays is tight tolerances. Because superdirectivity involves a partial cancellation of the element contributions at the main beam peak, with more cancellation for more superdirectivity, the tolerance of each element coefficient (excitation) becomes smaller (tighter) with more superdirectivity (Uzsoky and Solymar, 1956). A simple calculation has been made of these effects for Dolph–Chebyshev arrays by perturbing the center element of an odd array, finding the tolerance to reduce the directivity by 0.5 dB. This is not expected to be sensitive to sidelobe ratio, and a value of 20 dB was used. Calculations were made for $N = 3$ and 5 as a function of spacing, with the results shown in Figure 2.17. It was noted that the percentage error versus d/λ curve is linear up to spacings of roughly 0.1λ. For $N = 3$ the slope is 2 : 1, and for $N = 5$ the slope is 4 : 1. Thus for

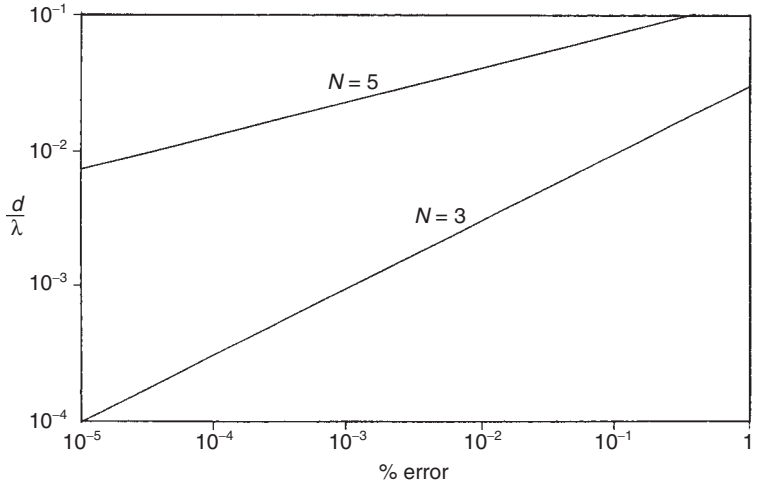

Figure 2.17 Center element roleance versus element spacing; 0.5 dB *D* Drop

$N = 3$, if the element spacing is halved, the tolerances must be four times tighter. The percentage tolerance for the center element, to maintain close (0.5 dB) to the expected directivity, is approximately given by:

$$\frac{100}{\sqrt{Q}} \tag{2.41}$$

but the constant varies with the number of elements.

Thus with $Q = 1000$, for example, the tolerance is 3.2%. Bandwidth and radiation resistance are more serious limitations of superdirective arrays.

An extreme example is the array of Yaru described above. An error in the center element excitation of only one part in 10^9 produces a directivity drop of roughly 3 dB. In general, the best way to evaluate tolerances for a given array design is to calculate the currents and then calculate the directivity change for a small change in one of the currents. Typically an amplitude error of σ_a (standard deviation) is equivalent to a phase error of σ_ϕ in radians.

2.5 MISCELLANEOUS SUPERDIRECTIVITY

Solymar (1958) found the maximum directivity of a line source whose distribution was a Fourier series. Superdirectivity can occur when the number of harmonics N exceeds the source L/λ.

Analogous situations between acoustics and electromagnetic waves were described by Kock (1959). These include waveguides, and other guiding structures, and wave diffraction. Of interest here is his demonstration of superdirectivity using five small loudspeakers with rheostats and reversing switches (normal excitation for comparison). Superdirectivity of about 4x was easily achieved!

An arc, or partial circle, of open loops or slitted cylinders with only one driven can be tuned for resonance by adjusting the gaps (King, 1989). At resonance it may be possible to produce a very narrowband peak of directivity (Veremy and Shestopalov, 1991). What degree of superdirectivity, if any, can be realized is not yet apparent. Measurements of an array of seven open loops on an arc with only one driven (Bokhari et al, 1992) are promising but not yet conclusive. This area is not yet well understood. Closely related is a circular (ring) array of short, parallel, dipoles, with only one excited. This ring can support a surface (slow) wave, and the closed ring can produce extremely sharp resonances (King et al., 2002; Fikioris, 1990, 1998). The small input resistance, narrow bandwidth, and narrow beams are characteristic of superdirectivity. It was shown by Janning and Munk (2002) that a planar array of short closely spaced dipoles could support a surface wave.

An analogy between superdirectivity and data processing to provide superresolution was provided by Buck and Gustincic (1967). Superresolution provides main beamwidth less than the Rayleigh limit λ/L (see Hansen, 1981a). Processing of the array outputs, for example, is by maximum entropy spectral analysis (Burg) or by maximum likelihood (Capon). The paper shows how noise limits the superresolution, just as errors limit superdirectivity.

2.6 MATCHING CIRCUIT LOSS MAGNIFICATION

A matching network for an electrically small antenna or for a superdirective array must cancel the large reactance and must transform the small radiation plus loss resistance to the nominal value, usually 50 ohms. Generally each element of an array will require a different matching network, although symmetric (broadside) arrays need fewer. If the matching network is composed of discrete L and C components, the low-R, high-X requirements will produce very large circulating currents in the overall circuit, consisting of the array element, the matching network, and the generator. These circulating currents will magnify the intrinsic loss to a much larger realized loss. Similarly, a distributed matching network under low-R, high-X conditions will have very large standing waves along the stubs and transformer sections. Again the intrinsic loss is magnified. In both cases the larger loss is due to power being proportional to voltage (or current) squared; the circulating currents or standing waves are large.

A transmission line transformer is typical. Let the matched loss be L and the antenna voltage standing wave ratio be VSWR. Then the actual loss L_a is (Moreno, 1948):

$$L_a = \frac{(\text{VSWR}+1)^2 L^2 - (\text{VSWR}-1)^2}{4 \bullet L \bullet \text{VSWR}} \tag{2.42}$$

For VSWR $\gg$ 1, the actual loss is:

$$L_a \simeq \frac{\text{VSWR} \bullet (L^2 - 1)}{4L} \tag{2.43}$$

Figure 2.18 shows the actual loss versus VSWR for intrinsic (matched) losses of 0.1, 0.2, 0.3, 0.5, 1, 2, 3, and 5 dB (Hansen, 1990). For $R \ll R_0$, the VSWR is VSWR $\simeq (R_0^2 + X^2)/RR_0$, whereas for $X \gg R_0$, VSWR $\simeq X^2/RR_0$. The latter holds also for $R \ll R_0$ and $X \gg R_0$. Some typical values are given in Table 2.3. For example, a case of $R/R_0 = 0.1$ and $X/R_0 = 10$ produces a VSWR = 1010. A matched loss of 0.01 dB becomes an actual loss of 3.35 dB; a matched loss of 0.1 dB becomes an actual loss of 11.01 dB. A more likely case, because the reactance ratio is usually higher, is $R/R_0 = 0.1$ and $X/R_0 = 30$, giving VSWR = 9010. A matched loss of 0.01 dB now yields an actual loss of 10.56 dB; a matched loss of 0.1 dB gives an actual loss of 20.2 dB.

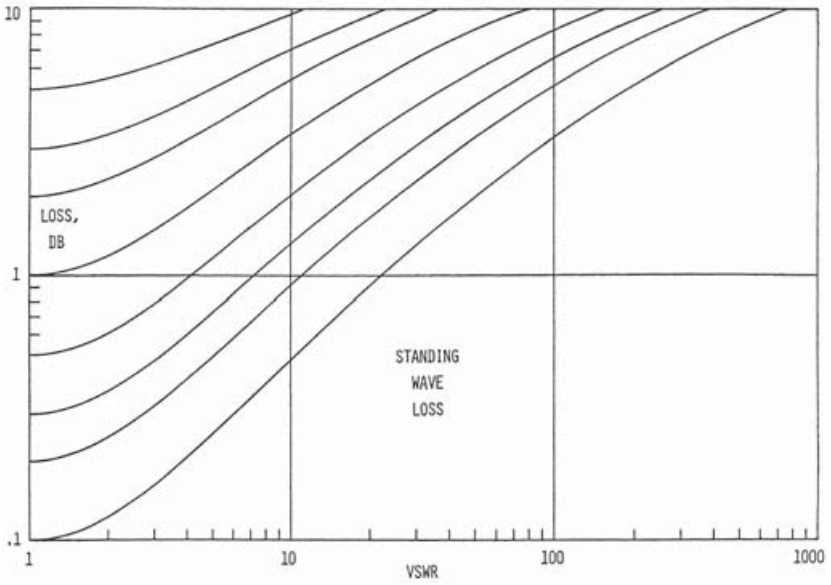

Figure 2.18 Line loss with mismatch

Table 2.3 VSWR from impedance mismatches

	X/R_0				
R/R_0	1	3	10	30	100
1	1.000	10.91	102.0	902.0	1.00×10^4
0.3	6.820	33.60	337.0	3004.0	3.334×10^4
0.1	20.05	100.0	1010.0	9010.0	1.000×10^5
0.03	66.68	333.4	3367.0	3.003×10^4	3.334×10^5
0.01	200.0	1000.0	1.010×10^4	9.010×10^4	1.000×10^6

2.7 NON-FOSTER MATCHING CIRCUITS

A new dimension in the impedance matching and impedance transformation of ESA and of superdirective antennas is now offered by Non-Foster circuits. These circuits produce negative resistance, negative inductance, or positive capacitance. They are Non-Foster in that their impedance circles the Smith chart with frequency the wrong way. Thus they violate Foster's reactance theorem for passive lossless circuits. Such circuits are also called negative impedance converters (NIC). It is also possible to transform impedances with such circuits.

NIC were developed at Bell Labs in the early 1930s and were used for many years in long-line telephony repeaters, where they provided both amplification and modest negative resistance, the latter to offset line losses. These repeaters made transcontinental telephone service possible and were used until microwave repeaters came into wide use after World War II. The BTL repeaters, of course, used vacuum tubes. To quote Linville (1963), "the ideal NIC is an active four-pole with input current equal to output current, and input voltage equal to the negative of the output voltage." Positive feedback is used to obtain these properties. As shown by Linville, the transistor quickly replaced the vacuum tube in NIC circuits. Applications include raising the Q of filters using negative resistance and negative and positive inductors at microwave frequencies, where conventional inductors are less attractive (Hara et al., 1988; El Khoury, 1995). The *MTT Transactions* contain many papers on filter applications. See Sussman-Fort (1998) for an extensive reference list. Papers on NIC topology include Tek and Anday (1989) and Sinsky and Westgate (1996). A novel technique was used by Pedinoff (1961) in which a tunnel diode biased into the negative conductance region was used with a slot antenna to provide amplification.

These concepts were applied to antennas by Mayes and Poggio in 1970. Negative impedance units were placed in series at several locations in the arms of a dipole (Mayes and Poggio, 1973; Poggio and Mayes, 1971). This was extended in an MS thesis under Mayes (Quirin, 1971) using Op Amps. Subsequently, transistors with much improved characteristics became available, allowing operation at microwave frequencies.

An early paper on non-Foster matching used two transistors to provide negative inductance for a loop antenna (Albee, 1976). Whether this was reduced to practice is not known. This was followed by Bahr (1976), who built a current inverting NIC to match a monopole antenna. A related approach uses an Op Amp with feedback to provide a charge amplifier, as opposed to a voltage amplifier (Ryan, 1983), for a short monopole (plate) antenna. Another patent concerns an Op Amp NIC applied to a loop antenna (Sutton, 1994). Op Amps are readily available but are not good choices, because of parasitics, poor dynamic range, poor efficiency, and noise. A significant advance was made by Skahill, Rudish, and Piero (1998), who matched a short dipole with a Khoury current conveyor using three transistors. A patent (2000) by these authors provides, in addition to the reactance match, a most important frequency squared transformer NIC that converts the short dipole radiation resistance to a constant value.

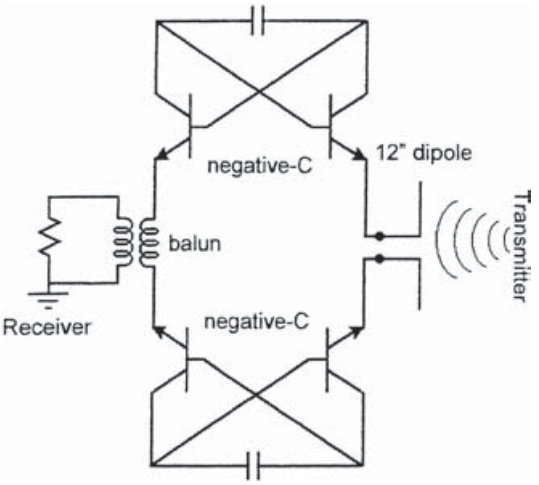

Figure 2.19 Measurement of short dipole N-F match. Courtesy of Rudish, R.M. and Sussman-Fort, S.E. Non-Foster Impedance Matching Improves S/N of Wideband Electrically-Small VHF Antennas and Arrays. *IASTED Conf on Antennas, Radar, and Wave Propagation,* Banff, Canada, 2005.

Because NIC employ positive feedback, stability is always a concern; parasitic and implementation defects are critical. Sussman-Fort and colleagues (1994, 1998) terminate an NIC in a one-port network designed to compensate for both active and passive parasitics. A negative inductance circuit was applied to a patch antenna (Kaya et al., 2004). Because patch antennas are easily matched, the extended bandwidth observed was probably due to the NIC losses. Non-Foster matching of a short dipole using a negative capacitance has produced typically a 10 dB improvement over more than an octave of frequency (Sussman-Fort and Rudish, 2005; Rudish and Sussman-Fort, 2005). Figure 2.19 shows the four transistor NIC used. A VHF monopole with N-F match developed for CECOM gave up to 6 dB improvement over a conventionally matched antenna (Sussman-Fort, 2006). Clearly a judicious use of Non-Foster matching can make a major improvement in receiving ESA. For transmitting ESA, the transistor circuit efficiency and the ability to handle the antenna current are critical. Research is ongoing; the use of Class E (switching) circuits in NIC holds promise.

Although not the subject of this book, Non-Foster circuits have advantages for phased arrays, either for matching or for connected arrays (see Hansen, 2003, 2004).

2.8 SD ANTENNA SUMMARY

An aperture can have any superdirectivity; an array can have limited superdirectivity. Both will suffer from low radiation resistance, narrow bandwidth, low efficiency, and tight tolerances. A modest superdirective ratio is useable. Small dipoles and loops are superdirective and share many of these problems. Q is of interest only if it is large, so that bandwidth = $1/Q$. Antennas with large VSWR need a matching

network with very low intrinsic loss. Here HTS can offer a significant advantage. We can have superdirectivity, but only a small supergain is useful. Non-Foster matching circuits appear to be the most promising approach to using SD antennas in the years ahead.

REFERENCES

Abramowitz, M. and Stegun, I.A., Eds. *Handbook of Mathematical Functions*, National Bureau of Standards, 1970.

Albee, T.K. *Broadband VLF Loop Antenna System*, U.S. Patent No. 3,953,799, April 1976.

Bach, H. Directivity of Basic Linear Arrays. *Trans. IEEE*, Vol. AP-18, Jan. 1970, pp. 107–110.

Bacon, J.M. and Medhurst, R.G. Superdirective Aerial Array Containing Only One Fed Element. *Proc IEE* Vol. 116, March 1969, pp. 365–372.

Bahr, A.J. Application of Active-Impedance Matching to Electrically Small Receiving Antenna. *Proc ECOM-ARO Workshop on Electrically Small Antennas, Ft. Monmouth, NJ*, Oct. 1976, pp. 199–204.

Bloch, A., Medhurst, R.G., and Pool, S.D. A New Approach to the Design of Super-Directive Aerial Arrays. *Proc IEE* Vol. 100, Sept. 1953, pp. 303–314.

Bloch, A., Medhurst, R.G., and Pool, S.D. Superdirectivity. *Proc IRE* Part III, Vol. 48, 1960, p. 1164.

Bokhari, S.A. et al. Superdirective Antenna Array of Printed Parasitic Elements. *Electronics Lett* Vol. 28, 2 July 1992, pp. 1332–1334.

Bouwkamp, C.J. and de Bruijn, N.G. The Problems of Optimum Antenna Current Distribution, *Philips Res Rep*, Vol. 1, 1947, pp. 135–158.

Brown, J.L. A Simplified Derivation of the Fourier Coefficients for Chebyshev Patterns. *Proc IEE* Vol. 105C, Nov. 1957, pp. 167–168.

Brown, J.L. On the Determination of Excitation Coefficients for a Tchebycheff Pattern, *Trans IEEE* Vol. AP-10, March 1962, pp. 215–216.

Buck, G.J. and Gustincic, J.J. Resolution Limitations of a Finite Aperture, *Trans IEEE* Vol. AP-15, May 1967, pp. 376–381.

Burington, R.S. *Handbook of Mathematical Tables and Formulas*, 5th Ed. McGraw-Hill, 1973, Section 365.12.

Butler, J.K. and Unz, H. Beam Efficiency and Gain Optimization of Antenna Arrays with Nonuniform Spacings. *Radio Sci* Vol. 2, July 1967, pp. 711–720.

Cheng, D.K. Optimization Techniques for Antenna Arrays. *Proc IEEE* Vol. 58, Dec. 1971, pp. 1664–1674.

Cheng, D.K. and Tseng, F.I. Gain Optimization for Arbitrary Antenna Arrays. *Trans IEEE* Vol. AP-13, Nov. 1965, pp. 973–974.

Cox, H., Zeskind, R.M., and Kooij, T. Practical Supergain. *Trans IEEE* Vol. ASSP-34, June 1986, pp. 393–398.

Dawoud, M.M. and Anderson, A.P. Design of Superdirective Arrays with High Radiation Efficiency. *Trans IEEE* Vol. AP-26, Nov. 1978, pp. 819–823.

Dawoud, M.M. and Hassan, M.A. Design of Superdirective Endfire Antenna Arrays, *Trans IEEE* Vol. AP-37, June 1989, pp. 796–800.

Dolph, C.L A Current Distribution for Broadside Arrays which Optimizes the Relationship between Beam Width and Side-Lobe Level. *Proc IRE* Vol. 34, 1946, pp. 335–348.

Drane, C.J. Derivation of Excitation Coefficients for Chebyshev Arrays. *Proc IEE* Vol. 110, Oct. 1963, pp. 1755–1758.

Drane, C.J. Dolph-Chebyshev Excitation Coefficient Approximation. *Trans IEEE* Vol. AP-12, Nov. 1964, pp. 781–782.

DuHamel, R.H. Optimum Patterns for Endfire Arrays. *Proc IRE* Vol. 41, May 1953, pp. 652–659.

El Khoury, S. The Design of Active Floating Positive and Negative Inductors in MMIC Technology. *IEEE Microwave Guided Wave Lett* Vol. 5, Oct. 1995, pp. 321–323.

Fikioris, G. Experimental Study of Novel Resonant Circular Arrays. *IEE Proc Microwave Antennas Propagation* Vol. 145, Feb. 1998, pp. 92–98.

Fikioris, G., King, R.W.P., and Wu, T.T. The Resonant Circular Array of Electrically Short Elements. *J Appl Physics*, Vol. 68, 1990, pp. 431–439.

Fong, T.S. On the Problem of Optimum Antenna Aperture Distribution. *J. Franklin Inst* Vol. 283, March, 1967, pp. 235–249.

Franz, K. Remarks on the Absorption Surfaces of Directive Aerials. *Hochfrequenztechnik Elektroakustik* Vol. 61, 1943, p. 51.

Gilbert, E.N. and Morgan, S.P. Optimum Design of Directive Antenna Arrays Subject to Random Variations. *Bell Sys Tech J* Vol. 34, May 1955, pp. 637–663.

Goward, F.K. An Improvement in End-Fire Arrays, *Proc IEE* Vol. 94, Part III, Nov. 1947, pp. 415–418.

Hansen, R.C. Formulation of Echelon Dipole Mutual Impedance for Computer. *Trans IEEE* Vol. AP-20, Nov. 1972, pp. 780–781.

Hansen, R.C. Fundamental Limitations in Antennas. *Proc IEEE* Vol. 69, Feb. 1981a, pp. 170–182.

Hansen, R.C. Some New Calculations on Antenna Superdirectivity. *Proc IEEE* Vol. 69, Oct. 1981b, pp. 1364–1366.

Hansen, R.C. Linear Arrays. In *Handbook of Antenna Design*, Rudge, A. W. et al., Eds. IEE/Peregrinus, 1983.

Hansen, R.C. Superconducting Antennas. *Trans IEEE* Vol. AES-26, March 1990, pp. 345–355.

Hansen, R.C. Hansen–Woodyard Arrays with Few Elements, *Microwave and Optical Tech Lett* Vol. 5, Jan. 1992, pp. 44–46.

HANSEN, R.C. *Phased Array Antennas*. John Wiley & Sons, 1998.

HANSEN, R.C. Antennas. Chapter 32 in *Reference Data for Engineers*, 9th Ed. Newnes, 2002.

HANSEN, R.C. Wideband Dipole Arrays Using Non-Foster Coupling. *Microwave Optical Tech Lett* Vol. 38, 20 Sept. 2003, pp. 453–455.

HANSEN, R.C. Non-Foster and Connected Planar Arrays. *Radio Sci* Vol. 39, 2004, RS4004, pp. 1, 14.

HANSEN, W.W. AND WOODYARD, J.R. A New Principle in Directional Antenna Design. *Proc IRE* Vol. 26, March 1938, pp. 333–345.

HARA S. ET AL. Broad-Band Monolithic Microwave Active Inductor and Its Applications to Miniaturized Wide-Band Amplifiers. *Trans IEEE* Vol. MTT-36, Dec. 1988, pp. 1920–1924.

HARRINGTON, R.F. Antenna Excitation for Maximum Gain. *Trans IEEE* Vol. AP-13, Nov. 1965, pp. 896–903.

JANNING, D.S. AND MUNK B.A. Effects of Surface Waves on the Current of Truncated Periodic Arrays. *Trans IEEE* Vol. AP-50, Sept. 2002, pp. 1254–1265.

JORDAN, E.C. AND BALMAIN, K.G. *Electromagnetic Waves and Radiating Systems*, 2nd Ed. Prentice-Hall, 1968.

KAYA, A. ET AL. Bandwidth Enhancement of a Microstrip Antenna Using Negative Inductance as Impedance Matching Device. *Microwave Optical Tech Lett* Vol. 42, Sept. 2004, pp. 476–478.

KING, R.W.P. Supergain Antennas and the Yagi and Circular Arrays. *Trans IEEE* Vol. 37, Feb. 1989, pp. 178–186.

KING, R.W.P. FIKIORIS, G., AND MACK, R.B. *Cylindrical Antennas and Arrays*. Cambridge Univ. Press, 2002.

KOCK, W.E. Related Experiments with Sound Waves and Electromagnetic Waves. *Proc IRE* Vol. 47, July 1959, pp. 1192–1201.

KOVÁCS, R. AND SOLYMÁR, L. Theory of Aperture Aerials Based on the Properties of Entire Functions of the Exponential Type. *Acta Physica Hung* Vol. 6, 1956, pp. 161–184.

KURTH, R.R. Optimization of Array Performance Subject to Multiple Power Pattern Constraints. *Trans IEEE* Vol. AP-22, Jan. 1974, pp. 103–105.

KYLE, R.F. Super-Gain Aerial Beam. *Elec* and *Radio Eng* Vol. 36, Sept. 1959, pp. 338–340.

LA PAZ, L. AND MILLER, G.A. Optimum Current Distributions on Vertical Antennas. *Proc IRE* Vol. 31, 1943, pp. 214–232.

LINVILL, J.G. Transistor Negative-Impedance Converters. *Proc IRE* Vol. 41, June 1953, pp. 725–729.

LO, Y.T. Array Theory. Chapter 11 in *Antenna Handbook*, Lo, Y.T. and Lee, S.W., Eds. Van Nostrand, 1988.

Lo, Y.T. et al. Optimization of Directivity and Signal-to-Noise Ratio of an Arbitrary Antenna Array. *Proc IEEE* Vol. 54, Aug. 1966, pp. 1033–1045.

Luke, Y.L. *Mathematical Functions and Their Approximations*. Academic Press, 1975, Table 4.4.

Margetis, D. et al. Highly Directive Current Distributions: General Theory. *Phys Rev E* Vol. 58, Aug. 1998, pp. 2531–2547.

Mayes, P.E. and Poggio, A.J. *Wire Antenna Multiply-Loaded with Active Element Impedances*. U.S. Patent No. 3,716,867, Feb. 1973.

Moreno, T. *Microwave Transmission Design Data*. Dover, 1948, Chapter 2.

Newman, E.H. et al. Superdirective Receiving Arrays. *Trans IEEE* Vol. AP-26, Sept. 1978, pp. 629–635.

Oseen, C.W. Die Einsteinsche Nadelstichstrahlung und die Maxwellshen Gleichungen. *Ann Phys* Vol. 69, 1922, p. 202.

Pedinoff, M.E. The Negative-Conductance Slot Amplifier. *Trans IRE* Vol. MTT-9, Nov. 1961, pp. 557–566.

Poggio, A.J. and Mayes, P.E. Bandwidth Extension for Dipole Antennas by Conjugate Reactance Loading. *Trans IEEE* Vol. AP-19, July 1971, pp. 544–547.

Pritchard, R.L. Optimum Directivity Patterns for Linear Point Arrays. *J Acoust Soc Am* Vol. 25, Sept., 1953, pp. 879–891.

Quirin, J.D. *A Study of High-Frequency Solid-State Negative-Impedance Converters for Impedance Loading of Dipole Antennas*. MS thesis, Univ. of Illinois, 1971.

Reid, D.G. The Gain of an Idealized Yagi Array. *J IEE* Vol. 93, Pt. IIIA, 1946, pp. 564–566.

Rhodes, D.R. On an Optimum Line Source for Maximum Directivity. *Trans IEEE* Vol. AP-19, July 1971, pp. 485–492.

Rhodes, D.R. *Synthesis of Planar Antenna Sources*, Clarendon Press, 1974.

Riblet, H.J. Discussion on a Current Distribution for Broadside Arrays which Optimizes the Relationship between Beam Width and Side-Lobe Level. *Proc IRE* Vol. 35, 1947, pp. 489–492.

Riblet, H.J. Note on the Maximum Directivity of an Antenna. *Proc IRE* Vol. 36, May 1948, pp. 620–623.

Ryan, P.A. *Low Profile Electric Field Sensor*, U.S. Patent No. 4.383,260, May 1983.

Rudish, R.M. and Sussman-Fort, S.E. Non-Foster Impedance Matching Improves S/N of Wideband Electrically-Small VHF Antennas and Arrays. *IASTED Conf. on Antennas, Radar, and Wave Propagation,* Banff, Canada, 2005.

Salzer, H.E. Calculating Fourier Coefficients for Chebyshev Patterns. *Proc IEEE* Vol. 63, 1975, pp. 195–197.

Sanzgiri, S.M. and Butler, J.K. Constrained Optimization of the Performance Indices of Arbitrary Array Antennas. *Trans IEEE* Vol. AP-19, July 1971, pp. 493–498.

Schelkunoff S.A. A Mathematical Theory of Linear Arrays. *Bell Syst Tech J* Vol. 22, 1943, pp. 80–107.

Seeley, E.W. Two- and Three-Loop Superdirective Receiving Antennas. *J Res NBS* Vol. 67D, March–April 1963a, pp. 215–235.

Seeley, E.W. VLF Superdirective Loop Arrays. *J Res NBS* Vol. 67D, Sept.–Oct. 1963b, pp. 563–565.

Sinsky, J.H. and Westgate, C.R. A New Approach to Designing Active MMIC Tuning Elements Using Second-Generation Current Conveyors. *IEEE Microwave Guided Wave Lett* Vol. 6, Sept. 1996, pp. 326–328.

Skahill, G., Rudish, R.M., and Piero, J.A. Electrically Small, Efficient, Wide-Band Low-Noise Antenna Elements. *Proc Antenna Applications Symp, Allerton, IL*, Sept. 1998, pp. 214–231.

Skahill, G., Rudish, R.M., and Piero, J.A. *Apparatus and Method for Broadband Matching of Electrically Small Antennas.* U.S. Patent No. 6,121,940, Sept. 2000.

Sokolnikoff, I.S. and Sokolnikoff E.S. *Higher Mathematics for Engineers and Physicists*, 2nd Ed. McGraw-Hill, 1941.

Solymar, L. Maximum Gain of a Line Source Antenna if the Distribution Function is a Finite Fourier Series. *Trans IRE* Vol. AP-6, July 1958, pp. 215–219.

Stearns, C.O. *Computed Performance of Moderate Size, Super-Gain Antennas.* NBS Report 6797, 5 Sept. 1961.

Stutzman, W.L. and Thiele, G.A. *Antenna Theory and Design*, 2nd Ed. John Wiley & Sons, 1998.

Sussman-Fort, S.E. An NIC-Based Negative Resistance Circuit for Microwave Active Filters. *Intl J Microwave Millimeter-Wave Computer-Aided Eng* Vol. 2, 1994, pp. 130–139.

Sussman-Fort, S.E. Gyrator Based Biquad Filters and Negative Impedance Converters for Microwaves. *Intl J Microwave Millimeter-Wave Computer-Aided Eng* Vol. 6, 1998, pp. 86–101.

Sussman-Fort, S.E. Matching Network Design Using Non-Foster Impedances. *Intl J RF Microwave Computer-Aided Eng* March 2006, pp. 135–142.

Sussman-Fort, S.E., and Rudish, R.M. Progress in Use of Non-Foster Impedances to Match Electrically-Small Antennas and Arrays. *Proc. Antenna Applications Symposium, Allerton, IL* 2005, pp. 89–108.

Sutton, J.F. *Active Antenna*. U.S. Patent No. 5,311,198, May 1994.

Tai, C.T. The Optimum Directivity of Uniformly Spaced Broadside Arrays of Dipoles. *Trans IEEE* Vol. AP-12, July 1964, pp. 447–454.

Taylor, T.T. A Discussion of the Maximum Directivity of an Antenna. *Proc IRE* Vol. 36, 1948, p. 1135.

Taylor, T.T. Design of Line-Source Antennas for Narrow Beamwidth and Low Sidelobes. *Trans IRE* Vol. AP-3, Jan. 1955, pp. 16–28.

Tek, H. and Anday, F. Voltage Transfer Function Synthesis Using Current Conveyors. *Electronics Lett* Vol. 25, Nov. 9, 1989, pp. 1552–1553.

Tseng, F.-I. and Cheng, D.K. Gain Optimization for Arbitrary Antenna Arrays Subject to Random Fluctuations. *Trans IEEE* AP-15, May 1967, pp. 356–366.

Uzkov, A.I. An Approach to the Problem of Optimum Directive Antennae Design. *Comp Rend Acad Sci URSS* Vol. 53, 1946, p. 35.

Uzsoky, M. and Solymar, L. Theory of Super-Directive Linear Arrays, *Acta Physica Hung* Vol. 6, 1956, pp. 185–205.

Veremy, V.V. and Shestopalov, V.P. Superdirective Antenna with Passive Resonant Reflector. *Radio Sci* Vol. 26, March–April 1991, pp. 631–636.

Voges, R.C. and Butler, J.K. Phase Optimization of Antenna Array Gain with Constrained Amplitude Excitation. *Trans IEEE* Vol. AP-20, July 1972, pp. 432–436.

Winkler, L.P. and Schwartz, M. A Fast Numerical Method for Determining the Optimum SNR of an Array Subject to a Q Factor Constraint. *Trans IEEE* Vol. 20, July 1972, pp. 503–505.

Yaru, N. A Note on Supergain Antenna Arrays. *Proc IRE* Vol. 39, Sept. 1951, pp. 1081–1085.

AUTHOR INDEX

Chapter 3

Superconducting Antennas

3.1 INTRODUCTION

The advent of high T_c superconducting materials has presented new opportunities for improving antenna performance. Many antenna workers are not familiar with the current findings on superconductors. Considered here are electrically small antennas, and matching of them, and millimeter wavelength antennas. Not included are SQUID devices that incorporate a loop or other antenna. These are primarily of interest as very low-frequency magnetic field sensors.

3.2 SUPERCONDUCTIVITY CONCEPTS FOR ANTENNA ENGINEERS

There are many excellent books on superconductivity; only a basic overview is given here. An excellent treatise on all aspects of high- and low-temperature superconductivity, including a thorough mathematical treatment, is by Tinkham (1996). A physical understanding, with a minimum of mathematics, is by Ginzburg and Andryushin (2004). And there are many others. Lancaster (1997) has a useful book on HTS applications including antennas. Table 3.1 shows a brief chronology up through the Fullerenes. It is interesting to note the first step toward HTS: In 1975 Sleight, Gibson, and Bierstedt discovered superconductivity in a barium lead bismuth metallic oxide at 13°K. This significant increase in T_c, and for a ceramic material, was a forerunner of HTS. In 1986 Bednorz and Muller discovered material that had $T_c = 35$°K, a major advance. This was quickly followed by Chu, who developed the first of the HTS family: YBCO, with $T_c = 92$°K.

Superconductors have two remarkable properties: zero DC resistance and magnetic flux expulsion except for a thin shell of λ thickness (Meissner effect). The superconducting state occurs when the temperature of certain materials drops below a critical temperature T_c; see Table 3.2. Then the material is in the lowest energy state, and conduction electrons form coupled pairs, called Cooper pairs, through phonon (lattice) interactions, for LTS (low temperature superconductors). These

Electrically Small, Superdirective, and Superconducting Antennas, by R. C. Hansen.

Table 3.1 Brief history of superconductivity

1911	Discovery by Onnes @ 4 K; H_g DC resistance = 0
1933	Meissner effect—H expulsion on cooling
1934	London—H penetration depth, two-fluid model of normal and SC electrons, flux quantization
1950	Ginzburg and Landau—macroscopic quantum theory
1956	Cooper—paired electrons
1957	BCS microscopic theory—H_c, Y_c relationship, etc.
1957	Abrikosov—Current vortices in type II materials, each containing one flux quantum
1961	Kunzler—high-field, high-current superconductors
1962	Josephson—tunneling effects
1965	Silver et al.—squid, SC loop with JJ
1975	Sleight et al.—Ba Pb Bi O = 13°K
1984	Yagubskii et al.—organic SC
1986	Bednorz and Muller—high-H_c materials—35°K
1987	Chu—YBCO materials—92°K
1991	Hebard et al.—doped fullerenes

Table 3.2 Some superconductor critical temperatures

Elements		
Al	1.2°K	
Sn	3.7	
Hg	4.2	
Pb	7.2	
Nb	9.3	
Alloys		
NbTi	10.5	
NbN	16	
Compounds		
Nb_3Sn	18.4	Widely used for magnets because of strong pinning forces
Nb_3Ge	23.2	
MgB_2	40	
Ceramics		
$La_2Ba_2Cu_1O_4$	35	Bednorz and Muller (April 1986)
$Y_1Ba_2Cu_3O_7$	92	Chu et al. (February 1987)
$Bi_2Sr_2Ca_2Cu_2O_{10}$	110	Asano and Hermann (1988)
$Th_2Ba_2Ca_2Cu_3O_{10}$	125	Beyers and Parkin (1988)

Cooper pair electrons flow without loss; they are coupled over the coherence length. For example, for LTS, for niobium it is roughly 44 nm; for aluminum it is 1600 nm. For HTS, the coherence length for YBCO is 140 nm. As temperature increases from 0°K, the thermal lattice vibrations excite some electrons out of the ground state,

Table 3.3 Penetration depth and coherence length

		λ	ξ	
Type I	Pb	39	87	All nm
	Nb	44	38	
	Sn	51	230	
Type II	Nb_3Sn	65	3	
	PbBi	200	20	
	YBaCuO	140	0.2–0.6	
	LaSrCuO	200	0.6	

Anderson, *Physics Vade Mecum*, AIP, 1989, Chap. 7.

breaking up some Cooper pairs. See Table 3.3 for penetration depth[1] λ and coherence length ζ. Crystal defects and impurities can change the coherence length, so purity is always a goal. The normal current flow produces loss. However the increase in resistivity is small until T_c is approached. As frequency increases from zero, the electron pair kinetic energy produces a delay that creates an electric field along the surface. An applied magnetic field can also force all electrons to normal; this is the critical field, H_c.

It is useful to compare a superconductor with a perfect electric conductor (PEC). As seen in the sketch of Figure 3.1, the PEC at any temperature and any applied magnetic field contains an internal magnetic field; current can flow without loss. For the superconductor, when a magnetic field is applied and the temperature lowered below T_c, the magnetic field is expelled, except at the surface. Again, current can flow without loss.

Bardeen–Cooper–Schrieffer theory makes a quantum mechanical formulation for the paired electrons. It relates critical temperature, critical magnetic field H_c, coherence length, etc. It represents LTS well, but only partially for HTS. For both LTS and HTS there are two types of materials: Type I and Type II. Type I materials are typically soft metallic elements, exhibiting the Meissner effect up to H_c. Coherence length is roughly comparable to penetration depth. The London penetration depth is the depth of current induced by a magnetic field. It is analogous to skin depth, which is the depth of current in a normal conductor. Type II materials have two critical magnetic fields, H_{c1} and H_{c2}. These have short coherence length and long penetration depth. The Meissner effect exists for fields up to H_{c1}; at H_{c2} the conductor is normal. Between H_{c1} and H_{c2} flux cores or vortices exist, with the spacing between them decreasing as H approaches H_{c2}. Each vortex contains one flux quanta; a supercurrent circulates around the core. Vortices are typically cylindrical, with radius of one or two coherence lengths. Table 3.4 gives critical fields for representative materials.

Superconductivity is not only destroyed by high current density, by high magnetic fields, or by high temperature, but also by high frequency, in particular by

[1] In most of this book λ is wavelength; in this chapter the SC terminology is used, except in 3.4.

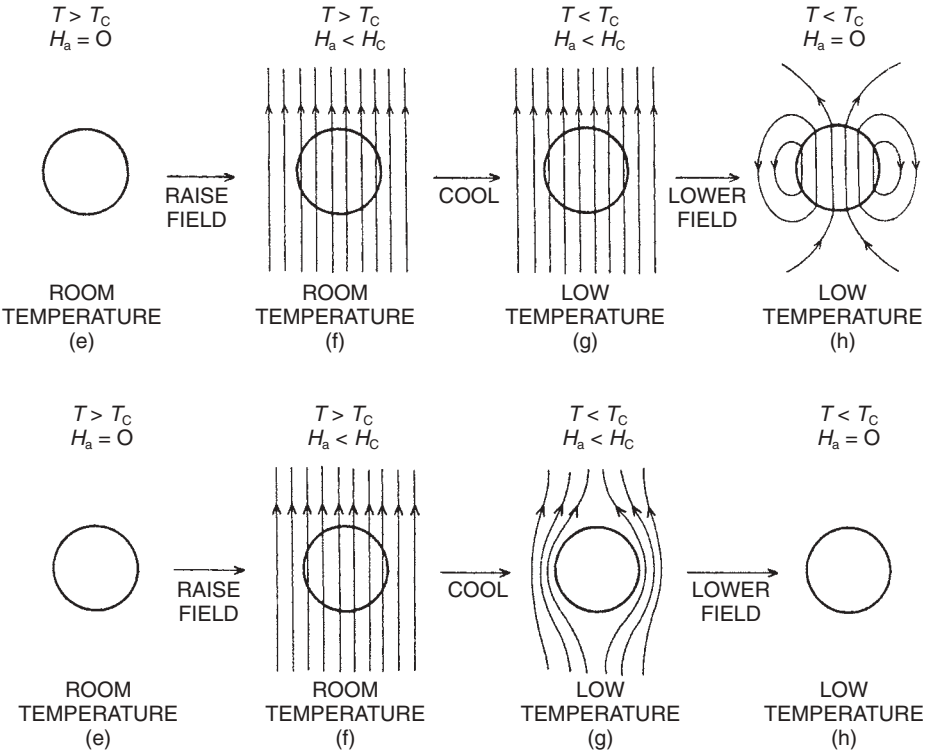

Figure 3.1 PEC versus SC

Table 3.4 Some superconductor critical fields

Material	H_{c1}	H_{c2}
Nb	1,600 at/cm	2,400
NbTi	2,800	88,000
Nb_3Sn	2,800	185,000

frequency greater than the energy gap frequency. For LTS the energy gap frequency is roughly 1 THz, whereas for HTS it is roughly 10 THz. Thus HTS are more suitable for submillimeter applications.

The HTS crystal structure is Perovskite; electrically active planes of copper and oxygen are sandwiched between other layers that are reservoirs of charge. Figure 3.2 is a sketch of YBCO. Such a crystal structure is highly anisotropic, with poor

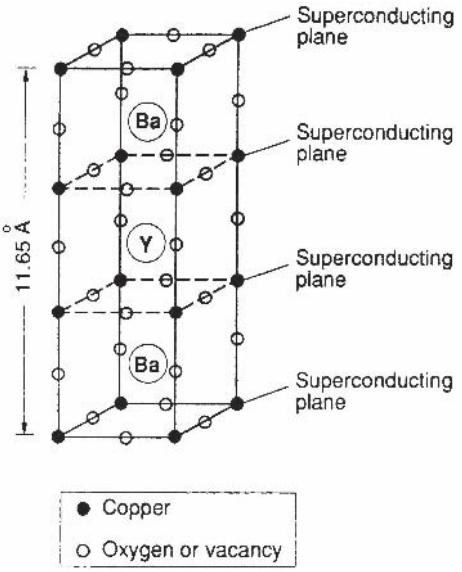

Figure 3.2 YBCO lattice

conductivity along the copper axis. Although a superconductor below T_c, the material, like most ceramics, is a poor conductor at room temperature. The SC current (Cooper paired electrons) flows along the CuO planes. Because of the crystal structure the electron pairing is more complex than that of the BCS theory. The two-fluid model is useful for HTS; a mixture of normal and SC currents flow. For the normal currents, $J = \sigma_1 E$. For the SC currents, the London equations apply:

$$\nabla \times J_{sc} = -H/\lambda^2, \quad \frac{dJ_{sc}}{dt} = \frac{E}{\mu_0 \lambda^2} \tag{3.1}$$

Typical data on surface resistivity versus frequency are shown in Figure 3.3, for copper at room temperature, and for copper and HTS at liquid nitrogen temperature. Data on the frequency where HTS resistivity is equal to that of copper at 77°K were given by Alford (1991). Data on LTS niobium were given by Piel and Muller (1991); measurements and BCS theory agree very well. The surface resistance, from measurements and theory, is given by:

$$R_s \simeq \frac{1}{2}\omega^2 \mu_0^2 \lambda^3 \sigma_1 \tag{3.2}$$

where σ_1 is the normal state conductivity and ω is angular frequency. Note that R_s varies as frequency squared. In contrast for a normal conductor the surface resistance varies as $f^{1/2}$. Surface reactance is simply:

$$X_s = \omega \mu_0 \lambda \tag{3.3}$$

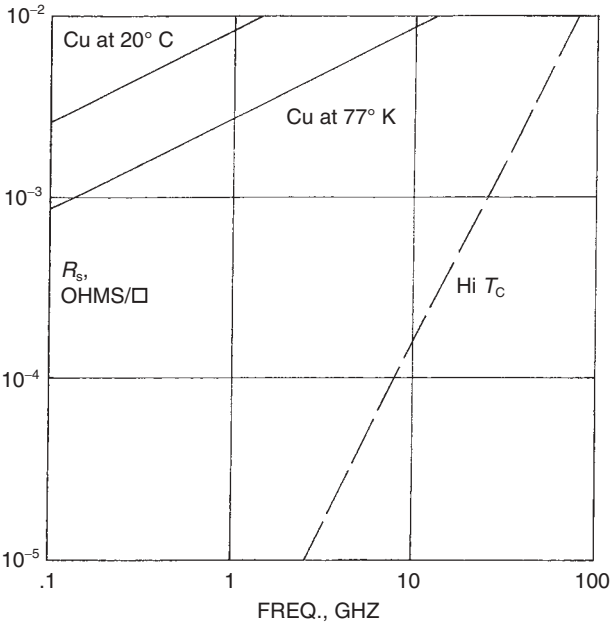

Figure 3.3 Surface resistivity trends

In both formulas for R_x and X_s, the penetration depth λ is:

$$\lambda = \frac{\lambda_o}{\sqrt{1-(T/T_c)^4}} \tag{3.4}$$

where λ_0 is the penetration depth at 0°K. Most antenna and circuit work now utilizes SC thin films, with the CuO plane parallel to the substrate. With films it is easier to control lattice defects and impurities in order to reduce RF losses. Substrates ideally should have a lattice match, have low loss and low ε, and be nonreactive with HTS at all processing temperatures.

An indication of how superconductors might affect antennas can be gleaned from considerations of external and internal fields. The performance of almost all antennas is governed by size and shape in free space wavelengths, that is external fields. Examples are dipoles, slots, spirals, log-periodics, Yagi–Uda, horns, and reflectors. Superconductivity generally has a small effect on external fields, so the size/shape of most antennas will not be reduced. Internal fields exhibit only loss, thereby reducing efficiency. Superconductors can improve efficiency, often at the expense of bandwidth. Most important, superconductors can make a significant increase in the efficiency of an impedance matching network.

It is useful to reflect on the progress of superconductivity. There have been three periods of spectacular progress, roughly 40 years apart. The period 1905–1911 saw liquefaction of helium, helium cryostats, discovery of mercury superconductivity, and discovery of tin and lead superconductivity. The period 1952–1962 saw micro-

scopic quantum theory, Cooper pairs, BCS theory, current vortices, Josephson effect, high-field superconductors, and superconducting magnets. And the period 1986–1991 saw the discovery of HTS, the YBCO family, the lanthanum family, fullerenes, and organics. Will we see room-temperature superconductors around 2030?

3.3 DIPOLE, LOOP, AND PATCH ANTENNAS

Immediately after the discovery of high-temperature superconductors antenna people looked at how these new materials might improve the performance of antennas. One company actually proposed building the surface of a dish antenna out of HTS in the vain hope that the typical dish aperture efficiency of 65% would be increased to close to 100%. Of course, the conduction loss in a dish antenna is usually less than 1% of the total loss, and the 65% is due to aperture taper and blockage losses. In what follows only antennas that have been built and tested are discussed. Antenna configurations incorporating Josephson junctions are outside the scope of this book.

With the discovery of HTS, LaBaCuO in 1986 by Bednorz and Muller, and YBaCuO in 1987 by Chu, it was inevitable that the new technology would be applied to antennas. Intensive activity was reported between 1988 and 1995. This work is reported by type of antenna. No measured data are reported here on ESA; it will appear later that none of the ESA needs HTS, only the matching network for short dipoles should employ HTS.

3.3.1 Loop and Dipole Antennas

Khamas et al. (1988) Wu et al. (1989), and Lancaster et al. (1992a) measured a short dipole and matching twin line, all made of YBCO, and compared results to a similar system made of copper (see Fig. 3.4). The HTS antenna gain was 12 dB higher. However, essentially all of the 12 dB improvement was due to the HTS matching (Hansen, 1990). Section 2.6 discusses matching network losses. The reduction in

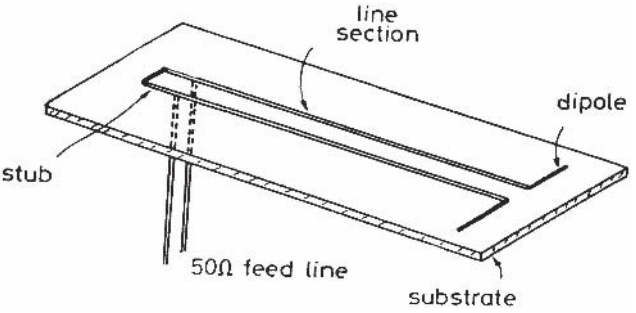

Figure 3.4 Short dipole with twin line match. Courtesy of Lancaster, M.J. et al. Supercooled and Superconducting Small-Loop and Dipole Antennas. *Proc IEE* Vol. 139, Pt. H, June 1992a, pp. 264–270.

gain of this configuration as the input power increased was noted by Gough et al. (1989); see also Portis et al. (1991). Dinger and colleagues (1990, 1991) calculated the efficiency for such a twin line fed dipole and showed that dielectric loss tangents should be less than 10^{-4}. Additional work on HTS dipoles was by He et al. (1990, 1991). A YBCO thick film loop and matching network was developed and measured by Lancaster et al. (1993; Fig. 3.5). Determination of loop-alone performance was made using backscatter measurements (Khamas et al., 1993; see Fig. 3.6). Multiturn loops made of BSCCO were tested by Itoh et al. (1993). Matching sections made of copper reduced the overall gain, due to matching loss. In addition the bandwidth was narrow as the loop radiation resistance was small compared to the reactance. Several ways of feeding small loops were compared by Ivrissimtzis et al. (1994a; Fig. 3.7). Effects of impurities on bandwidth were predicted with a two-fluid

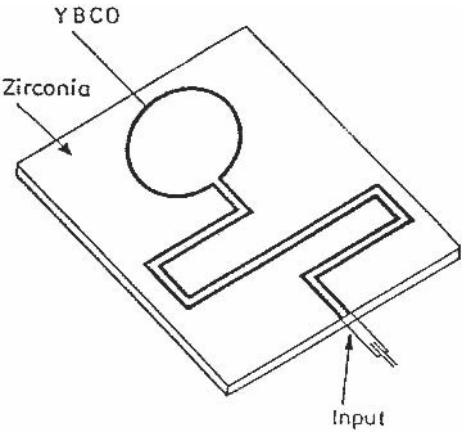

Figure 3.5 Loop and matching circuit. Courtesy of Lancaster, M.J. et al. YBCO Thick Film Loop Antenna and Matching Network. *IEEE Trans Appl Superconductivity* Vol. 3, March 1993, pp. 2903–2905.

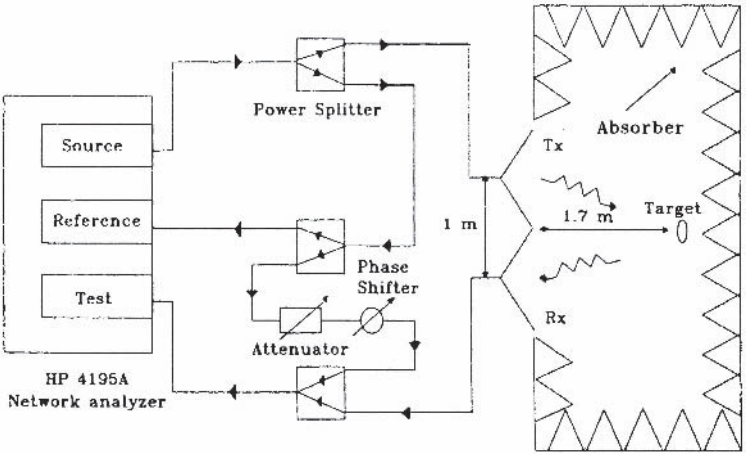

Figure 3.6 Backscatter measurement using nulling. Courtesy of Khamas, S.K. et al. Investigation of the Enhanced Efficiencies of Small Superconducting Loop Antenna Elements. *J Appl Physics* Vol. 74, 15 Aug. 1993, pp. 2914–2918.

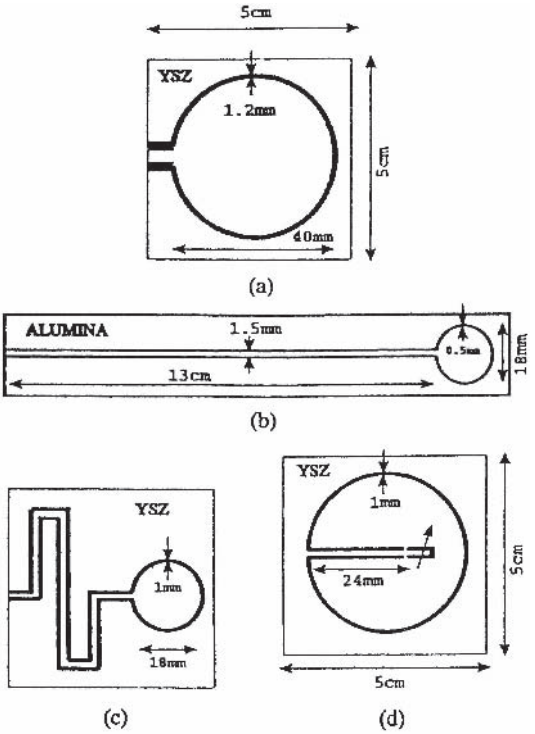

Figure 3.7 Loop feeding and matching: a) resonant loop; b) coplanar strip and capacitor c) coplanar strip meander; d) coplanar strip inside. Courtesy of Ivrissimtzis, L.P. et al. On the Design and Performance of Electrically Small Printed Thick Film $Yba_2Cu_3O_7$ Antennas. *IEEE Trans Appl Superconductivity* Vol. 4, 1994a, pp. 33–40.

model by Cook et al. (1992). A related study evaluated the efficiency of an HTS ESA over a lossy ground plane, using Sommerfeld integrals (Cook et al., 1994a; Cook et al., 1995). Environmental perturbations were investigated by James and Andrasei (1994). A novel technique is the control of loop or dipole radar cross section by temperature (Cook and Khamas, 1993) or by applied magnetic field (Cook and Khamas, 1994b). In both cases the RCS decreases as the surface resistance increases.

3.3.2 Microstrip Antennas

Work on arrays of microstrip patches is reported below; single patch efforts have been sparse. Richard et al. (1993) compared edge feeding and gap feeding. H-shaped patches have been investigated by Chaloupka et al. (1991) and by Lancaster and Hong (1998); see Figure 3.8. A meanderline patch fed by coax (Fig. 3.9) was constructed by Chaloupka (1992); Wang and Lancaster (1999) fed a meanderline patch by an H-shaped coupling aperture (Fig. 3.10). Resonant size is reduced to roughly $\lambda/10$. A meanderline antenna using EuBaCuO was described by Suzuki et al. (1992). Current density on patches has been measured using the kinetic inductance photo response (Newman and Culbertson, 1993). The real part of the surface impedance

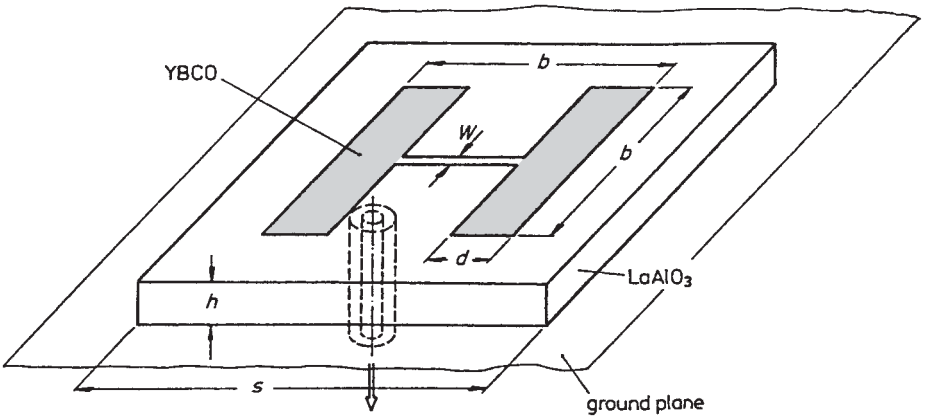

Figure 3.8 H-patch. Courtesy of Chaloupka, H. et al. Miniaturised High-Temperature Superconductor Microstrip Patch Antenna. *Trans IEEE* Vol. MTT-39, Sept. 1991, pp. 1513–1521.

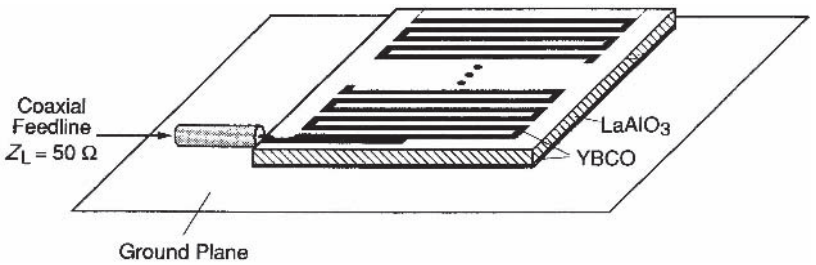

Figure 3.9 Meander patch. Courtesy of Chaloupka, H.J. High-Temperature Superconductor Antennas: Utilisation of Low r.f. Losses and of Nonlinear Effects. *J Superconductivity* Vol. 5, 1992, pp. 405–416.

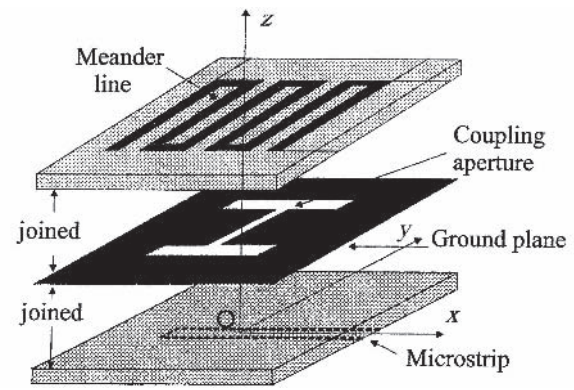

Figure 3.10 Aperture coupled meander patch. Courtesy of Lancaster, M.J., Wang, H.Y., and Hong, J.-S. Thin-Film HTS Planar Antennas. *Trans IEEE Appl Superconductivity* Vol. 8, Dec. 1998, pp. 168–177.

affects the patch input impedance, whereas the imaginary part alters the resonant frequency (Ali et al., 1999a). Yoshida et al. (2001; Tsutsumi et al., 2005) proposed a slot fed by coplanar waveguide, with a multisection matching circuit. The HTS matching section was critical, as the radiation resistance was less than 1 ohm. A bowtie patch with HTS matching circuit was tested by Chung (2001). Bandwidth was small compared to a bowtie dipole in free space.

3.3.3 Array Antennas

A superdirective array of two parallel dipoles in an endfire mode showed an increase in directivity, an increase in Q (Huang et al., 1991; Lancaster et al., 1992a), and a decrease in efficiency (Altshuler et al., 2005). A linear array of parallel dipoles was series fed with feed wires crossed between dipoles (Ivrissimtzis et al., 1994b, 1994c; see Fig. 3.11). Gain was improved but was less than the potential superdirectivity. Four parallel dipoles were excited in a superdirective endfire manner (Ivrissimtzis et al., 1995a; see Fig. 3.12). Gain was good, but bandwidth was narrow. This was extended to a 4×4 endfire dipole array (Fig. 3.13), with series feeding of each of the four subarrays and a corporate overall feed. Again gain was good, but bandwidth was narrow (Ivrissimtzis et al., 1995b). An endfire array of two helices and matching circuit in BSCCO was investigated by Itoh et al. (1993). Performance was several dB better than a copper array. A 4×4 12 GHz patch array with proximity

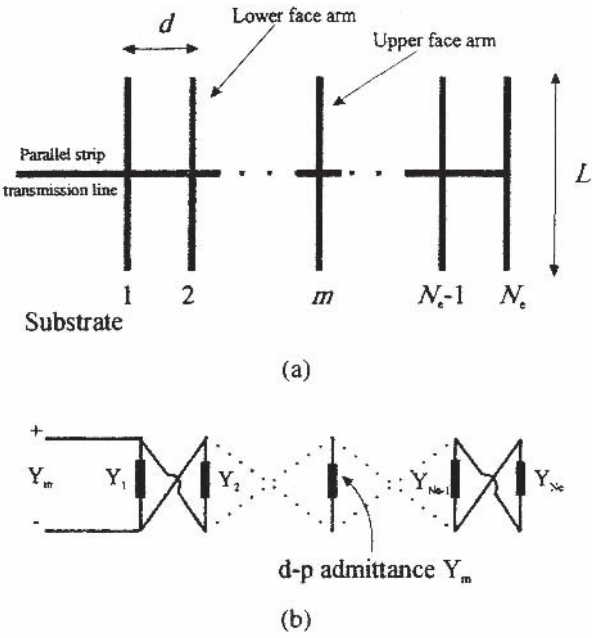

Figure 3.11 Series fed array: a) dipoles; b) equivalent circuit. Courtesy of Ivrissimtzis, L.P. et al. High Gain Printed Dipole Array Made of Thick Film High-T_c Superconducting Material. *Electronics Lett* Vol. 30, 6 Jan. 1994b, pp. 92–93.

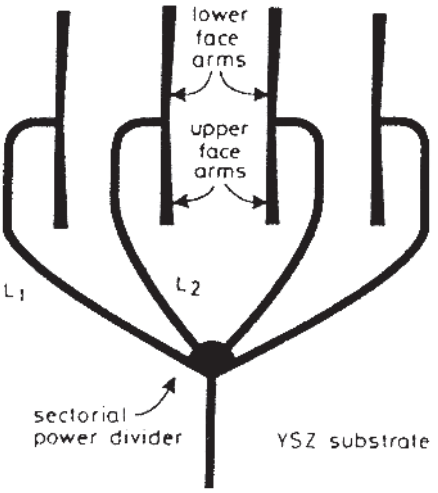

Figure 3.12 Endfire dipole array. Courtesy of Ivrissimtzis, L.P., Lancaster, M.J., and Alford, N. McN. Supergain Printed Arrays of Closely Spaced Dipoles Made of Thick Film High-T_c Superconductors. *IEE Proc Microwaves Antennas Propagation* Vol. 142, Feb. 1995a, pp. 26–34.

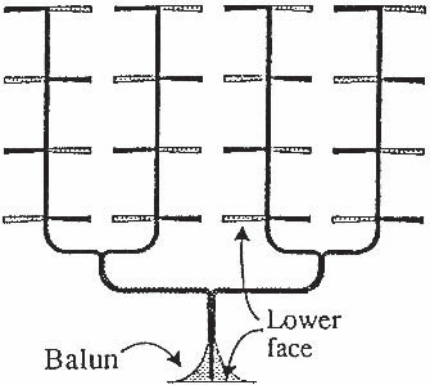

Figure 3.13 Endfire array with tapered Baluns. Courtesy of Ivrissimtzis, L.P., Lancaster, M.J., and Alford, N. McN. A High Gain YBCO Antenna Array with Integrated Feed and Balun. *Trans IEEE Appl Superconductivity* Vol. 5, June 1995b, pp. 3199–3202.

coupled feed network, all HTS, was developed by Herd et al. (1993; see Fig. 3.14). A two-layer 4 × 4 patch array was developed at 20 GHz (Herd et al., 1996; see Fig. 3.15). Another two-layer array is by Ali et al. (1999b). A broadside corporate fed 4 × 4 patch array at 20 GHz in YBCO was developed by Morrow et al. (1999). At 30°K gain was roughly 2 dB better than that of a copper equivalent array, but at 77°K the improvement was only about 0.5 dB. A 2 × 2 broadside patch array was built and tested by Richard et al. (1992). Another 2 × 2 patch array used phase rotation to produce circular polarization (Chung et al., 2003) at 12 GHz. Cryostat and mounting details were also provided (Chung et al., 2005). Gain over a comparable gold array was about 2 dB, probably because of the complexity of the HTS feed and matching network. A departure from YBCO was made by Lewis et al. (1992). They used thallium calcium barium copper oxide in an 8 × 8 patch array, with corporate feed, at 30 GHz (see Fig. 3.16). This is probably the most advanced

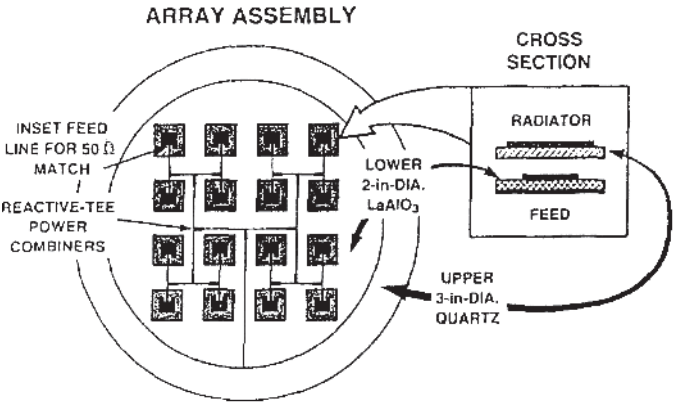

Figure 3.14 Proximity coupled patch array. Courtesy of Herd, J.S. et al. Experimental Results on a Scanned Beam Microstrip Antenna Array with a Proximity Coupled YBCO Feed Network. *IEEE Trans Appl Superconductivity* Vol. 3, March 1993, pp. 2840–2843.

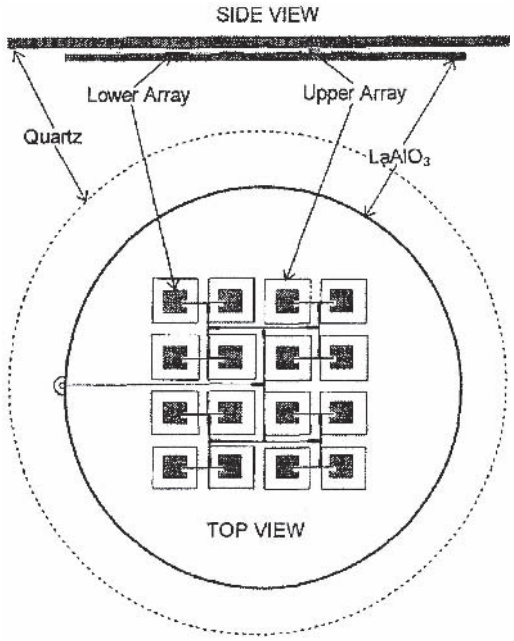

Figure 3.15 Multilayer patch array. Courtesy of Herd, J.S. et al. Twenty-GHz Broadband Microstrip Array with Electromagnetically Coupled High T_c Superconducting Feed Network. *Trans IEEE* Vol. MTT-44, July 1996, pp. 1384–1389.

application of HTS to arrays to date. A YBCO thin film patch array at 12 GHz showed improved gain over a comparison copper array, apparently because of feed loss reduction (Ali et al., 1999). Superdirective arrays used for adaptive beamforming or for multiport applications, because of the strong mutual coupling, benefit from the insertion of decoupling networks (Chaloupka, 1993, 2001; Chaloupka et al., 2003).

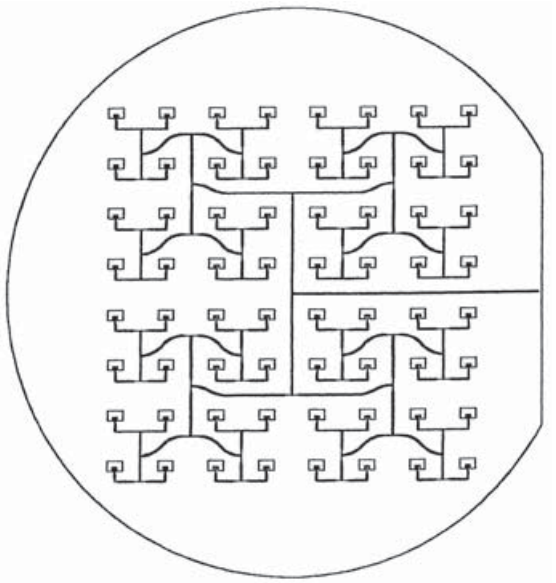

Figure 3.16 8 × 8 corporate fed patch array. Courtesy of Lewis, L.L. et al. Performance of TlCaBaCuO 30 GHz 64 Element Antenna Array. *Trans IEEE Appl Superconductivity* Vol. 3, 1992, pp. 2844–2847.

3.3.4 Millimeter Wave Antennas

Most reflector and array antennas have low dissipative losses (losses are primarily due to impedance mismatches). However at millimeter wavelengths, transmission line loss, whether waveguide, stripline, or microstrip, is important in determining the feasibility of an array. To illustrate this point, examples are calculated for both waveguide and microstrip planar arrays.

3.3.4.1 Waveguide Flat Plane Array

A planar array of waveguide slots is typically constructed of side-by-side waveguide linear slot arrays (sticks), with these fed by another waveguide at right angles, utilizing cross-guide couplers (see Hansen, 1998, Chap. 10.2). Often the array is divided into quadrants for monopulse operation. Resonant stick array design produces a fixed, broadside beam. For a square array of width L, the feed path length is $2L$. And for small to moderate loss, the array efficiency due to waveguide loss, is just:

$$\text{effic} = 1 - 4\alpha L \tag{3.5}$$

where α is the attenuation coefficient. Formulas for α are widely available and are not repeated here. For an example, the lower portion of a waveguide band is used: $\beta/k = 0.5$, and $a = 2b$, using common waveguide notation. Assuming the conductivity of copper, array efficiency due to guide loss is calculated for arrays of directivity 40, 50, and 60 dB (see Fig. 3.17). Gain then is the directivity minus the efficiency (in dB). Of course, for low efficiencies the results are only approximate, as the usual low loss assumptions have been used (tangential magnetic field at the waveguide walls is unchanged). Although

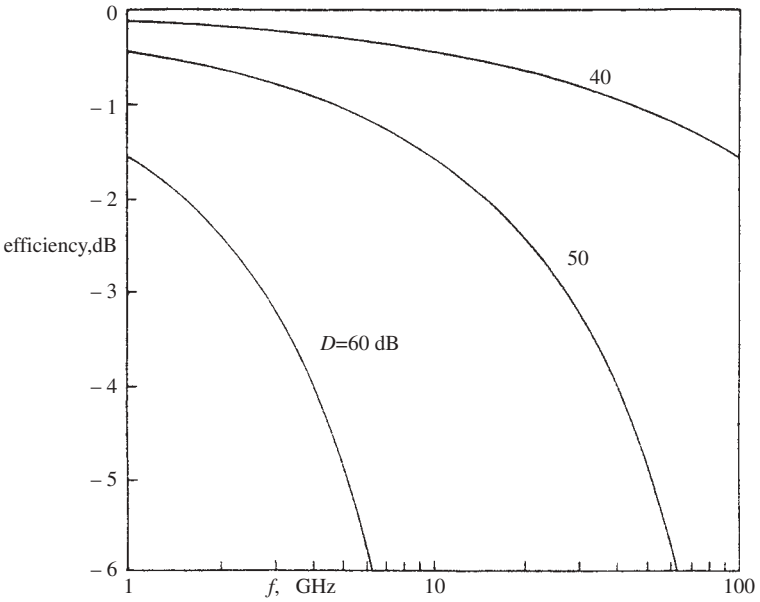

Figure 3.17 Waveguide slot flat plane array efficiency

the curves show that modest gain (40 dB) may be realizable at 100 GHz, the higher frequencies often require large gains to offset increased path loss.

Traveling wave array sticks have an effective path length of half (Begovich, 1966), or L, which reduces the losses compared with resonant arrays. However, the losses are still appreciable. Use of a corporate feed probably incurs an effective path length greater than $2L$, so its loss will exceed that of the resonant array. In practice, for all arrays, the actual loss will be greater, because of surface roughness, metal imperfections, etc. Thus waveguide loss has been a major factor against construction and utilization of high-gain arrays in the 40 to 100 GHz range.

Use of superconducting waveguides would in principle allow the efficiency to approach 0 dB, and thus high-T_c materials may allow a significant extension of array techniques.

3.3.4.2 Microstrip Planar Array

A microstrip array of patch elements is assumed, with loss only in the connecting microstrip lines. Because several approximate results for microstrip loss exist, that used here is given below (Pucel et al., 1968; Wheeler, 1977):

$$\frac{\alpha Z_0 h}{R} = \frac{\left[\dfrac{\dfrac{w'}{h}+\dfrac{w'}{\pi h}}{\dfrac{w'}{2h}+0.94}\right]\left[1+\dfrac{h}{w'}+\dfrac{h}{\pi w'}\left(\ln\dfrac{2h}{t}-\dfrac{t}{h}\right)\right]}{\left(\dfrac{w'}{h}+\dfrac{2}{\pi}\ln\left[2\pi e\left(\dfrac{w'}{2h}+0.94\right)\right]\right)^2} \tag{3.6}$$

where

$$\frac{w'}{h} = \frac{120}{Z_0} - \frac{2}{\pi}\left[1 + \ln\left(\frac{120\pi^2}{Z_0} - 1\right)\right] \tag{3.7}$$

In this formula, w/h has been written in terms of Z_0, for thin strips. The dielectric is air, to remove dielectric losses. Microstrip conductor width is w, thickness is t, and the spacing is h. A path length of L, giving efficiency equal to $1 - 2\alpha L$, is used. Parameters used in the calculation are $Z_0 = 50$, $h/\lambda = 0.03$, and $t/h = 0.01$. Figure 3.18 shows efficiency for arrays of directivity of 40, 50, and 60 dB, and the results are similar to those for waveguide arrays: Only modest gains are obtainable for 40–100 GHz.

Superconducting microstrip behavior is more complex than that of superconducting waveguide for several reasons. As edge current behavior is different, the strip conductors may be very thin without the high loss engendered by edge current singularities in normal conductors. And use of narrow strips allows the dielectric thickness to be reduced, thereby reducing dielectric losses (Kautz, 1979). If the dielectric loss needs to be reduced further, low-loss structures such as suspended-substrate microstrip or inverted microstrip can be used (Young and Itoh, 1988). The relative values of conductor and dielectric loss will depend on frequency, as the supercurrent component of surface resistance increases with the square of frequency, as predicted for low frequencies by the London two-fluid theory, and for frequencies near the energy-gap frequency by the Mattis–Bardeen theory (Kautz, 1978). It is assumed that the residual resistance component is negligible. It appears that microstrip of conventional dimensions could experience a loss reduction of the

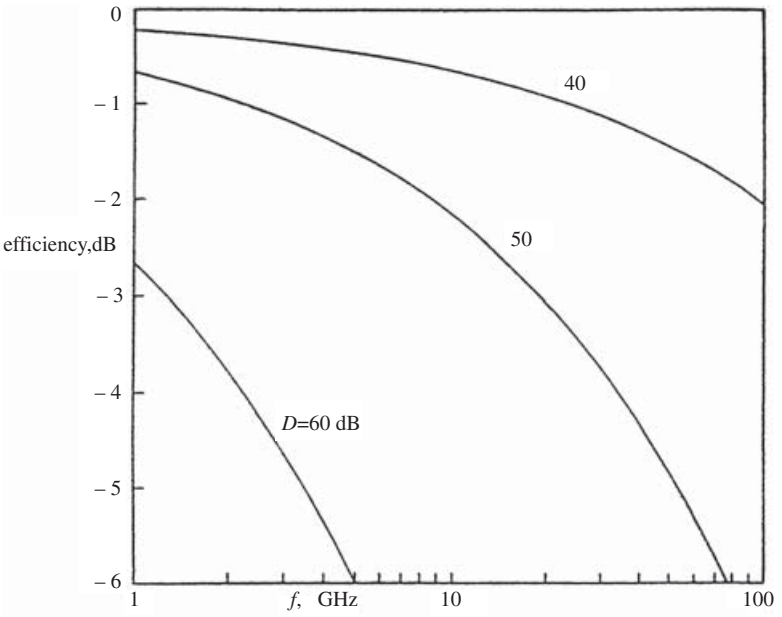

Figure 3.18 Microstrip flat plane array efficiency

order of 20 dB at 100 GHz, while thin film microstrip should show another 10 dB of loss reduction. Thus superconductors will allow high-gain microstrip arrays to be used at millimeter wavelengths.

3.3.5 Submillimeter Antennas

A slot antenna with quasi-optical mixer using an LTS (Nb) trilayer junction operates in the range of 400 to 850 GHz (Zmuidzines et al., 1992, 1995, 2004; Gaidis et al., 1996). For these short wavelengths, two parallel slots, with the trilayer SIS chip[2] in between, are all cooled to about 4°K by locating them on the cold finger of a helium Dewar. The incoming wave is focused on the double slot by a hemispherical silicon lens. This technology has been used in U.S. space probes. These SIS mixers apparently work below 4.5°K, so an HTS version may not be possible.

3.3.6 Low-Temperature Superconductor Antennas

One of the first experiments measured efficiency of a short dipole at 4°, 77°, and 290°K (Moore and Travers, 1966). Significant increases in efficiency were measured as the temperature was lowered. The dipole did not become superconductive; the material was not specified. Low-temperature measurements have been performed on a loop (Walker and Haden, 1969, 1977), and on an endfire array of lead-plated loops in a liquid helium environment (4.2°K). Efficiency rose to near 100% over room temperature, but the bandwidth became extremely narrow. Adachi (1976) worked on dipoles, and later on dipole arrays. Russian work using niobium has been reported: Pavlyuk et al. (1978) measured relative gain and Q for a loop and for a dipole; Krivosheev and Pavlyuk (1979) measured a two-loop endfire array; and Vendik et al. (1981) determined the input power a loop could accept while remaining superconductive.

3.4 PHASERS AND DELAY LINES

Phasers, or phase shifters, are used at each element of a phased array to steer the beam. For wide band arrays time delay (all time delay is "true") is also needed for frequency-independent beam steering. At microwave frequencies the loss, especially for long room temperature time delays, may become unacceptable. Superconductors possess an interesting property where the SC Cooper pair currents have kinetic inductance, allowing appreciable delay in a short segment of transmission line. Pond et al. (1987, 1989) measured LTS delay on a NbN transmission line; the dielectric loss was critical. With the kinetic inductance of the Cooper paired electrons goes loss; the SC layer thickness must be carefully chosen to reach an acceptable compromise between low phase velocity (thin film) and low loss (thick film). For a SC,

[2] See Tucker and Feldman (1985) for a comprehensive review of SIS technology.

the conductivity is complex, and it varies with the penetration depth and SC layer thickness (Ma and Wolff, 1996). The penetration depth changes with temperature, going to zero at T_c. The real part of conductivity relates to the loss, and the imaginary part relates to the kinetic inductance. Strong currents or strong magnetic fields will affect all parameters. Sheen et al. (1991) have formulated surface resistance, normal inductance, kinetic inductance, and current distribution for stripline, all as a function of penetration depth and film thickness. See also Ma and Wolff (1996) for formulations of complex conductivity and effective dielectric constant.

There was much interest in delay lines in the early 1990s. Liang et al. (1991) used YBCO on a lanthanum aluminum oxide substrate. A reflection configuration with PIN diode switches was used, with 4 bits of phase produced. Each bit utilizes a 3 dB hybrid and 2 diodes; see Figure 3.19. The difference in line length between the switched and unswitched lines gives the phase bit. Loss at 10 GHz was 1.1 dB, a value considerably less than that for copper phasers. Because a 4-bit phaser provides up to 0.9375λ of delay, the loss per wavelength was 1.2 dB. However, most of this loss was due to substrate loss, diode loss, and mismatch loss. Shen et al. (1991) built a spiral delay line in coplanar line, using ThBaCaCuO on a LaAlO substrate. Delay time was 11 ns, and the loss was 0.25 dB/ns at 8 GHz. Liang et al. (1993) worked spiral delay lines in YBCO; delays were 27 and 44 ns, with losses of 6 and 16 dB at 6 GHz. These losses are 0.22 and 0.36 dB/ns, and 0.042 and 0.061 dB/λ. A spiral YBCO delay line on sapphire (Liang et al., 1994) produced 9 ns of delay at 77°K. Surface resistance was 0.5 mohm at 10 GHz; insertion loss was 1.5 dB at 6 GHz. This is 0.167 dB/ns at 6 GHz. Also, at 6 GHz the delay line is 54λ long, giving a loss of 0.0278 dB/λ. Another spiral delay line (Hofer and Kratz, 1993) has 3-ns delay but no data on loss. Track et al. (1993) and Martens et al. (1993) built both NbN and YBCO delay lines, using a meanderline pattern. The delay was 8 ns, with a loss of 3 dB at 20 GHz, or 0.375 dB/ns. At 20 GHz this loss is 0.0125 dB/λ. Other work on meanderline delay lines was by Hattori et al. (1999) with 2.8-ns delay and loss at 70 K, and at 10 GHz, of 0.39 dB/ns or 0.039 dB/λ; by Hohenwarter et al. (1993), using NbN and coplanar waveguide, with 45-ns delay and with loss of

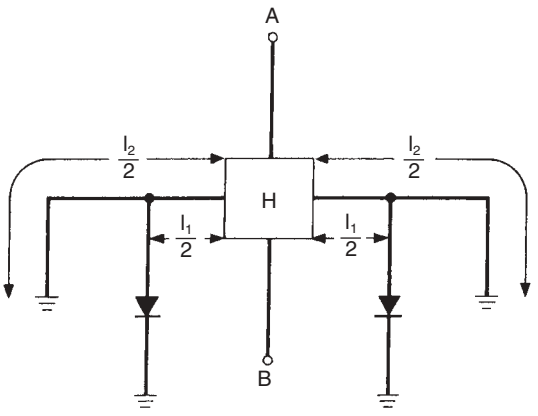

Figure 3.19 3 dB hybrid PIN diode phaser. Courtesy of Liang, G.C. et al. High-Temperature Superconductor Resonators and Phase Shifters. *IEEE Trans Appl Superconductivity* Vol. 1, March 1991, pp. 58–66.

0.01 dB/ns and 0.001 dB/λ at 10 GHz. Huang et al. (1993) developed a 3-ns YBCO delay line; loss at 8 GHz was 0.73 dB/ns or 0.092 dB/λ. Talisa et al. (1995) used a closely wrapped spiral of YBCO on LaAlO, in stripline. The line is 1.5 m long! See Figure 3.20. Surface resistance at 10 GHz and 77°K is 0.5 mohm. Delay is 45 ns. Loss is 2 dB at 10 GHz and 6 dB at 20 GHz. At 10 GHz, this loss is 0.0044 dB/λ, and at 20 GHz it is 0.0067 dB/λ. Loss per nanosecond is 0.044 dB/ns at 10 GHz and 0.133 dB/ns at 20 GHz. Fenzi et al. (1994) developed a 100-ns delay line using TBCCO on an LaAlO substrate with meandered coplanar waveguide; see Figure 3.21. Loss at 6 GHz was below 0.08 dB/ns, which is 0.013 dB/λ. This is the type of delay that might be suitable for wideband phased array steering. Fabrication details of a YBCO meanderline delayer using epitaxial liftoff were given by Koh and

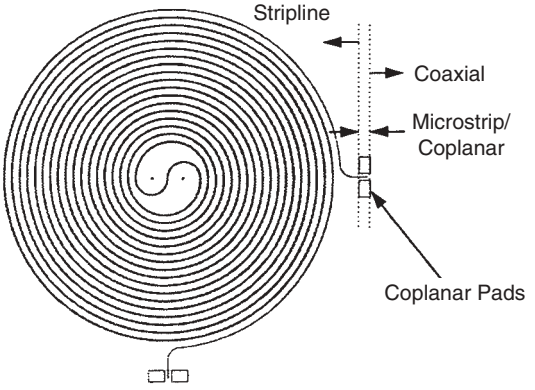

Figure 3.20 22.5 nanosec stripline delay line. Courtesy of Talisa, S.H. et al. High-Temperature Superconducting Wide Band Delay Lines. *IEEE Trans Appl Superconductivity* Vol. 5, 1995, pp. 2291–2294.

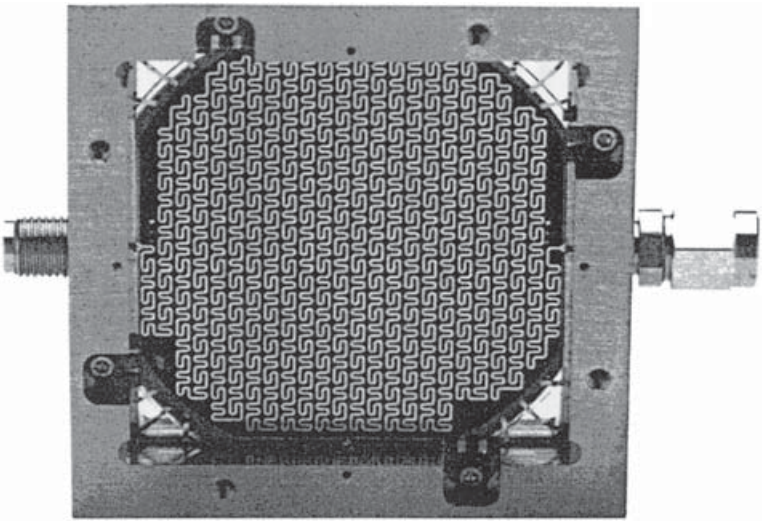

Figure 3.21 100 nanosecond delay line. Courtesy of Fenzi, N. et al. Development of High Temperature Superconducting 100 Nanosecond Delay Line. *Proc SPIE* Vol. 2156, 1994, pp. 143–151.

Hohkawa (1999). Important practical implementation considerations such as insulation package, cooler, vacuum package, and electronics package were discussed by Kapolnek et al. (1993). A convenient formula relates line length and delay:

$$L/\lambda = t_{\text{ns}} f_{\text{GHZ}} \tag{3.8}$$

A different approach uses an HTS transmission with many SQUID devices coupled to it. Each SQUID contains one Josephson junction. The first work was L TS using niobium (Durand et al., 1992). This was followed by an HTS YBCO (Takemoto-Kobayashi et al., 1992) delay line. A variable magnetic field on the SQUIDs changes the delay. The experimental model with 40 SQUIDs produced 60° of phase shift at 10 GHz. Problems of temperature, dynamic range, and complexity appear to make SQUID phasers less attractive than those using single line length.

3.5 SC ANTENNA SUMMARY

The field of superconducting antennas was changed by the emergence of three important principles (Hansen, 1990, 1991; Khamas et al., 1990). *Principle One*: Dipole-type ESA made of copper or aluminum have radiation resistance much larger than loss resistance; efficiencies are close to 100%. For example, a dipole 0.02λ long has a radiation resistance of 100 mohm, a value much larger than typical loss resistance. *Principle Two*: Loop-type ESA usually have radiation resistance well below loss resistance, so use of HTS will greatly increase loop efficiency. However Q (and bandwidth) are now controlled by radiation resistance alone; Q is unacceptably high. *Principle Three*: A network matching an ESA to 50 ohms sees a high VSWR, and this greatly increases the intrinsic loss in the matching network. Thus it may be concluded that HTS ESA are not useful or cost effective except in special circumstances. The matching circuit can benefit significantly by employing HTS components. HTS delay lines with long delays are promising for steering of wideband phased arrays. Millimeter wave arrays can benefit from HTS, not necessarily in the antenna elements, but in the feed network. Submillimeter antennas using integrated SIS sensors and antennas are a promising area.

REFERENCES

Adachi, S. et al. An Experiment on Superconducting Antennas. *Trans IECE Japan* Vol. J59-B, 1976, pp. 299–300.

Alford, McN.N. et al. Surface Resistance of Bulk and Thick Film $YBa_2Cu_3O_7$. *IEEE Trans Magnet* Vol. 27, March 1991, pp. 1510–1518.

Ali, M.I. et al. Effect of Surface Impedance on the Antenna Properties in Superconducting Microstrip Antenna. *Physica C* Vol. 325, 1999a, pp. 143–152.

Ali, M.I., Ehata, K., and Ohshima, S. Superconducting Patch Array Antenna on Both-Side YBCO Thin Film for Satellite Communication. *IEEE Trans Appl Superconductivity* Vol. 9, June 1999b, pp. 3077–3080.

Altshuler, E.A. A method for Matching an Antenna Having a Small Radiation Resistance to a 50-ohm Load. *Trans IEEE* Vol. AP-53, Sept. 2005, pp. 3086–3089.

Begovich, N.A. Frequency Scanning. In *Microwave Scanning Antennas*, Vol. 3, Hansen, R.C. Ed., Academic Press, 1966; Peninsula Publ., 1985.

Chaloupka, H.J. et al. Miniaturised High-Temperature Superconductor Microstrip Patch Antenna. *Trans IEEE* Vol. MTT-39, Sept. 1991, pp. 1513–1521.

Chaloupka, H.J. High-Temperature Superconductor Antennas: Utilisation of Low r.f. Losses and of Nonlinear Effects. *J Superconductivity* Vol. 5, 1992, pp. 405–416.

Chaloupka, H.J. Superconducting Multiport Antenna Arrays. *Microwave Optical Tech Lett* Vol. 6, Oct. 1993, pp. 737–744.

Chaloupka, H.J. HTS Antennas. In: *Microwave Superconductivity.* Weinstock, H. and Nisenoff, M., Eds., 2001, Kluwer Academic Publ., pp. 353–386.

Chaloupka, H.J., Wang, X., and Coetzee, J.C. A Superdirective 3-Element Array for Adaptive Beamforming. *Microwave Optical Tech Lett* Vol. 36, 20 March 2003, pp. 425–430.

Chung, D.-C. Broadband HTS Microstrip Antennas for Satellite Communication. *IEEE Trans Appl Superconductivity* Vol. 11, March 2001, pp. 107–110.

Chung, D.-C. et al. Circularly Polarized HTS Microstrip Antenna Array. *IEEE Trans Appl Superconductivity* Vol. 13, June 2003, pp. 301–304.

Chung, D.-C. et al. HTS Microstrip Antenna Array for Circular Polarization With Cryostat. *IEEE Trans Appl Superconductivity* Vol. 15, June 2005, pp. 1048–1051.

Cook, G.G. and Khamas, S.K. Temperature Control of Radar Cross-Section Using Electrically Small High-T_c Superconducting Antenna Elements for Stealth Applications. *Proc IEE* Vol. 140H, Aug. 1993, pp. 326–328.

Cook, G.G. et al. Predictions of the Efficiencies of Superconducting Small Antennas Connected to Lossy Ground Planes Using a Sommerfeld Integral Technique. *J Appl Phys* Vol. 76, 15 July 1994a, pp. 1266–1268.

Cook, G.G. and Khamas, S.K. Control of Radar Cross Sections of Electrically Small High Temperature Superconducting Antenna Elements Using A Magnetic Field. *Trans IEEE* Vol. AP-42, June 1994b, pp. 888–890.

Cook, G.G., Khamas, S.K., and Bowling, D.R. Efficiencies of Superconducting Small Antennas Connected to Lossless Disks Over Lossy Groundplanes. *Trans IEEE* Vol. AP-43, June 1995, pp. 631–633.

Cook, G.G. et al. Performance Prediction of High-T_c Superconducting Small Antennas Using a Two-Fluid-Moment Method Model. *Appl Phys Lett* Vol. 60, 6 Jan. 1992, pp. 123–125.

Dinger, R.J. and White, D.J. Theoretical Increase in Radiation Efficiency of a Small Dipole Antenna Made with a High Temperature Superconductor. *Trans IEEE* Vol. AP-38, Aug. 1990, pp. 1313–1316.

Dinger, R.J., Bowling, D.R., and Martin, A.M. A Survey of Possible Passive Antenna Applications of High-Temperature Superconductors. *Trans IEEE* Vol. MTT-39, Sept. 1991, pp. 1498–1507.

Durand, D.J. et al. The Distributed Josephson Inductance Phase Shifter. *IEEE Trans Appl Superconductivity* Vol. 2, March 1992, pp. 33–38.

Fenzi, N. et al. Development of High Temperature Superconducting 100 Nanosecond Delay Line. *Proc SPIE* Vol. 2156, 1994, pp. 143–151.

Gaidis, M.C. et al. Characterization of Low-Noise Quasi-Optical SIS Mixers for the Submillimeter Band. *Trans IEEE* Vol. MTT-44, July 1996, pp. 1130–1139.

Ginzburg, V.L. and Andryushin, E.A. *Superconductivity.* World Scientific, 2004.

Gough, C.E. et al. Critical Currents in a High-T_c Superconducting Short Dipole Antenna. *Trans IEEE* Vol. MAG-25, March 1989, pp. 1313–1314.

Hansen, R.C. Superconducting Antennas. *Trans IEEE* Vol. AES-26, March 1990, pp. 345–355.

Hansen, R.C. Antenna Applications of Superconductors. *Trans IEEE* Vol. MTT-39, Sept. 1991, pp. 1508–1512.

Hansen, R.C. *Phased Array Antennas*. John Wiley & Sons, 1998.

Hattori, W., Toshitake, T., and Tahara, S. A Reentrant Delay-line Memory Using a YBa2Cu3O7 Coplanar Delay Line. *IEEE Trans Appl Superconductivity* Vol. 9, June 1999, pp. 3829–3832.

He, Y.S. et al. Progress in High T_c Superconducting Ceramic Antennas. *Superconductor Sci Tech* Vol. 4, 1991, pp. S124–S126.

He, Y.S. et al. Liquid Nitrogen Temperature Superconducting Antennas Made from Metal Oxide Ceramics. *Cryogenics* Vol. 30, Suppl., 1990, pp. 946–950.

Herd, J.S. et al. Experimental Results on a Scanned Beam Microstrip Antenna Array with a Proximity Coupled YBCO Feed Network. *IEEE Trans Appl Superconductivity* Vol. 3, March 1993, pp. 2840–2843.

Herd, J.S. et al. Twenty-GHz Broadband Microstrip Array with Electromagnetically Coupled High T_c Superconducting Feed Network. *Trans IEEE* Vol. MTT-44, July 1996, pp. 1384–1389.

Hofer, G.J., and Kratz, H.A. High Temperature Superconductor Coplanar Delay Lines. *IEEE Trans Appl Superconductivity* Vol. 3, March 1993, pp. 2800–2803.

Hohenwarter, G.K.G. et al. Forty Five Nanoseconds Superconducting Delay Lines. *IEEE Trans Appl Superconductivity* Vol. 3, March 1993, pp. 2804–2807.

Huang, F. et al. A Superconducting Microwave Linear Phase Delay Line Filter. *IEEE Trans Appl Superconductivity* Vol. 3, March 1993, pp. 2778–2781.

Huang, Y. et al. A High Temperature Superconductor Superdirectional Antenna Array. *Physica C* Vol. 180, 1991, pp. 267–271.

Itoh, K. et al. High T_c Superconducting Small Antennas. *IEEE Trans Appl Superconductivity* Vol. 3, March 1993, pp. 2836–2839.

Ivrissimtzis, L.P. et al. On the Design and Performance of Electrically Small Printed Thick Film $Yba_2Cu_3O_7$ Antennas. *IEEE Trans Appl Superconductivity* Vol. 4, 1994a, pp. 33–40.

Ivrissimtzis, L.P. et al. High Gain Printed Dipole Array Made of Thick Film High-T_c Superconducting Material. *Electronics Lett* Vol. 30, 6 Jan. 1994b, pp. 92–93.

Ivrissimtzis, L.P. et al. High-Gain Series Fed Printed Dipole Arrays Made of High-T_c Superconductors. *Trans IEEE* Vol. AP-42, Oct. 1994c, pp. 1419–1429.

Ivrissimtzis, L.P., Lancaster, M.J., and Alford, N.McN. Supergain Printed Arrays of Closely Spaced Dipoles Made of Thick Film High-T_c Superconductors. *IEE Proc Microwaves Antennas Propagation* Vol. 142, Feb. 1995a, pp. 26–34.

Ivrissimtzis, L.P., Lancaster, M.J., and Alford, N.McN. A High Gain YBCO Antenna Array with Integrated Feed and Balun. *Trans IEEE Appl Superconductivity* Vol. 5, June 1995b, pp. 3199–3202.

James, J.R. and Andrasic, G. Environmental Coupling Loss Effects in Superconducting HF Loop Antenna Design. *Proc IEE Microwave Antennas Prop* Vol. 141, April 1994, pp. 94–100.

Kapolnek, D.J. et al. Integral FMCW Radar Incorporating an HTSC Delay Line with User-Transparent Cryogenic Cooling and Packaging. *IEEE Trans Appl Superconductivity* Vol. 3, March 1993, pp. 2820–2823.

Kautz, R.L. Picosecond Pulses on Superconducting Striplines. *J Appl Physics* Vol. 49, Jan. 1978, pp. 308–314.

Kautz, R.L. Miniaturization of Normal-State and Superconducting Striplines. *J Res NBS* Vol. 84, May–June 1979, pp. 247–259.

Khamas, S.K. et al. High-T_c Superconducting Short Dipole Antenna. *Electronics Lett* Vol. 24, 14 April 1988, pp. 460–461.

Khamas, S.K. et al. Significance of Matching Networks in Enhanced Performance of Small Antennas When Supercooled. *Electronics Lett* Vol. 26, 10 May 1990, pp. 654–655.

Khamas, S.K. et al. Investigation of the Enhanced Efficiencies of Small Superconducting Loop Antenna Elements. *J Appl Physics* Vol. 74, 15 Aug. 1993, pp. 2914–2918.

Koh, K. and Hohkawa, K. Fabrication of Superconducting Delay Line with GaAs Schottky Diode. *IEEE Trans Appl Superconductivity* Vol. 9, June 1999, pp. 3224–3227.

Krivosheev, E.F. and Pavlyuk, V.A. High-Gain Cryogenic Antenna Array. *Sov Tech Phys Lett* Vol. 5, Aug. 1979, pp. 384–385.

Lancaster, M.J. *Passive Microwave Device Applications of High-Temperature Superconductors.* Cambridge Univ. Press, 1997.

Lancaster, M.J. et al. Supercooled and Superconducting Small-Loop and Dipole Antennas. *Proc IEE* Vol. 139, Pt. H, June 1992a, pp. 264–270.

Lancaster, M. et al. Superconducting Antennas. *Superconducting Sci Tech* Vol. 5, 1992b, pp. 277–279.

Lancaster, M.J., Wang, H.Y., and Hong, J.-S. Thin-Film HTS Planar Antennas. *Trans IEEE Appl Superconductivity* Vol. 8, Dec. 1998, pp. 168–177.

Lancaster, M.J. et al. YBCO Thick Film Loop Antenna and Matching Network. *IEEE Trans Appl Superconductivity* Vol. 3, March 1993, pp. 2903–2905.

Lewis, L.L. et al. Performance of TlCaBaCuO 30 GHz 64 Element Antenna Array. *Trans IEEE Appl Superconductivity* Vol. 3, 1992, pp. 2844–2847.

Liang, G.C. et al. High-Temperature Superconductor Resonators and Phase Shifters. *IEEE Trans Appl Superconductivity* Vol. 1, March 1991, pp. 58–66.

Liang, G.C. et al. High-Temperature Superconducting Delay Lines and Filters on Sapphire and Thinned LaAO3 Substrates. *IEEE Trans Appl Superconductivity* Vol. 3, Sept. 1993, pp. 3037–3042.

Liang, G.C. et al. High-Temperature Superconductive Devices on Sapphire. *Trans IEEE* Vol. MTT-42, Jan. 1994, pp. 34–40.

Ma, J.-G. and Wolff, I. Electromagnetics in High-T_c Superconductors. *Trans IEEE* Vol. MTT-44, April 1996, pp. 537–542.

Martens, J.S. et al. HTS-Based Switched Filter Banks and Delay Lines. *IEEE Trans Appl Superconductivity* Vol. 3, March 1993, pp. 2824–2827.

Moore, J.D. and Travers, D.N. Radiation Efficiency of a Short Cryogenic Antenna. *Trans IEEE* Vol. AP-14, March 1966, p. 246.

Morrow, J.D. et al. Circularly Polarized 20-GHz High-Temperature Superconducting Microstrip Antenna Array. *IEEE Trans Appl Superconductivity* Vol. 9, Dec. 1999, pp. 4725–4731.

Newman, H.S. and Culbertson, J.C. Measurement of the Current-Density Distribution in High-Temperature Superconducting Microstrip by Means of Kinetic-Inductance Photoresponse. *Microwave Optical Tech Lett* Vol. 6, Oct. 1993, pp. 725–728.

Pavlyuk, V.A. et al. Superconducting Antenna. *Sov Tech Phys Lett* Vol. 4, Feb. 1978, p. 80.

Piel, H. and Muller, G. The Microwave Surface Impedance of High Temperature Superconductors. *Trans IEEE Magnet* Vol. 27, March 1991, pp. 854–862.

Pond, J.M., Claassen, J.H., and Carter, W.L. Measurements and Modeling of Kinetic Inductance Microstrip Delay Lines. *Trans IEEE* Vol. MTT-35, Dec. 1987, pp. 1256–1262.

Pond, J.M., Krowne, C.M., and Carter, W.L. On the Application of Complex Resistive Boundary Conditions to Model Transmission Lines Consisting of Very Thin Superconductors. *Trans IEEE* Vol. MTT-37, Jan. 1989, pp. 181–190.

Portis, A.M. et al. Power-Induced Switching of an HTS Microstrip Patch Antenna. *Supercond Sci Tech* Vol. 4, 1991, pp. 436–438.

Pucel, R.A., Masse, D.J., and Hartwig, C.P. Losses in Microstrip. *Trans IEEE* Vol. MTT-16, June 1968, pp. 342–350; see also MTT-16, Dec. 1968, p. 1064.

Richard, M.A., Bhasin, K.B., and Claspy, P.C. Superconducting Microstrip Antennas: An Experimental Comparison of Two Feeding Methods. *Trans IEEE* Vol. AP-41, July 1993, pp. 967–974; correction AP-52, March 2004, pp. 911–912.

Richard, M.A. et al. Performance of a Four-Element Ka-Band High-Temperature Superconducting Microstrip Antenna. *IEEE Microwave Guided Wave Ltrs* Vol. 2, April 1992, pp. 143–145.

Sheen, D.M. et al. Current Distribution, Resistance, and Inductance for Superconducting Strip Transmission Lines. *IEEE Trans Appl Superconductivity* Vol. 1, June 1991, pp. 108–115.

Shen, Z.-Y. et al. High T_c Superconducting Coplanar Delay Line with Long Delay and Low Insertion Loss. *IEEE MTT Symp Digest* 1991, pp. 1235–1238.

Suzuki, N. et al. Superconductive Small Antennas Made of Eu-Ba-CuO Thin Films. In *Advances in Superconductivity Vol. V*, Bando, Y. and Yamauchi, H., Eds. Springer-Verlag, 1992, pp. 1127–1130.

Takemoto-Kobayashi, J.H. et al. High-T_c Superconducting Monolithic Phase Shifter. *IEEE Trans Appl Superconductivity* Vol. 2, March 1992, pp. 39–44.

Talisa, S.H. et al. High-Temperature Superconducting Wide Band Delay Lines. *IEEE Trans Appl Superconductivity* Vol. 5, 1995, pp. 2291–2294.

Tinkham, M. *Introduction to Superconductivity* McGraw-Hill, 1996.

Track, E.K., Drake, R.E., and Hohenwarter, G.K.G. Optically Modulated Superconducting Delay Lines. *IEEE Trans Appl Superconductivity* Vol. 3, March 1993, pp. 2899–2902.

Tsutsumi, Y., Kanaya, H., and Yoshida, K. Design and Performance of an Electrically Small Slot Loop Antenna With a Mineaturized Superconduction Matching Circuit. *IEEE Trans Appl Superconductivity*, Vol. 15, June 2005, pp. 1020–1023.

Tucker, J.R. and Feldman, M.J. Quantum Detection at Millimeter Wavelengths. *Rev Mod Phys* Vol. 57, 1985, pp. 1055–1113.

Vendik, O.G., Kozyrev, A.B., and Morozik, V.P. Maximum Power of a Miniature Superconducting Radiator. *Sov Phys Tech Phys* Vol. 26, July 1981, pp. 888–890.

Walker, G.B. and Haden, C.R. Superconducting Antennas. *J Appl. Phys* Vol. 40, 1969, pp. 2035–2039.

Walker, G.B., Haden, C.R., and Ramer, O.G. Superconducting Superdirectional Antenna Arrays. *Trans IEEE* Vol. AP-25, Nov. 1977, pp. 885–887.

Wang, H.Y. and Lancaster, M.J. Aperture-Coupled Thin-Film Superconducting Meander Antennas. *Trans IEEE* Vol. AP-47, May 1999, pp. 829–836.

Wheeler, H.A. Transmission-Line Properties of a Strip on a Dielectric Sheet on a Plane. *Trans IEEE* Vol. MTT-25, Aug. 1977, pp. 631–647.

Wu, Z. et al. High T_c Superconducting Small Loop Antenna. *Physica* Vol. C162–4, 1989, pp. 385–386.

YOSHIDA, K. ET AL. Superconducting Slot Antenna with Broadband Impedance Matching Circuit. *IEEE Trans Appl Superconductivity* Vol. 11, March 2001, pp. 103–106.

YOUNG, B. AND ITOH, T. Loss Reduction in Superconducting Microstrip-Like Transmission lines. *IEEE 1988 Microwave Theory Tech Symp Digest* 1988, pp. 453–456.

ZMUIDZINAS, J. AND LEDUC, H.G. Quasi-Optical Slot Antenna SIS Mixers. *Trans IEEE* Vol. MTT 40, Sept. 1992, pp. 1797–1804.

ZMUIDZINAS, J. AND RICHARDS, P.L. Superconducting Detectors and Mixers for Millimeter and Submillimeter Astrophysics. *Proc IEEE* Vol. 92, Oct. 2004, pp. 1597–1616.

ZMUIDZINAS, J. ET AL. Low-Noise Slot Antenna SIS Mixers. *IEEE Trans Appl Superconductivity* Vol. 5, June 1995, pp. 3053–3056.

AUTHOR INDEX

Subject Index

Electrically Small, Superdirective, and Superconducting Antennas, by R. C. Hansen.